

https://dspace.org/

Sediment patterns and source areas within the Letaba River, Kruger National Park, South Africa

Mugwabana, Tondani Tshifaro

2018

https://hdl.handle.net/10539/25860

Mugwabana, Tondani Tshifaro (2018) Sediment patterns and source areas within the Letaba River, Kruger National Park, South Africa, University of the Witwatersrand, Johannesburg, <http://hdl.handle.net/10539/25860>

Downloaded from a DSpace repository. https://dspace.org/

Sediment patterns and source areas within the Letaba River, Kruger National Park, South Africa

Submitted by: Tondani Mugwabana

Student number: 418215

Qualification: Masters of Science by Dissertation

Submitted to: Geography Division, School of Geography, Archaeology and Environmental Studies, University of the Witwatersrand



Contents

List of figures iv
List of tables viii
Abbreviations ix
Abstract x
Declaration xi
Acknowledgements xii
Chapter 1: Introduction 1
1.1. Background 1
1.2. Aim and Objectives 3
1.2.1. Aim 3
1.2.2. Objectives 4
Chapter 2: Study area 5
2.1. Location of study area 5
2.2 Geological history, soils and topography 7
2.3 Rainfall 10
2.4 River Discharge 10
Chapter 3: Literature Review 13
3.1 Characteristics of semi-arid catchments 13
3.2. Characteristics of bedrock-influenced channels 14
3.3 Mechanisms of bedrock erosion 15
3.4 Floods as modifiers of river systems 16
3.5 Flood modifications in rivers across the world 18
3.6 Grain sizes and distributions 19
3.7 Sediment provenance 23
3.8 Processes affecting heavy mineral assemblages 24
3.9 Multivariate mixing models 27
Chapter 4: Methodology 31
4.1. Desk based methods 31
4.2. Geomorphic mapping and landform identification 32
4.3 Laboratory work 35
4.3.1 Grain size analysis 35
4.3.2 Heavy minerals 37
4.3.3 X-ray Fluorescence Spectroscopy 38

4.3.4 Organic matter content 38
4.4 Analysis 39
4.5 Modified Collins mixing model 41
4.5.1 Running of the mixing model 42
4.5.2 Accuracy of the mixing model 43
Chapter 5: Results 44
5.1 Channel forms 44
5.2 Field descriptions 44
5.3.1 Grain size distributions 72
5.3.2 Grain sizes on different geomorphological features 75
5.3.3 Impact of tributaries 76
5.4 Grain size and underlying geology 77
5.5 Mineral analysis 80
5.5.1 Heavy mineral assemblages 80
5.5.2 Heavy minerals in tributaries 81
5.5.3 Spatial distributions of heavy minerals 86
5.6 Magnetic susceptibility 89
5.7 Trace elements 92
5.8 Mixing of sediments 95
Chapter 6: Discussion 100
6.1 Landforms, sediments and grain size analysis 100
6.2 Mineral analysis 104
6.3. Magnetic susceptibility 106
6.4 Trace element distribution 107
6.5 Mixing models and sediment sources 111
6.5.1 Sediment sources 111
6.5.2 Sediment source apportionment at different sampling sites 112
7. Conclusions 114
7.1 Implications of this study for river management 115
7.2 Limitations of this study 116
Reference list 117
Appendices i
Appendix A: Example of results obtained from Gradistat on Excel 2010. i
Appendix B: Table indicating grain size parameters for each site following Gradstat analysis. ii

Appendix C: Table indicating the mode, sediment name, kurtosis and sorting obtained from Gradstat analysis. iv

Appendix D: Table indicating Organic matter measured at different sites. vi

Appendix E: Table indicting the minerals counted on the thin section of each sample site. vii

Appendix F: Example of the Python script used for running the mixing model. x

Appendix G: Table indicating the correlation coefficient between trace elements xi

Appendix H: Table indicating the eigenvalues obtained following principal component analysis... xii

Appendix I: Table indicating the relationship between grain sizes and trace elements. Significant statistical relationships at P>0.5. xiii

Appendix J: Table indicating relationships between trace elements and minerals within the sediment. Qz=quartz, plg=plagioclase, cpy=clinopyroxene, olv=olivine, hbld=hornblende, bio=biotite, mg=magnetite, hm=hematite, il=ilmenite, zcn=zircon, opy=orthopyroxene, grt=garnet, rt=rutile, tml=tourmaline. Significant statistical relationships at P>0.5 marked in bold. xiv

List of figures

Fig. 2.1: Location of the Letaba River (boxed) within the Kruger National Park and South Africa. Produced by Wendy Phillips. Department of Geography, Archaeology and Environmental Studies. 17 September 2015.

Fig. 2.2: Image of the Letaba Catchment and the location of the Letaba River within the Kruger National Park (hatched) and the 15 data collection sites.

Fig. 2.3: The underlying geology of the Letaba River within the Kruger National Park.

Fig. 2.4: Discharge measuring stations, where data was collected, within the Letaba catchment. B8H008-Letaba Ranch, B8H034-Blach Heron Dam, B8H018-Engelhardt Dam.

Fig. 2.5: Discharge volumes for 3 measuring stations between 2006 and 2015 in the measuring stations within the Great Letaba River. Station names: B8H008 (Great Letaba at Letaba Ranch), B8H034 (Great Letaba at Black Heron Dam), B8H018 (Great Letaba at Engelhardt Dam).

Fig. 3.1: Variable grain sizes and substrate listed in order of resistance to erosion, with the arrow indicating increase in resistance (from Wohl 2015).

Fig. 4.1: Image of the Letaba River and the data collection sites for this research.

Fig. 4.2: Image of Differential GPS (dGPS) used to measure transects across the river channel.

Fig. 4.3: Image of the top sediment being sampled into a plastic sampling bag.

Fig. 4.4: A: Image of sieves of different intervals used to sort sediments in their different grain sizes. B: Image of a scale used to measure the weight of the sieved sediment.

Fig. 4.5: (a): Image of pressed pallets. (b): Image of Mowiol binder, grinder and press used in the preparation of pallets.

Fig. 4.6: Workflow processes of a sediment mixing model (Haddadchi *et al.,* 2013).

Fig. 4.7: The locations of the source sampling sites along the Letaba River.

Fig. 5.1: Data collection sites within the Letaba River.

Fig. 5.2: (a) View of the Groot Letaba River with a vegetated sandbar formed within the channel, flow direction is indicated in the red arrows. (b) View of flat-topped sandbars formed at the intersection between the two rivers, with an abandoned channel cutting through the sandbars. (c) View of subaqueous sand dunes that have formed on the dry Klein Letaba River. Flow direction is indicated with the red arrows.

Fig. 5.3: (a) Geomorphic features along site 1. The red dots also indicate the area where the transect was taken across the river, (b) the transect and sample numbers along site 1.

Fig. 5.4: IView of the Letaba River at the Shimuwini Dam, site 4a. The river is 10-12 m wide and tens of centimetres deep. Red arrow indicates flow direction.

Fig. 5.5: View of site 4b indicating vegetated sandbars present separating the channel into multiple channels. Red arrow indicates flow direction.

Fig. 5.6: (a) Geomorphic features along site 4. (b) The transect and sample numbers along site 4

Fig. 5.7: (a) View of the Letaba River and at the Phalaborwa Bridge, site 5. (b) View of an inactive channel between ridge-like sandbars. The inactive channel is characterised by a collection of dark coarse gravel. (c) The narrow Letaba River flowing under the Phalaborwa Bridge. (d) Cobbles of up to 10 cm in diameter present in inactive channels (pen for scale). Red arrows indicate flow direction.

Fig. 5.8: The transect and sample numbers at site 5.

Fig. 5.9: Views of site 6 (a,b,c) indicating elevated sandbars and abundant *Phragmites mauritianus* present as riparian vegetation. The red circle on (b) indicates the entrance of the Makoforo River tributary.

Fig. 5.10: (a) Views of the Letaba River meandering between vegetated sandbars, site 7, (b) sandstone bedrock pavement present near the rivers, (c) large bedrock outcrop with a 3m wide pothole (Person for scale). Arrow indicates flow direction.

Fig. 5.11: Geomorphic features at site 7.

Fig. 5.12: Image of the wide and dry Nwanedzi River which is a tributary of the Letaba River. The arrow indicates the flow direction.

Fig. 5.13: (a) View of the flat-topped sandbars on the floodplain and the position of the present day active channel. The red arrow indicates the flow direction, (b) view of the different layers of a flat topped sandbar. Pen indicates scale.

Fig. 5.14: The geomorphic features at site 9 and data collection sites are indicated in red.

Fig. 5.15: Image (a,b) of the Letaba River upstream of the Engelhardt dam. The river consists of a straight deep channel, with no outcrops. The red arrows indicate the flow direction.

Fig. 5.16: (a) The geomorphic features at site 10, (b) the transect and sample numbers at site 10. The red dots indicate where the transect was taken.

Fig. 5.17: Image of the river just downstream the Engelhardt Dam, characterised by bedrock outcrops and sandbars.

Fig. 5.18: (a) Site 12 characterised by bedrock outcrops, (b) a 20/20 cm square indicating the cobbles present in this reach.

Fig. 5.19: (a) Geomorphic features at site 12. The red dots indicate the area where the transect was taken, (b) the river profile and sample numbers at site 10.

Fig. 5.20: (a,b) View of site 13 showing the river reach characterised by multiple channels flowing between diorite outcrops. The red arrow indicates the flow direction.

Fig. 5.21: (a) Geomorphic features at site 13. The red dots indicate where the transect was taken, (b) the river profile and sample numbers along site 13.

Fig. 5.22: (a,b) View of low-water bridge at site 14, which acts as a barrier to trap sediment and only allows very little water to pass through, (c) bedrock outcrop covered in round potholes. Arrows indicate flow direction, the marker indicates scale.

Fig. 5.23: (a) Geomorphic feature at site 14. (b) The transect and sample numbers at site 14.

Fig. 5.24: (a) View of mixed bedrock and alluvium at site 15, (b) boulders up to 1.5 m deposited on the floodplain, (c) abrasion marks present on a boulder on the floodplain (blue arrow). Red arrows indicate flow direction.

Fig. 5.25: The transect and sample numbers at site 15.

Fig. 5.26: The mean grain sizes throughout the Letaba River, within the Kruger National Park.

Fig. 5.27: Scatter plot of kurtosis values of sediment within the Letaba River, in a downstream direction. The blue arrows indicate the locations of tributaries.

Fig. 5.28: Scatter plot of skewness values of sediment within the Letaba River, in a downstream direction. The blue arrows indicate the locations of tributaries.

Fig. 5.29: Sorting values for individual samples from upstream to downstream. The blue arrows indicate the tributaries.

Fig. 5.30: Grain size distributions at different channel reaches. The site numbers are arranged in the downstream direction.

Fig. 5.31: Heavy minerals present in the sediment. (a,b) Columnar zircon inclusion in quartz grain from site 10, in plain light and crossed polars. (c) Zircon inclusion in quartz grain at site 15. (d) Columnar zircon inclusion in quartz grain at site 14. (e) Zoisite and clinopyroxene from site 3. (f) Subhedral zoisite included in quartz grain at site 9 and muscovite grains in the groundmass and present as inclusions in quartz grains. (g) Tourmaline grain from site 10. (h) Rutile inclusion in quartz grain from site 5. (i) Large sub-rounded olivine grain form site 14. (j) Orthopyroxene and clinopyroxene grains from site 3. (k) Large orthopyroxene and clinopyroxene from site 1. (l) Subhedral epidote grain from site 7. (m) Subrounded olivine grain with plagioclase inclusions from site 15. (n) Subhedral olivine grain which is slightly altered from site 9. Qz=quartz, Zr=zircon, Zs=zoisite, Tr=tourmaline, Rt=rutile, Olv= olivine, cpx=clinopyroxene, opx=orthopyroxene, plg=plagioclase, Epi=epidote.

Figure 5.32: Images of magnetite (mg), ilmenite (il) and hematite (hm). (a) Anhedral hematite grain with inclusions of magnetite. (b) Hematite inclusions in olivine grain. (c) Angular inclusion of hematite in quartz grain with inclusions of ilmenite and magnetite. (d) Subrounded magnetite grain with inclusions of ilmenite. (e) Subrounded ilmenite grain with inclusions of magnetite and hematite. (f) Hematite with lamellae of magnetite (pinkish). (g) Ilmenite with lamellae of hematite. (h) Angular grain of magnetite. (i) Subrounded grain of magnetite with inclusions of hematite. (j) Subhedral inclusions of magnetite and hematite in quartz grain. (k) Ilmenite grain with magnetite (pinkish) and

hematite (white) lamellae. (i) Irregular magnetite inclusion in quartz grain. Mg=magnetite, hm=hematite, Qz=quartz, il=ilmenite.

Fig. 5.33: The abundance of minerals at different river reaches.

Fig. 5.34: Magnetic susceptibility values throughout the Letaba River.

Fig. 5.35: Scatter plot of the relationship between mean grain sizes and magnetic susceptibility.

Fig. 5.36: The trace elements which are present in the sediment and their abundances.

Fig. 5.37: The predicted percentage contributions tributaries, channel bank and channel bed from the different data collection sites.

Fig. 5.38: The overall relative predicted contributions from tributaries, channel bank and channel bed within the Letaba River.

Fig. 5.39: The percentages obtained from calculating the mean absolute errors of the mixing model.

Fig. 5.40: The percentage contributions from tributaries, channel banks and channel bed throughout the mapped section of the Letaba River.

Fig. 6.1. The concentrations of 5 trace elements at sample 4-1 and 4-2. Trace elements are seen to decrease towards the present day active channel.

List of tables

Table 4.1. The channel types found within the Sabie River which displays the same channel types as the Letaba River. Numbers indicate the occurrence of each unit (Van Niekerk *et al*., 1995, p. 74).

Table 4.2: Grain size parameters and the characteristic values (Blott and Pye, 2001).

Table 4.3: The optical properties of some heavy minerals which were identified, namely; zircon, magnetite and ilmenite. Adapted from Lynn *et al*. (2008).

Table 5. 1: Mean grain size values on different geomorphic features.

Table 5.2: The mean grain sizes, sorting, skewness and kurtosis values before and after a tributary.

Table 5.3: The underlying geology and grain size parameters of sediment collected along the Letaba River.

Table 5.4: Minerals of individual grains recorded at different river reaches (qtz=quartz, plag=plagioclase, ortho=orthoclase, cpx=clinopyroxene, olv=olivine, hbld=hornblend, bt=biotite, il=ilmenite, hm=hematite, opx=orthopyroxene, msc=muscovite, epd=epidote, zirc=zircon, rut=rutile, tour=tourmaline, grt=garnet). The columns highlighted in pink indicate tributaries.

Table 5.5: The number the number of magnetite, ilmenite and hematite grains counted in the sediments collected from the Letaba River.

Table 5.6: Magnetic susceptibility values, the number of magnetite, hematite and magnetite and the underlying geology.

Table 5.7: Relationships between the different components. The bold values indicate values showing significant relationships. Values statistically significant at P<0.5.

Table 5.8: The mean and standard deviation of source samples and sediment collected on different geomorphic features.

Table 5.9: Significance values of the trace elements after the Kruskal Wallis H-test was performed. The bold values indicate values that are statistically significant. Values are statistically significant at P<0.05.

Table 5.10: The significance values of trace elements after discriminant function analysis was performed. The bold values indicate values that are statistically significant. Values are not statistically significant at P<0.05.

Abbreviations

XRF - X-Ray Fluorescence

MS - magnetic susceptibility

KNP - Kruger National Park

Abstract

Sediment distributions vary across a river system depending on the hydraulic processes operating at different river reaches and affect flow regimes and influence the formation of landforms. The research was conducted in the Letaba River which is sourced in the Eastern Escarpment and flows through Kruger National Park (KNP), South Africa. It flows across bedrock types including granite and granitic gneiss, and volcanic and sedimentary rocks of the Karoo Supergroup. This underlying geology has played a role in the development of the river system, geomorphology and sediment patterns. This study aims to understand sediment sources and dynamics on the KNP section of the Letaba River as it flows through the KNP, focusing on the distribution of grain sizes, heavy minerals and minor trace elements in the different storage areas within the river system, and identifying the potential sediment source areas with the use of a multivariate sediment mixing model. Field data collection involved geomorphic mapping along river reaches within KNP, and geomorphic features such as sandbars, subaqueous dunes, levees, overbank deposits and bedrock outcrops were identified. Sediment samples were collected from the main river channel and four tributaries. Results of grain size analysis based on the Folk and Ward method indicate that the majority of the sediments present on geomorphic features are coarse grained, negatively skewed and mesokurtic to leptokurtic. The presence of overbank deposits and coarse grain sizes indicates that the river geomorphology is modified by the occurrence of floods. The distribution of heavy mineral assemblages highlights the role of hydraulic processes in the distribution of minerals derived from the underlying geology. X-ray fluorescence analysis of the sediment measured a total of 18 trace elements within the sediment. The trace elements that were identified are: Zr, Ba, Cr, Sr, V, Ni, Cu, Zn, Rb, Y, Co, Pb, Th, Ga, Sc, Nb, Mo, U, and are listed in order of abundance. Results from the multivariate sediment mixing model indicate that the highest relative contribution of sediment is derived from the channel bed (55%), followed by the channel bank (28%), and the tributaries contributing the lowest proportion (17%) of the sediment. The results of this study highlight spatial patterns of morphological features, the influence of floods in the development of the river system and the identification of relative percentage contributions from potential sediment sources. This can be used to determine the role of tributary floods in sediment erosion and transport along the main river channel. This research can also be used to inform catchment management plans aimed at reducing erosion and sediment influx into the Letaba River.

Keywords: sediment, grain sizes, geomorphic features, sediment sources, multivariate sediment mixing model, Letaba River.

Declaration

This study presents the original work by the author and has not plagiarized the work of others. Where use has been made of the work of other authors it is acknowledged in the text accordingly. This dissertation has not been submitted before for any degree or examination at any other University.

Signature: ……..

Tondani Mugwabana, Student number 418215

Date: 27 March 2018

Acknowledgements

I would like to acknowledge everyone who played a role in assisting me in completing this dissertation. I would first like to thank my supervisor Prof. Jasper Knight, for his guidance, patience and support. I would also like to thank the National Research foundation (NRF) for providing funding for this research. A special thanks is also given to Calvin Opiti who assisted me with the creation of algorithms in order to run the sediment mixing models.

Chapter 1: Introduction

1.1. Background

The sediment dynamics of a river system are important as landform development and river flow regimes are directly affected by these dynamics. Sediment in rivers maintain habitats, is a medium for transporting nutrients throughout the river, and sediment can protect a river from the effects of flooding (Arnold *et al.,* 1995). Sediment patterns also determine the geomorphic features present within a river system and this in turn determines the type and distribution of riparian vegetation and organisms (van Coller *et al*., 1997). However the presence of too much sediment can have a detrimental effect on river systems. These effects include the destruction of riverine habitats and ecosystems, alterations in the flow regime, reduction in water quality, and siltation in dams (Kingsford, 2000; Bunn *et al.,* 2002; Batalla *et al*., 2004; Terrio, 2006). The factors that influence the transport of sediment between storage areas within a river system include the surrounding vegetation, catchment area, slope, morphology, tectonics, underlying geology and climate (Heritage *et al*., 1997; Fryirs *et al*., 2007; Baartman *et al.,* 2013). Sediment movement is dependent on the flow of water and the connectivity of landforms within a river system (Fryis *et al.,* 2007). The climatic region of the river system plays a vital role as the climate determines the availability of water in the river throughout the year (Kale, 2003; Thompson *et al.,* 2013). Semi-arid regions are prone to long dry periods and short heavy rainfall events, and the magnitude and frequency of these heavy rainfall and associated flood events are a major determining factor for morphological development in semi-arid river systems (Heritage *et al*., 2015). This unique characteristic of semi-arid regions makes these regions vulnerable to the effects of climate change, which will ultimately affect the sediment patterns in these catchments (Heritage *et al.,* 2015). It is thus essential to understand these regions in more detail in order to better manage and reduce the effects of climate change. The sources of sediment within a river system can either be from the underlying geology, the adjacent floodplain, channel bed or channel bank erosion, or from tributaries during flood events (Russell *et al.,* 2001; Gruszowski *et al*., 2003; Evrard *et al.,* 2011; Cox *et al.,* 2015). Sediment influx into the Letaba River has increased over recent decades and has caused the channel to display more alluvial dominated channel types and modifications in the channel flow regime (Heritage *et al*., 1997).

Within the past 15 years, the Limpopo Province in South Africa, where the study area is located, has experienced flooding events in the years 2000 (Heritage *et al.,* 2001), 2004 and 2006 (Maponya *et al*., 2012), 2012 (Heritage *et al*., 2015) and 2013 (Spaliviero *et al*., 2014) and these flooding events played a role in the sediment movement within the Letaba River and surrounding rivers within the Kruger National Park (KNP). The geomorphology of the

Olifants and Sabie rivers, which are also within KNP, were also altered due to these flood events (Heritage *et al.,* 2015). The Sabie River experienced changes following the 2000 flood, when riparian vegetation was removed and large quantities of sediment were deposited into the channel. This resulted in a change in channel types from bedrock-influenced to more alluvial-dominated channels, due to increased sediment influx (Heritage *et al.,* 2004). After the 2012 extreme flood, both the Olifants and Sabie rivers experienced stripping of stored sediment and resulted in an increased exposure and erosion of bedrock-outcrops, and the channel shifted once more to being bedrock-influenced (Heritage *et al.*, 2015). The Olifants and Sabie rivers have been the focus of several sediment and geomorphic studies within KNP (Rountree *et al*., 2000; Heritage *et al.,* 2015; Eze *et al*., 2016; Gyamfi *et al.,* 2016) and little research exists within the Letaba River, thus there is an urgent need to fill this gap in order to fully understand the functioning of this river.

The Letaba catchment has also been modified by human activities through the construction of dams (Heritage *et al*., 2001). Recently, the Department of Water Affairs and Forestry has proposed to increase the capacity of Tzaneen Dam and the construction of a dam in the Groot Letaba River, which is upstream of the Letaba River (DWAR, 2010). The dams are being constructed to meet the increasing demand of water for domestic, industrial and irrigation purposes (DWAF, 2010). The construction of these dams will pose more stress on the already scarce water resource in this river as it will cause increased degradation of the catchment and increased alluviation, downstream effects such as siltation, and any flood events may intensify changes to existing sediment patterns (DWAF, 2010). It is also suggested that the construction of these dams will result in increased river bed erosion during floods and the outcome will be increased sediment production (DWAF, 2010). Dams have been reported to have destructive effects in other parts of the world, and these effects include changes in the river flow regimes (Batalla *et al*., 2004), changes in sediment delivery to downstream reaches (Walling *et al.,* 2003; Phillips, 2004) and changes in riverine biodiversity (Kingsford, 2000; Bunn *et al*., 2002).

Sediment patterns and the positioning of landforms within the river channel have an impact on riverine habitats and ecosystem services (van Coller *et al*., 1997; Meissner *et al.,* 2016). Understanding of sediment patterns is important because it will increase the ability to predict the effects of sediment changes on landform dynamics, biodiversity and ecosystem services, brought on by the construction of dams and increased flooding as a result of climate change. In order to implement effective catchment management plans, it is essential to understand the driving forces of sediment pattern dynamics (van Niekerk *et al*., 1995). Van Wilgen *et al*. (2016) stated that it is essential to have embedded and continuous research in South African National Parks to ensure that scientific research can inform and be incorporated into park management plans. In this way, management plans will consider and maintain the integrity and functions of river landforms and sediment patterns. Studies of river sediment dynamics have typically included observations and measurements of: river landforms and geomorphic mapping, surface and subsurface sediments, stratigraphy, grain

size parameters, grain shape, mineralogy, sediment movement during floods, floodplain sedimentation and sediment yield (e.g. Folk and Ward, 1975; Friedman, 1979; McLaren, 1979; McLaren *et al.,* 1985; Bui, 1989; Roman *et al*., 1999; Wachecka-Kotkoswska *et al.,* 2011). Sediment research on the Letaba River has been limited to calculating sediment yields and modelling stream flow (Katambara *et al*., 2010). However, this research did not attempt to identify the sources of sediment. Previous studies have used different techniques to identify sediment sources in rivers across the world. The direct methods include mapping, surveying, photogrammetry, suspended sediment flux monitoring and remote sensing (Walling *et al*., 2001), calculating erosion vulnerability indices and sediment fingerprinting (Collins *et al*., 2002). The use of sediment mixing models is a growing method for scientific research on sediment provenance and source areas, and has been used in rivers across the world to inform on catchment management plans (Russell *et al*., 2001; Gruszwoski *et al*., 2003; Haddadchi *et al*., 2013, 2014a, 2014b; Lin *et al.,* 2015; Tiecher *et al*., 2015). This method offers quick and reliable results (Kouhepeima *et al.,* 2011). However, only a few researchers have used sediment mixing models to identify sediment sources in South African rivers (Miller *et al*., 2013; van der Waal *et al*., 2015; Manjoro *et al*., 2017). Research to identify sediment sources within the Letaba River has never been conducted, and this research will fill the gap in knowledge lacking on the sediment patterns of this river.

In this study, the sediment patterns and landforms of the Letaba River will be studied, with particular emphasis on grain size, trace element concentrations and heavy mineral proportions. The arrangement of geomorphic features will be highlighted in order to understand sediment patterns and sediment dynamics. Emphasis will also be placed on the mixing of sediment from tributary sources and an attempt will be made to identify potential sediment source contributions to the sediment within the river using a sediment mixing model. Understanding how the influx of tributary sediment affects river properties is important in order to identify how tributary floods impact on the already high sediment yields within this river. The scientific knowledge produced in this research can be incorporated into management schemes of this river and surrounding rivers in this semi-arid region, and can also be used in monitoring programs to understand geomorphic changes in this river system.

1.2. Aim and Objectives

1.2.1. Aim

The aim of this research is:

To understand the sediment sources and dynamics of the Letaba River as it flows through the Kruger National Park, by investigating the distributions of grain sizes, heavy minerals and trace elements in different landforms within the river system.

1.2.2. Objectives

In view of the above aim, the objectives of this study are:

1. Map geomorphological features within the Letaba River, in order to produce geomorphic maps of different river reaches and identify sediment storage areas and the relationships between grain sizes and geomorphic features;
2. Determine patterns of heavy mineral assemblages, magnetic susceptibility and trace elements by collecting sediment samples on geomorphic features in order to identify sediment patterns;
3. Identify potential sediment source contributions using the modified Collins sediment mixing model in order to identify major sediment sources at the downstream river reaches and the processes responsible for sediment generation.

Chapter 2: Study area

2.1. Location of study area

The Letaba River is situated in the north-eastern part of South Africa (Fig. 2.1) and covers an area of approximately 13,400 km^2 (Moon *et al*., 2001) but drains an area of 3300 km^2 within KNP (Kotschy *et al.,* 2000). The Letaba catchment is located within the Luvuvhu/Letaba Water Management area in South Africa (State of the Rivers Report, 2001). The Letaba River has two major tributaries which are the Molotsi and Klein Letaba, and other minor tributaries include the Tsende and Shipikana, which are situated within KNP (Heritage *et al.,* 2001). The Middle Letaba and the Letsitele rivers also form part of the tributaries that flow into the Letaba and the river joins the Olifants River at the border with Mozambique (DWAF, 2006). The catchment is characterised by a mountainous region in the west and low lying area in the east (State of the Rivers Report, 2001). The main controlling factor of different climatic conditions is the variable topography of the region (State of the Rivers Report, 2001; Katambara *et al*., 2010).

The Letaba River is a bedrock influenced channel (Moon *et al*., 2001) and within KNP the river is underlain by granite and granite gneiss as well as volcanic and sedimentary rocks of the Karoo Supergroup which form part of the sediment source within the river (Heritage *et al*., 2001). The Letaba River within KNP is characterised by some very sandy river reaches with narrow bedrock channels flowing between the dense sand (DWA, 2006; Sinha, 2015). The water within the Letaba catchment (Fig. 2.2) is used mainly for irrigation, industry and domestic water uses (DWAF, 2006) and within KNP the river water creates habitats for fish, mammals, birds and reptiles (State of the Rivers Report, 2001). The available water of the Letaba River does not meet the full demand for irrigation, ecological, industrial and domestic uses due to water scarcity (Katambara *et al*., 2010; Sinha, 2015). Sinha (2015) suggested that the effects of climate change in the Letaba River include intensification of rainfall seasons, increasing temperatures, amplification of dry seasons and an increased frequency of extreme climatic events which will further alter the river system geomorphology.

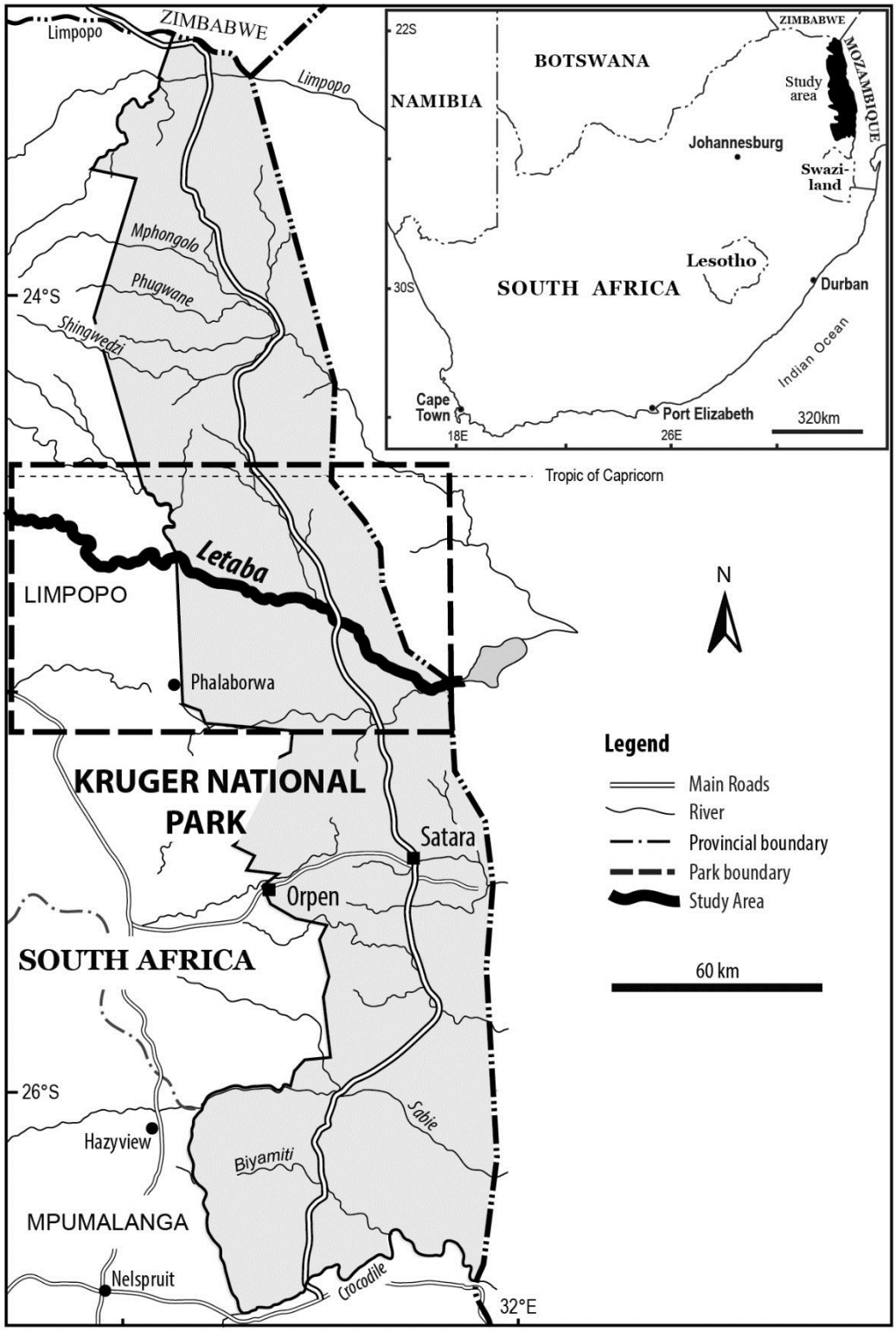


Fig. 2.1: Location of the Letaba River (boxed) within the Kruger National Park and South Africa. Produced by Wendy Phillips. Department of Geography, Archaeology and Environmental Studies. 17 September 2015.

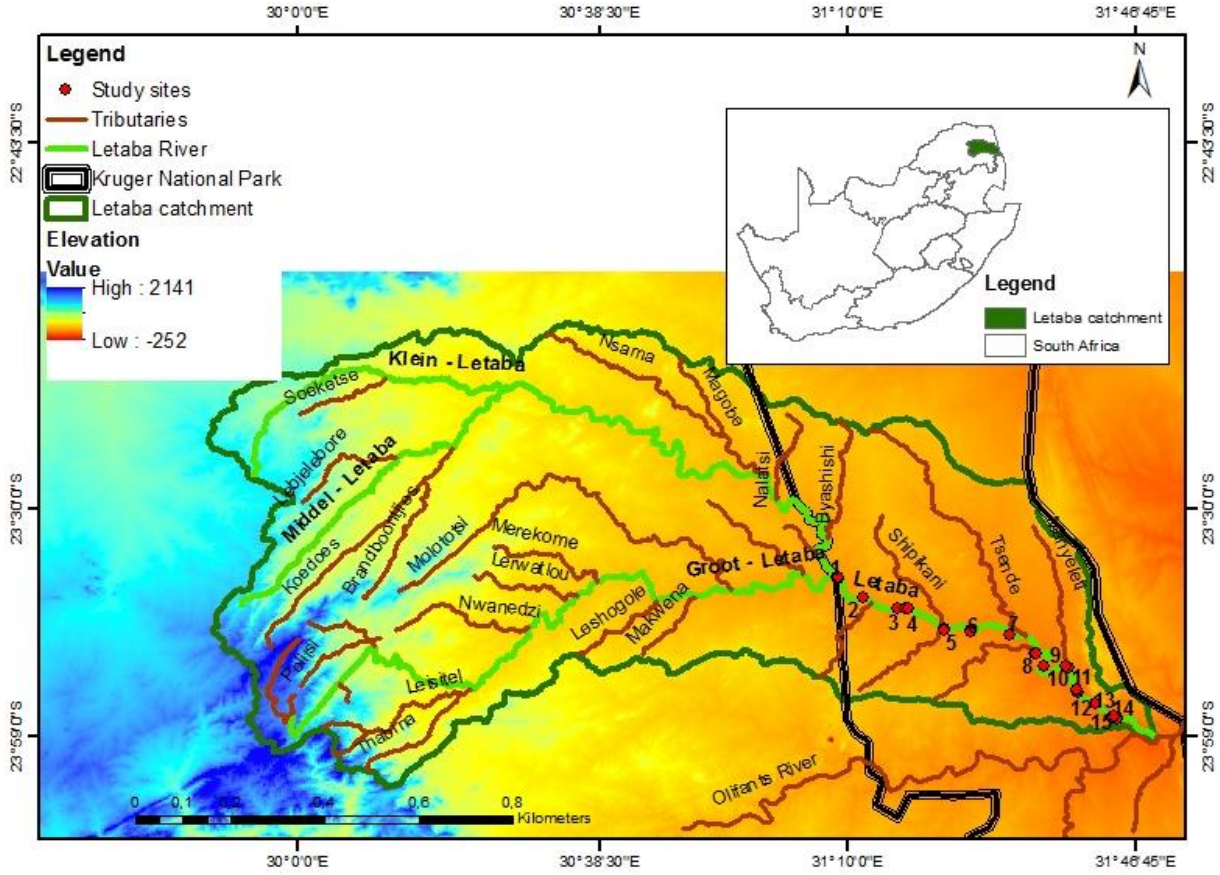


Fig. 2.2: Map of the Letaba Catchment and the location of the Letaba River within the Kruger National Park and location of the 15 data collection sites.

2.2 Geological history, soils and topography

The deposition of the Murchison Greenstone belt occurred between 3009 and 2097 million years ago (Ma) and consists of rocks which were deformed through the intrusion of the Archean granite suite which occurred between 3000 and 2700 Ma (McCarthy *et al.,* 2005). The Archaean granite suite was formed by intrusions of slow cooling basaltic magma which crystallized to form coarse-grained rocks (McCarthy *et al*., 2005) The Timbavati Gabbro was then deposited during the Precambrian (1100 Ma) above the Archean granite suite. Sedimentary rocks of the Karoo Supergroup were deposited between 310 and 182 Ma (McCarthy *et al*., 2005; Viljoen, 2015). The Dwyka Group of the Karoo Supergroup was initially deposited due to melting of glacial ice, followed by deposition of the Ecca Group, Beaufort Group and finally the Stormberg Group, as the climate in South Africa became more arid (McCarthy *et al*., 2005). Deposition of sediments of the Karoo Supergroup terminated during the Permian (182 Ma) when basaltic lavas of the Drakensberg Group flowed and covered the sedimentary rocks, and dolerite dykes and sills intruded the sedimentary rocks (McCarthy *et al*., 2005). This period of basalt deposition was followed by the deposition of rhyolites and granophyres that make up the Lebombo Mountains, which

was initiated by rifting as the continent of Gondwana split (McCarthy *et al*., 2005; Viljoen, 2015). The area surrounding KNP experienced periods of uplift, planation and fluvial incision which ultimately developed the present day topography and landforms of KNP (Viljoen, 2015). Erosion took place in particular in the Neogene (20 Ma), followed by tectonic uplift around 5 Ma (McCarthy *et al.,* 2005). During the period of erosion, the rocks of the Eastern Escarpment and the Lebombo Mountains were eroded and resulted in the development of the Lowveld province through which the Letaba River flows within KNP (McCarthy *et al*., 2005; Viljoen, 2015).

Within KNP, the Letaba River is underlain by granite and granitic gneiss as well as volcanic rocks of the Karoo Supergroup which form part of the sediment source within the river (Heritage *et al*., 2001) (Fig. 2.3). The Letaba River flows over Karoo volcanic rocks of the Lebombo monocline which consists of the Letaba Basalt Formation, Sabie River Basalt Formation, Jozini Rhyolite Formation and Karoo sediments (Erlank, 1984). The basalt of the Letaba Basalt Formation is made of olivine and pyroxene and contains oxides and trace elements of potassium, titanium, rubidium and barium (Erlank, 1984). The olivine present in the basalt of the Letaba Basalt Formation is very rich in magnesium and is referred to as picrate, due to its high magnesium content and is present as large phenocrysts of olivine (Bristow *et al.,* 1989). The basalt rocks of the Sabie River Basalt formation contain very little olivine and are thus low in magnesium (Bristow *et al.,* 1989). The Jozini Rhyolite Formation consists of plagioclase, clinopyroxene, magnetite, quartz, zircon, olivine and ilmenite (Erlank, 1984). The Karoo sediments consist of reworked volcaniclastics, sandstones, siltstones and shales (Erlank, 1984). The volcanics, shales and sandstones of the Karoo Supergroup dip at shallow angles to the east (Viljoen, 2015) and are underlain by basaltic rocks and Timbavati Gabbros (Bristow *et al*., 1989). Several dykes of basalt, dolerite and granophyre intrusions are prevalent along the river and cut through the Karoo sequence (Bristow *et al*., 1989).

The dolerite weathers into clayey soils and sedimentary rocks weather into soils with a sandy texture, the granites weather into gravely soils and the basalts into sandy clays (Venter, 1986). In terms of topography, the Letaba catchment in KNP is divided into three regions with variable altitudes. The confluence between the Klein Letaba and Groot Letaba River is characterised by plains and open hills, with an altitude between 200 and 475 m. This area is characterised by clayey soils (State of the Rivers Report, 2001). The area farther downstream towards the confluence with the Olifants River is characterised by low relief, an altitude of 175 to 425 m and shallow black, brown or red clayey soils (State of the Rivers Report, 2001). The landscape at the confluence with the Olifants River contains hills and an undulating rocky terrain with gorges and ravines along the river and an altitude between 150 and 500 m. This area is characterised by shallow stony soils produced by the weathering of rhyolite and granophyre (State of the Rivers Report, 2001).

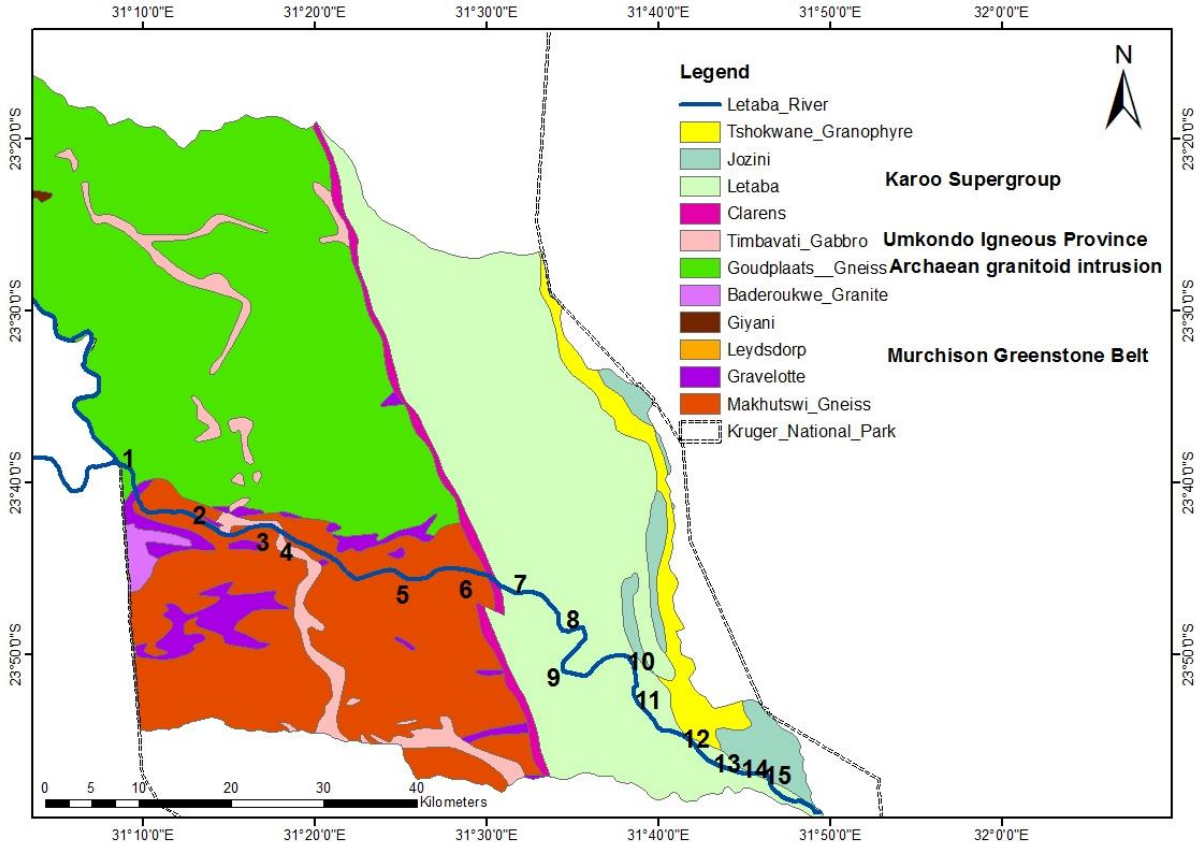


Fig. 2.3: Map of the underlying geology of the Letaba River within Kruger National Park, based on McCarthy *et al.* (2005).

There is a distinct relationship between the underlying geology, the geomorphology of the river and the landscapes that have formed there (Gertenbach, 1983; Viljoen, 2015). In this area, pediments were developed during the Neogene erosion phase (Viljoen, 2015). Weathering of granites has resulted in 'onion skin' morphology (Viljoen, 2015). The erosion of Timbavati gabbro has resulted in the formation of blocky ridges (Viljoen, 2015). Distinctive drainage patterns have developed as a result of the underlying geology (Viljoen, 2015). River incision in areas with abundant granitic rocks is characterised by a dendritic drainage pattern, and areas where rhyolite is dominant are characterised by trellis drainage pattern (Viljoen, 2015). The erosion of rhyolite ridges has given rise to gorges, potholes and linear channel reaches (Viljoen, 2015). Steep outcrops or koppies of granites called the Shamiriri and Shithabure are present at the Olifants and Letaba river confluence (Gertenbach, 1983). Karoo sediments represent a low lying landscape characterised by shallow slopes (Gertenbach, 1983).

The geology of the tributaries of the Letaba River that flow within KNP is similar to that of the Letaba River. The Ngwenyeni River tributary flows over granite, gneiss and syenite intrusions (Gertenbach, 1983). The Tsende River is underlain by granite, amphibole and

dolerite intrusions (Gertenbach, 1983). These form part of the sediment sources that flow into the Letaba River.

2.3 Rainfall

The Letaba catchment is characterised by high climatic variability. The Eastern Escarpment headwater area is climatically different to the middle and lower reaches of the river. The Eastern Escarpment in the western part of the Groot Letaba River has an altitude higher than 2000 m and receives annual rainfall of 650-1325 mm, which is more than is received in lower reaches located within KNP (State of the Rivers Report, 2001). The Letaba catchment within KNP is semi-arid and receives an average of 450 mm of rainfall per year (Moon *et al*., 2001). The confluence between the Klein Letaba and Groot Letaba River is at the eastern KNP boundary, which is a low lying area, and high sediment loads carried by the Klein Letaba River are deposited at the confluence due to a decrease in gradient and because of the mixing of waters from the two rivers. The low lying area receives highly variable annual rainfall of between 325 and 975 mm per year (State of the Rivers Report, 2001). The area of the Letaba River's confluence with the Olifants River near the Lebombo Uplands has rainfall of 400-950 mm per year. Rainfall usually occurs in the summer months between October and March (DWAF, 2012). Rainfall events have played a major role in influencing the geomorphology of the river. Following the extreme floods that occurred in 2012, large quantities of sediment were eroded and deposited into the rivers within KNP. The Olifants and Sabie rivers experienced high sediment deposition and this shifted the rivers from bedrock-influenced channels to displaying more alluvial-dominated channel types (Heritage *et al.,* 2015).

2.4 River Discharge

The average monthly discharge volumes for the Letaba River at the Letaba Ranch were analysed for the years 2006 to 2015 at different gauging stations (Fig. 2.4). The Letaba catchment experiences highly variable climate characterised by long dry periods and short periods of rainfall, and has experienced flooding in some years followed by years of droughts (Maponya *et al*., 2012). The years where there were high rainfall values are characterised by high water volumes, and the years with low rainfall are characterised by lower volumes of water within the river, and this ultimately affects river sediment patterns and geomorphology (Heritage *et al*., 2015). The rainfall data indicate that extremely high flow volumes were experienced in the years 2006, 2011, 2013 and 2014 (Fig. 2.5). The highest peak discharges volumes were experienced in the Engelhardt Dam (station B8H018) in the year 2013, with discharges reaching 563 $m^3 s^{-1}$. Downstream reaches (B8H034 and B8H018) experienced higher discharge volumes (Fig. 2.5). The higher water volumes may be influenced by increased inputs of water from tributaries and the spatial variability of storm events within the catchment.

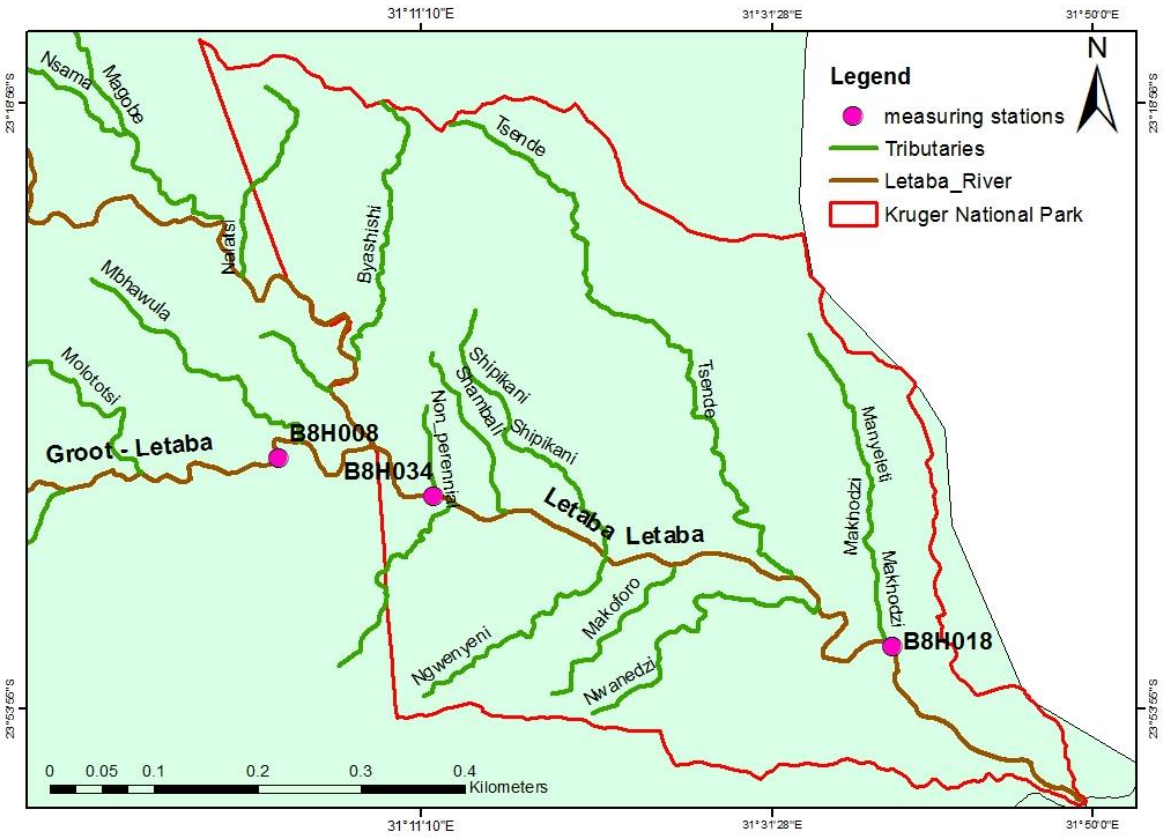


Fig. 2.4: The discharge measuring stations (pink dots), where data was collected, within the Letaba catchment. B8H008: Letaba Ranch, B8H034: Black Heron Dam, B8H018: Engelhardt Dam.

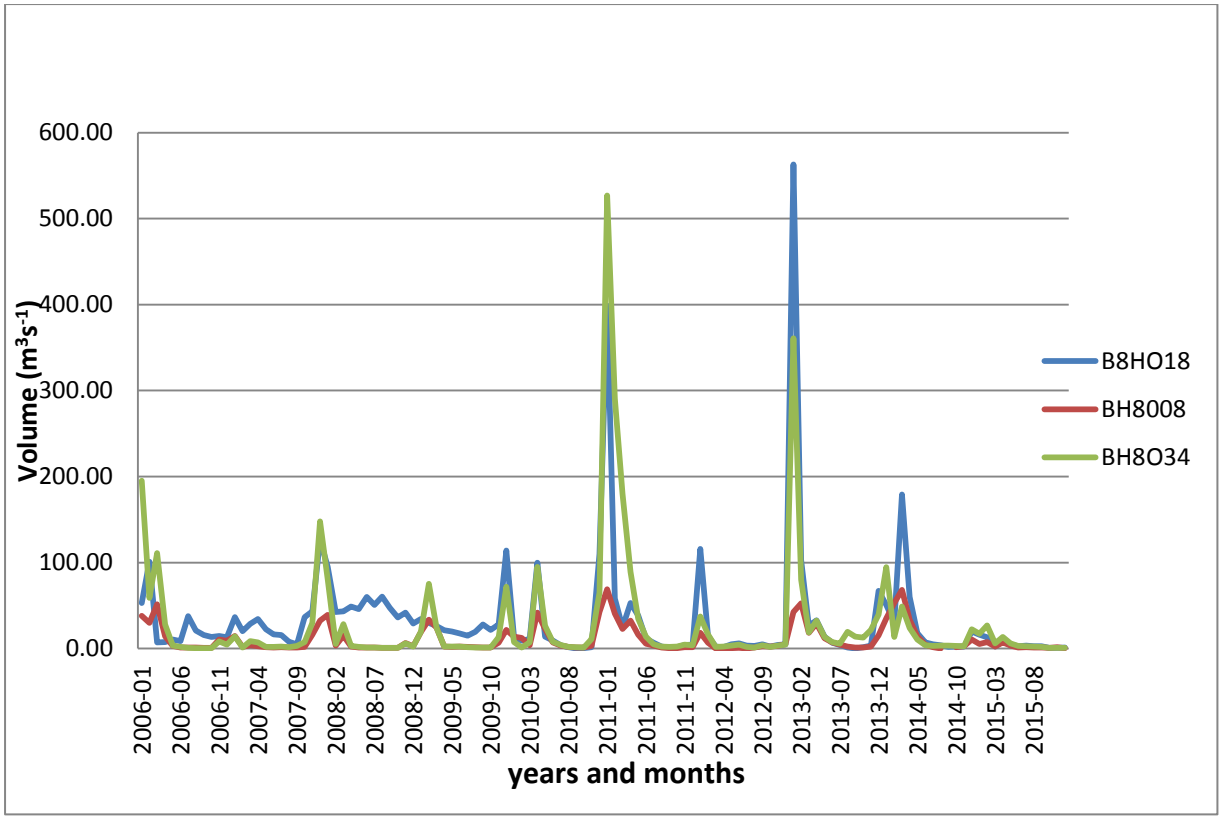


Fig. 2.6: Discharge volumes for 3 measuring stations between 2006 and 2015 in the measuring stations within the Great Letaba River. Station names: B8H008 (Great Letaba at Letaba Ranch), B8H034 (Great Letaba at Black Heron Dam), B8H018 (Great Letaba at Engelhardt Dam).

Chapter 3: Literature Review

Semi-arid rivers consist of combinations of bedrock and loose sediments within the channel and on the surrounding floodplain. Hence, bedrock-influenced channels consist of very little alluvium and abundant outcrops (Montgomery *et al*., 1996; Tinkler *et al*., 1998; Rountree *et al*., 2000; Whipple, 2004; Turowski *et al*., 2008). The morphology of these types of channel systems is dependent on underlying geology, channel geometry, sediment supply and climatic conditions of the catchment (Knighton, 1998; Kale, 2004; Thompson *et al.,* 2015; Surian *et al*., 2016). Bedrock incision has a primary role in the development of these channel systems (Hancock *et al.,* 1998). Floods are also an essential tool for transporting sediment, and sediment provenance and grain size distribution studies are essential to understand sediment patterns and mineral assemblages. The topics discussed in this chapter include characteristics of semi-arid catchments, characteristics of bedrock-influenced channels, mechanisms of bedrock erosion, floods as modifiers of the landscape, sediment provenance, and the description of grain size properties within bedrock-influenced channels.

3.1 Characteristics of semi-arid catchments

Semi-arid regions are prone to long dry periods and short heavy rainfall events, and the resulting flood events have important impacts on the morphology and dynamics of river systems (Heritage *et al*., 2015). Semi-arid regions also experience very high evaporation rates which add to the aridity of the region (Bull *et al*., 2002). It is the high variability in climate which distinguishes them from other river environments (Bull *et al*., 2002). Long term river changes are influenced by intense flood events (Heritage *et al*., 2015). These events erode the bedrock and increase sediment input, thus altering river behaviour, and the catchment may become dominated by alluvial-influenced channels (Heritage *et al*., 2015). Alternatively, extreme floods can strip away the alluvium which has accumulated during the dry season and thus results in the bedrock being exposed, and switching to bedrock-influenced channels (Heritage *et al*., 2015). This switching behaviour has been noted in several studies (e.g. Sklar *et al.,* 2001; Dean *et al.,* 2013; Thompson *et al.,* 2013; Omengo *et al.,* 2016), indicating the influence of floods on the geomorphology and sediment patterns of rivers. Low river flows have also been noted to bring about changes in sediment patterns (Schumm and Lichty, 1963; Burkham, 1972; Wolman, 1978). The influence of low flows has not been focused on in recent studies, however, but it is essential to consider both high and low flow events in order to understand sediment patterns and the processes influencing these patterns in semi-arid regions.

Fryirs *et al.* (2007) discussed the notion that energy within a channel influences the amount of sediment that moves between different landforms. Dean *et al.* (2013) took this notion forward by stating that one of the controls on geomorphic responses to a flood is a decrease in steam power due to high sediment flux, and this ultimately affects the amount of

sediment deposited within the channel. After a study conducted in the Rio Grande River, USA, Dean *et al*. (2013) indicated that geomorphic changes that occur after extreme floods include increased channel width, floodplain scour, meander migration, vegetation stripping and bar formation. A particular example locally is the Sabie River, which is similar to the Letaba River in that it has a bedrock-influenced channel, and is situated in a semi-arid region (Heritage *et al.,* 2015). The morphologies found on the Sabie River are influenced by variable flow regimes, irregular sediment influxes and variable riparian vegetation assemblages (Heritage *et al*., 2015). These factors concur with those that Dean *et al.* (2013) put forward as the main determinants of channel response to flood events.

3.2. Characteristics of bedrock-influenced channels

Bedrock-influenced channels are characterised by bedrock outcrops which influence flow characteristics of the river system, and with minimal alluvial cover over long time intervals (Montgomery *et al*., 1996; Tinkler *et al*., 1998; Rountree *et al*., 2000; Whipple, 2004; Turowski *et al*., 2008). In bedrock channels, sediment transport capacity is higher than that of the sediment flowing into the channel (Montgomery *et al*., 1996; Whipple, 2004). Tinkler and Wohl (1998) defined bedrock channels as channels where more than 50% represents exposed bedrock and the bedrock influences flow patterns and sediment pathways. Turowski *et al*. (2007) refined this definition by stating that in order for a bedrock channel to widen or shift its bed, erosion of the bedrock boundary has to take place, and this property distinguishes it from other channel types as bedrock influences the flow rate and rates of bedrock erosion. The amount of alluvium within a river channel at a given time is also important as sediment acts as an erosive tool as it strikes bedrock during channel flow and cuts down into the riverbed if it is concentrated in areas where the bed shear stress is highest (Tinkler *et al*., 2005). Channel reaches with low stream power and low shear stress are characterised by widespread alluvial cover (Whitbread *et al.,* 2015). Bedrock channels in semi-arid regions usually contain narrow valleys with high relief, and are characterised by flashy flows and high peak discharges that bring about a high degree of change in fluvial landscapes (Knighton, 1998; Kale, 2003; Hooke, 2016).

The morphology of bedrock-influenced channels has been proposed to be influenced by a number of factors and it important to understand what these factors are in order to understand channel control variables. Pazzaglia *et al*. (1998) proposed that bedrock channel reaches are influenced by rock type, for example resistant sandstone beds are characterised by narrow valley bottoms and gorges. In the Scottish Highlands, Whitbread *et al.* (2015) confirmed that bedrock influenced channels are narrower and deeper than alluvial channels. A different conclusion was drawn by Wohl (2015) and Whitbread *et al.* (2015) who suggested that channel slope and gradient were more important, as these determine the position of bedrock and alluvial reaches. However, channel slope and gradient would be most important in areas with steep slopes which influence discharge rates. It is clear, therefore, that there are several underlying factors which influence the morphology of

bedrock-influenced river systems and that the controlling variables depend on the different characteristics within each river channel and reach.

3.3 Mechanisms of bedrock erosion

The erosion of bedrock has been suggested as a source of sediment within bedrock-influenced river systems (Whitbread *et al.,* 2015; Surian *et al.,* 2016). Bedrock in these channel types can be eroded through abrasion, quarrying, cavitation and plucking (Hancock *et al.,* 1998; Whipple *et al*., 2000; Sklar *et al*., 2001; Richardson *et al*., 2005). Seidl *et al*. (1992) suggested that vertical wearing, scour and knickpoint propagation are responsible for erosion of bedrock channels and resulting increases in channel depth. Lateral erosion of bedrock is responsible for bedrock channel widening and the resultant increase in sediment supply (Whitbread *et al*., 2015; Surian *et al.,* 2016).

Sediment entrained in river flow collides with the bedrock surface and the impact can cause grains and rock fragments from the bedrock to be detached in the process of abrasion (Hancock *et al.,* 1998). Tinkler *et al*. (2005) indicated that high sediment cover in transit can erode the channel walls, but Sklar *et al*. (2001) stated that low supply rates of coarse sediment acts as a tool that abrades bedrock whereas too much alluvial sediment insulates the bedrock from erosion. Thus alluvial sediments have been shown to act as a tool of erosion, but once a threshold has been exceeded, the sediments act to protect the bedrock. However, Hancock *et al.* (1998) stated that the amount of sediment in a river system cannot be used to predict the amount of erosion that will take place in a given time, but rather the concentration of a specific grain size is an important factor.

Wohl and Merritt (2001) studied bedrock channel reaches and confirmed that the major factors controlling bedrock channel morphology are hydraulic driving forces and the characteristics of the bedrock and its resistance, but this study was focused on only large scale morphological features. Richardson *et al.* (2005) studied small scale morphological features such as flutes and potholes, and found that these mechanisms also apply at these scales. Schanz *et al.* (2016) identified strath terrace development and meandering in channels underlain by sedimentary rocks in the Willapa and Nehalem River basins, USA. Detached blocks of bedrock were also present in channels of less resistant bedrock in the West Fork Teanaway River, USA, indicating the importance of rock resistance in river morphology development (Collins *et al.,* 2016). However, anthropogenic removal of vegetation was also suggested to have increased sediment supply and the rate of bedrock incision.

The strength of the bedrock has an influence on channel width, channel slope, sinuosity, shear stress and rate of bedrock erosion (Hancock *et al.,* 2011; Allen *et al.,* 2013; Spotila *et al.,* 2015; Schanz *et al.,* 2016). Channel width plays a fundamental role in bedrock erosion as narrow channels exert energy on the channel bed, but as the channel width increases

erosion becomes more pronounced at the channel margins (Yanites *et al*., 2010b; Allen *et al.,* 2013). In order to fully understand the effect of lithology on bedrock channel morphology, Allen *et al.* (2013) studied the Siwaliks River in northwest Himalayas. The empirical data collected indicated that channels with resistant bedrock display narrow and steep channel forms, whereas channels underlain by less resistant bedrock were shallow and wide. Similar results were found by Whittaker *et al.* (2007) in the central Italian Apennines. However the bedrock-influenced New River in North America displayed wider bedrock reaches when compared to alluvial reaches (Spotila *et al.,* 2015). This contrast was attributed to erosion at discontinuities by plucking which resulted in lateral erosion and widening of the channel. This indicates that the strength of bedrock is not the only factor that determines the behaviour of bedrock channels. Variations in channel form downstream together with variable steepness have been attributed to differences in substrate strength (Allen *et al.,* 2013). River reaches characterised by resistant bedrock will display high sinuosity due to an increase in lateral erosion following high magnitude floods (Allen *et al.,* 2013). However Yanites *et al.* (2010b) noted variations in morphological response of river reaches with similar bedrocks in central Taiwan, and attributed the bedrock incision and morphology of the river to differences in uplift rates.

Underlying geology has been suggested to control erosion rates and channel morphology (Wohl *et al.,* 1998; Turowski *et al.,* 2007; Allen *et al*., 2013; Collins *et al*., 2016), while Yanites *et al.* (2010b) proposed channel width as the most important factor and Amos *et al.* (2007), Yanites *et al.* (2010) and Whittaker *et al.* (2007) attributed erosion to tectonic uplift rate. Friable rocks are eroded more rapidly by abrasion and resistant rocks are eroded by plucking and crushing, which requires greater unit stream power (Collins *et al.,* 2016). Resistant bedrock experiences vertical erosion due to narrow channel formation, and less resistant bedrock experiences lateral erosion which causes the channel to widen rapidly (Schanz *et al*., 2016; Collins *et al.,* 2016). However, narrow channels also experience lateral erosion at channel boundaries where sufficient sediment supply is able to act as abrading tools (Yanites *et al.,* 2010b; Allen *et al.,* 2013).

3.4 Floods as modifiers of river systems

Considering that the occurrence of floods has been proposed to be the mechanism responsible for the development of semi-arid river systems (Wolman *et al.,* 1978; Kale, 2003; Kale *et al.,* 2004,) this section will discuss morphological changes within river systems caused by floods and the factors that influence these changes. Floods have different meanings to different authors but magnitude of river discharge and velocity produced by the flood are conventionally accepted as determining factors of a flood (Wolman *et al.,* 1960; Rajaguru, 1995; Gupta, 2000; Kale *et al.,* 2004; Dean *et al.,* 2013; Hooke, 2016). Understanding what defines a flood is essential to understanding its geomorphological effects (Baker, 1994). Floods cause modifications of a river system and a measure of these modifications is known as geomorphic effectiveness (Wolman *et al.,* 1960; Kale *et al.,* 2004;

Dean *et al*., 2013). Geomorphic effectiveness is the ability of a flood event to alter the form of the landscape (Wolman *et al.,* 1960). The competency of a large flood to modify the geomorphology of a river can also be used to measure the geomorphic effectiveness of a flood (Wolman *et al.,* 1978). Furthermore, a certain threshold needs to be crossed for geomorphic modifications to take place (Yanites *et al.,* 2010b; Allen *et al.,* 2013). However, these thresholds differ across river systems and are not well known for semi-arid catchments. Magilligan (1992) argued that in humid, alluvial channels, the minimum unit stream power needed to produce major geomorphic change is 300 W m^{-2}. Rare large flood events in the Katherine Gorge in Australia which are experienced every 100 years produced discharges of 6000 $m^3 s^{-1}$ and have transported boulders up to 3 m within the river (Baker *et al.,* 1987). However, in the Herbert Gorge, Australia, the flow conditions that are required to transport boulders between 1-3 m diameter is a discharge of 1500 $m^3 s^{-1}$ at rapids, which exhibits maximum shear stress and stream power (Wohl, 1992).

The geomorphic effectiveness of a climatic event differs with the spatial distribution of the event, the size of the drainage basin, the morphological features present, and the timing and location of erosion within the river (Wolman *et al.,* 1978; Lewin, 1989; Cenderelli *et al*., 2003). The duration of the flood is just as important (Knighton, 1998). Huckleberry (1994) reported on two floods of high magnitude that occurred in 1983 and 1993 in the Gila River, Arizona, USA. The 1983 flood produced a large peak discharge but had minimal effects on river geomorphology when compared to the 1993 flood (Huckleberry, 1994). The reason why the 1993 flood was more effective in modifying the river system was because it lasted longer and produced a greater volume of water, with discharges higher than 230 $m^3 s^{-1}$ for 17 days (Huckleberry, 1994). The Nogalte River in southeast Spain experienced discharges of < 2500 $m^3 s^{-1}$ during the 2012 flood, but resulting morphological changes were not as great as expected, possibly due to the short duration of the flood or that the channel might be adapted to high magnitude flood events (Hooke, 2016). However, Magillian *et al.* (2015) reported different results of high geomorphic effectiveness caused by a short duration flood in 2011 on the Saxtons River, southeast Vermont, USA. Geomorphic effectiveness also varies spatially within a river system because different features and lithologies have different thresholds of erosion (Wolman *et al.,* 1978). A good measure of the effectiveness of a flood is the boulder shear stress or the ability of a flood to transport large boulders (Kale, 2003). However, Wolman *et al.* (1960) and Kale *et al.* (2004) stated that the amount of suspended sediment carried during a flood of high magnitude is also a measure of effectiveness. The differences in the conclusions drawn by these studies might be related to the location of the study sites, where rivers in high relief areas would generate high flows capable of carrying large boulders, whereas flat areas would most likely transport suspended sediment (Kale, 2003).

The time interval between high magnitude floods has been used as a parameter to measure the effectiveness of a flood (Wolman *et al.,* 1978). Kale *et al.* (2004) indicated that when floods occur consecutively with a low recurrence interval (about 5 years), the geomorphic

effectiveness might be minimal, but if the recurrence interval is high the flood may appear to have greater geomorphic effectiveness.

3.5 Flood modifications in rivers across the world

Floods can adjust river morphologies at different reaches across a river system (Wohl, 2014). High flood magnitudes cause large modifications in fluvial systems because large volumes of water are flushed into the channel, which results in erosion at some river reaches and deposition at others (Wohl, 2014). Spatial variability in geomorphic modifications in a river system can be expected, as the flood magnitude is considered to be low in large catchments (Lewin, 1989) and where the stream power increases downstream (Knighton, 1998). Spatial variations in the characteristics of a flood, sediment supply and erodibility of channel boundaries all influence different modifications in river morphology (Cenderelli *et al*., 2003). Magnitude and frequency of a flood event determines the effectiveness of the flood in modifying channel morphology (Wolman *et al.,* 1978; Gupta, 2000; Kale *et al.,* 2004).

The magnitude and frequency of floods vary depending on the region (topics or subtropics) and the meteorological systems supplying the moisture (Huckleberry, 1994). However, Huckleberry (1994) did not consider the influence of geology on floor discharge, velocity or rates of erosion. Geology has been suggested as the main controlling factor of geomorphic changes that occur during and following a flood (Lewin, 1989; Kale, 1990, 1998; Baker *et al.*. 1998; Cenderelli *et al*., 2003; Surian *et al*., 2016; Hooke, 2016). Hooke (2016), however, discussed the interplay between geology and the magnitude of a flood event, based on differences between the Nogalte and Torrealvilla rivers (Spain) after a major flood in 2012. The flood effects were more severe in the Nogalte River which experienced large magnitude flows while the Torrealvilla River had a moderate flow and less severe modifications (Hooke, 2016). The geomorphic modifications in the Nogalte River were more severe because the river flows over schist which produces easily erodible loose gravel, and the intensity of rainfall was higher, as opposed to the Torrealvilla River which flows over more resistant marl (Hooke, 2016). The geomorphic changes in the Nogalte River were more closely related to peak discharge and stream power, and the modifications in the Torrealvilla River were more closely related to velocity, shear stress and unit power (Hooke, 2016). The high erosion rates in bedrock-influenced reaches of the Lockyer Valley, southeast Australia, were attributed to high stream power values characteristic of knickpoint development in confined reaches (Thompson *et al.,* 2013). Similar conclusions were drawn by Surain *et al.* (2016) who attributed channel widening to flood power and valley confinement. The limiting factor in these studies is that the underlying geology and magnitude of the flood were the only factors considered, and other influences such as anthropogenic influences prior to the floods were not included. Kochel *et al.* (2016) indicated that extreme geomorphic modifications of the Susquehanna River tributaries, USA, were related to deforestation and channel modification which made the river more vulnerable to the effects of high magnitude floods.

Overbank deposits form by the deposition of coarse grained sediment on the floodplain. Overbank deposition occurs during flood events when the river channel gets overfilled and water and sediment spills on to the floodplain (Owens *et al*. 1999, Bridge *et al*. 2003). In overbank deposits, the coarser sediment is deposited adjacent to the active channel whereas the finest sediment is deposited distally (Bridge *et al*., 1979; Marriot, 1992; Muller *et al*., 1999; Owens *et al*., 1999; Bridge *et al*., 2003). Owens *et al.* (1999) used sediment cores to measure the rate of overbank sedimentation on the Tweed River, Scotland, and identified that more sediment was stored on the floodplain when compared to the channel bed. However, this was based on suspended sediment which can be carried during both high and low flows and might not always represent sediment deposited by a flood. Marriot (1992) examined sediment grain size distributions following a flood on the Severn River, UK, and identified that sand was deposited 20 m from the present channel and finer sediment on the edge of the floodplain. However, on other river systems, overbank deposits do not display this trend. Following a 2013 flood on the Abu River, Japan, Yamada *et al.* (2016) used field surveys and aerial photographs to examine flood deposits. They identified that coarse and fine sediment was deposited simultaneously adjacent to the active channel, and there was no distinctive pattern of deposition with distance from the channel. Omengo *et al.* (2016) used sediment cores and fallout radionuclide concentrations to identify overbank sedimentation rates in the Tana River, Kenya. The results indicate that overbank deposits were fine grained but that sedimentation rates decreased with distance from the main channel depending on floodplain topography and the presence of vegetation. Thus, modifications caused by floods vary between river systems. The differences in the sediment patterns characteristic of overbank deposits in the studies mentioned above, indicate that more research is needed to understand these deposits in order to generate a universal definition characteristic of overbank deposits.

3.6 Grain sizes and distributions

The movement of sediment between landscape elements such as hillslopes, floodplains and channels influences the geomorphological units that develop within river catchments (Baartman *et al*., 2013). Sediment patterns vary in different channel reaches mainly because sediment movement differs according to catchment characteristics such as surrounding vegetation, morphology, slope, catchment area, tectonics and anthropogenic effects (Fryirs *et al.,* 2007). Other variables include geometry of the river channel (Jung *et al.,* 2013), the magnitude and frequency of heavy rainfall events (Huang, 2011) and sediment availability (Favaro *et al*., 2015). River reaches with an increasing depth and smaller width are characterised by high river discharge and are able to carry more sediment (Jung *et al.,* 2013; Favaro *et al*., 2015). The type of flow influences the type and amount of sediment that is transported in the river channel (Hudson, 1997; Chanson, 1999). The mechanisms responsible for bedload transport are rolling, sliding and saltation (Chanson, 1999) from the surrounding catchment (Mentling *et al.,* 2015). The composition and grain sizes of sediment

depend on sediment compositions from the total watershed and local hillslopes as well as the channel bed (Mentling *et al.,* 2015).

Sediment grain size distribution has been widely used to infer sediment provenance, transport and depositional history (Folk and Ward, 1957; Friedman, 1979; McLaren, 1979; Bui *et al.,* 1989). McLaren (1979) noted that properties of grain size distributions depend on the characteristics of the source material and sedimentary processes of erosion, selective deposition and final deposition of sediment. As sediment grains move down a river system, grain size is modified through abrasion as the grains collide with the bedrock and other grains present in the flow (Hancock *et al.,* 1998; Attal *et al.,* 2009). Attal *et al.* (2009) noted that lithology, attrition or wear, mass loss and fragmentation that control pebble abrasion during fluvial transport. Resistant lithologies have lower abrasion rates than softer lithologies (Mueller *et al.,* 2016). In order to determine sediment source, grain size parameters such as average and modal grain size, sorting, skewness and kurtosis have been used (Roman *et al.,* 1999; Wachecka-Kotkowska *et al.,* 2011). McLaren *et al.* (1985) suggested that the transport capacity of grains is dependent on grain size and that finer grains are more likely to be transported, resulting in a negatively skewed distribution. However, Rubey (1933) suggested that sediment settling and transport is dependent on sediment density. When energy is high, sediment becomes coarser, better sorted and positively skewed, but under lower energy conditions, sediment becomes finer and more negatively skewed (McLaren *et al.,* 1985).

Grain sizes are also influenced by flow velocity (Friedman, 1967). Discharge rates determine the total amount of sediment transported (Jung *et al.,* 2013). Fluctuations in discharge have been related to temporal variations in grain size distributions (Walling *et al.,* 1987). A decrease in the discharge of the Huange River, China, over a 50-year period resulted in the overall decrease in total sediment transported by the river (Wang *et al.,* 2006). Channel geometry also plays a role in grain size distributions. Rivers with narrow channels will transport coarser sediment because the unit stream power is higher (Mentling *et al.,* 2015). Steep channel slopes enhance the mixing of sediments as unit stream power is higher and the composition of the sediment will reflect that of the channel bed lithology more than that contributed from other sources (Mentling *et al.,* 2015). Different hydrodynamic conditions are characteristic of different channel reaches depending on channel slope, channel width and depth, climate and river discharge (Mentling *et al*., 2015). The morphology of the streams in the Luquillo Mountains, Puerto Rico, is strongly influenced by the variable lithologies and hydraulic forces such as discharge, slope and stream power (Pike *et al.,* 2010). High stream power has been attributed to high abrasion rates and thus impacting on the grain size distribution (Chatanantavet *et al.,* 2010; Pike *et al.,* 2010; Mentling *et al.,* 2015).

Abrasion is responsible for the production of smaller grain sizes (Chatanantavet *et al.,* 2010; Miller *et al*., 2014; O'Connor *et al.,* 2014; Cox *et al.,* 2015) and has been linked to

downstream fining (Chatanantavet *et al.,* 2010; Pike *et al.,* 2010; Miller *et al*., 2014; Mentling *et al.,* 2015) observed in many river channels. Abrasion rates depend on the travel distance of sediment grains and are shorter for less resistant rocks and longer for more resistant rocks, which ultimately controls the grain size distribution (Sklar *et al.,* 2006). However, abrasion can also reduce sediment flux as some grains are completely dissolved during transport (O'Connor *et al.,* 2014). Contradictory trends of downstream coarsening have been observed in some studies (Mueller *et al.,* 2016), indicating that a combination of different mechanisms are responsible for grain size distributions within a channel (Mentling *et al.,* 2015). The resistance of bedrock within a river channel determines the production of sediment (Wohl, 2015). Furthermore, discharge and sediment supply provides erosive tools as the volume of grains influence abrasion, which is thus governed by stream power (Wohl, 2015). However the entrainment of abundant coarse sediment in the water column reduces flow velocity, thus impacting the sorting and distribution of variable grain sizes (Mueller *et al.,* 2016).

Underlying geology plays a role in determining the composition and grain sizes of sediment and in determining the balance between bedload and suspended load within a river system (Mueller *et al.,* 2016). In channels underlain by granite, eroded grains are coarse because of lower abrasion rates (Mueller *et al.,* 2016; Mentling *et al.,* 2015). High abundance of ultramafic rocks in the bedload of rivers in Westland, New Zealand, was attributed to the low abrasion rates of ultramafic rocks which make them more durable during transport. A downstream fining trend was related to the contribution of sediment from tributaries (Cox *et al.,* 2015). Pike *et al.* (2010) showed that volcaniclastic rocks had abundant cobbles and boulders, metamorphic rocks produce more sand-sized grains, granodioritic rocks had both sand and large boulders, and alluvial streams were characterised by cobbles. Other sources of sediment came from landslides which contributed boulders into the main river channel (Pike *et al.,* 2010). Variable grain sizes and erosion rates are shown in Fig. 3.1, and the initial grain size will determine whether a grain will be present in fine or coarse grain size intervals (Wohl, 2015).

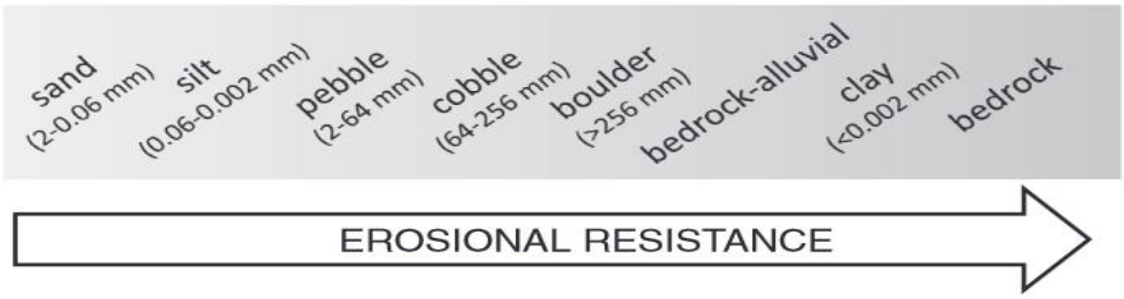


Fig. 3.1: Variable grain sizes and substrate listed in order of resistance to erosion, with the arrow indicating increase in resistance (from Wohl, 2015).

Mentling *et al.* (2015) proposed that a combination of factors influences grain sizes and size distributions, including hydrodynamic conditions, differential fining of variable lithologies, differential abrasion rates due to channel slope, and contributions from hillslopes. Mueller *et al.* (2016) used the occurrence of different lithologies and variable erosion and abrasion rates to explain the distribution and grain size changes of sediments in a downstream direction. The results indicated that the durability of resistant rock types determines grain size, and the concentration of sediment in different grain size classes changes as a function of variable lithologies and abrasion. Abrasion of friable schist produces an abundance of sand-sized grains when compared with greywacke and ultramafic rocks in the Westland rivers in New Zealand (Cox *et al.,* 2015). In western Oregon, USA, sedimentary rocks were abraded into fine grains and transported as suspended load (O'Connor *et al.,* 2014). The underlying geology not only plays a role in the generation of sediment but also in sediment supply (O'Connor *et al.,* 2014). As less resistant sediment is transported downstream, high abrasion rates decrease sediment concentration and thus decreasing total sediment volume deposited in downstream reaches (O'Connor *et al.,* 2014).

Mentling *et al.* (2015) suggested that selective transport can also influence grain size distributions. Miller *et al.* (2014) suggested that abrasion occurs in two phases, with rounding in the first phase and reduction in grain size in the second phase once rounded grains have been formed, and that the grain size distribution depends on both abrasion and selective deposition. Similarly, Miller *et al.* (2016) observed a downstream evolution in grain size and shape and concluded that abrasion controls downstream reduction in grain mass and selective sorting is responsible for downstream reduction in grain size. Chatanantavet *et al.* (2010), however, suggested that selective sorting would only play a role in the grain size distribution where there are small grain sizes and low channel slopes. The effect of sediment influx from other sources such as hillslopes and tributaries was not considered.

In the Westland rivers in New Zealand, bedload composition is influenced by sediment flux from tributaries which mix with main channel sediment and changes the resulting bulk composition (Cox *et al.,* 2015). Variation in bedrock lithology has an influence on creation of sediment through abrasion, the presence of discontinuities such as faults or joints, overall sediment supply, and rate of downstream reduction in grain size (O'Connor *et al.,* 2014). The supply of sediment from external sources other than the channel bed plays an important role in grain size distributions. In areas where there is supply from hillslopes or tributaries, abrasion can have an insignificant effect on grain size distributions (Sklar *et al.,* 2006). Abrasion can only cause downstream fining if the grain size of the sediment entering the system reduces in size in the downstream direction. Within a river channel, changes in grain size distribution occur as sediment moves across different lithologies, or at tributary junctions, or in areas of variable channel geometries (Sklar *et al.,* 2006). The impacts of sediment flux from external sources represent an ongoing topic of research, and the influence of these sediments varies between river systems.

Cox *et al.* (2015) proposed that downstream transport, sediment supply, tectonics and Quaternary glaciation has impacted on the evolution of bedload within the Westland rivers in New Zealand. Glacial sediments can be a sediment store and contribute coarse grains to rivers when deglaciation occurs (Cox *et al.,* 2015). However, this is only applicable to glaciated areas and storage processes may differ in other river systems. Sediment in bedrock channels is stored for only brief periods. However sediment can be stored for longer in alluvial channels depending on grain size and valley geometry (Wohl, 2015). The storage of sediment within different channel types with different transport and abrasion rates has implications for resulting grain size distributions.

3.7 Sediment provenance

The study of sediment provenance involves tracing the origin of sediments and the processes that occurred until the sediment reaches the present day basin or channel (Caracciolo *et al.,* 2016). Detrital minerals are mineral fragments that are transported through the river system and are incorporated in the sedimentary record (Garzanti, 2016). Detrital minerals in sedimentary rocks undergo mechanical and chemical weathering during multiple transport episodes, and changes to the mineral grains that occurred during these episodes can be traced back to elucidate sediment provenance and history (Garzanti, 2016). Sediment provenance studies have utilised trace elements (Bahlburg, 1998), petrographic data of minerals (Garzanti *et al*., 2007b) and grain sizes (Weltje *et al*., 2004) in order to identify the production of sediment, characteristics of sediment source areas and erosional and depositional patterns. Quantitative analytical techniques that have been used in order to analyse sediment provenance include petrographic analysis of minerals (Caracciolo *et al.,* 2016), grain sizes and size distributions (Rubey, 1933; von Eynatten *et al.,* 2012) and chemical composition of minerals (Garçon *et al*., 2014). The methods that have been used to analyse minerals include X-ray spectrometry, electron microprobe analysis and petrographic modal analysis (Tsikouras *et al.,* 2011; von Eynatten *et al.,* 2012; Caracciolo *et al.,* 2016).

Magnetic susceptibility (MS) is the measure of magnetic minerals in the soil and has been widely used as a tracer to identify sediment sources in fluvial environments (Maher, 1998; Blake *et al.,* 2006; Lyons *et al.,* 2010; Mzobe, 2014; Pulley *et al.,* 2016; Rowntree *et al.,* 2017). Heavy minerals influence MS readings of mixed sediments from different sources (Jadot *et al.,* 2015). Every mineral found in sediment has a degree of magnetism, some stronger than others (Mullins, 1977; Liu *et al.,* 2012). Minerals with very weak magnetism include quartz and carbonates and are known as diamagnetic, and minerals such as silicates and clays are known as paramagnetic (Liu *et al*., 2012). Minerals such as magnetite and maghemite have a strong magnetic property known as ferrimagnetism (Mullins, 1977). Another type of magnetism which is characteristic of hematite is known as antiferromagnetism (Mullins, 1977) and has a weaker magnetic property than ferrimagnetic minerals (Maher, 1998). A positive correlation between grain sizes and MS has been identified (Maher, 1998; Hatfield *et al.,* 2009). However, some authors have reported the

relationship between grain sizes and MS to be nonlinear (Foster *et al.,* 1998; Blake *et al*., 2006; Oldfield *et al.,* 2009). In order to overcome this challenge, researchers have used a single grain size interval in order to measure MS (Hatfield *et al.,* 2009; Rowntree *et al*., 2017). Pulley *et al.* (2016) however indicated that a single grain size interval may affect the accuracy of the results as other grain sizes are overlooked. This indicates that there is uncertainty associated with the relationship between grain size and MS, and more research is required to overcome these uncertainties.

3.8 Processes affecting heavy mineral assemblages

Heavy minerals are present as accessory minerals in a variety of rock types and can be used to identify sediment source areas (von Eynatten *et al.,* 2012). Stable heavy minerals which are commonly found in sediment in low quantities include zircon, rutile, tourmaline and kyanite, and heavy minerals which are least stable and found in large quantities include olivine, clinopyroxene, orthopyroxene, garnet and epidote, and these minerals originate from the underlying lithologies (Morton *et al.,* 1999). Heavy minerals are commonly present in the fine grain size interval, between 125 to 63 µm, when compared to other minerals found in sandstone (Morton *et al.,* 1999). The distribution of heavy minerals in a river system depends in part on the energy of the transporting medium (Morton *et al.,* 1999). During sedimentary cycles, heavy minerals are altered and the stability of the minerals is influenced by environmental and climatic conditions (Morton *et al*., 1999; Ando *et al*., 2012; Garzanti *et al*., 2013). The processes that affect heavy mineral assemblages and geochemical characteristics include physical sorting during transport and deposition, mechanical abrasion during transport and dissolution during weathering, and burial (Morton *et al.,* 1999). Variability in heavy mineral ratios within a river system is affected by processes of weathering, abrasion and sorting (von Eynatten *et al.,* 2012). According to Rubey (1933), heavy minerals are concentrated in fine grain size fractions due to sorting. Heavy minerals can also be altered by weathering during temporary storage in a river system, and mineral abundances may be influenced by the complete dissolution of unstable minerals (Morton *et al.,* 1999). Alteration of heavy minerals also occurs during recycling episodes in subduction complexes (Garzanti *et al*., 2013).

During burial diagenesis, unstable minerals of the parent rock are dissolved depending on the depth of burial and this alters heavy mineral assemblages in the daughter rock (Garzanti *et al.,* 2013). Ando *et al.* (2012) focused on the effects of weathering and diagenesis on mineral surface textures and concluded that different heavy minerals display similar corrosion features during the different stages of weathering. Ando *et al*. (2012) proposed that corrosion features on heavy minerals can be used to identify sediment provenance. During weathering, heavy minerals undergo five successive stages, namely; unweathered, corroded, etched, deeply etched, and the final skeletal stage which completely alters the shape of the grain (Ando *et al.,* 2012). Climate plays a fundamental role in weathering as it determines the time period over which the grain will be weathered before it is transported (Ando *et al.,* 2012). The alteration of heavy minerals during the sediment cycle can pose a

problem of accuracy in sediment provenance studies (Morton *et al.,* 1999; Garzanti *et al.,* 2013). However, Morton *et al.* (1999) suggested that the overprinting characteristics acquired during the sediment cycle such as changes in colour, habit, internal structure and geochemical changes, can be used to successfully determine the provenance of sediments. Garzanti *et al.* (2007a) stated that understanding present day conditions of climate, topographic setting, sedimentary processes, lithology and tectonic setting will aid in understanding heavy mineral compositions and abundances.

Grain size is also an important factor when conducting sediment provenance studies. Depending on the rock type and rock forming processes, a mineral may occur as either a coarse or fine grain in the parent rock. Von Eynatten *et al*. (2012) used variations in the grain size of the same mineral group to identify whether the grain is of igneous or metamorphic origin, concluding that grains of igneous origin have larger grain sizes. This has been noted in tourmaline grains, which appear as coarse grains in granitic rocks but are smaller in metapelitic rocks (von Eynatten *et al.,* 2012). Differences in grain size fractions within a sample have been attributed to the settling velocities of different minerals (Rubey, 1933; Garzanti *et al.,* 2007b). Rubey (1933) used Stokes' Law to explain the settling velocity of minerals. The volume and density of minerals and the density and viscosity of the transport medium determine the velocity at which a certain mineral grain will be deposited. During transport, high density minerals will settle together with coarse grained low-density minerals due to equivalent setting velocities, and the finer grains will be transported and deposited at a different location (Rubey, 1933). It has been noted that when assessing grain size distributions, heavy mineral concentrations fall in the fine tail and coarse low-density minerals that settled with the heavy minerals fall in the coarse tail (Rubey, 1933). Analysing a single grain size is regarded as a potential source of bias since heavy minerals are present in different grain sizes, and this has been attributed to initial grain size in parent rocks, different erosional processes and sources (bedrock, terraces or soils) as well as differential transport (Garzanti *et al.,* 2007b). The challenge with using one grain-size fraction in heavy mineral analysis is deciding which size to use, because analysis of heavy minerals can be undertaken using several different size fractions. Rubey (1933) suggested a minimum of two grain-size intervals should be used. Garzanti *et al.* (2007b) stated that various grain size intervals larger than 2 diameters need to be considered.

Caracciolo *et al.* (2016) used detrital amphibole and pyroxene to investigate the provenance of Tertiary volcaniclastic sediments in Thrace, Bulgaria. The results indicated contributions from three different volcanic areas. Highly resistant heavy minerals such as zircons may be transported and reworked with sediments and thus can be effectively used for sediment provenance studies (Thomas, 2011). Thomas (2011) used detrital zircons found in sandstones and their zircon ages and found that the sediment was deposited from the Rockies and Appalachian Mountains into the Grand Canyon, USA. Garzanti *et al.* (2013), however, suggested that zircon can be unreliable in provenance analysis as it is very resilient and the age spectra can remain the same over sequential sedimentary cycles. Furthermore,

von Eynatten *et al.* (2012) noted that the use of a single grain may be biased, for example, the use of zircon alone may limit the representation of zircon-free lithologies thus limiting the accuracy of the provenance study.

Sediment provenance researchers have used heavy minerals to assess provenance using different techniques such as bulk sediment (Garzanti *et al.,* 2007b), multi-mineral (Tsikouras *et al.,* 2011) and single-mineral analysis (von Eynatten *et al.,* 2012). Single grain analysis focuses on variabilities in a mineral group which were created during weathering, transport or burial, and can be used to identify the lithology and age of source rocks (von Eynatten *et al.,* 2012). Heavy mineral concentrations vary depending on source rocks (Garzanti *et al.,* 2007b). Rocks with very few heavy minerals include sedimentary, low-grade metasedimentary and felsic rocks, while mafic igneous rocks and high temperature metamorphic rocks contain abundant heavy minerals (Garzanti *et al.,* 2007b). Depending on rock forming processes, minerals from the same mineral group can have variable chemical compositions and can be present in different grain size fractions (Tsikouras *et al.,* 2011). Tsikouras *et al.* (2011) suggested that hydraulic sorting would be the primary factor affecting present mineral abundances. They used tourmaline, garnet, spinel and zircon and the multi-mineral technique to identify sediment provenance in the Scotian Basin in Canada, and concluded that the majority of sediments were reworked from the Appalachian orogen. Garzanti (2016) reviewed the techniques used in provenance studies and suggested that an integrated approach including bulk sediment, multi-mineral and single mineral analysis is essential for accurate provenance studies. Garzanti *et al.* (2007b) used bulk-sediment analysis to show that the concentration of heavy minerals in modern sands is a reflection of mineral composition in the parent rock. Garzanti (2016), however, suggested that fragile minerals dissolve during burial diagenesis, and this may have implications for the usefulness of bulk-sediment technique in sediment provenance studies.

Within river systems, tributaries can lead to differences in mineral assemblages recorded. Garzanti *et al.* (2005) used heavy minerals to identify sediment mixing and to calculate the sediment contribution from different tributaries. Garzanti *et al.* (2006) found that the majority of sediment on the River Nile was contributed by the River Atbara and Blue Nile, based on the heavy mineral assemblages characteristic of each river. Heavy mineral assemblages and abundances in Nile River sediments were attributed to the underlying geologies of tributaries, the climate in sub-catchments, and fractionation during sediment transport (Garzanti *et al.,* 2006).

The area within the river channel where sampling is conducted also has implications for provenance studies. The chemical variation of minerals can be used to determine the water depth during sampling (Garçon *et al*., 2014). Suspended sediment and bedload differ in catchments with variable lithologies. Garçon *et al*. (2014) based on isotopic data concluded that grains from basalts are usually found in the suspended sediment and grains from other lithologies within the catchment were present as bedload. Resulting differences in grain

sizes of the weathered rock can have implications for the distribution of different mineral assemblages.

3.9 Multivariate mixing models

Sediment source fingerprinting studies involve the discrimination of tracers with characteristic properties of source sediments, and the use of tracers in multivariate sediment mixing models to estimate the contribution from each source (Collins *et al.,* 1997). Multivariate sediment mixing models have been widely used to assess the percentage contribution of different sediment sources within a river system (Collins *et al.,* 1997, 2010a, 2010b; Motha *et al.,* 2003; Fox *et al.,* 2008; Evrard *et al.,* 2011; Miller *et al.,* 2013; Haddadchi *et al.,* 2014a, 2014b; Smith *et al.,* 2014; Pulley *et al.,* 2017). These mixing models include the Bayesian (Cooper *et al.,* 2015), Slattery, Collins, Motha, Hughes, modified Collins (Collins *et al.,* 2010a), Landwehr, and Modified Kandwehr models (Haddadchi *et al.,* 2014a). Smith *et al.* (2014) used the Collins mixing model to discriminate between surface and subsurface sediment sources in an agricultural catchment of the Tamar River, England. A low degree of sediment source discrimination in this area suggests the influence of land use changes in cultivated and pasture fields (Smith *et al.,* 2014). Collins *et al.* (2010b) used the modified Collins mixing model to study the contribution of suspended sediment from farm track surfaces, cultivated topsoil and channel banks in the Piddle River catchment, England. The results indicated that erosion from farm track surfaces was an important source of suspended sediment to the river. Haddachi *et al.* (2014b) used both the Hughes and modified Collins mixing models to assess sediment contribution to suspended and bed material in the Taleghani catchment, Iran. The results indicated that crop fields contributed the highest sediment percentage during flood events with high sediment concentrations, and channel banks contributed the highest percentage during flood events with low sediment concentrations (Haddadchi *et al.,* 2014b).

The choice of potential sediment sources is often informed by land use and land cover within the catchment. Hughes *et al.* (2009) identified that sheetwash, gully and rill erosion resulted in channel banks being the dominant source areas to the Fitzberg River, Australia. Sediment from gully erosion was the major contributor of sediment in various river systems (Evrard *et al.,* 2013; Wilkinson *et al.,* 2013). Carter *et al.* (2003) identified two different source contributions to upstream and downstream reaches of the Aire and Calder rivers, England. The results indicated that channel bank sources contributed the highest percentage of sediment in upstream reaches, and topsoil from cultivated land contributed the majority of sediment in lower reaches (Carter *et al.,* 2003). Wilkinson *et al.* (2013) attributed the highest percentage sediment contribution to subsurface soil sources in the Burdekin River Basin, Australia. The relative contribution of sediment from tributaries and channel banks were very low. Pulley *et al.* (2015a) argued that some land uses are less useful as diagnostic sediment sources areas than others. They tested the potential of magnetic minerals, fallout radionuclides, geochemical signatures and organic matter and identified that there were large differences between tracer group predictions. An example

of this is tracers that were measured from agricultural sources and anthropogenic inputs from urban areas (Devereux *et al.,* 2010), where the dominant tracers in these source areas differ significantly. This is a limiting factor within sediment mixing models, where high within-group variability increases the uncertainty obtained from mixing models (Pulley *et al.,* 2015a). In order to test the accuracy of this assumption, Palazón *et al.* (2015) used artificial mixtures of sediment and confirmed that within-group variability needs to be low in order to reduce uncertainty. However, the use of artificial mixtures of sediment might not always be an accurate representation of sediment in the field, and some researchers have used mathematical methods to reduce the uncertainty associated with within-group variability. These methods include cluster analysis and principal component analysis (Walling *et al.,* 1993; Walling and Woodward, 1995; Pulley *et al.,* 2017).

The type of mixing model used has been proposed to affect the resultant combination of possible sediment sources (Haddadchi *et al.,* 2014a; Smith *et al.,* 2014; Manjoro *et al.,* 2017). Another factor that determines the accuracy of mixing models is source group classification, as this will affect the input data for the model (Pulley *et al.,* 2017). Some studies have used erosional processes such as sheetwash, rill and gully erosion (Hughes *et al.,* 2009; Gellis *et al.,* 2011; Evrard *et al.,* 2013) as a way of classifying sediment source types. Other studies have used spatial sources such as urban areas (Devereux *et al.,* 2010) or geological patterns (Laceby *et al.,* 2015). Since source group classification depends on land use and management goals that have been set, the source apportionment may be biased and neglect other potential sources (Collins *et al.,* 2017).

Tracer properties that have been used in mixing models include fallout radionuclides (Guzmán *et al.,* 2013; Pulley *et al.,* 2015a), minor and major trace elements (Devereux *et al.,* 2010; Haddadchi *et al*., 2014a; Lamba *et al*., 2015; Pulley *et al.,* 2015a), trace element ratios, organic matter content (Smith *et al.,* 2014) and mineral magnetism (Manjoro *et al.,* 2017). Martinez-Carreras *et al.* (2008) used a multivariate mixing model in the Wollefsbach catchment, Luxembourg, and identified that uncertainties in mixing model outputs arise from the number of tracers used in the model. However, not all trace elements identified within the sediment can be successfully used to discriminate sources, as some trace elements lack spatial variability. Manjoro *et al.* (2017) argued that the number of tracers used did not change the performance of the model. Another area of uncertainty in the accuracy of mixing models is the effect of changes in the physical and geochemical properties of particles (Koiter *et al.,* 2013; Smith *et al.,* 2014; Haddadchi *et al.,* 2016). Particle size and organic matter content tend to change from source to sink depending on transport and storage processes (Koiter *et al.,* 2013). Koiter *et al.* (2013) and Laceby *et al.* (2015) suggested that it is important to have prior knowledge of the geochemistry of tracers and the transformations that might occur during transport and deposition. The <63 µm particle size fraction has been widely used in sediment mixing studies to reduce the uncertainties associated with particle size differences (Devereux *et al.,* 2010; Nosrati *et al.,* 2014; Lamba *et al*., 2015; Pulley *et al.,* 2015b). Haddadchi *et al.* (2016) examined the effects

of grain size on the accuracy of mixing models in Emu Creek, Queensland, Australia. They showed that results obtained from single grain sizes may differ from those obtained from aggregated samples. Pulley *et al.* (2015a) demonstrated that organic matter and particle size did not have an effect on the differences that were observed in source prediction for different tracer groups. However, Kouhpeima *et al.* (2011) emphasised that it is essential that tracer properties selected should have a conservative behaviour, meaning that the physical and geochemical characteristics of the tracer should not change from source to sink. They also noted that further research is required in order to fully understand the effect that conservativeness of tracer properties has on the accuracy of mixing models. Koiter *et al.* (2013) suggested that selecting fingerprints that are less likely to change during transport might be used as a way to reduce uncertainty. However, the testing of all possible tracers may be time consuming. Mukundan *et al*. (2012) suggested that a standardised procedure needs to be developed for selecting tracers. Koiter *et al.* (2013) further emphasised that a framework needs to be developed which will guide researchers on the most appropriate tracers for different environments and river systems. Thus it is essential to study river systems in order to create a database of the most appropriate tracers to use.

This also brings up the issue of sampling location. Haddadchi *et al.* (2016) emphasized that sediment samples collected close to source will show a high proportion of sediment from that source. Sedimentary rock sources were dominant in riverbed sites and metamorphic rock sources were dominant in the downstream parts of the catchment (Haddachi *et al*. 2015). Fryirs (2013) emphasised that contributing areas of sediment to a river will vary depending on the magnitude and frequency of rainfall events. Thus Collins *et al.* (2017) suggested that the sampling period and number of samples should be planned accordingly. This is because some tracers such as organic matter may change during different seasons and agricultural crop rotations may alter the geochemistry of the sediment. The importance of sampling period was shown by Devereux *et al.* (2010) in the Anacostia River, Maryland, USA. Different erosional processes were seen to cause temporal variations in potential sources of sediment. Similar results were obtained by Foucher *et al.* (2015) from a lowland catchment in France where the dominant sediment source was surface runoff during flood events, and subsurface sources during low flow periods.

A lot of uncertainty has been associated with mixing models; however these models have been successfully used to estimate sediment contribution from various sources and can influence development of appropriate catchment management strategies aimed at reducing sediment influx from potential source areas (Collins *et al*., 2001; Hillier, 2001; Russell *et al*., 2001; Gruszwoski *et al*., 2003; Kouhpeima *et al.,* 2011; Wilkinson *et al.,* 2013; Laceby *et al.,* 2015; Tiecher *et al.,* 2015; Manjoro *et al.,* 2017). The modified Collins model has been widely used in order to identify sediment sources (Collins *et al.,* 2010a, 2010b; Evrard *et al.,* 2011; Haddadchi *et al.,* 2013, 2014a; Wilkinson *et al.,* 2013; Laceby *et al.,* 2015; van der Waal *et al*., 2015). The Collins model works on the assumption that the concentration of tracers in the sampled sediment is the same as the concentration found in the source

sediment (Kouhpeima *et al.,* 2011). The modified Collins model incorporates all the uncertainties that were mentioned above and thus reduces uncertainty associated with mixing models by including weightings which are obtained from discriminant function analysis (Collins *et al.,* 2010a). Particle size differences are also accounted for in the model (Collins *et al.*, 2010a). However, there is a lack in the application of these models in the South African context.

A South African example is that of the Mkabela Basin, KwaZulu-Natal, where sediment sources varied depending on land use and soil type (Miller *et al.,* 2013). Fine grained sediment was attributed to vegetable field sources and coarse grained sediment was attributed to steep sugar cane fields. Another example is that of an unnamed catchment in the Eastern Cape where the modified Collins mixing model together with trace elements and magnetic susceptibility values were used to identify the sources of suspended sediment (Manjoro *et al.,* 2017). Results indicated an increased contribution from rill and gully erosion. Van der Waal *et al.* (2015) used magnetic susceptibility values and the modified Collins model in the Thina catchment, Eastern Cape, and showed that the underlying sedimentary rocks contributed the highest relative percentage of sediment to the river.

Chapter 4: Methodology

This research seeks to identify major sediment sources within the Letaba River and map the geomorphology of the river within and outside of KNP as well as investigate factors that affect river geomorphology and sediment patterns. This chapter explains the methods that were employed in this research as well as the techniques that were used for analysing the data that were collected. The methods used in this research include desk based mapping, collection of data in the field, analysis of sediment in the lab, and a final analysis of all the research findings.

4.1. Desk based methods

Landsat 8 images with a pixel resolution of 30 m for 30 September 2015 were acquired from the USGS website. These images were used because they can be downloaded for free and provide coverage of the study area during the field sampling period of this research. The images were pre-processed using the ENVI v5.2 image processing software in order to prepare them for digitizing. The pre-processing steps include atmospheric corrections in order to make the images clearer. Atmospheric corrections were done through Gram-Schmidt Pan sharpening, which is a function on ENVI, where a single band image was merged with a multispectral image in order to improve the resolution of the image. The images were then mosaicked and colour balanced using ENVI, in order to combine the images and get a complete coverage of the study area. The final output image after mosaicking was used to digitize the different channel types within the river using ArcGIS v10.3 software. Microsoft Excel v2010 software was used to construct cross profiles of the river at different locations using Differential GPS (dGPS) data collected in the field.

4.1.1 Digitizing geomorphic features

The Letaba River consists of five main channel types: bedrock anastomosing, alluvial braided, mixed pool-rapid, alluvial single thread, and mixed bedrock-alluvial anabranching, similar to those reported from the adjacent Sabie River (Table 4.1). These channel types are distinguished by the presence of different geomorphological features such as braid bar, rock pool, boulder bed, riffle and terrace. ArcGIS v10.3 software was used to digitise these geomorphic units and channel types, from the Landsat images and field data, by drawing polygons around these features and labelling them as was done following the methods used by Heritage *et al*. (1997). This procedure was done by creating shapefiles for multiple and single channels, boulder beds, bedrock pavements, bedrock outcrops, bare sandbars, vegetated sandbars, sand dunes, floodplain, bedrock core bars, bedrock pools, crevasse splay deposits and dams. The position of the units was inferred from notes that were made in the field, Landsat images and dGPS points.

Table 4.1. The channel types found within the Sabie River (van Niekerk *et al*., 1995) which displays similar channel types as the Letaba River. Numbers indicate the occurrence of each unit at each river reach. (1)=Definite occurrence, (2)=Probable occurrence, (3)=Rare occurrence (based on observation). (Source: Van Niekerk *et al.,* 1995, p. 74).

Geomorphological Units	**Channel Type**	**Description**
Lateral bar (1), River cliff (2), Apical pool (2), Point bar (2), Rip channel (2), Pool(1), Riffle (2),Rock Pool (1), Rapid (2), Floodplain (2), Terrace (2)	Single Thread	Uniform single channel river. Limited bedrock outcrops or braided bars associated with active channel. May be bedrock or alluvial.
Braid bar (1), Lateral bar (1), Braid channel (1), River cliff (3), Apical pool (3), Point bar (3), Rip channel (1), Cutoff channel (2), Armoured area (2), Floodplain (2), Levee (3), Alluvial distributary (1), Terrace (2), Alluvial backwater (3)	Alluvial Braided	Multi-channel system with impermanent distributaries on alluvium. Channel convergence and divergence occurs on the scale of channel width.
Rock pool (1), Rapid (1), Bedrock core bar (1), Waterfall (1), Boulder bed (2), Armoured area (2), Lee bar (2), Rock distributary (2), Rock backwater (2)	Bedrock Anastomosing	Multi-channel system of permanent bedrock distributaries. Sediment may accumulate on topographic highs.
Rock pool (1), Rapid (1), Bedrock core bar (2), Lee bar (2), Braid bar (3), Lateral bar (2), Pool (3), Riffle (3), Cataract (2), Boulder bed (2), Armoured area (2), Floodplain (2), Alluvial distributary, Terrace (2), Rock backwater (2)	Pool/Rapid	System of shallow, faster, steeper bedrock dominated rapids and associated upstream backwater pools.
Alluvial islands (1), Floodplain (1), Bedrock pavement (1), Levee (1), Lateral bar (2), Boulder bed (3), Rapid (2), Pool (2), Lee bar (2)	Mixed bedrock-alluvial Anabranching	Multi-channel system that converges and diverges around vegetated semi-permanent ridges or islands. Islands are formed of bedrock and/or alluvium.

4.2. Geomorphic mapping and landform identification

Fieldwork involved mapping of 15 sites representing different river reaches along the Letaba River within KNP, over a period of 5 days. The geomorphological features such as in-channel and flood bars, terraces, floodplains, levees, sand dunes and crevasse splay deposits, characteristic of each channel type, were mapped along the area of interest by making annotated field notes and taking photographs of the area, and this was incorporated with what has already been mapped using satellite imagery. The sites were chosen because each site represented a different channel type and thus the 15 sites represented the different channel types mentioned above. Sampling was conducted by collecting sediments starting

from the river terrace towards the main active channel in order to analyse grain size differences and changes in heavy mineral proportions across the river. In total, 49 sediment samples were collected at the 15 sites from the top (2 cm) surface sediment on each geomorphic feature along the river channel, as mentioned above, in order to obtain representative samples (Fig. 4.1). The top 2 cm was chosen as it represents the sediment that is prone to be eroded and transported during a rainfall event and represent the most recently deposited sediment (Kouhpeima *et al.,* 2013; Miller *et al.,* 2013). Sediments were also collected from 4 tributaries for further analysis (Fig. 4.1).

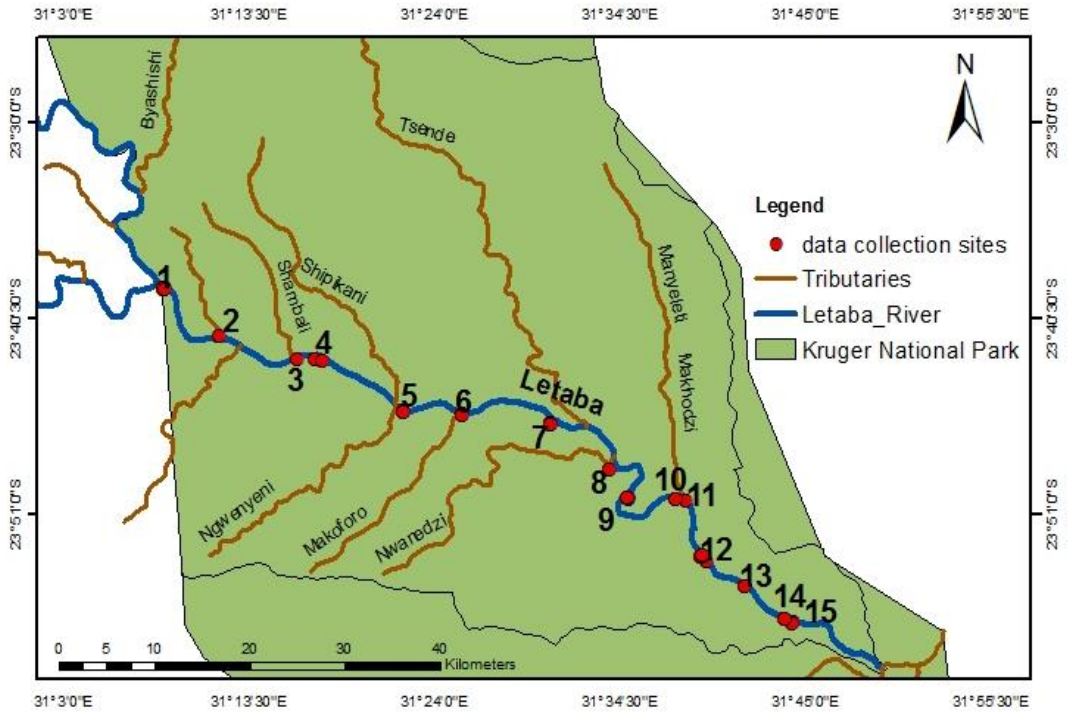


Fig. 4.1: Map of the Letaba River and the data collection sites 1-15 for this research.

dGPS readings were taken at each location where samples were collected, in order to locate these sites on a geomorphic map. In total, 10 transects across the river channel were measured using the dGPS in order to construct cross sectional profiles of the river (Fig. 4.2). A transect was done at different river reaches as defined by changes in channel type, and were also the locations where samples were collected. Each transect was measured by collecting coordinates and elevation values at locations along the transect, perpendicular to the river channel axis, and were plotted using Sigmaplot v10.3 software. Sediment properties at each channel type and geomorphic features were all noted. MS measurements were made (in 10^{-6} m^3 kg^{-1} SI units), which is a measure of the concentration of magnetic minerals within the sediment, using a SM-30 pocket-size MS meter at each of the sites where samples were collected, with about 1-3 readings for each site depending on the number of samples for each site (Balsam *et al*., 2011). MS values indicate the strength of magnetism in the sediment. The sampling sites were chosen to include the different

underlying geologies. Balsam *et al.* (2011) suggested that the formation of soil can be correlated to MS values and the formation of soil develops as rainfall increases. With increasing rainfall, magnetic grains increase in concentration as iron oxides are broken down by the rainfall (Balsam *et al*., 2011). Thus MS values were measured from the floodplain towards the active channel in order to identify how the magnetic grains evolve across the river channel. The MS readings were collected by placing the MS meter on the land surface and recording the value that appears on the meter. A total of 45 readings was recorded in the field on sediment in different river reaches. High MS values mean that there is a high concentration of magnetic minerals, and low readings mean a deficiency of magnetic minerals. MS values were correlated with the concentrations of iron oxide minerals including magnetite, hematite and ilmenite. The grain sizes of minerals have also been seen to impact on MS readings (Hatfield *et al.,* 2009), thus MS readings were also correlated with mean grain size. Bedrock geology was mapped by identifying exposed bedrock units along the river reaches where available.



Fig. 4.2: Image of dGPS unit used to measure transects across the river channel.



Fig. 4.3: Image of top sediment being sampled into a plastic sampling bag.

4.3 Laboratory work

Data collected in the field were analysed by different lab techniques. Bulk sediment samples collected in the field were analysed in order to identify grain sizes and heavy mineral proportions. Grain sizes were analysed by using sieves at 0.25 phi intervals using the Gradistat software (Blott and Pye, 2001) to obtain the moment measures of the grain size distributions. The heavy mineral assemblages were assessed using a petrographic microscope and trace element proportions were assessed using X-ray fluorescence on samples <63 µm and >63 µm respectively.

4.3.1 Grain size analysis

Researchers have used grain size and shape analysis in order to identify sediment provenance, transport and sediment depositional histories (Friedman, 1979; Bui *et al.,* 1989). In order to identify sediment sources, grain sizes were analysed. Sieves at 0.25 phi intervals from 2 mm to 63 µm were used to identify the grain size distribution of individual samples (Fig. 4.4). Sieves were stacked and manually shaken for 2 to 3 minutes and sediment grains were separated according to their grain sizes (Collins *et al*., 2010). The sediment on the different sieves was weighed and the values recorded. The mass on each sieve was examined in Excel using the Gradistat program which calculates statistical parameters such as the mean, mode, sorting, skewness and kurtosis for each sample using the Folk and Ward (1957) graphical method and moments method (Blott and Pye, 2001). The mean grain size is the average grain size for each sample (Masselink *et al.,* 2015). The mode represents the most frequently-occurring grain size in the sample (Lewis *et al.,* 1994). The sediment can either be unimodal (meaning one mode), bimodal (two modes), trimodal

(three modes) or polymodal (more than one mode). The characteristic values of grain size parameters reported in the literature are indicated in Table 4.2. Sediment sorting is determined by the standard deviation of the distribution and can be used to determine energy conditions during transport and deposition (Lewis *et al.,* 1994; Masselink *et al.,* 2015). Sorting can range from well sorted to poorly sorted, with high standard deviation values representing poorly sorted sediments and low values representing well sorted sediments. Skewness indicates how symmetrical the grain size distribution is (Lindholm, 2012). Negative skewness indicates an abundance of coarse grains and positive skewness indicates an abundance of fine grains (Masselink *et al.,* 2015). Kurtosis describes the sharpness of peak of the grain size distribution (Masselink *et al.,* 2015). Kurtosis can also be used to identify the depositional environment of the sediments (Masselink *et al*., 2015).

Table 4.2: Summary of grain size parameters and the characteristic values (Blott and Pye, 2001).

Sorting		Skewness		kurtosis	
Very well sorted	<0.35	Very fine skewed	0.3 to 1.0	Very platykurtic	<0.67
Well sorted	0.35 to 0.50	Fine skewed	0.1 to 0.3	Platykurtic	0.67 to 0.90
Moderately well sorted	0.50 to 0.70	Symmetrical	0.1 to -0.1	Mesokurtic	0.90 to 1.11
Moderately sorted	0.70 to 1.00	Coarse skewed	-0.1 to -0.3	Leptokurtic	1.11 to 1.50
Poorly sorted	1.00 to 2.00	Very coarse skewed	-0.3 to -1.0	Very leptokurtic	1.50 to 3.00

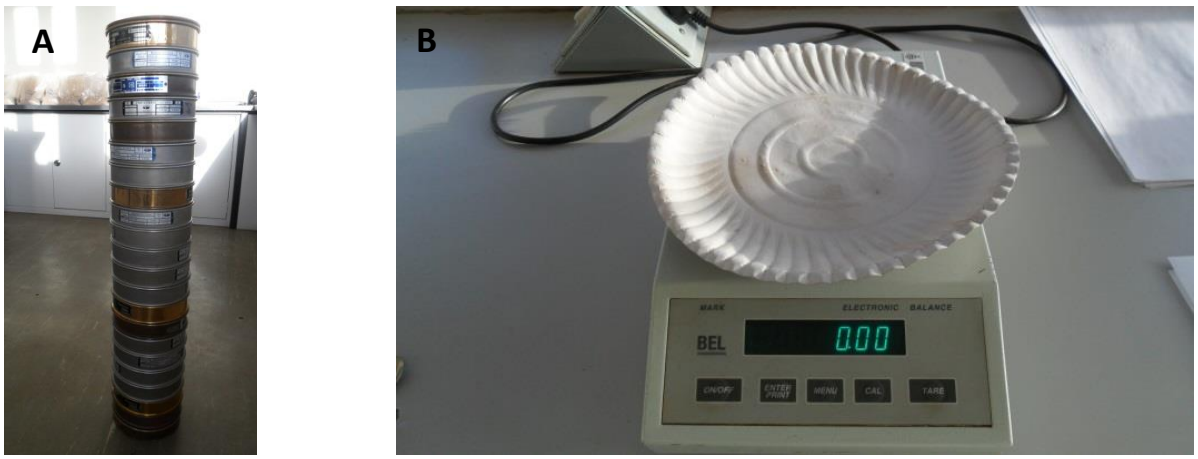


Fig. 4.4: (A) Image of sieves of different intervals used to sort sediments in their different grain sizes. (B) Image of a balance used to measure the weight of the sieved sediment.

4.3.2 Heavy minerals

Heavy minerals can be used to identify the source of sediments and are usually found in trace amounts (Lynn *et al*., 2008). Heavy minerals include magnetite, zircon and ilmenite (Lynn *et al*., 2008). Once grain sizes were analysed, the proportions of heavy minerals were investigated using a petrographic microscope. Grain sizes <2 mm for each sample were placed on a glass slide, containing oil for mounting, which is about 46 by 26 mm, and cover slips were placed over the glass slide and then heated before further analysis. There were between 300 and 500 grains on each glass slide. One thin section was prepared for each sample. The thin sections had to be polished to allow for identification of minerals. The mineral properties that were observed under the microscope include colour, pleochroism, habit, cleavage, twinning, relief, Becke line and birefringence (Lynn *et al.,* 2008). The optical properties of common heavy minerals are presented in Table 4.3.

Table 4.3: The optical properties of some heavy minerals identified, namely; zircon, magnetite, ilmenite, biotite and olivine. (Adapted from Lynn *et al*., 2008).

Mineral name					
	Zircon	Magnetite	Ilmenite	Biotite	Olivine
Crystalline system	Tetragonal	Isometric	Hexagonal		Orthorhombic
Colour	Colourless to pale	Black with metallic lustre	Blue-grey to black	Red, brown, green	Yellowish green, reddish brown
Relief	Positive, very high			High positive	Moderate
Refractive index	1.925-1.993				1.670 - 1.690
Birefringence	0.060-0.062				
Extinctive angle	Parallel				
Interference figure	Uniaxial (+)				Biaxial (+)
Habit		Octahedral crystals	Tabular crystals	Tabular crystals	

A petrographic microscope was used for analysing the modal abundances of heavy minerals. Pictures of the samples were taken using an Olympus DP2 Twain camera together with the AnalySIS getIT v5.2 software. Minerals such as magnetite, ilmenite and hematite were identified under reflected light at a magnification of 40x and the remaining minerals, olivine, clinopyroxene, orthopyronene, biotite, muscovite, hornblende, rutile, zircon, tourmaline, zoisite, plagioclase, orthoclase, were identified under transmitted light at a magnification of 4x and 10x. The thin section was divided into 9 equal parts and mineral abundances were counted from these points. In order to obtain the mineral abundances, individual minerals were counted, resulting in a total number of 200 to 300 minerals counted on each thin section.

4.3.3 X-ray Fluorescence Spectroscopy

The analysis of heavy mineral proportions was also conducted using X-ray fluorescence (XRF) spectroscopy, which is a faster method for obtaining trace element proportions. The grains of 48 samples which were collected from the Letaba River were again sieved with a sieve interval of <63 µm in order to enable analysis with the spectrometer (Shaltout *et al*., 2011). The samples were prepared by adding Mowiol, which is an organic binder, to a 5 g sample, then combining the mixture until the Mowiol dissolved into the sample. The mixture was then poured into a steel cup and pressed at a pressure of 10 tons, creating pallets for further analysis using a spectrometer (Fig. 4.5). The XRF works by emitting short wavelength radiation on the minerals, the minerals then absorb this radiation based on their chemical composition (La Tour, 1989; Potts *et al*., 2008).

The wavelength dispersive X-ray spectrometer is used for this analysis. The X-ray beam source is reflected against the prepared samples at different angles for different minerals because they reflect at different angles. The minerals are then 'excited', the 'excited' minerals release energy and this energy is reflected onto a collimator which narrows the beam. The beam is then reflected onto a crystal which intensifies the wavelength of the reflected beam. The beam that was reflected onto the crystal will be reflected on to a detector which measures the angle and intensity of the wavelength, and the measured intensity of this energy indicate the proportion of minerals present and thus identifying the quantities of heavy minerals (La Tour, 1989; Potts *et al.,* 2008). Each element will reflect X-rays at a different angle and at a different intensity and this indicates the type of element and the concentration of the element. The Pro-trace software is used to convert wavelength into concentration of the elements.

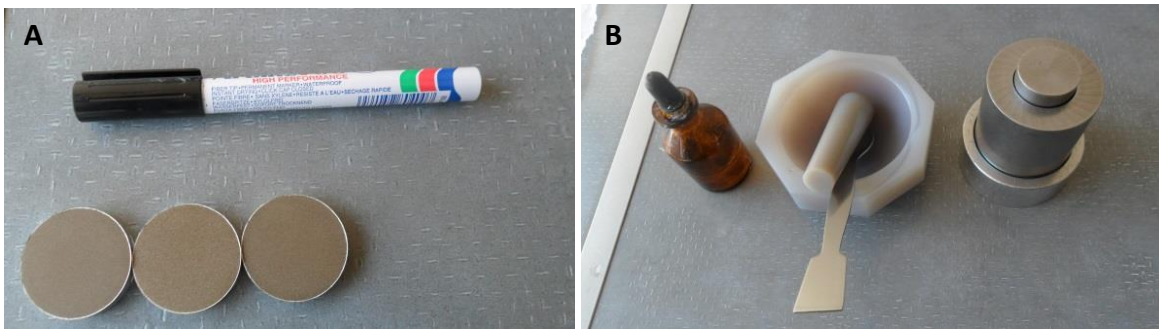


Fig. 4.5: (a): Image of pressed pellets. (b): Image of Mowiol binder, grinder and press used in the preparation of pellets.

4.3.4 Organic matter content

The organic matter content of the sediment samples was determined using loss on ignition analysis. With this method, the percentage of organic matter in the samples was calculated by comparing the weight of the sample before and after being burned in a furnace, the mass loss being related to the organic matter present in the sample. The crucibles used in the

analysis were first weighed before sediment was placed in them and weighed. The crucibles were placed in a furnace and burned for 8 hours at 430˚C. After this time, the furnace was switched off and the samples left to cool. The crucibles were then removed from the furnace using tongs. The crucibles were reweighed and their weights recorded. The weight of the crucibles with sediment before ignition was subtracted from the weight after ignition, from which the percentage of combustible organic matter could be calculated. The results of this analysis are given in Appendix D and were used in the mixing model.

4.4 Analysis

Principal component analysis was performed using SPSS v23, in order to reduce the dimensionality of the data and identify significant relationships between the trace elements present in the samples (Haddadchi *et al.,* 2013). Sediment provenance studies involve identifying potential sediment sources, selecting properties which can distinguish these sources and comparing these properties to those of sediment collected throughout the river system (Walling *et al.,* 2008). These distinguishing properties can be used in a sediment mixing model in order to identify the relative contribution from potential sediment sources. The sediment samples were divided into source samples and river sediment samples. Source samples represent the sediment collected from potential sediment sources including tributaries, and the river samples are those used to assess how the sediment from the different sources have mixed during transport. The sediment from source and river samples were all analysed through XRF for trace element concentrations. The mean and standard deviation of trace element concentrations in the source and river sediments were analysed in Microsoft Excel 2010, in order to calculate the variability within the trace element concentrations. High variability means that the sediment can be distinguished according to its different sources. The mixing model used in this study is the modified Collins model (Haddadchi *et al.,* 2013), also known as the Monte Carlo numerical mixing model (Wilkinson *et al.,* 2013). The main principle in the application of this model is that the concentration of a particular tracer in the sampled sediment is the same value as the source sediment (Kouhepeima *et al.,* 2011). This model was chosen because it has been successfully used in identifying potential sediment sources in previous studies (Collins *et al*., 2010; Haddadchi *et al.,* 2013, 2014a), and the choice of the mixing model was dependent on the availability of tracers to be used as model input. Sediment fingerprinting with mixing models is useful for sediment source identification because it provides a direct approach for identifying sediment sources for different river reaches, as opposed to other methods such as soil erosion tracers, photogrammetry and surveying (Haddadchi *et al*., 2013). Sediment mixing models work by “unmixing” the sediment and apportioning percentage contributions to the potential sediment sources that have been identified (Collins *et al.,* 1997; Haddachi *et al.,* 2013; Smith *et al.,* 2014).

Haddadchi *et al.* (2013) developed a workflow of the processes needed in order to identify sediment sources (Fig. 4.6). Samples are initially collected, then analysed in the lab for distinguishing characteristics called 'tracers', which are used to identify different sediment sources. Statistical methods are then applied to the results and an appropriate mixing model is then used (Haddadchi *et al.,* 2013). These tracers may include sediment colour, grain sizes, different heavy mineral populations, or trace element concentrations (Haddadchi *et al*., 2013). The tracers used in this present study are the minor trace elements identified from XRF. Two statistical tests of the tracers were conducted in order to determine which to use in the mixing model. These tests were the Kruskal Wallis H-test and stepwise multivariate discriminant function analysis (e.g. Collins *et al*., 1997; Kouhpeima *et al.,* 2013; Miller *et al.,* 2013; Haddadchi *et al.,* 2014a; Smith *et al.,* 2014; Manjoro *et al.,* 2017). The Kruskal Wallis test identifies tracers that will be useful in distinguishing the various sources (Smith *et al.,* 2014; Manjoro *et al.,* 2017). Discriminant function analysis tests the trace elements that passed the Kruskal Wallis test, and the number of tracers which are correctly classified into the potential source category (Manjoro *et al.,* 2017). The results of the discriminant function analysis are based on the Wilk's lambda algorithm which indicates the tracers which are correctly classified into the potential source groups (Kouhpeima *et al.,* 2013). The statistical tests were done using SPSS v24 software. The source categories that were used include sediment from tributaries, the channel bed, and channel banks. The source samples consisted of a total of 4 samples from tributary sources, 2 samples from the channel bank, and 2 samples from the channel bed (Fig. 4.7). Only one sample was collected from sites 2, 4, 6 and 9. Two sediment samples were collected from site 1 and site 8, thus making it 6 sampling locations.

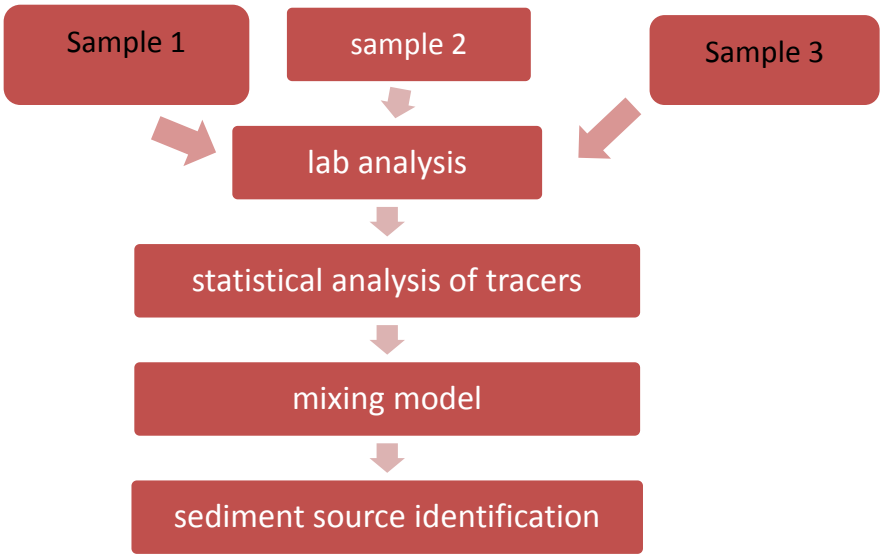


Fig. 4.6: Workflow processes of a sediment mixing model. (Adapted from Haddadchi *et al*., 2013).

4.5 Modified Collins mixing model

Collins *et al.* (2010) proposed a modified mixing model (eq 1) which was used in this project to identify potential sediment sources along the Letaba River. Within this model, the source type contributions must all be positive and the total of the source type contributions must be equal to 1 (Collins *et al.,* 1997).

$$\sum_{i=1}^{n} \{ (C_i - (\sum_{s=1}^{m} P_s S_{si} Z_s O_s SV_{si}))C_i \}^2 W_i \quad (1)$$

where: Ci=concentration of fingerprint property (e.g. concentration of trace elements); (i) is the floodplain sediment collected from the sub-catchment outlet; Ps=the optimised percentage contribution from source category (s); Ssi=mean concentration of fingerprint property (i) in source category (s); Z= particle size correction factor for source category (s); O=organic matter content correction factor for source category (s); SVsi= weighting representing the within-source variability of fingerprint property (i) in source category (s); Wi=tracer discriminatory weighting; n=number of fingerprint properties comprising the optimum composite fingerprint; m=number of sediment source categories.

The modified Collins mixing model includes additional parameters and W_i has a different meaning, compared to the original Collins model (Collins *et al.,* 2010). The multivariate mixing model uses the mean and standard deviation of the tracers in each source group and calculates the relative contributions by minimizing the sum of squares of the relative errors produced for each tracer (Collins *et al*., 2010). The additional parameter is SVsi, indicating within-source variability of the different tracer properties, and this weighting influences the smallest calculated standard deviation of the tracer properties that have the greatest influence on the solution of the equation (Collins *et al*., 2010). The weighting representing the within-source variability was obtained by calculating the variance of the fingerprint concentrations in the different source categories in Microsoft Excel 2010. The W_i parameter represents the tracer discriminatory weighting. This value is obtained by using discriminant function analysis and is based on the number of tracers which are classified correctly into the potential source category (Collins *et al.,* 2010). The tracer discriminatory weightings were obtained when calculating the discriminant function analysis in SPSS v24 software. The organic matter content correction factor is another parameter used to reduce uncertainty (Collins *et al*., 2010). The correction factor was calculated by obtaining the ratio between the organic matter of the sediment samples and the mean values from the source type categories.

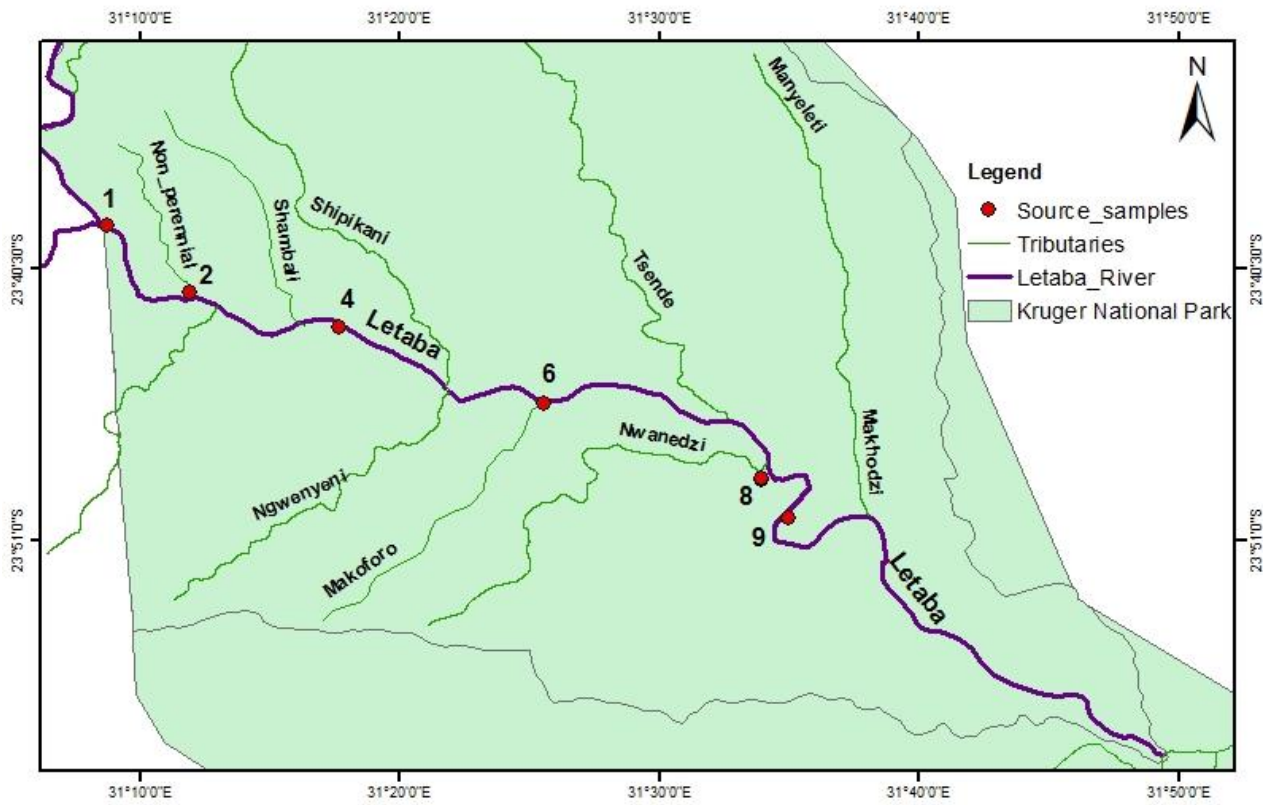


Fig. 4.7: The locations of the source sampling sites 1-9 along the Letaba River.

4.5.1 Running of the mixing model

Python v2.7.8 was used in order to run the model. A script with the formula was created for the model in the Python software (Appendix F). Columns were created in Excel 2010 for the data obtained for each variable within the formula, and a *.csv file was created for each of the trace elements. The model was repeated for each trace element at each source category in order to calculate the source contributions. In order to understand the sources of sediment in the downstream direction, the model needs to be applied using source samples that lie upstream of each site, thus the model was only run for the downstream sites 10 to 15, as these are located downstream of all of the source sampling sites. These upstream sediment source samples provided a suitable number of samples in order to calculate the parameters that were needed to run the model. The relative source apportionments from each source were estimated from the modelled results by calculating the overall mean estimated contribution from each source and dividing it by the estimated mean obtained from each source for all the sediment samples collected from the different sites.

4.5.2 Accuracy of the mixing model

The accuracy of the mixing model was assessed using the Mean Absolute Error (MAE) (Hughes *et al.,* 2009; Haddadchi *et al*., 2014a) for individual and group sediments according to (eq 2):

$$\text{MAE}=\frac{\sum_{j=1}^{m} |X_j - Y_j|}{m} \quad (2)$$

where Xj is actual percentage of sources in mixture sediments, Yj is calculated contribution of each source (j) and m is the number of sources (m = 3).

The MAE compares the tracer concentrations within the samples and the modelled results obtained from the mixing model (Kouhpeima *et al.,* 2013). Walling *et al.* (2000) indicated that the, in order for the model results to be considered as reliable, the errors must be <15%.

Chapter 5: Results

Fieldwork was done during September 2015 and sampling was performed over five days. The fieldwork involved sampling and mapping within KNP from the confluence of the Groot Letaba and Klein Letaba rivers to the confluence of the Groot Letaba with the Olifants River (Fig. 5.1). The results of this research are presented in this chapter. The first section includes field descriptions and geomorphological maps of the Letaba River. The second section presents the grain size analysis, grain size distributions, correlation between grain size and underlying geology and MS values. The third section deals with the heavy minerals present within the sediments and the mineral assemblages at different river reaches. The fourth section outlines the trace elements present within the sediments sampled in the river.

5.1 Channel forms

The Letaba River is characterised by an east-flowing channel meandering between bedrock outcrop and sand bars. The Letaba River within KNP is characterised by variable channel types such as bedrock-influenced channels, alluvial-influenced channels and mixed bedrock-alluvial channels, depending on the amount of bedrock and alluvium present. Below is a description of morphological features present within the studied river reaches. The data were collected over 15 different sites with variable morphological features (Fig. 5.1). Meandering channels and vegetated sandbars characterize alluvial channels. Diorite and basalt outcrops represent channel reaches that are bedrock-influenced as these rock types are resistant to erosion. Bedrock core bars, pavements and steep channel banks are characteristic of these reaches. The geomorphic maps produced provide the spatial patterns and configuration of landforms and the key features that make up these river landscapes.

5.2 Field descriptions

Site 1 (23˚38.920'S, 31˚8.750'E)

The Klein Letaba and Groot Letaba rivers meet at this sandy river reach. The Klein Letaba River was dry during the time of sampling. The Klein Letaba river bed contains fine grained subaqueous dunes, mud cracks and granite gneiss outcrops 1 m in length (Fig. 5.2). The subaqueous sand dunes trend southwest and are 20-50 cm in height. The Groot Letaba River contains multiple channels that flow between vegetated sandbars (Fig. 5.3a). The channel is 1 to 4 m wide and contains several small flat sand bars with grassy vegetation on top. The floodplain of the Groot Letaba River is characterised by three large flat topped sandbars 10 to 12 m wide (Fig. 5.2). The majority of the sediment appears to be brought in from the dry Klein Letaba River, thus reducing the size of the Groot Letaba River channel at the confluence. The transect across this river shows a steep erosional slope, followed by a low elevation floodplain, with sandbars that slightly increase floodplain elevation (Fig. 5.3b).

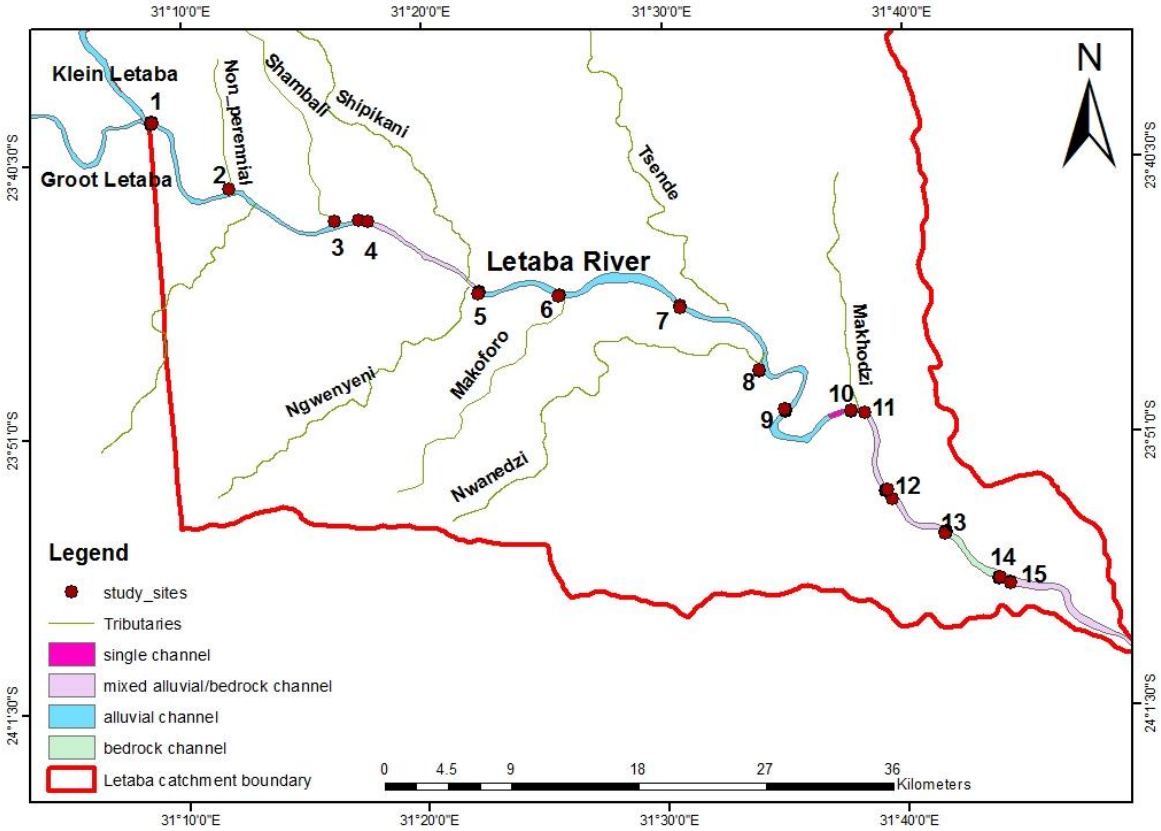


Fig. 5.1: Data collection sites 1-15 on the Letaba River within KNP.



Fig. 5.2: (a) View of the Groot Letaba River with a vegetated sandbar formed within the channel, flow direction is indicated by the red arrow.

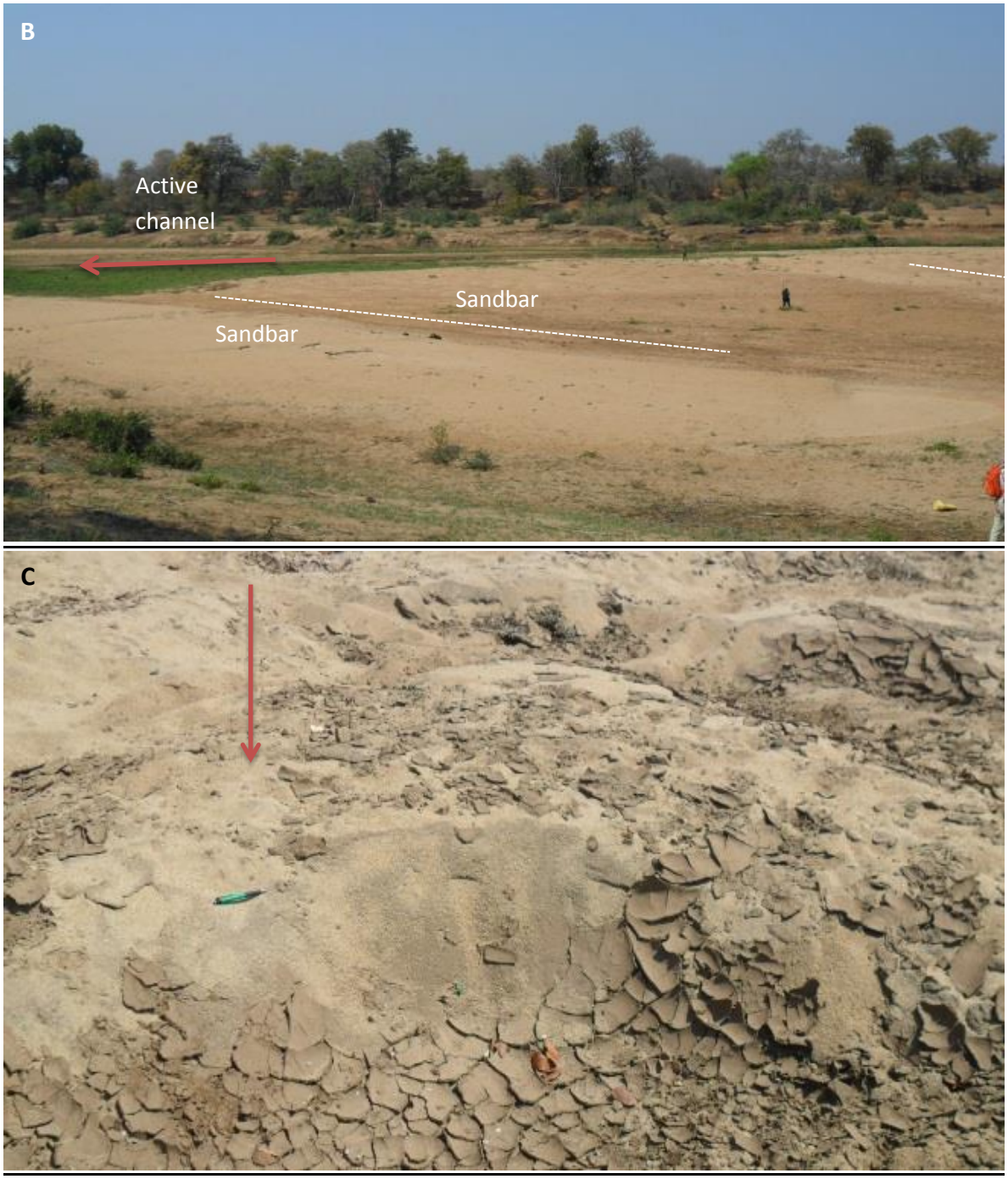


Fig. 5.2: (a) View of the Groot Letaba River with a vegetated sandbar formed within the channel, flow direction is indicated by the red arrow. (b) View of flat-topped sandbars formed at the intersection between the two rivers, with an abandoned channel cutting through the sandbars. (c) View of subaqueous sand dunes on the bed of the dry Klein Letaba River. The pen indicates the scale. Flow direction is indicated with the red arrow.

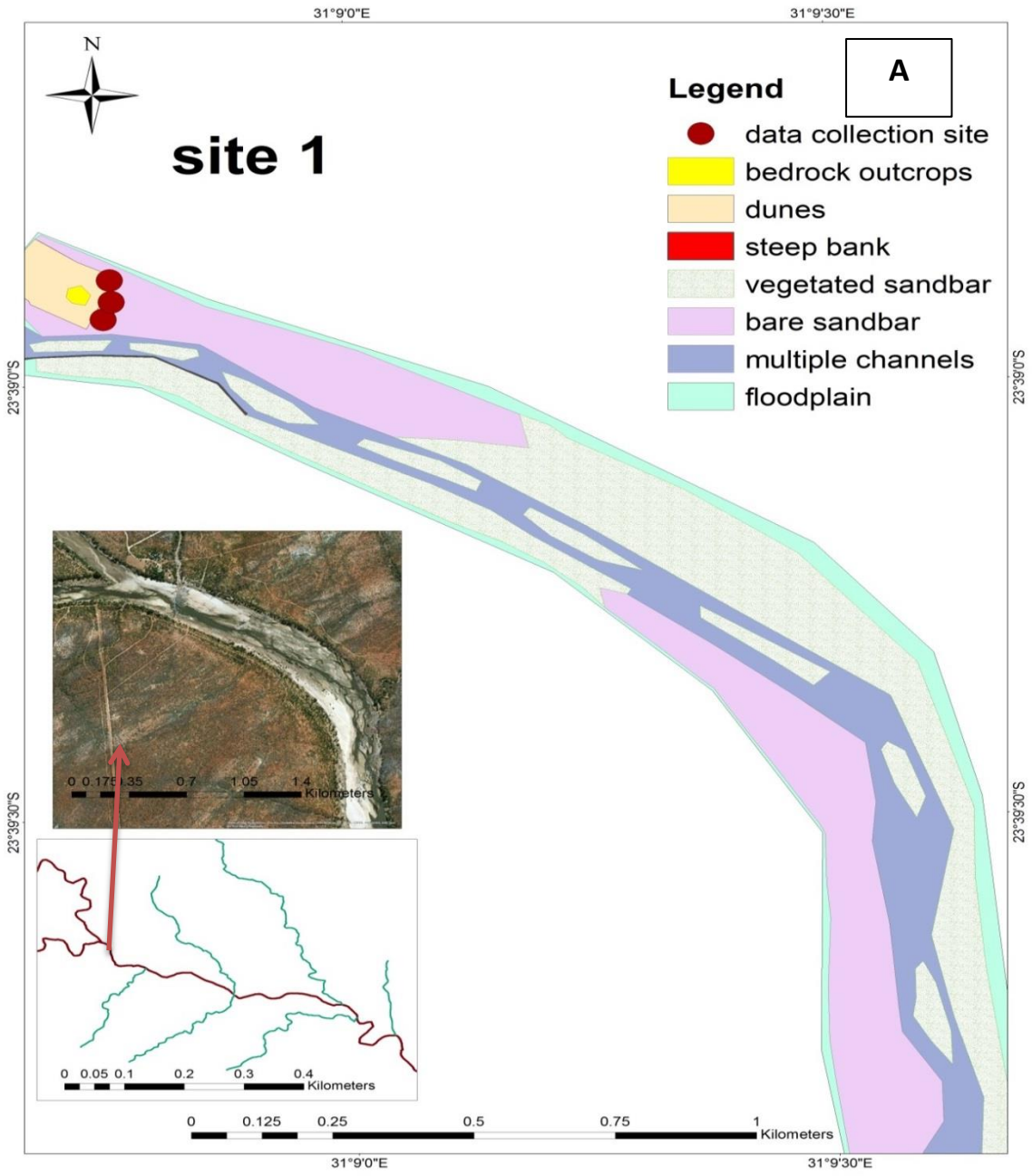


Fig. 5.3: (a) Geomorphic features at site 1. The red dots also indicate the area where the transect was taken across the river.

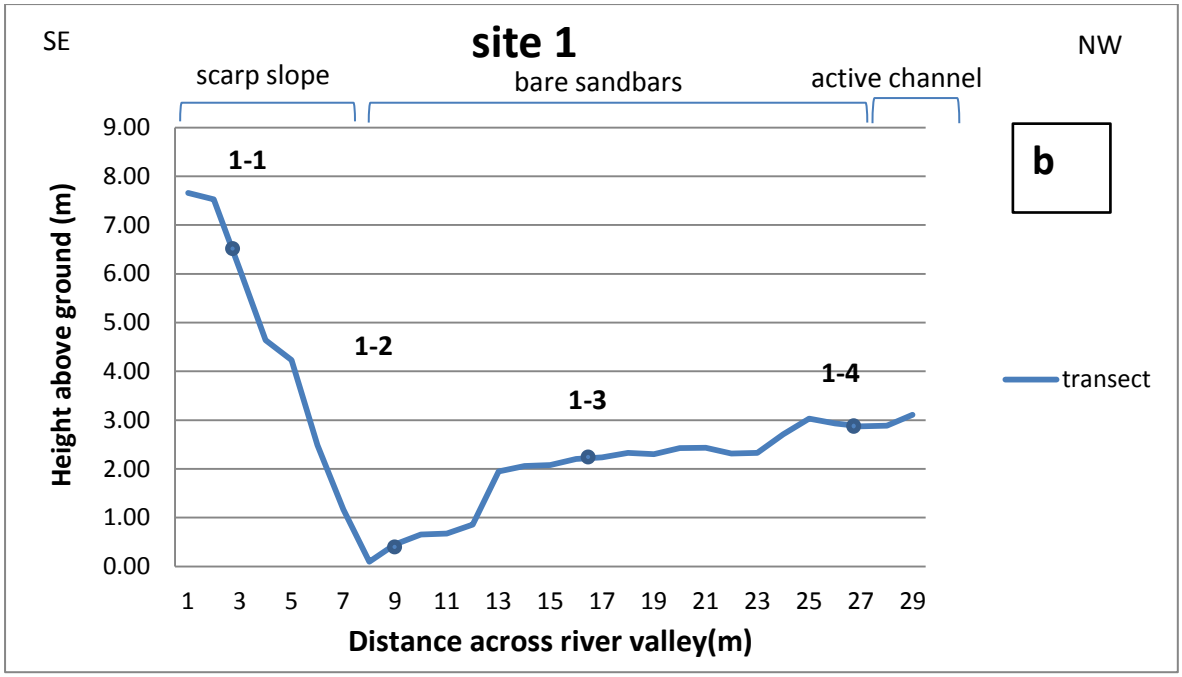


Fig. 5.3: (b) The transect and sample numbers at site 1.

Site 2 (23˚41.462'S, 31˚11.905'E) and site 3 (23˚42.730'S, 31˚17.282'E)

These sites represent tributaries of the Letaba River. Site 2 is a non-perennial river which enters the Letaba River 9.36 km downstream of the confluence of the Klein and Groot Letaba rivers. The river is 8 m wide and the river bed was covered with gravel at the time of sampling. Site 3 is the Shambali River which enters the Letaba River 18 km downstream of this confluence. This river is 10 m wide and the river bed is made of medium to coarse grained sediment and granite and granitic gneiss boulders up to 1 m dimensions. This river was dry during the time of sampling but the flow direction is south east, towards the Letaba River. Both rivers are very narrow with steep terraces on both sides of the river, indicative of erosional incision during high flows.

Site 4(a) (23˚42.730'S, 31˚17.284'E)

A low water bridge submerged under the water has resulted in a visible break of channel gradient at this river reach. There are very few bedrock outcrops of 30 cm in height which make up about 2% of the material within the river channel, however the majority of the channel contains no sandbars or outcrops (Fig. 5.4). There are however outcrops of diorite and boulders of granite of up to 60 cm in diameter on the edges of the river. A steep river bank 20 cm in height characterises this river reach. The scarp slope is less steep and gradually becomes flatter downstream as the river widens.



Fig. 5.4: View of the Letaba River at the Shimuwini Dam, site 4a. The river is 10-12 m wide and tens of cm deep. The arrow indicates flow direction.

Site 4 (b) (23˚42.775'S, 31˚17.688'E)

Multiple sandbars are present within the river channel and water hyacinths are present on the sand bars and these separate the channel into 5 narrow channels (Fig. 5.5). The presence of sediment and outcrops is representative of a mixed bedrock-alluvial channel type (Fig. 5.6a). Outcrops of diorite and granite up to 1 m diameter on the edges of the river mark the contact between a granite intrusion and diorite. Fine grained sediment is deposited between these outcrops and these make up bedrock-cored bars. The floodplain consists of a large mass of sand and large boulders up to 2 m diameter are present 40 m from the main channel, indicating the highest flood level during past flood events (Fig. 5.6a). The river has a steep scarp 4 m in height, which is indicative of erosional incision during floods (Fig. 5.6b). The erosional slope is followed by a flat floodplain and variations in the height of the floodplain caused by the presence of diorite and granite outcrops (Fig. 5.6b).



Fig. 5.5: View of site 4b indicating vegetated sandbars separating multiple channels. Red arrow indicates flow direction.

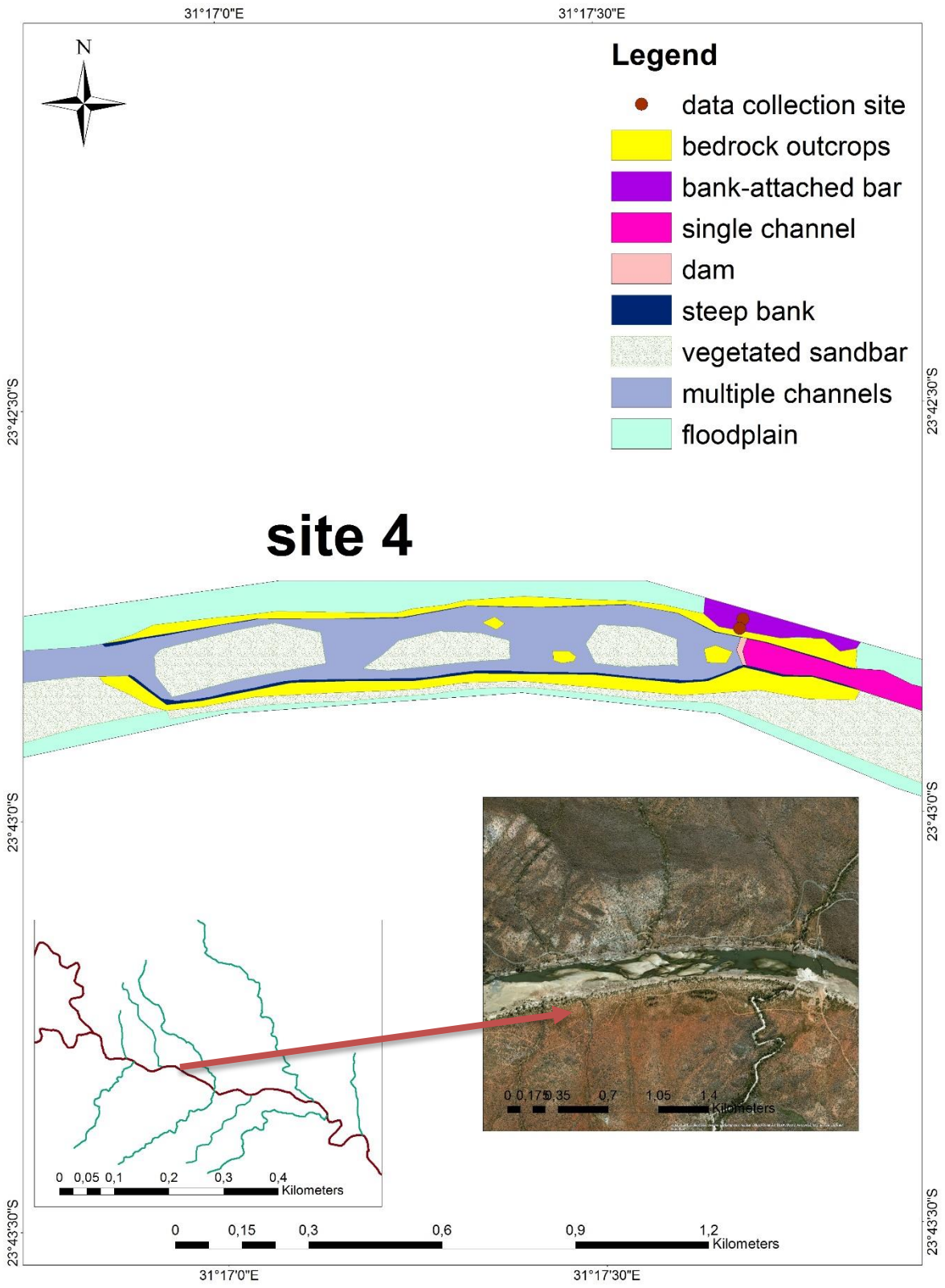


Fig. 5.6: (a) Geomorphic features at site 4b.

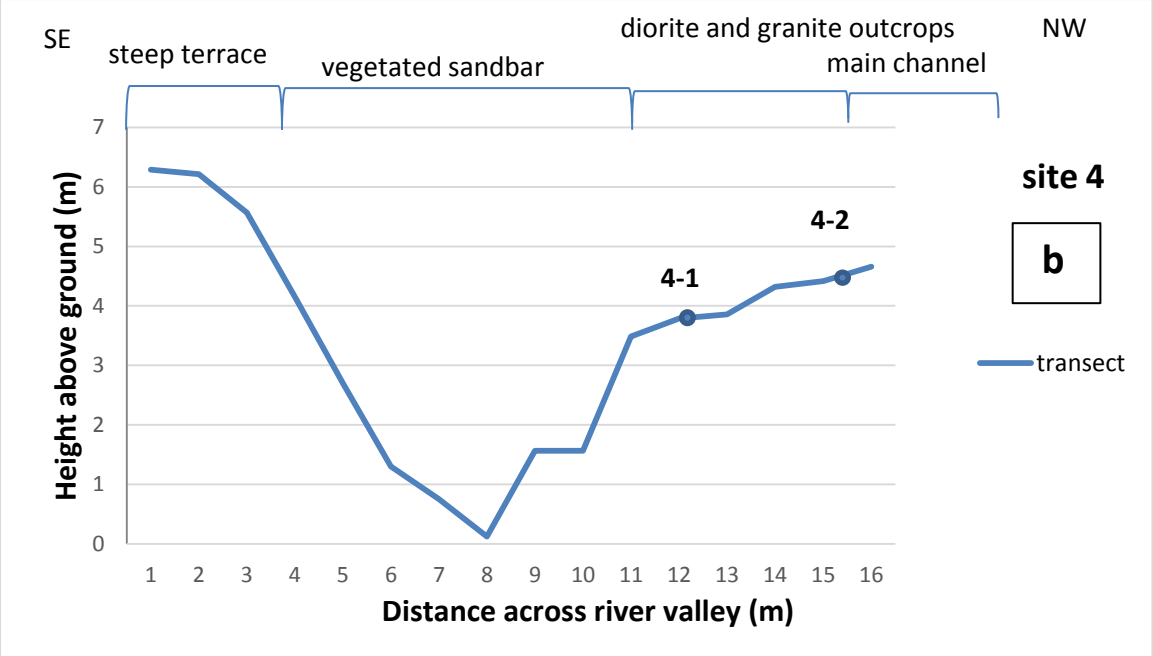


Fig. 5.6: (b) The transect and sample numbers at site 4b.

Site 5 (23˚45.531'S, 31˚22.281'E)

The Mopani/Phalaborwa Bridge separates the very narrow river channel (Fig. 5.7a). This river reach is characterised by multiple ridge-like sand bars and inactive channels and a narrow stream at the end of the bridge (Fig. 5.7b). There are three large sandbars of 2 m cross-sectional length on the floodplain, separated by inactive channels. The inactive channels are identified by a collection of basalt, granite and quartzite cobbles up to 10 cm diameter at a lower elevation than the sand bars. The main river channel is surrounded by boulders (up to 30 cm diameter) of basalt, which are present on the river bank. The river has a flat-topped steep scarp slope up to 5 m high (Fig. 5.7c). The transect indicates a steep erosional slope and an uneven profile caused by ridge-like sandbars and inactive channels present on the floodplain (Fig. 5.8).



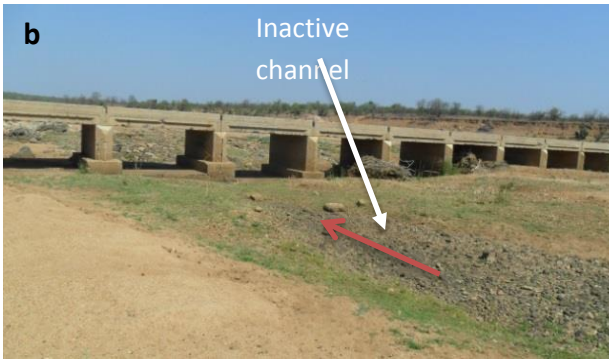




Fig. 5.7: (a) View of the Letaba River and the Phalaborwa Bridge, site 5. (b) View of an inactive channel between ridge-like sandbars. The inactive channel is characterised by a collection of dark coarse gravel. (c) The narrow Letaba River flowing under the Phalaborwa Bridge. (d) Cobbles present in the inactive channel (pen for scale). Red arrows indicate flow direction.

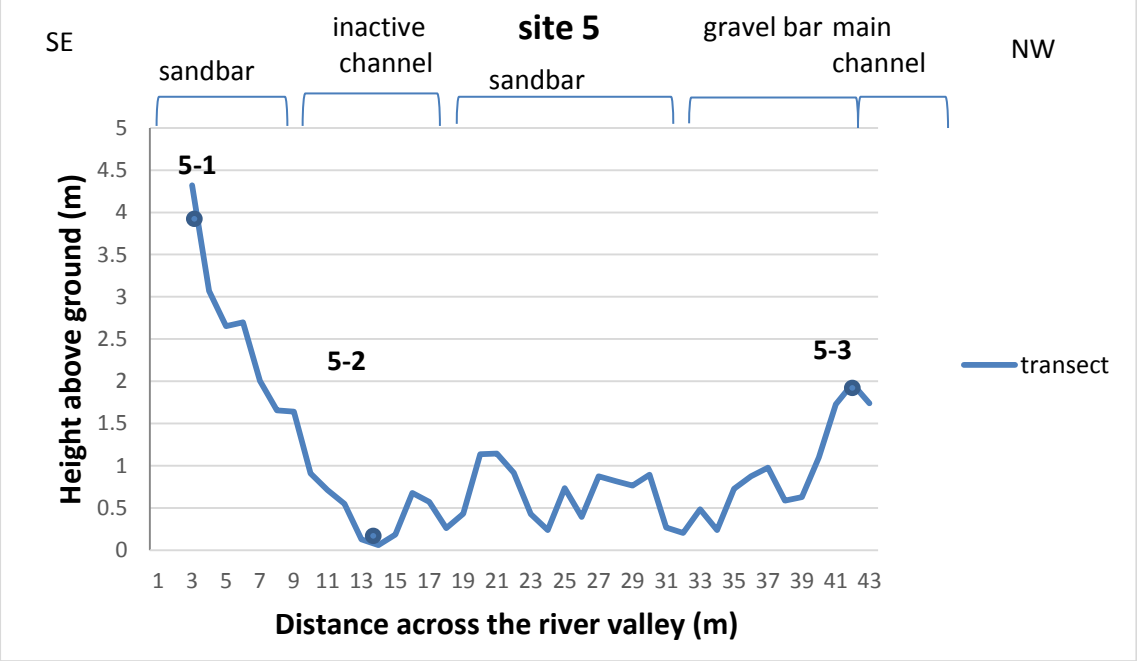


Fig. 5.8: The transect and sample numbers at site 5.

Site 6 (23˚45.680'S, 31˚25.610'E)

This river reach is characterised by multiple channels separated by large sandbars (Fig. 5.9). The first channel just after the steep scarp face is separated into two channels by a sandbar and has a shallow river bank. This channel is then followed by a sandbar up to 30 cm high which is covered in reeds and shrubs. Next to the sandbar is an inactive channel with gravel 1-5 cm in diameter. This inactive channel fills up during periods of heavy rainfall and deposits gravel on its river bed. Another sandbar up to 30 cm high separates the inactive channel from another shallow active channel. The channel is a single sinuous channel

surrounded by water hyacinths. The floodplain consists mostly of grass, bare sand and a few shrubs. There are no visible bedrock outcrops within this river reach. It represents an anastomosing sand-dominated channel type.



Fig. 5.9: Views of site 6 (a,b,c) indicating elevated sandbars and *Phragmites mauritianus* present as riparian vegetation. The red circle on (b) indicates the entrance of the Makoforo River tributary.

Site 7 (23˚46.166'S, 31˚30.637'E)

This sandy river reach consists of multiple sandbars and channels that meander around the sandbars (Fig. 5.10a). A massive sandstone outcrop and boulders are present at the edge of the river channel. The river channel starts off as a single sinuous channel which then separates into four shallow channels by flat-topped sandbars which are 1-2 m wide. The channels then converge in the downstream direction. The surrounding floodplain is characterised by a coarse grained un-vegetated sandbar 1 m high and 10 m across (Fig. 5.11). Sandstone outcrops present at the edge of the river are up to 6 m high and show water level marks indicating water levels during periods of flooding. One of the boulders contains a 3 m-wide rounded pothole which is indicative of high erosion rates by a bedload abrader during floods (Fig. 5.10c). This river reach represents an alluvial braided channel type as there are no bedrock outcrops present within the channel.







Fig. 5.10: (a) View of the Letaba River meandering between vegetated sandbars at site 7. (b) Sandstone bedrock pavement present near the river. (c) Large bedrock outcrop with a 3 m wide pothole (Person for scale). Arrow indicates flow direction.

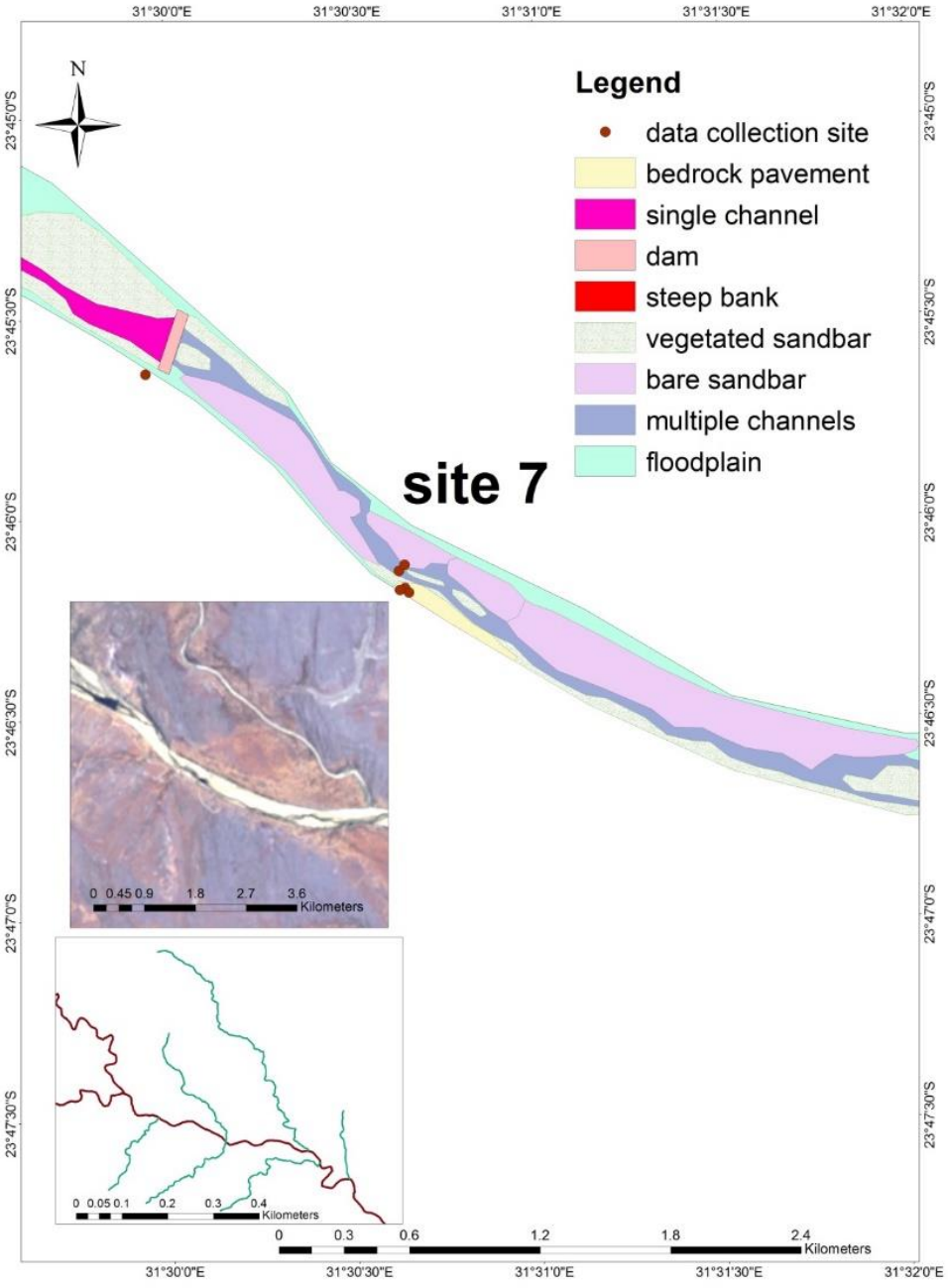


Fig. 5.11: Geomorphic features at site 7.

Site 8 (23˚48.640'S, 31˚33.929'E)

The Nwanedzi River is a tributary of the Letaba River and it was dry at the time of sampling. The river valley is up to 12 m wide, representing one of the largest tributaries to the Letaba River. The river is characterised by a steep scarp face 4 m high and contains a fining upwards sequence of grain size distributions indicating the deposition of cobbles during previous flood events (Fig. 5.12). The river bed consists of gravel between 2 mm and 30 cm in diameter.



Fig. 5.12: Image of the wide and dry Nwanedzi River, a tributary of the Letaba River, at site 8. The arrow indicates the flow direction.

Site 9 (23˚ 50.149'S, 31˚34.990'E)

This channel reach consists of four flat-topped sand bars and a sinuous main channel (Fig. 5.13a). The sandbars are 30 cm to 1 m high, followed by a lower elevation inactive channel with coarse grained sediment, parallel to the main active channel. The main active channel consists of sandbars covered by vegetation, and the channel is divided into three channels 2 to 8 m wide, which converge and divide continuously in this river reach. The river bank is 20 cm in height and contains abundant reeds. This river reach also consists of a shallow backwater channel perpendicular to the active channel (Fig. 5.14). This channel is 4 m wide and is characterised by shallow ponds and boulders up to 5 cm in diameter and likely gets filled during heavy rainfalls. The river is surrounded by a steep scarp slope up to 2 m high eroded by floodwaters. Fig. 5.13b shows the cross section of an eroded sandbar indicating different periods of sheet flows, with fine grained sediment at the bottom and coarse sediment at the top layers.

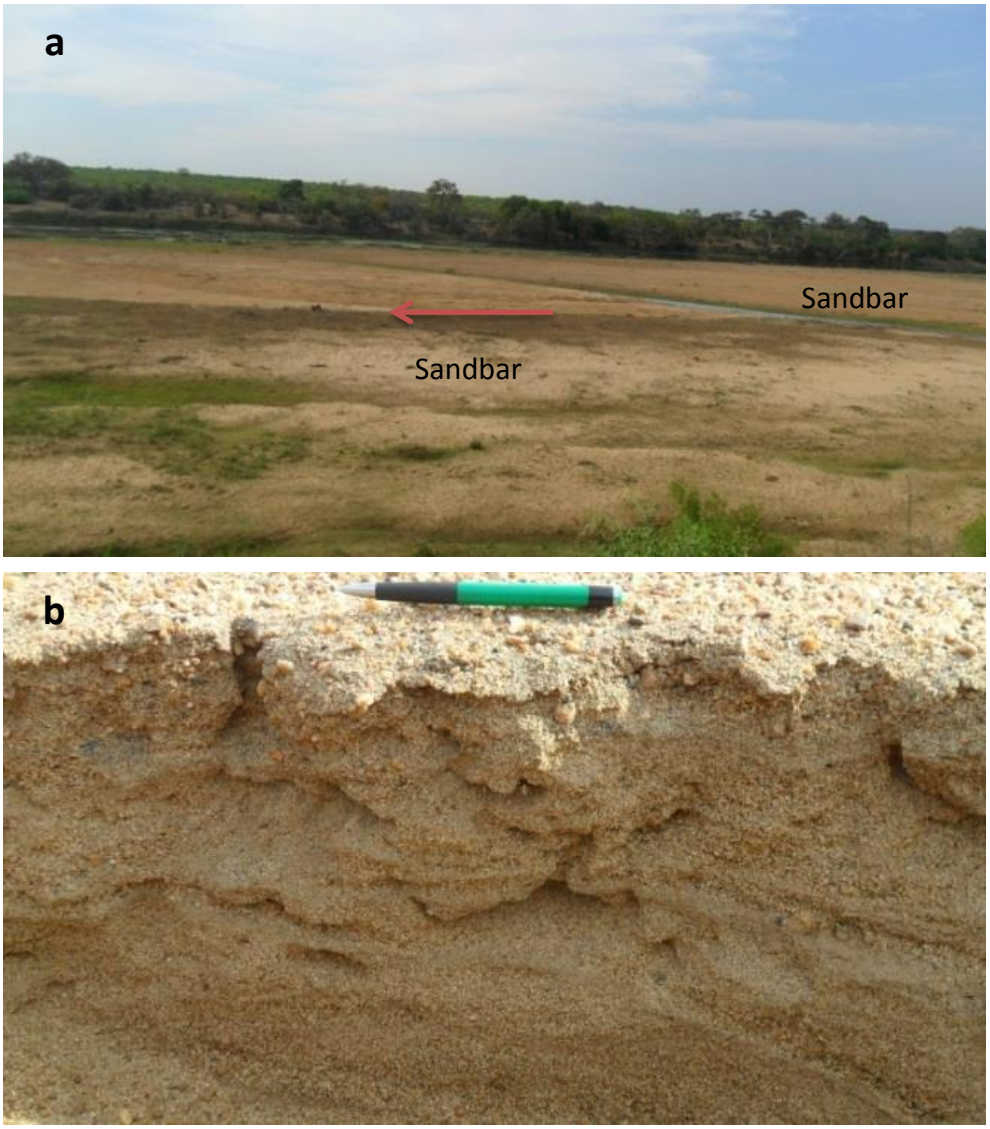


Fig. 5.13: (a) View of flat-topped sandbars on the floodplain and position of the present day active channel, site 9. The red arrow indicates the flow direction. (b) View of the different layers of a flat topped sandbar. Pen indicating scale.

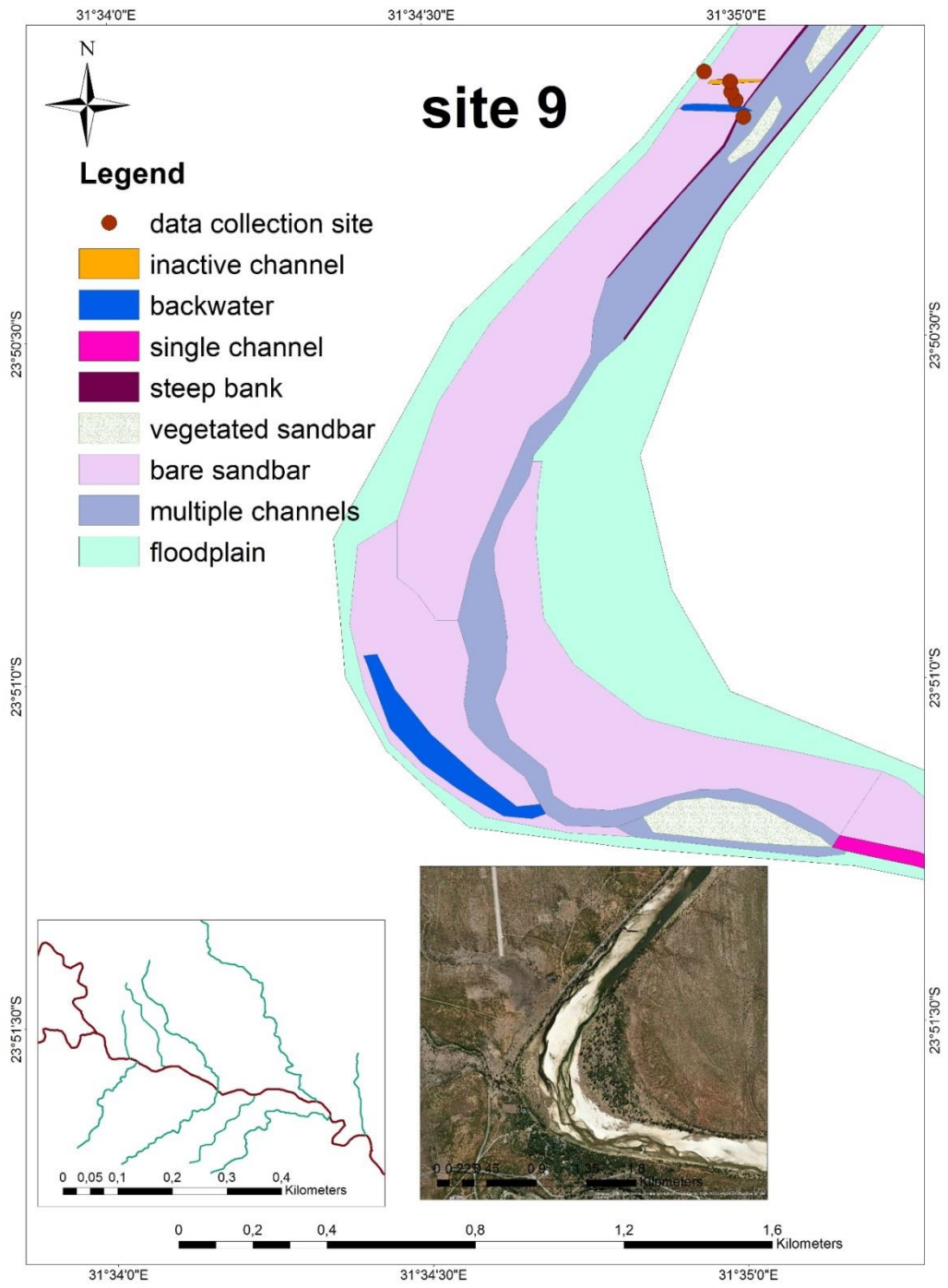


Fig. 5.14: The geomorphic features at site 9 and data collection sites indicated in red.

Site 10 (23˚50.199'S, 31˚37.736'E)

This river reach is fairly straight with no bedrock outcrops or sand bars present within the river channel (Fig. 5.15). The river bank is flat with water hyacinth present along the edge of the river channel. Vegetation is prominent and reduces in quantity away from the river bank until there is only grass present. Tall trees are present just after the shallow scarp slope of the river. This river reach is made up only one single wide river channel (Fig. 5.16a). The transect of this river has a concave profile, starting off as steep, followed by a shallow

profile and ends off with a slight increase in height associated with the active channel (Fig. 5.16b).



Fig. 5.15: Image (a,b) of the Letaba River upstream of the Engelhardt dam. The river consists of a straight deep channel, with no outcrops. The red arrows water flow direction.

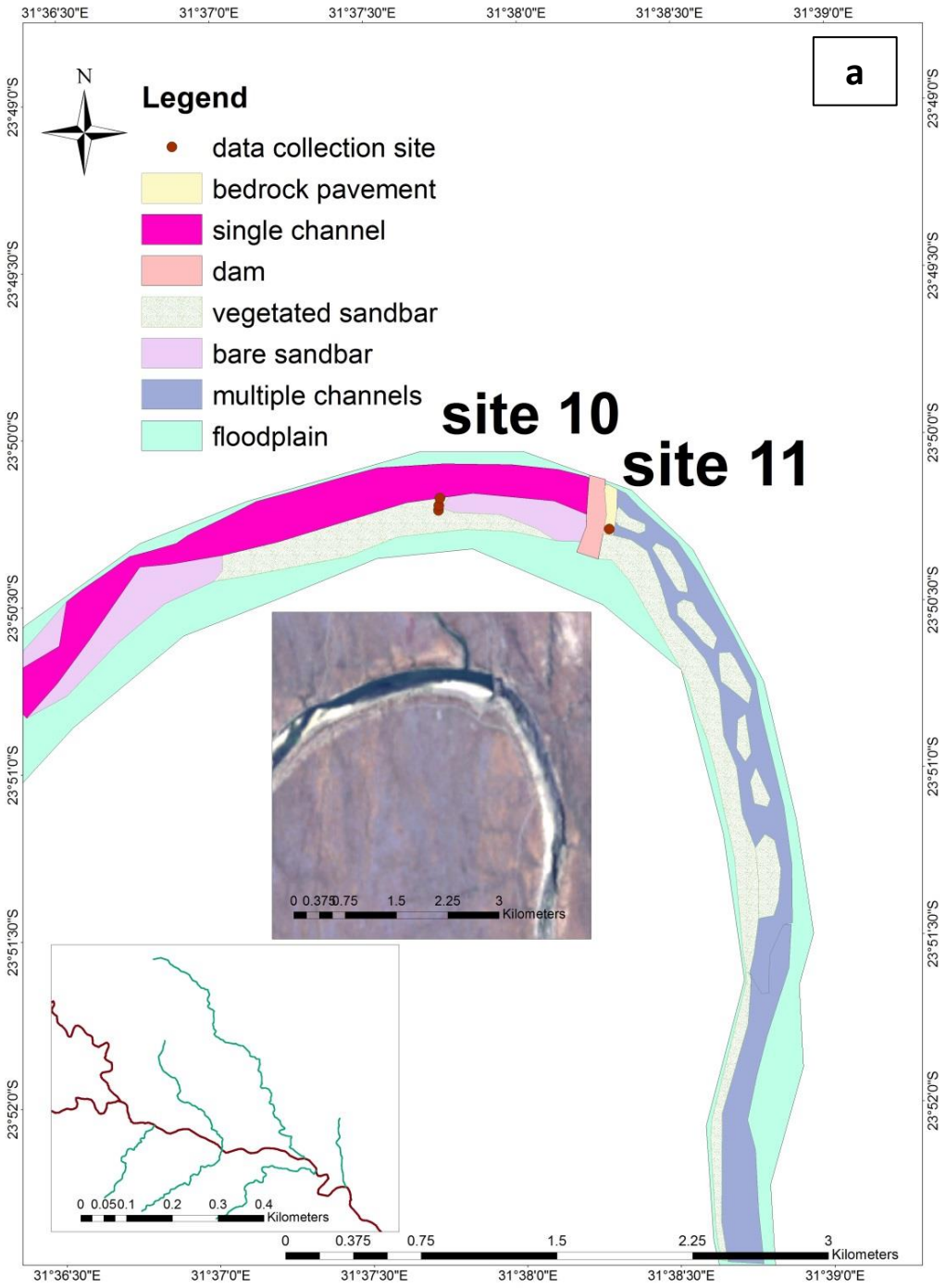


Fig. 5.16: (a) The geomorphic features at site 10 and site 11.

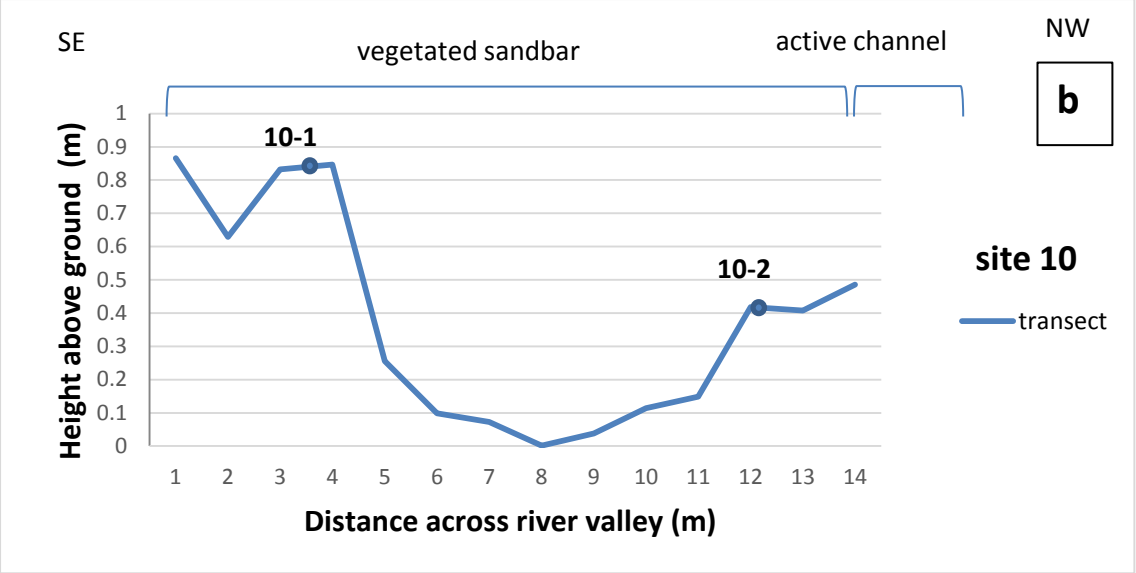


Fig. 5.16: (b) The transect and sample numbers at site 10.

Site 11 (23˚50.279'S, 31˚39.182'E)

This river reach represents the area downstream of the Engelhardt Dam within the Letaba River (Fig. 5.17). A total of three shallow channels were observed with both sandbars and bedrock present between the channels. The sand bars are partially vegetated with grass, water hyacinth and *Phagmites mauritianus* (Fig. 5.17a). A northeast dipping bedrock pavement composed of granite and basalt is present where the dam structure is built. The river bank is flat, however the scarp slope is up to 2 m high.



Fig. 5.17: Image of the river just downstream the Engelhardt Dam, characterised by bedrock outcrops and sandbars. Red arrow indicates water flow direction.

Site 12 (23˚53.241'S, 31˚39.182'E)

A basalt bedrock pavement dominates this river reach with about 20% vegetation and 5% fine grained sediment between the outcrops (Fig. 5.19a). A total of 5 deep channels meander between the bedrock outcrops. The river bank is fairly flat with a steep scarp slope 3 m high surrounding the river channel. Fig. 5.18b shows a mix of poorly sorted quartz, granite, diorite and basalt cobbles, indicating sediments washed in and deposited by high water discharge. The floodplain consists of sand bars 30 cm in height just before the river bank. The river transect indicates a steep erosional slope and uneven river profile due to the diorite outcrops present within the channel (Fig. 5.19b).



Fig. 5.18: (a) Site 12 characterised by bedrock outcrops. (b) A 20/20 cm square indicating the cobbles present in this reach.

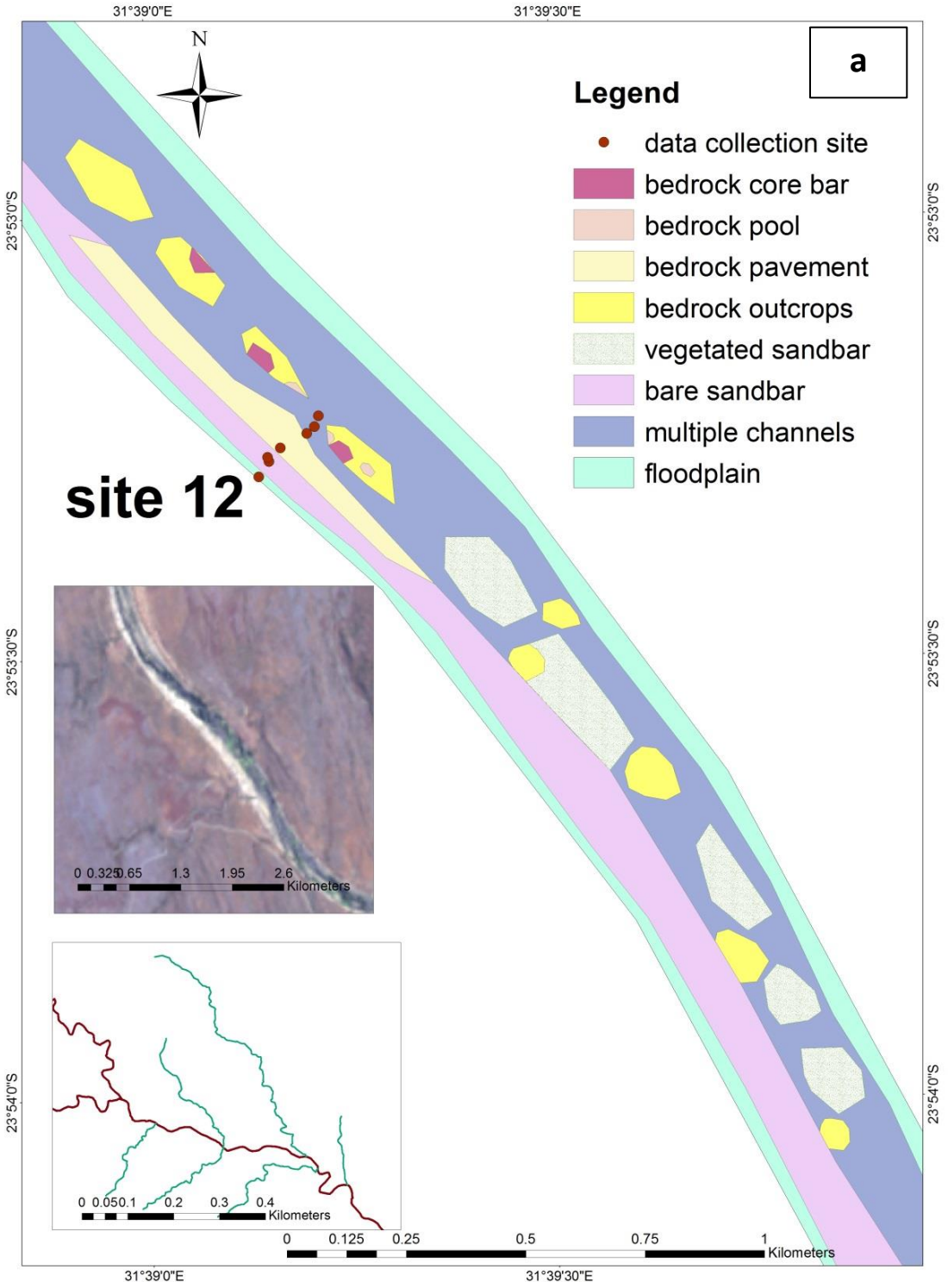


Fig. 5.19: (a) Geomorphic features at site 12. The red dots indicate the area where the transect was taken.

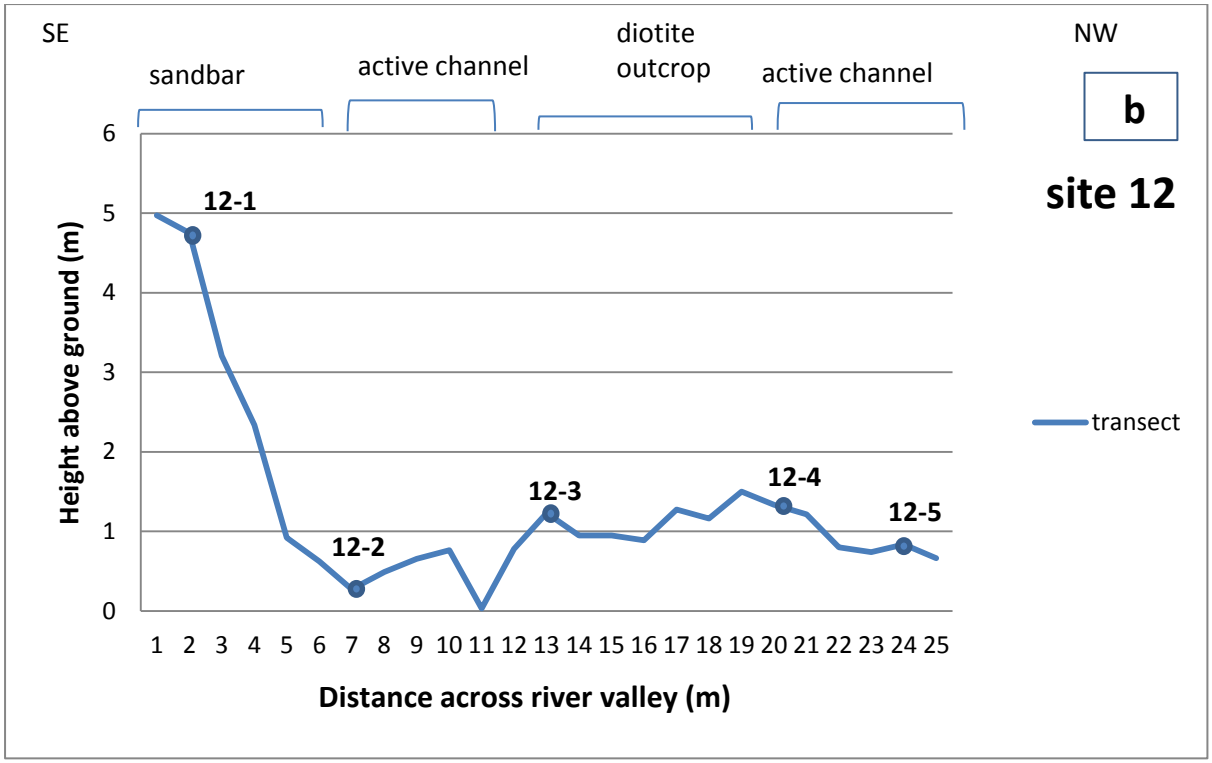


Fig. 5.19: (b) The river profile and sample numbers at site 12.

Site 13 (23˚54.873'S, 31˚41.633'E)

This river reach is characterised by abundant diorite outcrops 40 cm to 2 m high with coarse sand and very little vegetation between the outcrops (Fig. 5.20). The river begins with a break in slope of the river bank and consists of multiple channels 2 to 10 m wide flowing between diorite outcrops. Bedrock cored bars are dominant features at this site (Fig. 5.21a). The floodplain consists of fine sand to gravel (up to 2 cm in diameter), with little to no vegetation present. The sediment on the floodplain coarsens away from the main channel. A diorite boulder bed is present 50 m from the main river channel. The floodplain also consists of elongate clusters of gravel, indicating that the river flowed on the floodplain at some point. The transect of the river shows an uneven valley profile due to the presence of bedrock outcrops on the floodplain and within the river (Fig. 5.21b).

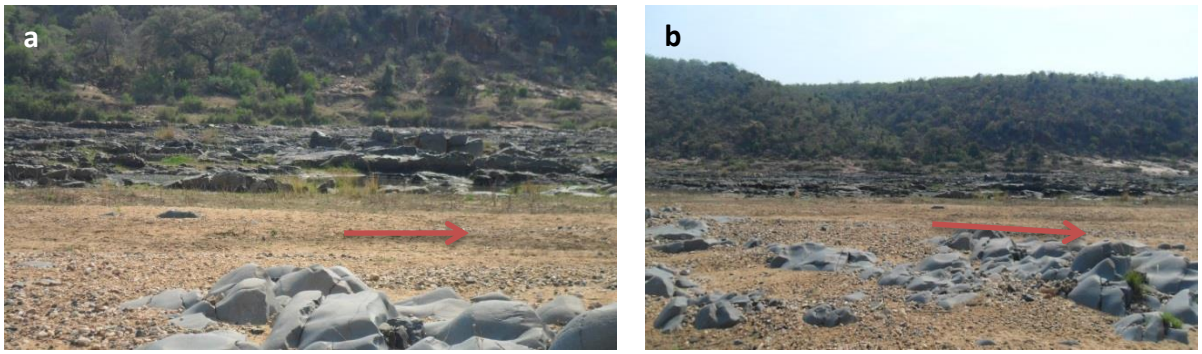


Fig. 5.20: (a,b) View of site 13 showing the river reach characterised by multiple channels flowing between diorite outcrops. The red arrows indicate flow direction.

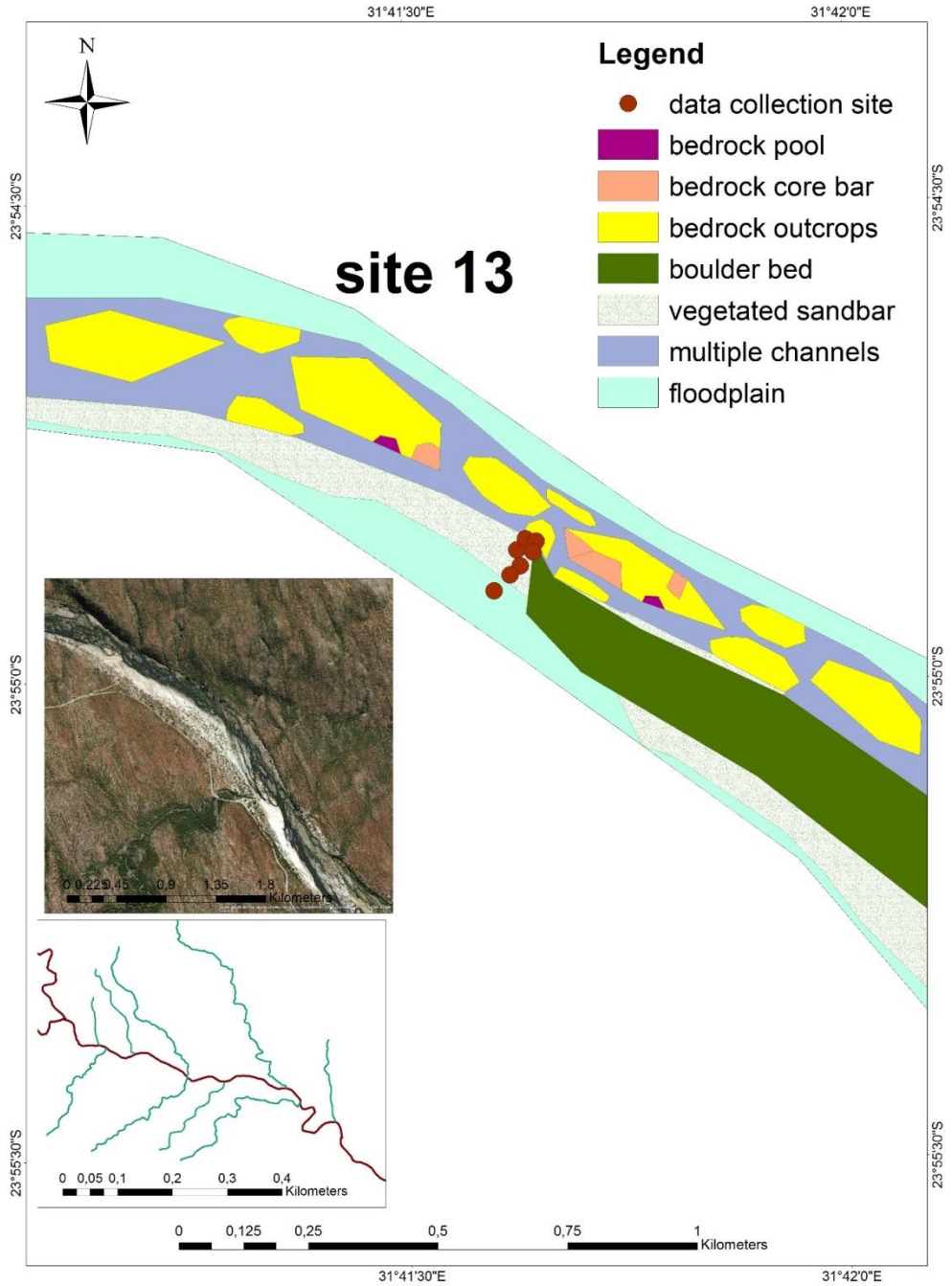


Fig. 5.21: (a) Geomorphic features at site 13. The red dots indicate where the transect was taken.

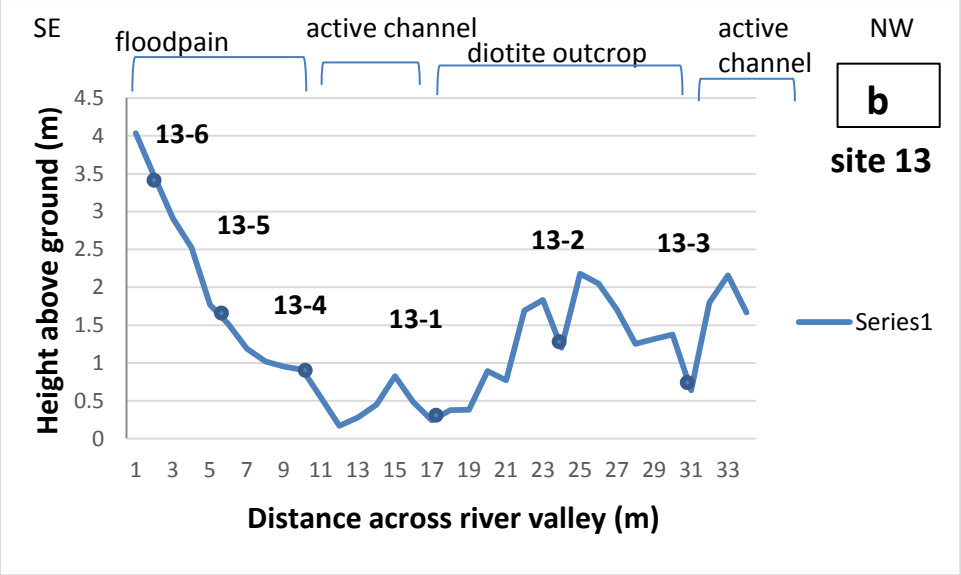


Fig. 5.21: (b) The river profile and sample numbers along site 13.

Site 14 (23˚54.594'S 31˚43.869'E)

A low water bridge divides the channel and ultimately influences the channel types present in this river reach (Fig. 5.22). The upstream side of the bridge is covered in coarse sediment forming sandbars, with three (2 m wide) bedrock outcrops visible between the sediment (Fig. 5.22a, b). The bedrock outcrops are covered with circular potholes which are indicative of abrasion during high water levels (Fig. 5.22c). The low water bridge acts as a barrier to hinder sediment movement, however water moves through the bridge which separates the channel into multiple channels (Fig. 5.22a) separated by patches of water hyacinth and bedrock outcrops. Approximately 5% cover of fine sediment is present between the outcrops. A bedrock pavement 6 m long is present on the floodplain with sandbars and vegetation dominating the floodplain on the downstream side of the river (Fig. 5.23a). The transect of the river shows a flat river valley, with a steep erosional lateral slope (Fig. 5.23b).



Fig. 5.22: (a,b) View of low-water bridge at site 14 which acts as a barrier to trap sediment and only allows very little water and sediment to pass through. (c) Bedrock outcrop covered in round potholes. The arrows indicate flow direction, the marker indicates scale.

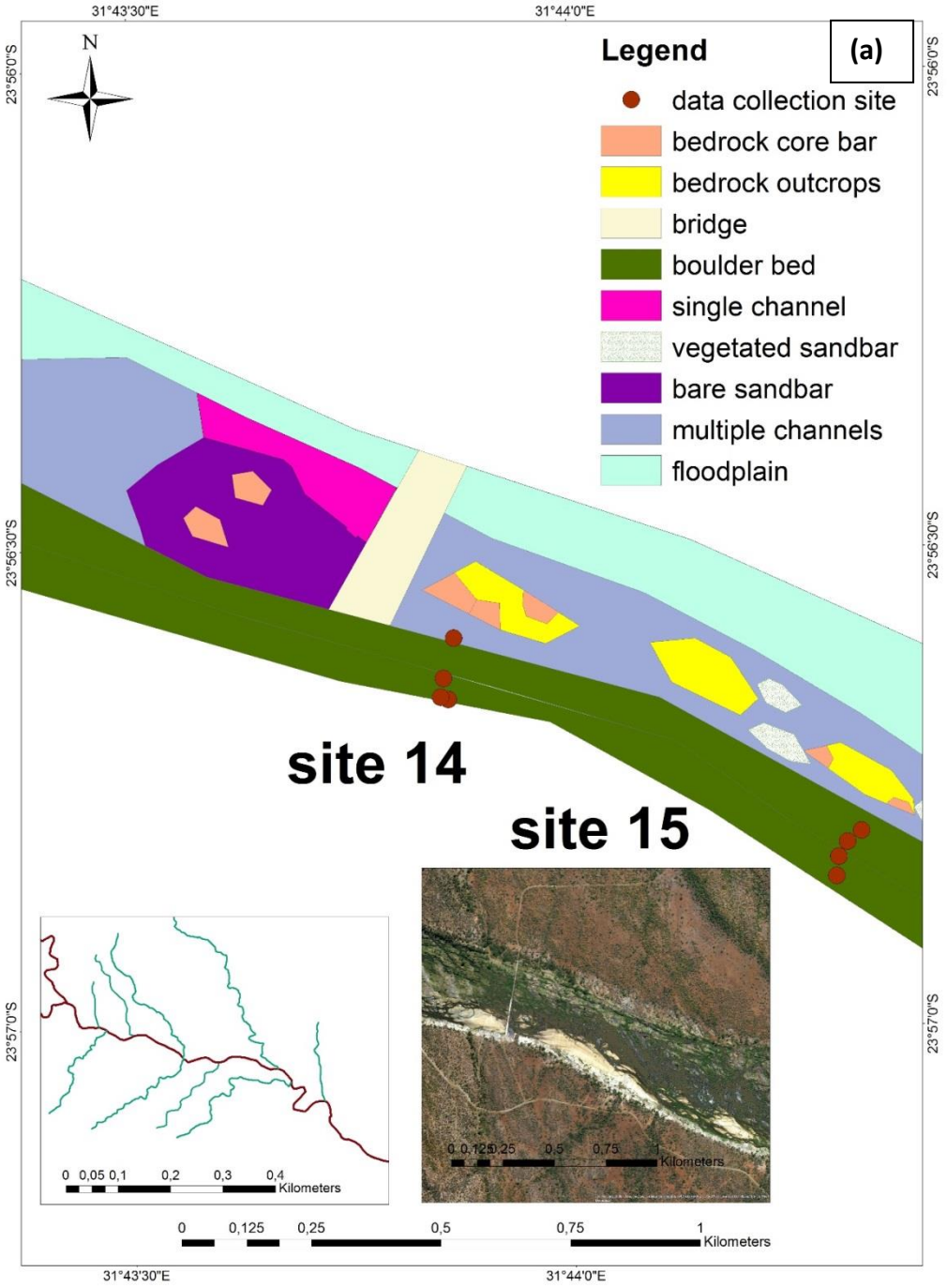


Fig. 5.23: (a) Geomorphic feature at site 14.

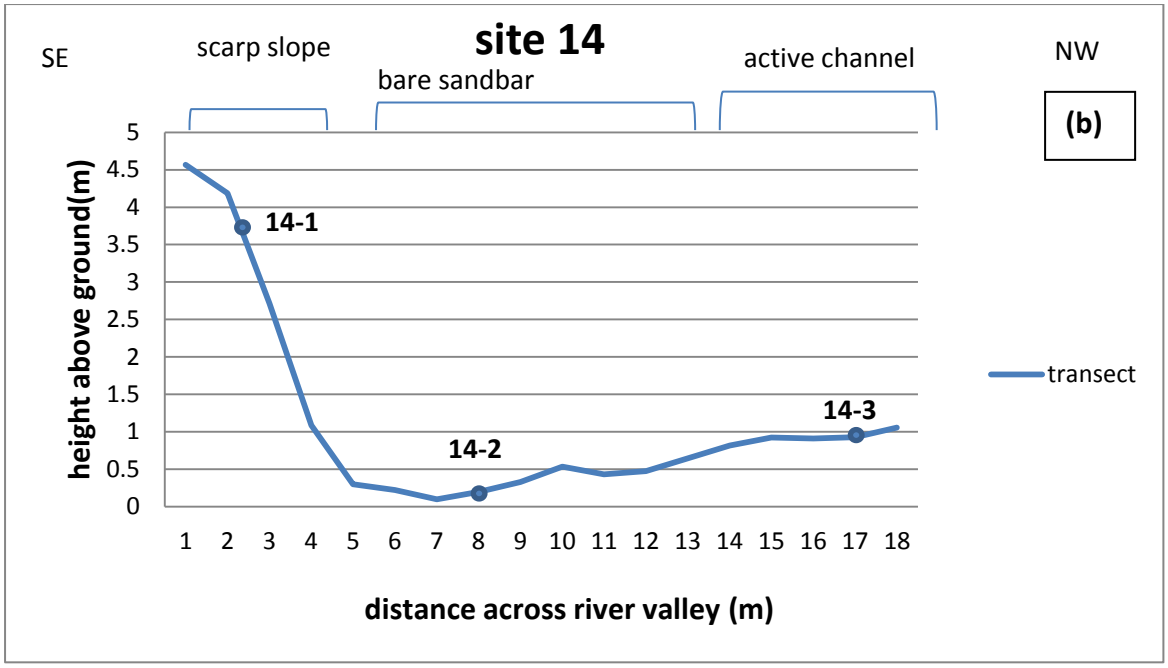


Fig. 5.23: (b) The transect and sample numbers at site 14.

Site 15 (23˚56.819'S, 31˚44.318'E)

Bedrock outcrops and sediment are present between the multiple channels in this river reach, representing a mixed bedrock-alluvial channel (Fig. 5.24a). Basalt bedrock outcrops, about 30 cm to 50 cm high, divide five shallow channels with around 50% coarse sediment, forming sandbars between the channels. The floodplain is characterised by boulders of up to 1.5 m diameter, which make up 60% of the floodplain (Fig. 5.24b). These boulders consist of sandstone, basalt, diorite and granite. These boulders represent periods of flooding as only water moving at a high velocity can deposit boulders of this size. Scour and abrasion marks are present on the boulders indicating contact between the boulders during transport (Fig. 5.24c). About 80% of the water in this river reach is covered by water hyacinth, with backwater ponds formed adjacent to the main river channel. The transect of the river indicates an uneven floodplain due to the large boulders present (Fig. 5.25).



Fig. 5.24: (a) View of mixed bedrock and alluvial river at site 15, (b) boulders up to 1.5 m diameter deposited on the floodplain, (c) abrasion marks present on a boulder on the floodplain (blue arrow). Red arrows indicate flow direction.

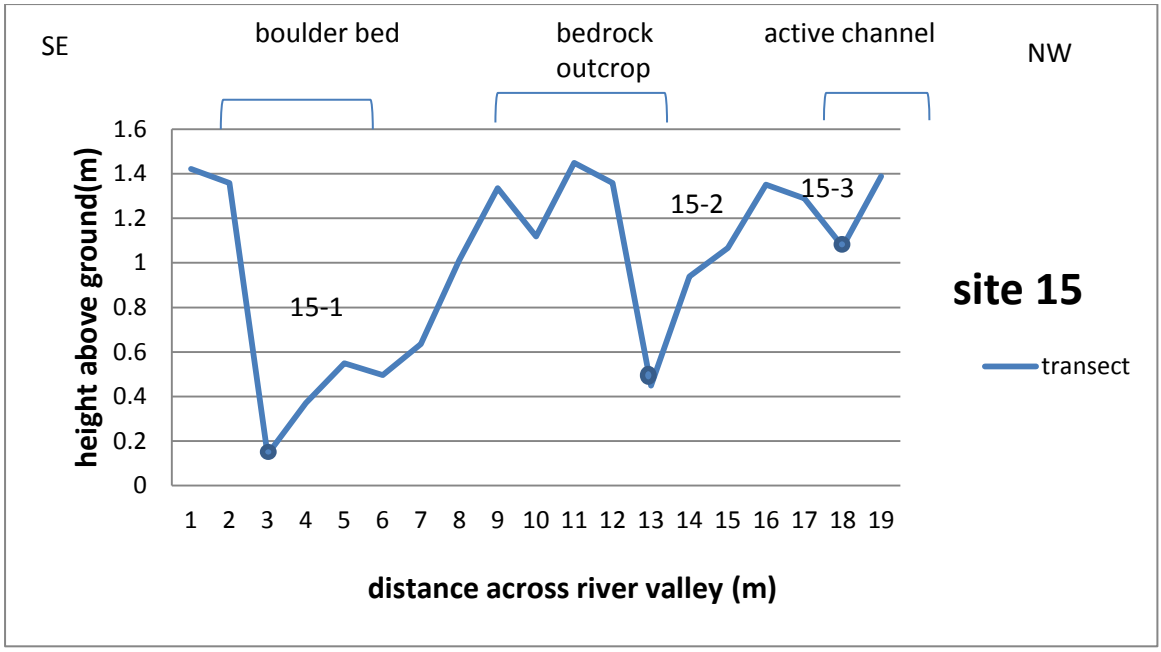


Fig. 5.25: The transect and sample numbers at site 15. The location of site 15 is shown in Fig. 15.23a.

5.3 Grain size analysis

5.3.1 Grain size distributions

The Letaba River consists of variable grain sizes ranging from large boulders, gravel, sand sized particles and fine to very fine particles. When considering the river from upstream to downstream, overall sediments are moderately sorted to moderately well sorted, representing 45% and 33% of all samples respectively. Mean grain size increases in a downstream direction with a range in particle size from 0.016 µm to 2.5 mm diameter (Fig. 5.26). The kurtosis values range from 0.664 to 1.669, indicating mesokurtic to very leptokurtic distributions (Fig. 5.27). The majority (49%) of samples are mesokurtic, with the rest of the samples displaying leptokurtic (41%), very leptokurtic (6%), platykurtic (2%) and very platykurtic (2%) distributions (Fig. 5.27). Sediments characterised by high kurtosis values are moderately well sorted to poorly sorted. Skewness values range from -0.529 to 0.266 indicating fine skewed to very fine skewed symmetry (Fig. 5.28). The grain sizes display a distribution which is coarse skewed, symmetrical, fine skewed and very fine skewed, with fine skewed symmetry being dominant (Fig. 5.28). Overall, 88% of the samples are negatively skewed indicating deposition in low energy environments.

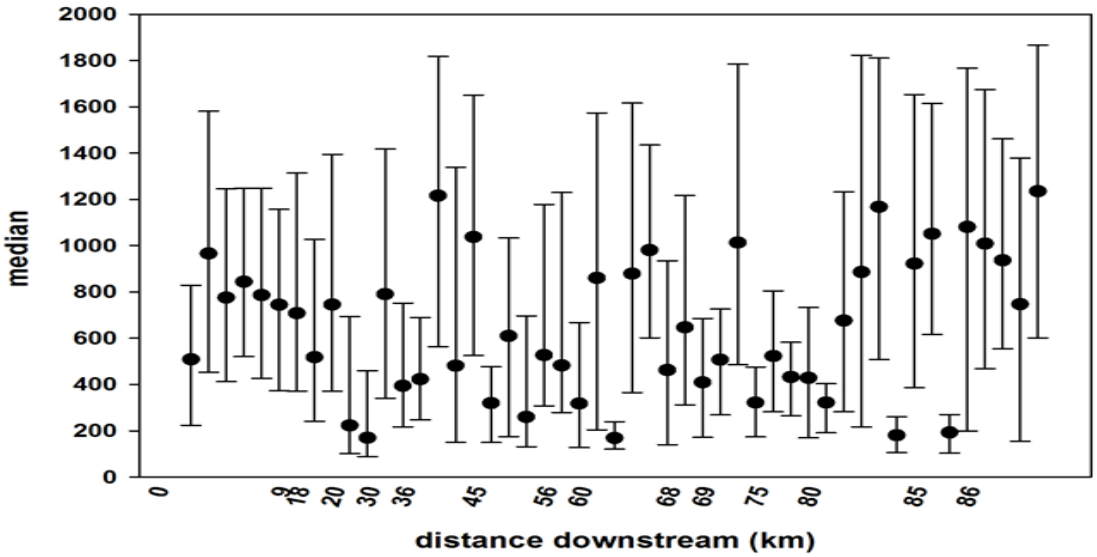


Fig. 5.26: The median grain sizes throughout the Letaba River within KNP.

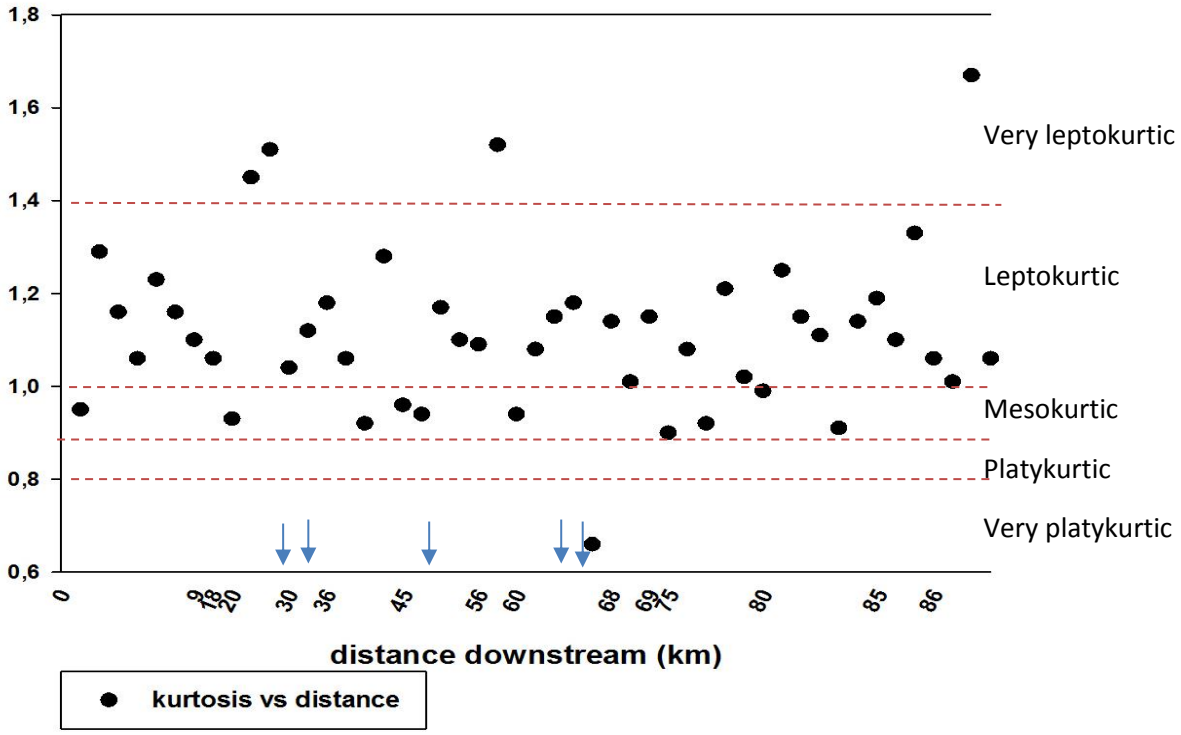


Fig. 5.27: Scatter plot of kurtosis values of sediment within the Letaba River, in a downstream direction. The blue arrows indicate the locations of tributaries.

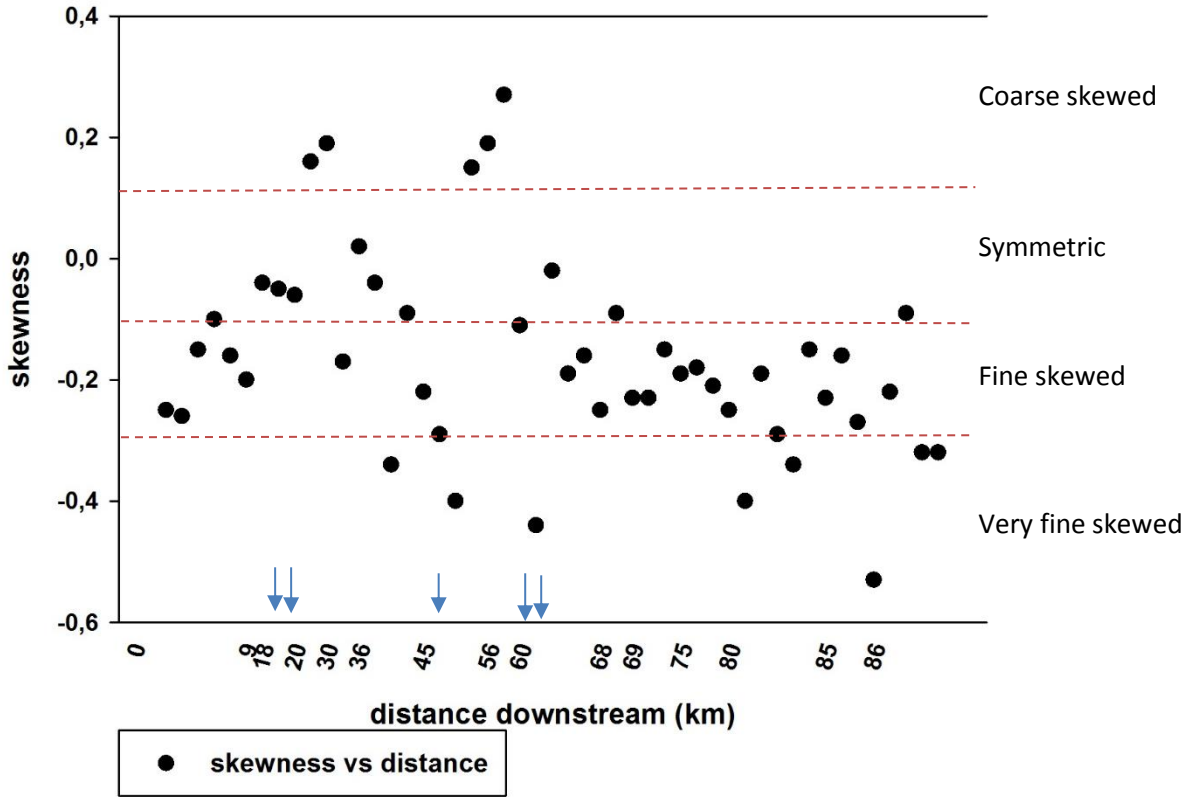


Fig. 5.28: Scatter plot of skewness values of sediment within the Letaba River, in a downstream direction. The blue arrows indicate the locations of tributaries.

The majority of the sediment collected is moderately sorted (45%) or moderately well sorted (33%) (Fig. 5.29). Only 7 (14%) of the samples are poorly sorted and 4 (8%) samples are well sorted. There is no visible trend in the sorting values from upstream to downstream, which could be because the samples were collected from different geomorphic features, which are governed by variable hydraulic processes. Samples from tributaries range from moderately well sorted to poorly sorted. The sediment collected from the non-perennial tributary and the Shambali River is moderately sorted. Sediment from the Makoforo River is moderately well sorted; while sediment from the Nwanedzi River is moderately sorted to poorly sorted.

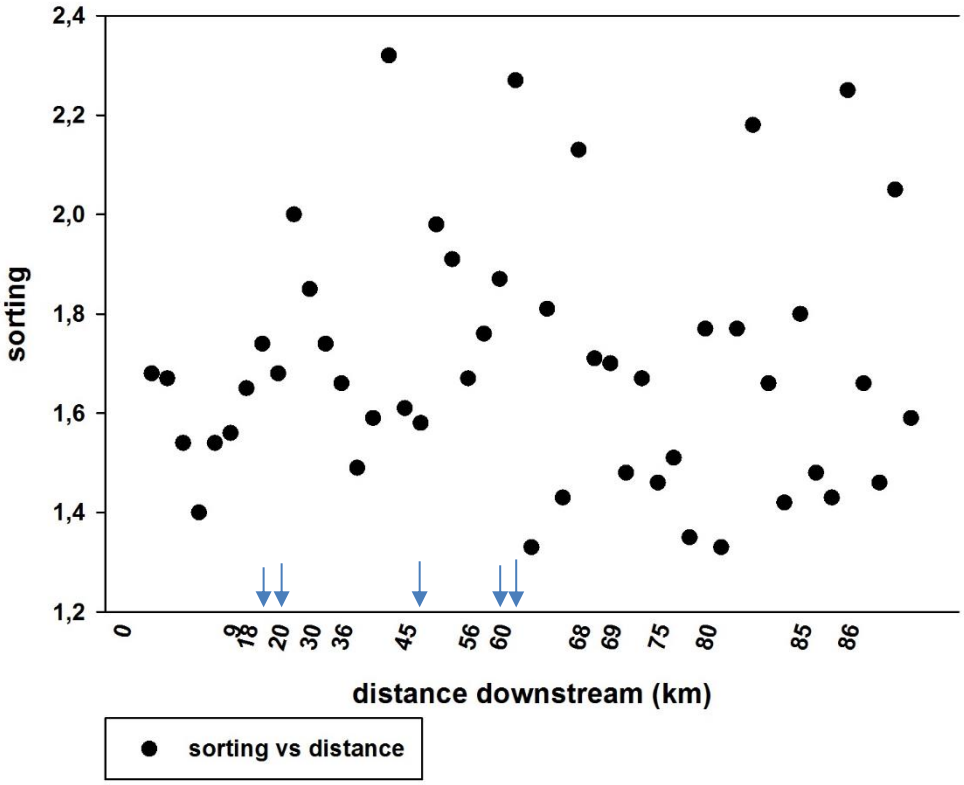


Fig. 5.29: Sorting values for individual samples from upstream to downstream. The blue arrows indicate the tributaries.

5.3.2 Grain sizes on different geomorphological features

Sediment samples were grouped according to where they had been collected, in order to see how the sediment is stored in different landforms of the river. These groups include sediment collected on bedrock and sandbars separating the channels, on the floodplain, on active channels, on the channel banks, and from tributaries. The downstream increase in sediment grain size is more visible from floodplain deposits (Table 5.1). The sediment on the floodplain is stored as sandbars, between vegetation, and as unconsolidated sand sheets. Sediment is medium to coarse sand with grain size ranging from 181 to 1155 µm. The sediment is moderately to well sorted with kurtosis values between 0.94 and 1.45 (mesokurtic to leptokurtic). Sediment is also stored as bedrock-cored bars in which sediment is stored in hollows between outcrops within an active river channel. This sediment is either deposited during high water levels or formed by bedrock weathering. This sediment is medium to coarse sand with grain sizes ranging from 105 to 1784 µm and with standard deviation of 1.33 to 2.18, indicating moderately to well sorted. Sediment stored as sandbars within the active channel, that separate the channel into multiple channels, is negatively skewed, indicating deposition in a low energy environment (McLaren and Bowles, 1985). The tributary beds consist of slightly very fine gravelly sand to coarse sand with mean grain sizes of 292 to 735 µm, and contribute medium to coarse sand when entering the

Letaba River. However, sediment from the tributaries display the lowest mean grain sizes, possibly because there were only a few samples collected.

Table 5.1: Mean grain size values (µm) of samples from different geomorphic features.

	Sandbar	**Bedrock**	**Active channel**	**Tributary**	**Floodplain**
Mean grain size (µm)	753.80 419.60 460.30 1011.20 538.30 858.20 960.70 514.70	980.50 302.60 396.70 418.30 634.00 811.10 173.40 1075.30	834.60 175.60 171.10 1121.10 564.30 876.80	516.10 735.80 295.40 670.00 292.70	471.90 925.10 709.70 224.90 504.50 278.00 634.20 383.40 485.00 307.00 1032.40 181.30 803.50 922.90 1155.50
Total no. of samples	8	8	6	5	15

5.3.3 Impact of tributaries

In order to fully understand the impact of tributaries on sediment characteristics, the grain sizes of samples on the main river upstream and downstream of the tributaries were compared (Table 5.2). The mean grain sizes before the tributary are lower compared to mean grain sizes after the tributary entry. This increase is possibly caused by coarser sediment contributed to the main channel by the tributaries. The sediment before and after tributaries are negatively skewed, indicating fine skewed sediment distributions from the tributary into the main river. Kurtosis values in the upstream reach (site 1) decrease after the sediment has mixed (values changing from 1.097 to 1.057, respectively). Kurtosis values at sites 12 and 13 increase from 0.929 to 1.446. Sorting values from site 10 and 11 change from moderately well sorted before the tributary to moderately sorted after the tributary. The sediment samples were collected from different parts of the channel where geomorphic features may have controlled flow conditions. Hence, this could be the reason why the grain sizes are distributed this way.

Table 5.2: Mean grain sizes, sorting, skewness and kurtosis values before and after incoming tributaries

Grain size characteristics	Site 10 and site 11		Site 12 and 13		Site 6		Site 1	
	Before	After	Before	After	Before	After	Before	After
Mean grain size (μm)	434	980.5	387.86	767.166	292.7	1121.1	709.7	834.6
Sorting	1.59	1.667	1.484	1.719	1.576	1.594	1.647	1.396
Skewness	-0.229	-0.154	-0.058	0.157	-0.298	-0.342	-0.041	-0.103
kurtosis	1.08	0.899	0.929	1.446	0.959	1.056	1.097	1.057
n	2	1	5	6	1	3	1	6

5.4 Grain size and underlying geology

The percentages of the different grain size intervals in all the samples are indicated in Fig. 5.30. It can be seen that the grain sizes of the sampled sediment differ considerably throughout the variable river reaches. Very coarse sand and coarse sand dominate the sediments within this river, with only 6 of the samples being dominated by fine sand (Fig. 5.30). The percentages of the different grain size intervals are also indicated in Appendix B. Grain sizes are discussed with respect to the underlying geology in order to determine any relationship between these (Table 5.3). The confluence between the Klein and Groot Letaba rivers is underlain by granitic gneiss is characterised by a high percentage of coarse and very coarse sediment. The Shambali River, which is a tributary of the Letaba River, is underlain by gabbro and is characterised by very coarse to medium sand. Site 4, downstream of this tributary, is underlain by granodiorite and consists of fine to very fine sediment. Further downstream on the same bedrock type, there is an increase in medium sand which then becomes very coarse to medium sand with increased distance. Site 7 is underlain by sandstone and sediment is coarse to medium sand, with fine sand making up a very small percentage. The Nwanedzi River (site 8), another tributary of the Letaba River, is underlain by basalt and characterised by coarse to medium sand. The rest of the Letaba River is underlain by basaltic rock and follows the same trend of medium to coarse sand. At site 13, there is a sudden shift in the characteristics of the sediment. The percentage of very coarse sand increases, making up the majority of the sediment.

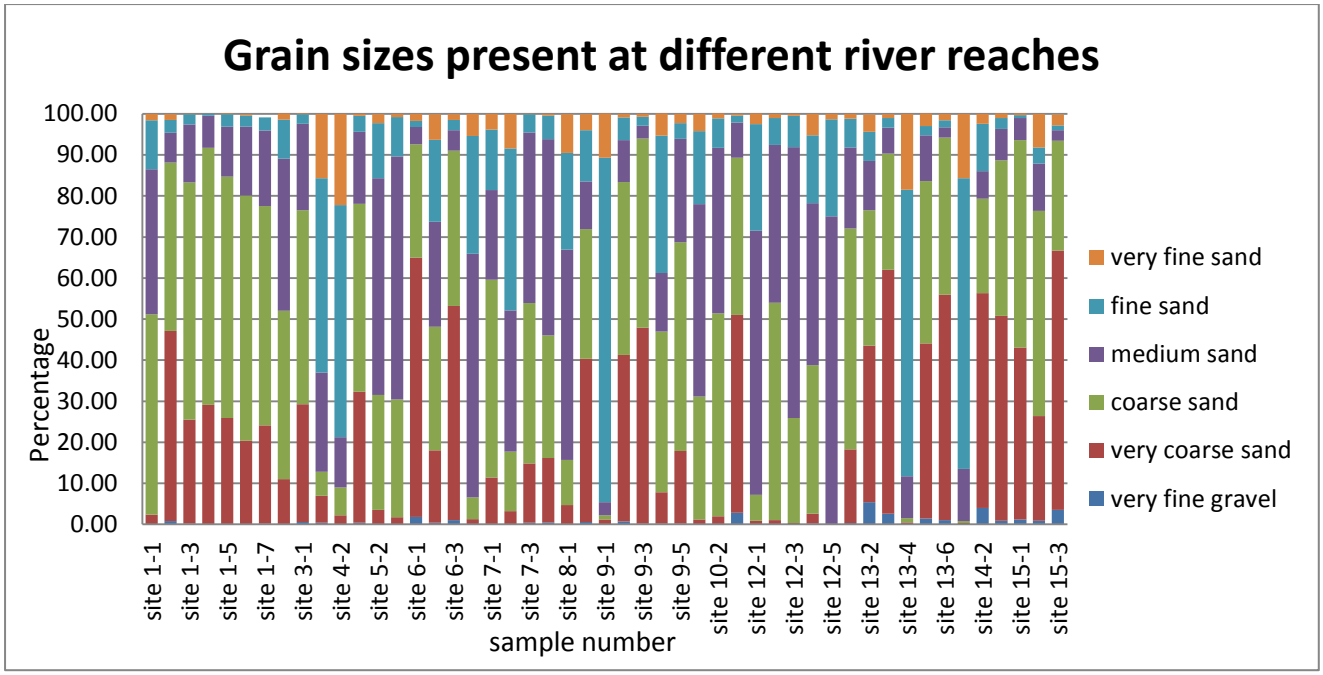


Fig. 5.30: Grain size distributions at different channel reaches. The site numbers are arranged in a downstream direction.

Table 5.3: The underlying geology and the generalized grain size parameters of sediment collected along the Letaba River.

	Lithology		Grain size parameters				
		Sand size	Mean	Sorting	Skewness	Kurtosis	Mode
Site							
1	Leucocratic strongly migmatised biotite gneiss	Medium to coarse sand	471.9-925.1	1.396-1.677	Symmetrical to fine skewed negative (-0.25 to -0.04)	Mesokurtic to leptokurtic (0.95 to 1.23)	Unimodal to bimodal
2	Medium grained granodiorite/ tonalitic biotite gneiss	Coarse sand	516.1	1.741	Symmetrical (-0.05)	Mesokurtic (1.06)	Trimodal
3	Gabbro, olivine gabbro	Coarse sand	735.8	1.676	Symmetrical (0.06)	Mesokurtic (0.93)	Unimodal
4	Medium grained granodiorite/ tonalitic biotite gneiss	Fine sand	224.9-175.6	1.845-2.002	Coarse skewed (0.16 to 0.19)	Leptokurtic to very leptokurtic (1.45 to 1.51)	Trimodal to polymodal
5	Medium grained granodiorite /tonalitic biotite gneiss	Medium to fine sand	402.7-753.8	1.494-1.736	Symmetrical to fine skewed (-0.04 to 0.02)	Mesokurtic to leptokurtic (1.04 to 1.18)	Unimodal to bimodal

6	Medium grained granodiorite/ tonalitic biotite gneiss	Medium to very coarse sand	292.7-1121.1	1.576-2.319	Symmetrical to very fine skewed (-0.34 to -0.09)	Mesokurtic to leptokurtic (0.92 to 1.28)	Unimodal to polymodal
7	Fine grained sandstone, siltstone	Medium to coarse sand	278-564	1.673-1.983	Very fine skewed to coarse skewed (-0.40 to 0.27)	Mesokurtic to leptokurtic (0.94 to 1.17)	Unimodal to trimodal
8	Basic volcanic rocks (tholeiitic, picrite basalts)	Medium to coarse sand	295.4-670	1.868-2.274	Very fine skewed to fine skewed (-0.44 to -0.11)	Very leptokurtic to mesokurtic (0.94 to 1.52)	Bimodal to trimodal
9	Basic volcanic rocks (tholeiitic, picrite basalts)	Fine to coarse sand	171.1-960.7	1.33-2.128	Symmetrical to fine skewed (-0.25 to -0.02)	Leptokurtic to very platykurtic (0.66 to 1.18)	Unimodal to trimodal
10	Basic volcanic rocks (tholeiitic, picrite basalts)	Medium sand	383.4-485	1.479-1.702	Fine skewed (-0.23)	Mesokurtic to leptokurtic (1.01 to 1.15)	Bimodal to polymodal
11	Basic volcanic rocks (tholeiitic, picrite basalts)	Coarse sand	980.5	1.677	Fine skewed (-0.15)	Platykurtic (0.90)	Unimodal
12	Basic volcanic rocks (tholeiitic, picrite basalts)	Medium to coarse sand	302.6-514.7	1.332-1.771	Very fine skewed to fine skewed (-0.40 to -0.19)	Mesokurtic to leptokurtic (0.92 to 1.21)	Unimodal to trimodal
13	Basic volcanic rocks (tholeiitic, picrite basalts)	Fine to very coarse sand	634-1075.3	1.417-2.183	Very fine skewed to fine skewed (-0.39 to -0.19)	Mesokurtic to leptokurtic (0.91 to 1.25)	Unimodal to polymodal
14	Basic volcanic rocks (tholeiitic, picrite basalts)	Fine to coarse sand	181.3-968.6	1.43-2.245	Fine to very fine skewed (-0.22 to -0.53)	Mesokurtic to leptokurtic (1.06 to 1.33)	Unimodal to trimodal
15	Basic volcanic rocks (tholeiitic, picrite basalts)	Coarse to very coarse sand	691.8-1155.5	1.461-2.052	Symmetrical to very fine skewed (-0.32 to -0.09)	Mesokurtic to very leptokurtic (1.01 to 1.67)	Unimodal to bimodal

5.5 Mineral analysis

5.5.1 Heavy mineral assemblages

The modal abundance of different minerals was analysed using a petrographic microscope. The heavy minerals that were identified from sediment samples include clinopyroxene, olivine, hornblende, biotite, zircon, orthopyroxene, muscovite, garnet, epidote, rutile, tourmaline and zoisite, with quartz, plagioclase and orthoclase making up the light minerals (Table 5.4).

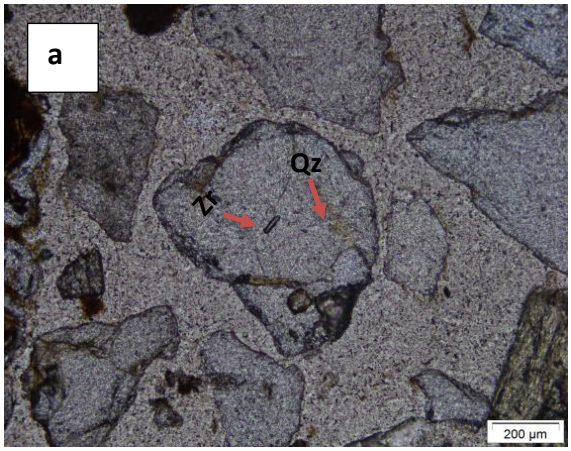
The most abundant mineral is quartz, followed by biotite and muscovite. Opaque minerals make up between 11.6% to less than 1%, with magnetite being the most dominant opaque mineral. The grain sizes of the minerals also vary from fine to coarse at different river reaches. An example of the different sizes of olivine grains at site (9) and (14) can be seen in Fig. 5.31 (l) and (n). Minerals such as zircon also exist as inclusions in quartz grains as can be seen in Fig. 5.31 (a-d). Site 1 at the confluence of the Groot and Klein Letaba rivers is underlain by migmatised biotite gneiss. There is abundance of orthopyroxene and muscovite in samples from this site with orthopyroxene making up 33.2% of the heavy minerals present. Site 4 is underlain by granodiorite and contains high values of clinopyroxene, magnetite (7.4%), biotite (17.8%) and muscovite (12%). Site 7 is underlain by fine grained sandstone and siltstone. Sediment in this site is abundant in clinopyroxene, micas and zoisite. The sediment at site 9, which is underlain by basalt, is abundant in olivine, biotite, epidote and rutile. Table 5.4 shows the mineral assemblages present at each site. Sites 1, 8 and 14 seem to be enriched by a similar source because of the presence of abundant orthopyroxene. The highest proportions of magnetite, Ilmenite and hematite are found in site 4, 5 and 13.

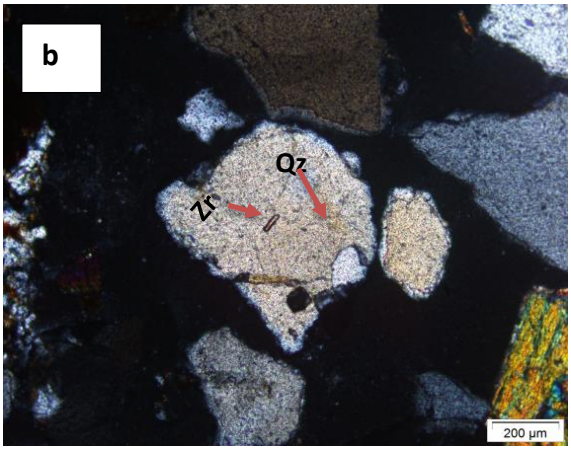
Table 5.4: Minerals of individual grains recorded at different river reaches (qtz=quartz, plag=plagioclase, ortho=orthoclase, cpx=clinopyroxene, olv=olivine, hbld=hornblend, bt=biotite, mg=magnetite, il=ilmenite, hm=hematite, opx=orthopyroxene, msc=muscovite, epd=epidote, zirc=zircon, rt=rutile, tour=tourmaline, gt=garnet). The rows highlighted in pink indicate samples from tributaries.

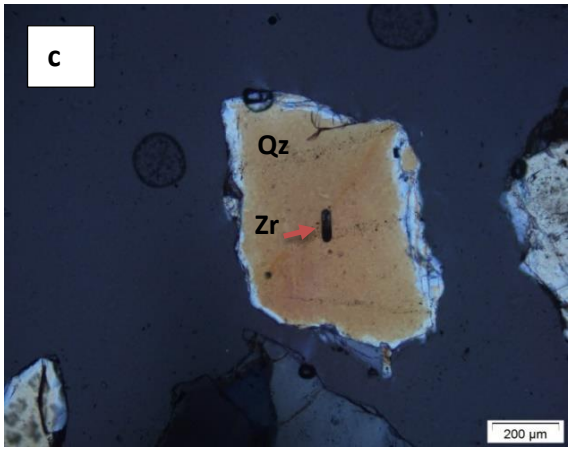
Site	qtz	plag	opx	cpx	olv	hbld	bt	mg	il	hm	opx	msc	epd	zirc	rt	tour	zoi	gt	n
1	150	10		13	4	7	22	23	8	10	138	13	5	4	9				416
2	201			24	28	7	7	12	3	3	10	30	3	10	30	3	1	1	373
3	171	15	6	20	2		20	8	2	4	10	15		10					283
4	311	5		17		3	111	46	14	33		75	7	13	8				623
5	263					13	68	70	25	35		40	20	11	51	6			602
6-4	282			9	5	5	18	8	4	3	2	8	7	4	15				370
6	388		4	23	5	7	70	9	3	4	11	32	8	4	39	2	2		611
7	273	2		31	2	9	102	27	13	15	9	95	22	1	20	7	4	1	632
8	174	9			21	12	40	18	16	16	15	29	9	13	27	2			401
9	342	10		11	15	8	35	19	7	10	6	36	25	8	16	6	4	1	559
10	221		5	12	5	3	18	17	8	11	11	29	10	6	9		2		367
11	239	6		28	15	9	122	9	5	10	10	96	43		73	19	1	4	689
12	235			24	5	10	58	20	10	10	7	36	14	12	34	10			485
13	266	15	5	28	14	5	12	42	11	19	19	28	7	6	13		2	3	495
14	212		3	5	9	8	18	9	4	5	38	15	10	15	14		2		367
15	219	6		35		13	177	21	7	9		33		4					517

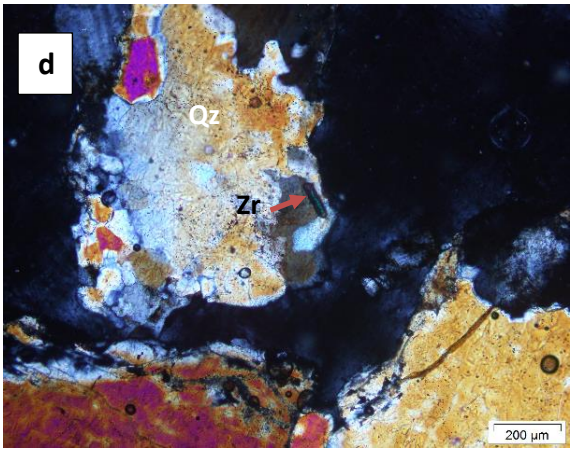
5.5.2 Heavy minerals in tributaries

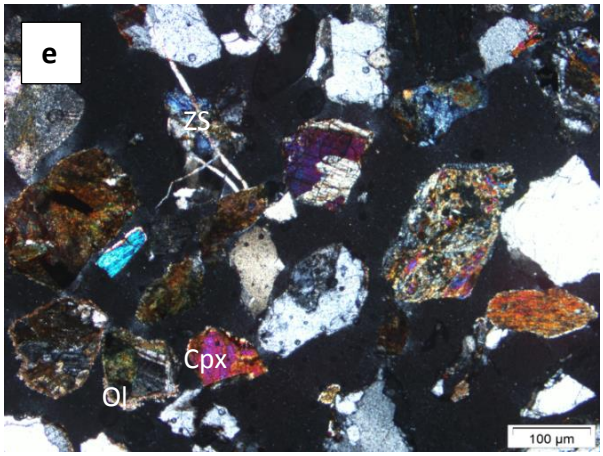
The tributaries pass through similar bedrock geologies as the main Letaba River. Site 2 is a non-perennial tributary. The sediment in this river is abundant in olivine (7.5%), clinopyroxene (6.4%) and muscovite (8.4%) (Table 5.4). Site 3 is the Shambali River which is underlain by coarse-grained gabbro. The sediment in this tributary is abundant in large subhedral clinopyroxene (7.06%) grains of about 5 µm in size, and abundant columnar zircon grains (3.5%) that are present as inclusions in quartz grains. Subhedral zoisite grains around 2 µm in size make up less than 1% of the minerals present (Fig. 5.31f). Site 8 is the Nwanedzi River which is one of the large tributaries entering the Letaba River and is underlain by basalt. This river sediment here is abundant in olivine (5.2%), biotite (9.9%), muscovite (7.2%) and rutile (6.7%) (Table 5.4). The olivine grains exist as large grains with a fine grained groundmass of euhedral plagioclase (Fig. 5.31n). The Makoforo River enters the Letaba River at site 6 and is underlain by tonalitic biotite gneiss. Sediment from this tributary is abundant in rutile (4.1%) and biotite (4.8%). At this point zircon is present as inclusions which lie at a parallel orientation in quartz. The non-perennial Shambali and Makoforo rivers contain very low percentages of magnetite, ilmenite and hematite making up only between 0.8 to 3.2%. The Nwanedzi River contains high percentages of magnetite (4.4%), ilmenite (3.9%) and hematite (3.9%), when compared to other tributaries.

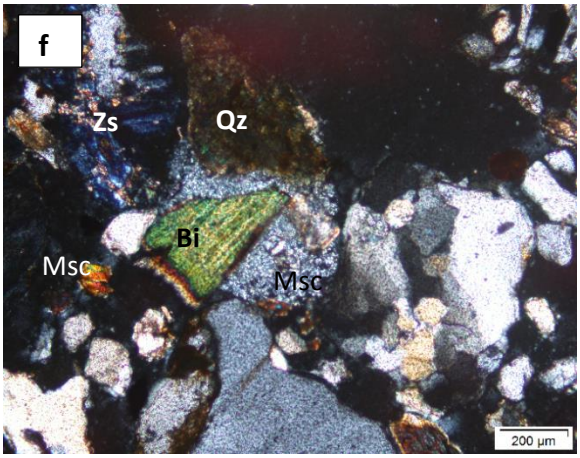

a
Qz
200 µm

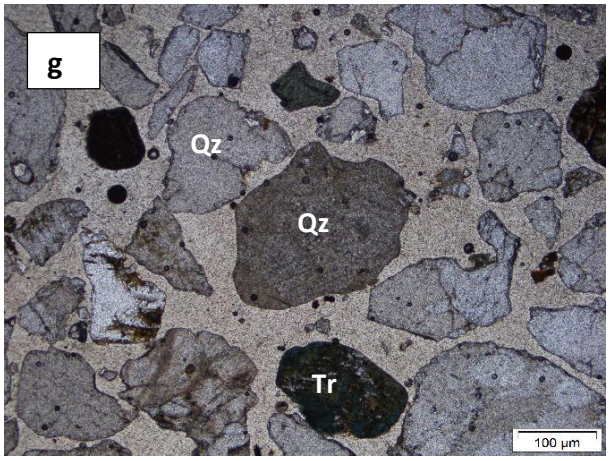

b
Qz
200 µm

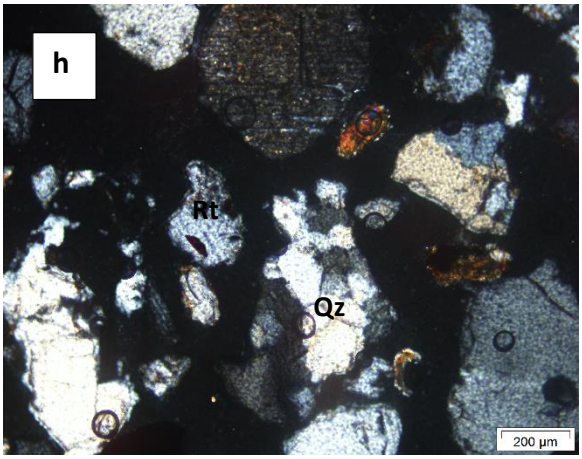

c
Qz
Zr
200 µm

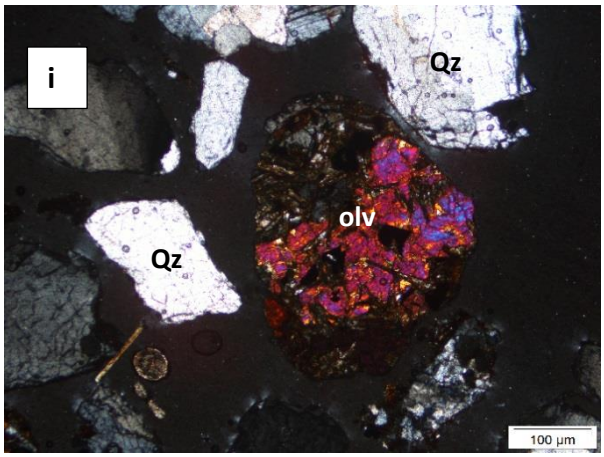

d
Qz
Zr
200 µm

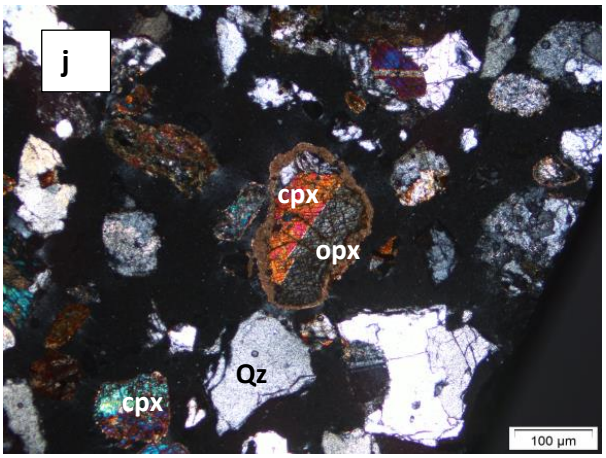

e
ZS
Cpx
Ol
100 µm

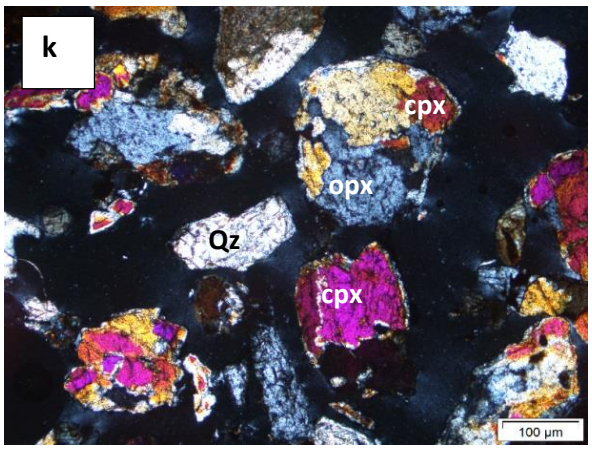

f
Zs
Qz
Bi
Msc
Msc
200 µm

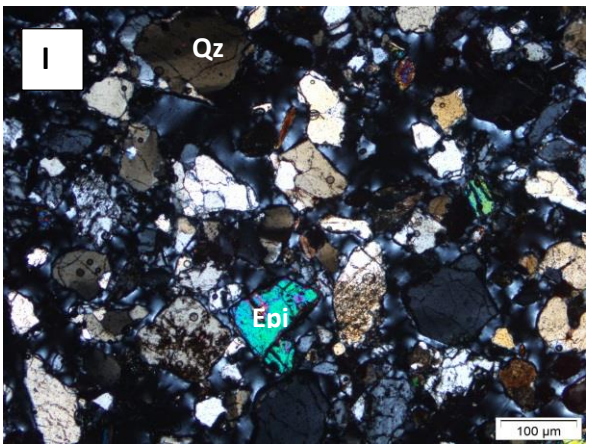

g
Qz
Qz
Tr
100 µm

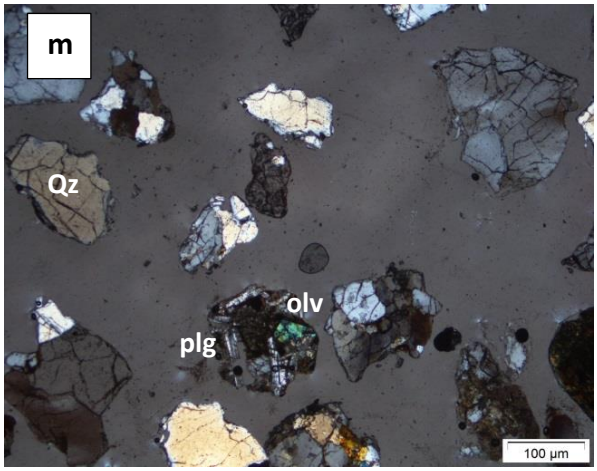

h
Rt
Qz
200 µm


i
Qz
olv
Qz
100 µm


j
cpx
opx
Qz
cpx
100 µm


k
cpx
opx
Qz
cpx
100 µm


l
Qz
Epi
100 µm


m
Qz
olv
plg
100 µm

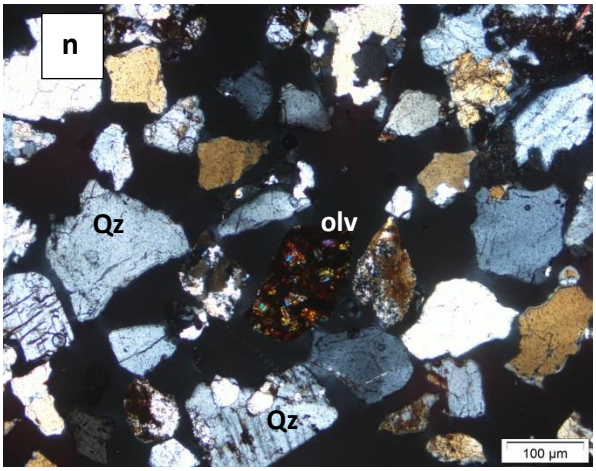
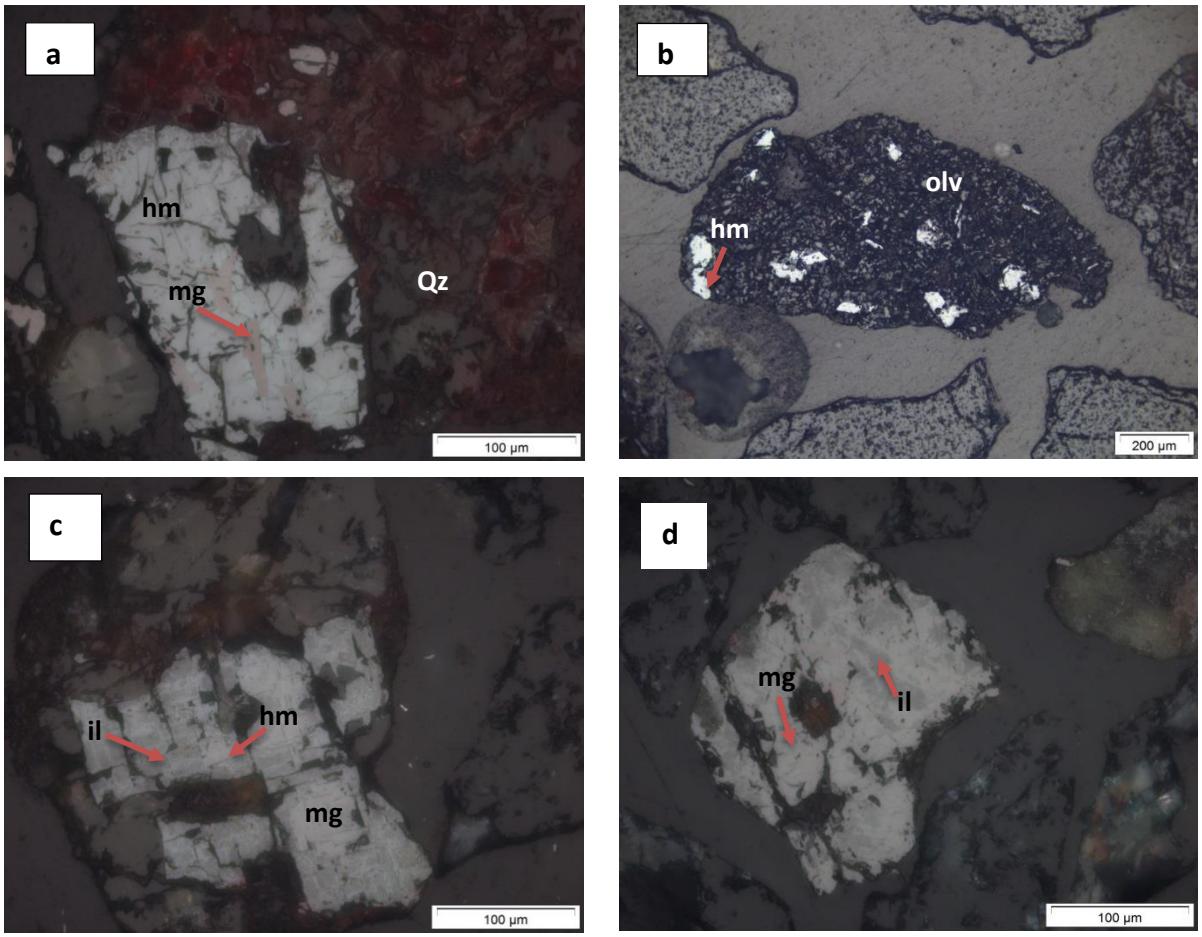
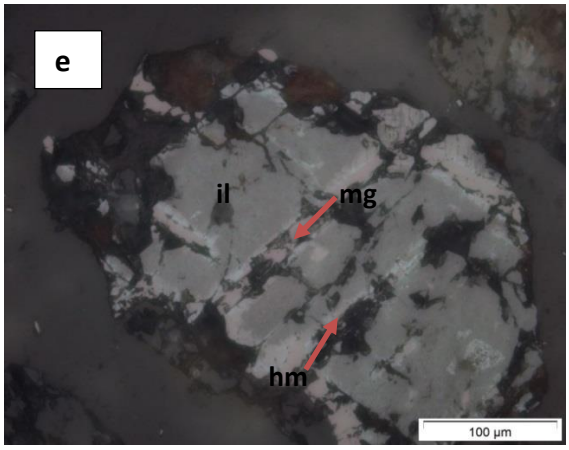
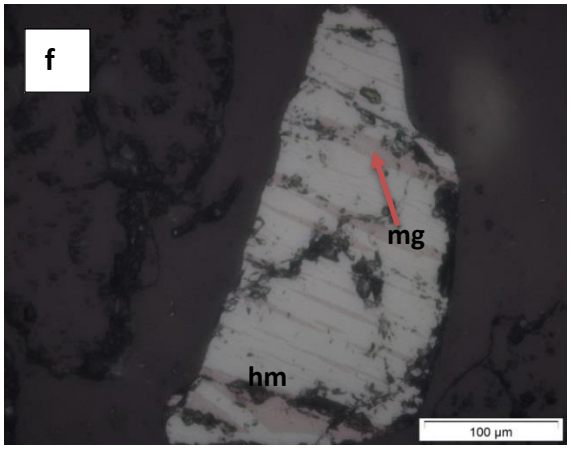

n
Qz
olv
Qz
100 µm

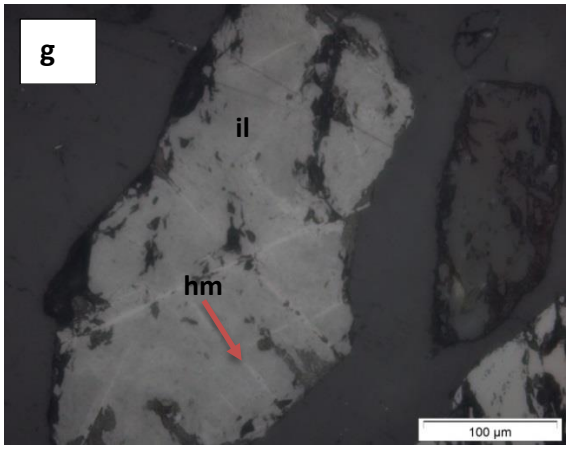
Fig. 5.31: Images from polished slides indicating minerals present in the sediment. (a,b) Columnar zircon inclusion in quartz grain from site 10, in plain light and crossed polars, (c) zircon inclusion in quartz grain at site 15, (d) columnar zircon inclusion in quartz grain at site 14, (e) zoisite and clinopyroxene from site 3, (f) subhedral zoisite included in quartz grain at site 9 and muscovite grains in the groundmass and present as inclusions in quartz grains, (g) tourmaline grain from site 10, (h) rutile inclusion in quartz grain from site 5, (i) large sub-rounded olivine grain from site 14, (j) orthopyroxene and clinopyroxene grain from site 3, (k) large orthopyroxene and clinopyroxene from site 1, (l) subhedral epidote grain from site 7, (m) subrounded olivine grain with plagioclase inclusions from site 15, (n) subhedral olivine grain which is slightly altered from site 9. Qz=quartz, Zr=zircon, Zs=zoisite, Tr=tourmaline, Rt=rutile, Olv= olivine, cpx=clinopyroxene, opx=orthopyroxene, plg=plagioclase, Epi=epidote.

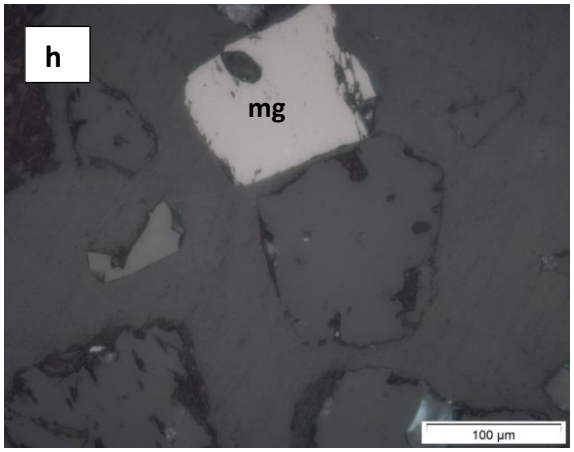
Heavy minerals such as magnetite, ilmenite and hematite exist together and can be seen using reflected light (Fig. 5.32). The minerals either exist as individual grains or as inclusions in other minerals.

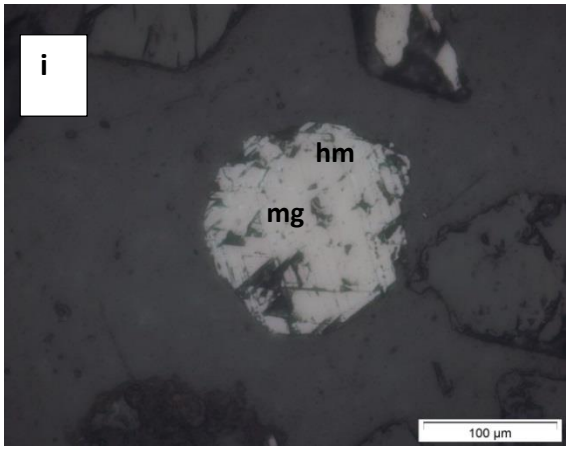


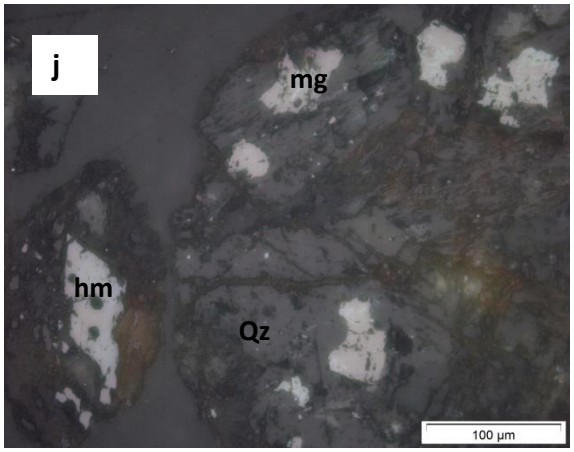

e
il
mg
hm
100 µm

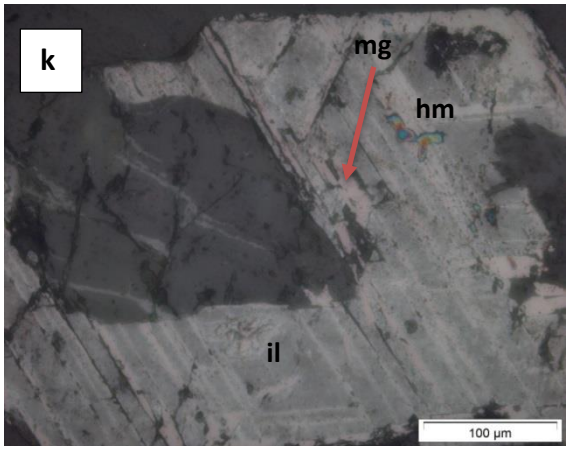

f
mg
hm
100 µm


g
il
hm
100 µm


h
mg
100 µm


i
hm
mg
100 µm


j
mg
hm
Qz
100 µm


k
mg
hm
il
100 µm

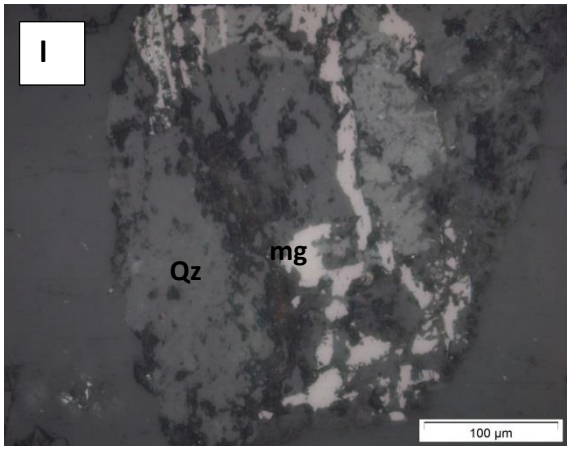

l
Qz
mg
100 µm

Figure 5.32: Images of magnetite (mg), ilmenite (il) and hematite (hm) and quartz (Qz). (a) anhedral hematite (white) grain with inclusions of magnetite (pink) at site 8, (b) hematite inclusions in olivine grain at site 15, (c) angular inclusion of hematite in quartz grain with inclusions of ilmenite (grey) and magnetite at site 12, (d) subrounded magnetite grain with inclusions of ilmenite at site 1, (e) subrounded ilmenite grain with inclusions of magnetite and hematite at site 2, (f) hematite with lamellae of magnetite (pinkish) at site 5, (g) ilmenite with lamellae of hematite at site 9, (h) angular grain of magnetite at site 7, (i) subrounded grain of magnetite with inclusions of hematite at site 13, (j) subhedral inclusions of magnetite and hematite in quartz grain at site 14, (k) ilmenite grain with magnetite (pinkish) and hematite at site 9 (white) lamellae, (l) irregular magnetite inclusion in quartz grain at site 6. Mg=magnetite, hm=hematite, Qz=quartz, il=ilmenite.

5.5.3 Spatial distributions of heavy minerals

The percentages of heavy minerals in different river reaches indicate variable mineral assemblages throughout the river. Site 1 at the confluence of the Groot and Klein Letaba rivers is abundant in orthopyroxene, which is lacking in other river reaches (Table 5.4). Olivine is present as large euhedral to subhedral grains up to 20 µm diameter. Site 4 was supplied by a source rich in muscovite and biotite which make up a large percentage of the minerals present. Site 5 is also abundant in biotite and muscovite. Very low percentages of magnetite, ilmenite and hematite are found at site 6. The sediment from this river reach is abundant in biotite, clinopyroxene and rutile, the latter of which is present as inclusions in quartz grains (Fig. 5.31h) and are also present as individual grains. A clinopyroxene-rich sediment source is reflected at site 7 where it makes up 5% of the sample. Site 7 is abundant in subrounded zoisite grains of up to 10 µm diameter. The most abundant magnetite, hematite and ilmenite minerals are found at site 5. Site 9 marks the beginning of a basaltic lithology, which is abundant in clinopyroxene, olivine and zoisite. Biotite and muscovite are the most abundant minerals together with rutile grains in this site. Apart from quartz, biotite is the second most abundant mineral present within the sediment (Fig. 5.33). Samples shown in Fig. 5.33 are placed in order, from upstream to downstream. Orthopyroxene is abundant in sediment from site 1 and is present in minimal quantities until site 13 and 14, which are also enriched in orthopyroxene with mean values of 19% and 38% respectively. Magnetite is present in large quantities at site 4, site 5 and site 13, with mean values of 46%, 70% and 42% respectively.

Table 5.5: The proportion of magnetite, ilmenite and hematite grains counted in sediments collected from the Letaba River. Mg=magnetite, il=ilmenite, hm=hematite.

	Active channel			Tributary			Floodplain			n
	mg	il	hm	mg	il	hm	mg	il	hm	
Percentage of grains counted	7.8	6.0	2.4	1.2	0.3	0.3	7.6	2.8	2.4	
	3.3	1.2	1.0	0.8	0.4	0.4	0.4	0.3	0.1	
	0.8	0.4	0.3	1.7	1.6	1.6	1.5	0.6	0.6	
	1.7	0.4	0.7	1.9	1.4	1.6	0.7	0.3	0.2	
	15.8	6.8	2.6	0.8	0.4	0.4	0.7	0.6	0.3	
	3.1	2.4	1.8				0.5	0.3	0.3	
	1.8	1.2	0.8				0.5	0.2		
							0.8	0.2	0.2	
n	34.5	18.5	9.8	6.4	4.3	4.3	12.8	5.3	4.1	100

Opaque heavy minerals were chosen in order to highlight the variability of the concentrations of heavy minerals in the active present day channel, the tributaries and the floodplain (Table 5.5). The concentrations of opaque minerals differ spatially, depending on whether the sediment was collected from the floodplain or active channel. The present floodplain has the highest concentrations of magnetite, ilmenite and hematite with percentages ranging from 0.3% to 15.8%. The percentage of minerals counted on the floodplains range between 0.1% and 7.6%. Tributaries contributed low concentrations of opaque minerals, with values ranging between 0.3% and 1.9%.

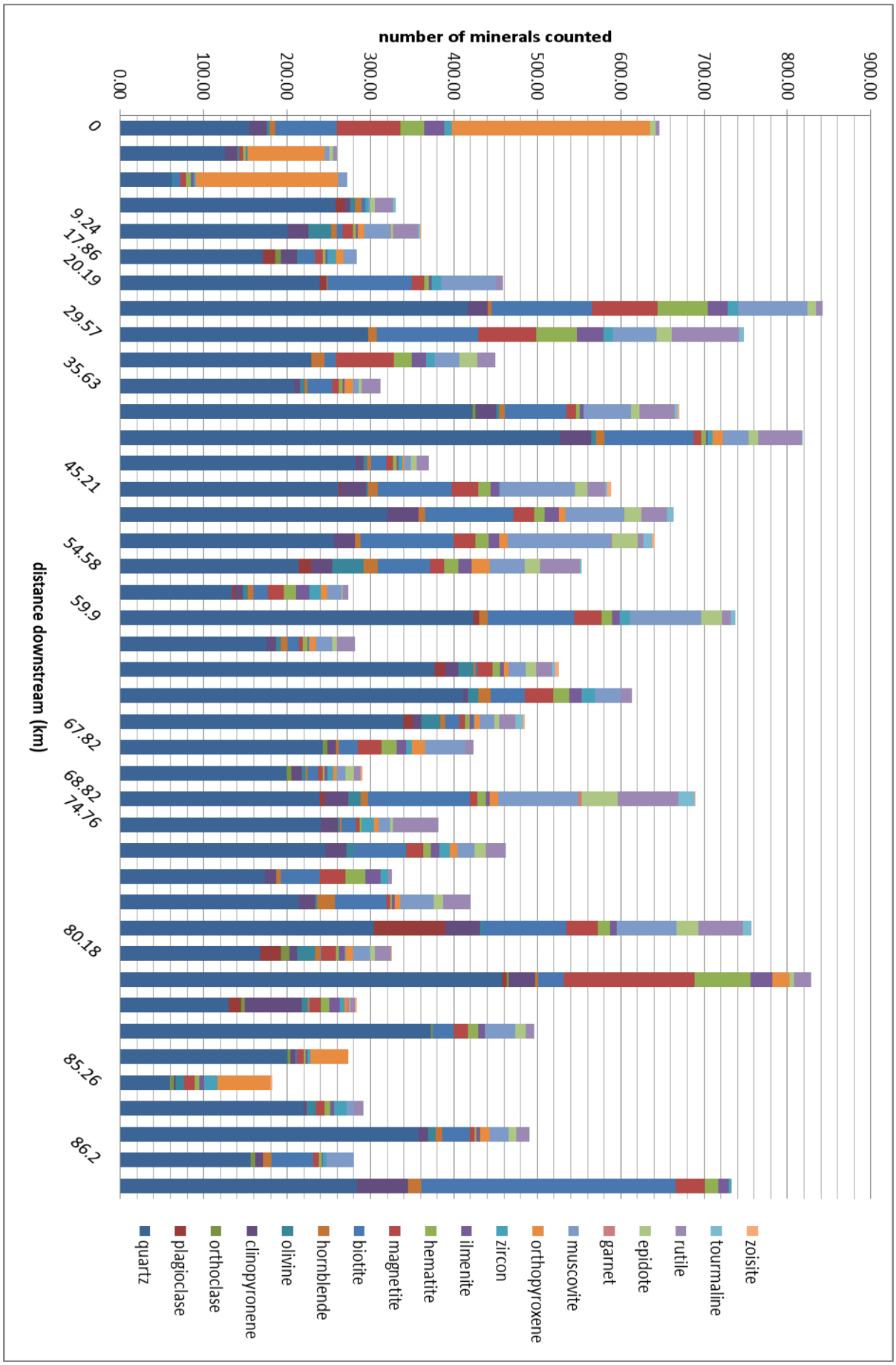


Fig. 5.33: The abundance of minerals at different river reaches

5.6 Magnetic susceptibility

Magnetic susceptibility (MS) is a measure of the concentration of magnetic minerals within the sediment (Murdock *et al.,* 2013). MS does not display a clear trend from floodplain to the main river channel, but there is a downstream increase in MS values along the Letaba River (Fig. 5.34). This trend corresponds with the increase in mean grain size thus indicating that MS values may be related to the grain size distribution. To investigate this relationship further, a scatter plot was constructed between magnetic susceptibility and mean grain sizes (Fig. 5.35). The R^2 value is 0.002, indicating that there is a very weak relationship between mean grain sizes and magnetic susceptibility. The highest MS values are found in sites 1, 12, 13 and 15, with the highest value of $3.15\times10^{-6}m^3kg^{-1}$ found at site 1. The lowest values are found in sample 6-1 and 5-1, with values of 0.13 $10^{-6}m^3kg^{-1}$ and $0.25\times10^{-6}m^3kg^{-1}$, respectively. There is a low variability between the MS values throughout the river. All the MS values at site 13 are greater than 1 and range from $1.70\times10^{-6}m^3kg^{-1}$ to $2.06\times10^{-6}m^3kg^{-1}$.

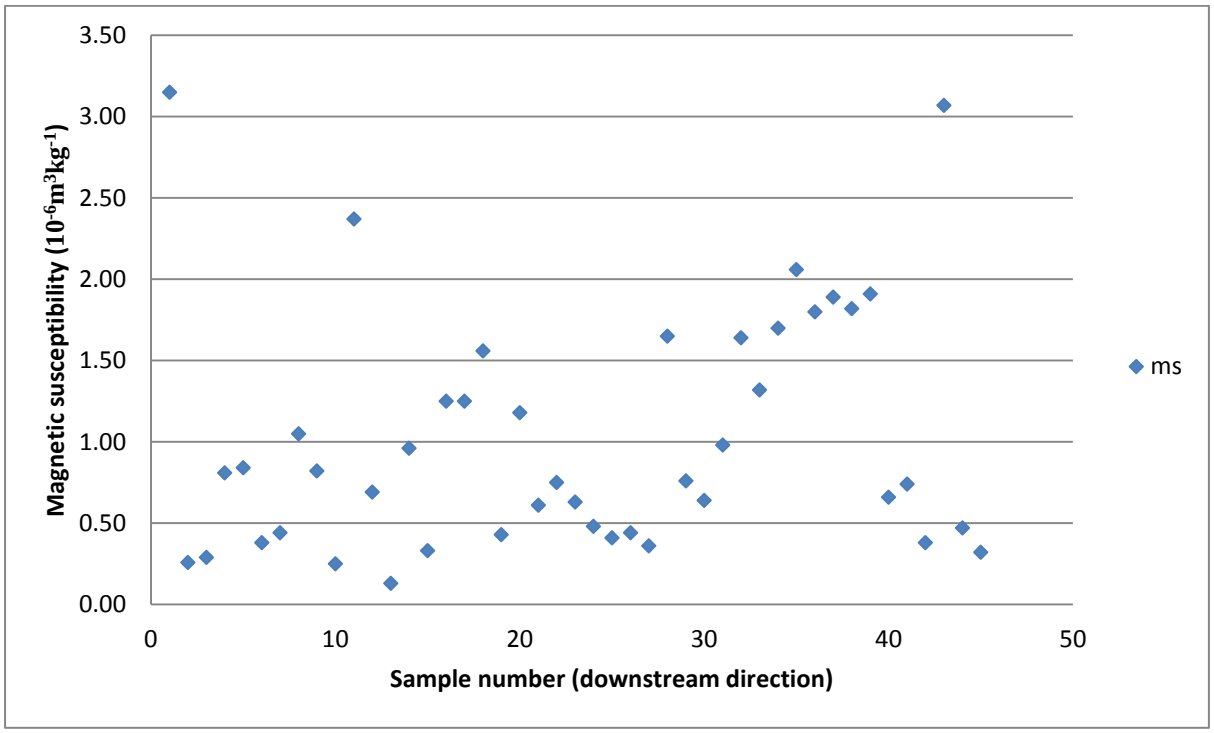


Fig. 5.34: Magnetic susceptibility values at selected sections of the Letaba River.

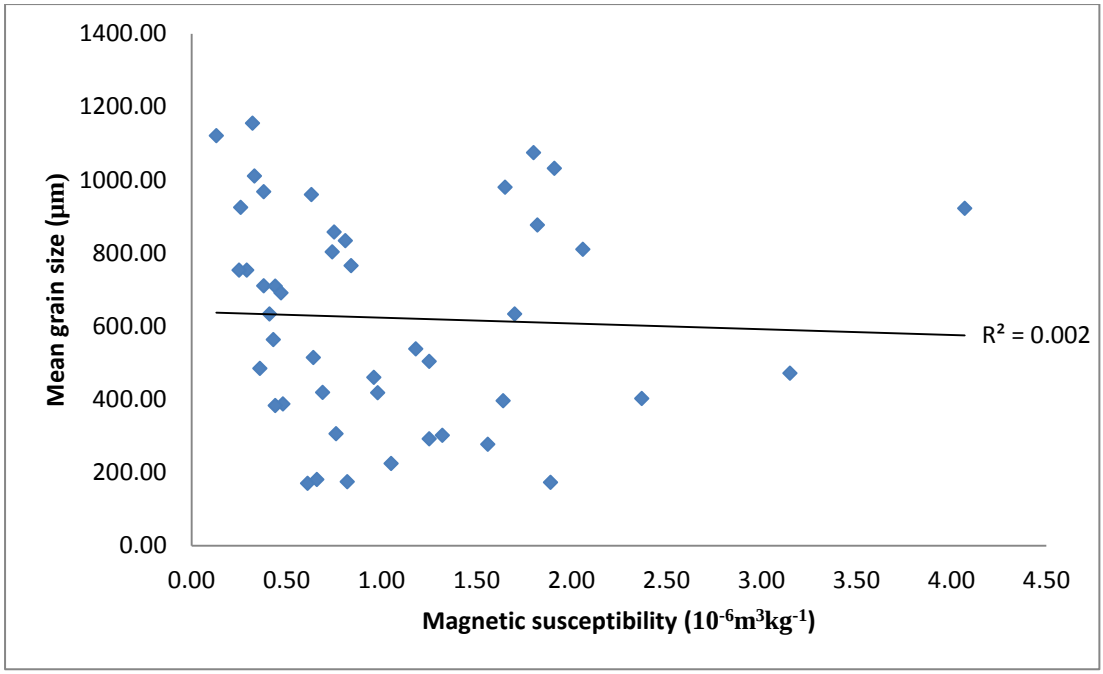


Fig. 5.35: Scatter plot of the relationship between mean grain sizes and magnetic susceptibility.

Table 5.6 indicates the MS values at different sites as well as the percentages of counted magnetic minerals, magnetite, hematite and ilmenite. The samples with high MS values include sample 1-1, sample 5-2, sample 13-2 and sample 15-1 with MS values of $3.15\times10^{-6}m^3kg^{-1}$, $2.37\times10^{-6}m^3kg^{-1}$, $2.06\times10^{-6}m^3kg^{-1}$, $3.07\times10^{-6}m^3kg^{-1}$, respectively. The samples with high MS values also have a high number of magnetic minerals, with percentages ranging between 4.5% and 17.7%. However, not all samples with high values of opaque minerals have high MS readings. An example of this can be seen from sample 4-2, with magnetic mineral percentages of 8.8%, 13.1% and 7.7%, respectively, with an MS reading of $0.82\times10^{-6}m^3kg^{-1}$. Sample 5-1 has 7.9% magnetite, 10.4% hematite and 10.2% ilmenite minerals with an MS reading of $0.25\times10^{-6}m^3kg^{-1}$. Low MS values were recorded at sample 1-2, sample 1-3, sample 5-1 and sample 6-1 with MS values $0.26\times10^{-6}m^3kg^{-1}$, $0.29\times10^{-6}m^3kg^{-1}$, $0.25\times10^{-6}m^3kg^{-1}$ and $0.13\times10^{-6}m^3kg^{-1}$, respectively. Sample 1-3 and sample 6-1 have a low concentration of opaque minerals. When considering the underlying geology, sandstone reaches have high MS readings ranging between $0.43\times 10^{-6}m^3kg^{-1}$ to $1.56\times10^{-6}m^3kg^{-1}$. Reaches underlain by basalt have MS readings ranging from $0.32\times10^{-6}m^3kg^{-6}$ to $3.07\times10^{-6}m^3kg^{-1}$. Magnetic susceptibility values not only range from site to site but also range between samples of each within each site.

Table 5.6: Magnetic susceptibility values, the percentage of magnetite, hematite and magnetite and the underlying geology.

Site	**MS value** $10^{-6}m^3kg^{-1}$	**Mean grain size (µm)**	**Magnetite (%)**	**Hematite (%)**	**Ilmenite (%)**	**Underlying geology**
1-1	3.15	471	8.5	6.1	7.7	leucocratic strongly migmatised biotite gneiss
1-2	0.26	925	0.4	0.7	0.3	
1-3	0.29	753	0	0	0	
1-4	0.81	834	0	0	0	
1-5	0.84	766	0	0	0	
1-6	0.38	710	0	0	0	
1-7	0.44	709	0.7	1.0	1.3	
4-1	1.05	224	1.6	1.3	1.0	leucocratic granodioritic /tonalitic biotite gneiss
4-2	0.82	175	8.8	13.1	7.7	
5-1	0.25	753	7.9	10.5	10.3	leucocratic granodioritic /tonalitic biotite gneiss
5- 2	2.37	402	7.7	4.5	5.8	
5-3	0.69	419	0	0	0	
6-1	0.13	1121	0.9	0.8	1.0	leucocratic granodioritic /tonalitic biotite gneiss
6-2	0.96	460	1.2	1.0	1.3	
6-3	0.33	1011	1.1	1.0	0.9	
6-4	1.25	292	0.9	0.8	0.9	
7-1	1.25	504	4.0	3.2	3.2	fine grained sandstone/ siltstone
7-2	1.56	278	2.8	2.8	5.5	
7-3	0.43	564	0	0	0	
7-4	1.18	538	0	0	0	
9-1	0.61	171	3.8	2.6	3.2	basic volcanic rocks (theolites, picrite basalts)
9-2	0.75	858	0.5	1.0	0.6	
9-3	0.63	960	2	1.9	1.6	
9-4	0.48	388	4	4.1	4.8	
9-5	0.41	634	0.7	1.3	1.2	
10-1	0.44	383	3.1	4.0	3.9	basic volcanic rocks (theolites, picrite basalts)
10-2	0.36	485	0.5	0.7	0.9	
11-1	1.65	980	0	0	0	
12-1	0.76	307	0.6	0.4	0	
12-2	0.64	514	2.2	2.0	3.5	
12-3	0.98	418	4	5.2	5.9	
12-4	1.64	396	0.4	0.6	1.0	
12-5	1.32	302	0	0	0	
13-1	1.7	634	1.9	0.9	2.3	basic volcanic rocks (theolites, picrite basalts)
13-2	2.06	811	17.7	14.8	8.4	

13-3	1.8	1075	0	0	0	
13-4	1.89	173	1.4	2.5	4.0	
13-5	1.82	876	2.0	3.0	2.6	
13-6	1.91	1032	0.9	0.4	0.7	
14-1	0.66	181	1.4	1.3	1.6	
14-2	0.74	803	1.1	2.0	1.2	basic volcanic rocks (theolites, picrite basalts)
14-3	0.38	968	0.6	0.4	1.2	
15-1	3.07	922	0	0	0	
15-2	0.47	691	0.7	0.6	0.7	
15-3	0.32	1155	4.0	3.4	3.8	
n			100	100	100	

5.7 Trace elements

Following analysis of the <63 µm fraction of the sediment sample by XRF, the trace elements present in the sediment are indicated in Fig. 5.36. The most abundant minerals present include Zr, Ba, Sr and Cr, with the highest concentrations of these minerals being 2607 ppm, 740 ppm, 448.8 ppm and 863 ppm respectively. The highest quantities of Zr are found at sites 2, 5, 7, 9, 12 and 14 with values of 2262.91 ppm, 1544.23ppm, 1660.78 ppm, 1321.39 ppm, 2511.84 and 1666.14 ppm respectively. The trace elements are present in different quantities throughout the variable river reaches and the elements vary within each sampling site. The confluence between the Klein Letaba and Groot Letaba rivers (site 1), for example, is mostly abundant in Ba and Zr; and Zr has the highest percentage at site 2. The minerals present in low quantities include U, Mo, Sc and Pb with the highest concentrations of these being 6.6 ppm, 3.2 ppm, 29.5 ppm and 30.8 ppm respectively.

Correlations between the trace elements are indicated in Appendix G. A positive relationship exists between the elements Sc, V, Co, Cu, Zn, Y, Ga and Nb. A strong correlation of 0.91 exists between Sc and V. A positive relationship exists between the elements Sc, V, Co, Cu, Zn, Y, Ga and Nb. A strong correlation of 0.91 exists between Sc and V. A positive relationship also exists between Th, Cr, Zr, Y, Ni, Pb, U and Ga. The elements that have a strong relationship with very fine gravel include Sc, V, Zn, Ga and Nb with significance values ranging from 0.52 to 0.71 (Appendix I).

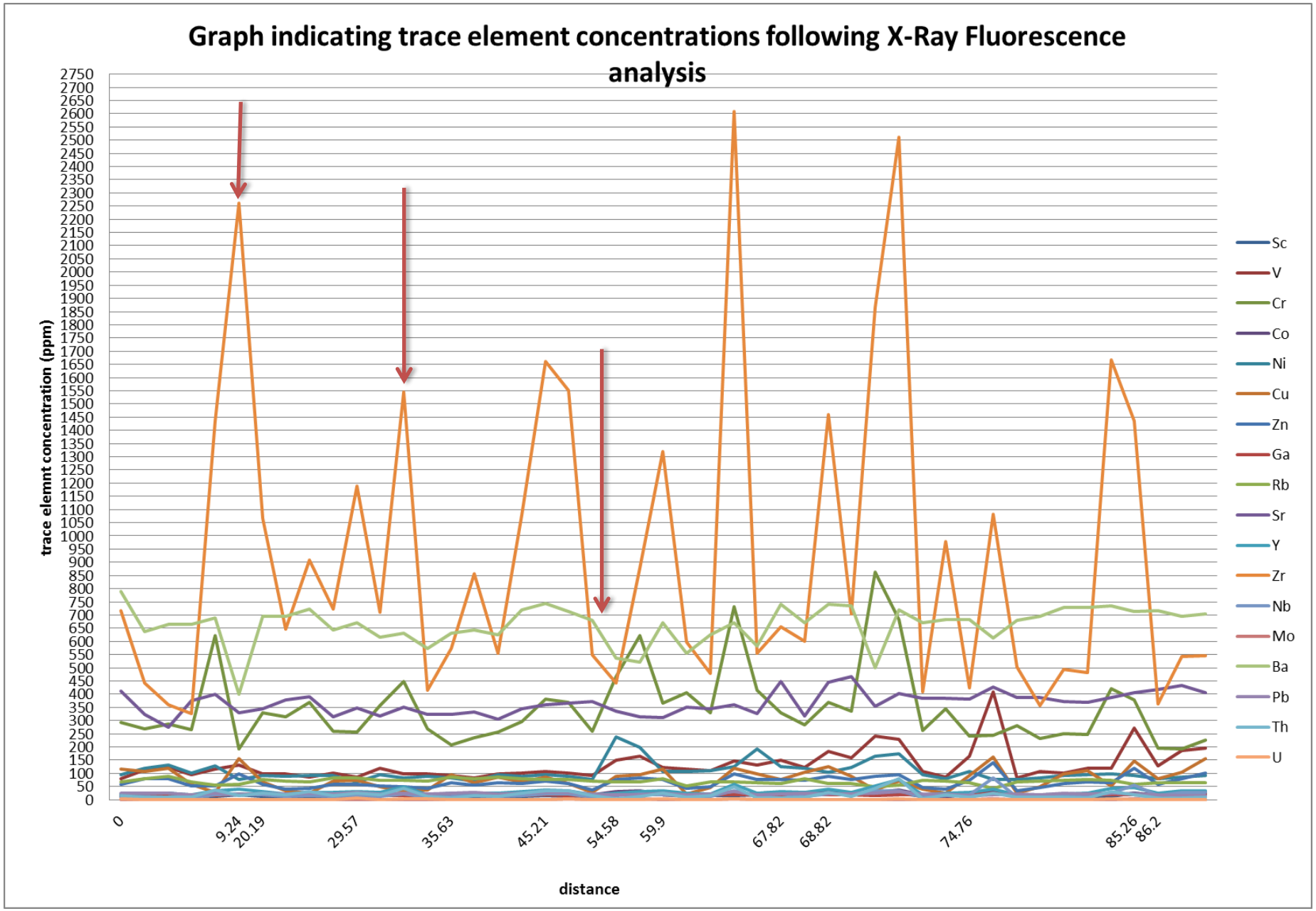


Fig. 5.36: The trace elements which are present in the sediment and their abundances. The red arrows indicate the entrance of tributaries.

Table 5.7: Relationships between the different components. The bold values indicate values showing significant relationships at P<0.5.

	Component	
	1	**2**
Zn	**0.952**	-0.067
V	**0.878**	-0.276
Sc	**0.873**	-0.171
Nb	**0.784**	-0.354
Cu	**0.737**	0.465
Ga	**0.695**	0.458
Co	**0.693**	-0.335
U	-0.440	-0.190
Sr	0.385	-0.134
Mo	0.318	0.022
Th	0.050	**-0.941**
Cr	0.170	**-0.889**
Zr	0.177	**-0.865**
Y	0.471	**-0.795**
Ni	0.367	**-0.698**
Pb	-0.249	**-0.675**
Rb	-0.450	**0.520**
Ba	0.083	0.219

Following analysis of the trace elements through Principal Component analysis, the results of the relationships between the different components are summarised in table 5.7. There is a relationship between the first component which is Sc and Zn, V, Sc, Nb, Cu, Ga and Co (Table 5.7). A positive relationship also exists between the second component, which is V and Th, Cr, Zr, Y, Ni, Pb and Rb (Table 5.7).

Correlation coefficient analysis was used to examine the relationships between trace elements and heavy minerals present in the sediment and the results are indicated in Appendix I. A high significance value of 0.61 exits between zircon and Zr. Zircon also has a high significant relationship with Y, Nb and Mo. Plagioclase and Mo have a significance value of 0.74. Olivine has a significant relationship with Ba and Th, with values of 0.58 and 0.2 respectively. A significant relationship can also be seen between garnet and Co, Ga, Sr, Y and Ba. A significant relationship exists between magnetite and V and Nb, with weak relationships between magnetite and Sc, Zn, Ga, Rb, Mo and U.

5.8 Mixing of sediments

The mean and standard deviations of the source samples and sediment collected on different geomorphic features in the variable river reaches were calculated in order to elucidate the distribution and variability of the trace elements throughout the river (Table 5.8). The elements with the highest standard deviation within the source and river samples include V, Cr, Zr, Ni and Ba and the elements with the lowest standard deviation are U, Mo and Ga. The high variability of mean and standard deviations of the trace elements within source samples indicates that the trace elements can be used to distinguish the variable source categories.

Table 5.8. The mean and standard deviation of source samples and sediment collected on different geomorphic features.

Tracers	Source samples		River samples	
	Mean (ppm)	Standard deviation	Mean (ppm)	Standard deviation
Sc	17.7175	5.73668	15.59153	3.65537
V	167.385	100.98017	125.13538	45.76742
Cr	341.2675	145.84421	346.87794	147.16325
Co	24.63	6.1866930	21.52025	4.71502
Ni	122.37125	61.066866	102.78948	27.45849
Cu	94.02125	45.73571	75.58846	36.03502
Zn	79.25	29.62660	65.12333	19.72047
Ga	18.98875	3.018506	17.90769	1.53219
Rb	64.59375	13.07974	70.68102	8.71082
Sr	349.61625	37.72934	369.49897	42.90753
Y	30.7725	6.450111	30.72717	12.31866
Zr	935.82125	594.5956	924.24512	589.95868
Nb	25.74125	23.86651	18.33487	9.20148
Mo	1.29375	0.832242	1.14410	0.69449
Ba	584.2825	102.99952	679.31564	55.27140
Pb	19.63	2.13592	23.22846	3.24365
Th	14.53875	8.00340	20.05230	15.41020
U	0.085	0.24041	0.88897	1.54203

Two statistical tests were conducted in order to determine which trace elements to use in the mixing models; namely the Kruskal Wallis H-test and discriminant function analysis. The results of the Kruskal Wallis H-test are indicated in Table 5.9, indicating that V, Cr, Co, Sr, Ba, Pb and U are the only elements with statistical significance.

Discrimination function analysis was then tested on these 7 trace elements in order to test the ability of the minerals to distinguish different source areas and the results are indicated in Table 5.10. The minerals with high statistical significance include V, Cr and Co and these minerals will be used in the mixing models in order to identify sediment sources. These minerals are all transition metals and principal component analysis indicated a significant relationship between the two trace elements V and Co (Table 5.10). It can be seen that it is

not always elements with the highest overall concentrations that will be useful for discriminating between sources, but the variability within the concentrations of individual trace elements is the main determining factor.

Table 5.9: Significance values of the trace elements after the Kruskal Wallis H-test was performed to differentiate between sediment form different sources. The bold values indicate values that are statistically significant at P<0.05.

	Chi-Square	Sig.
Sc	17.918	0.118
V	23.867	**0.021**
Cr	31.642	**0.002**
Ni	15.396	0.220
Co	30.660	**0.02**
Cu	12.596	0.372
Zn	14.889	0.248
Ga	8.681	0.730
Rb	20.697	0.055
Sr	25.408	**0.013**
Y	11.617	0.477
Zr	17.475	0.133
Nb	16.947	0.152
Mo	8.799	0.720
Ba	22.410	**0.033**
Pb	21.208	**0.047**
Th	18.879	0.092
U	23.171	**0.026**

Table 5.10: The significance values of trace elements after discriminant function analysis was performed, which indicates which tracers were correctly classified into the different source categories. The bold values indicate values that are statistically significant at P<0.05.

Wilks' Lambda

Test of Function(s)	Wilks' Lambda	Chi-square	df	Sig.	% of source samples classified correctly
V	.007	177.730	84	**.000**	75
Cr	.036	119.379	66	**.000**	64
Co	.133	72.635	50	**.020**	81
Sr	.266	47.737	36	.091	58
Ba	.526	23.161	24	.510	52
Pb	.809	7.624	14	.908	61
U	.932	2.537	6	.864	45

The modelled relative contributions from each site were calculated and are indicated in Fig. 5.37. Contributions from the channel bed are the highest at sites 10, 12 and 14, indicating the importance of channel erosion at these river reaches. Channel bank contributions are high only at site 13, with the channel bank contributing 62% of the sediment.

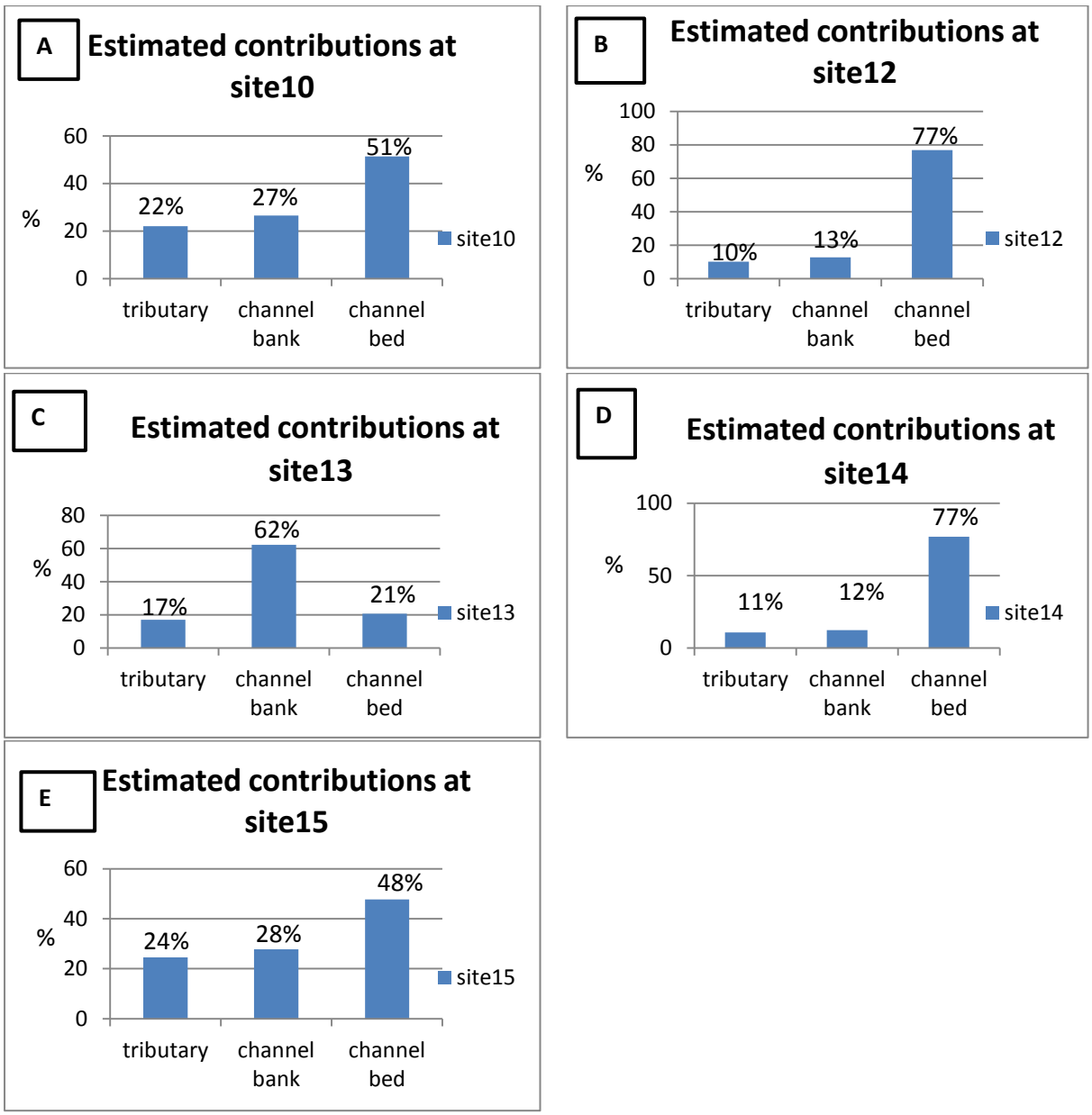


Fig. 5.37: The predicted percentage contributions of tributaries, channel bank and channel bed from the different data collection sites.

The overall relative percentages are indicated in Fig. 5.38. Results from the modified Collins model indicate that the channel bed contributed the most sediment, with a value of 55%. The channel bank contributed 28% to the sediment. According to the Collins model, the tributaries contributed the lowest overall percentage of sediment to the floodplain sediment in the downstream reaches of the river, with a value of 17%.

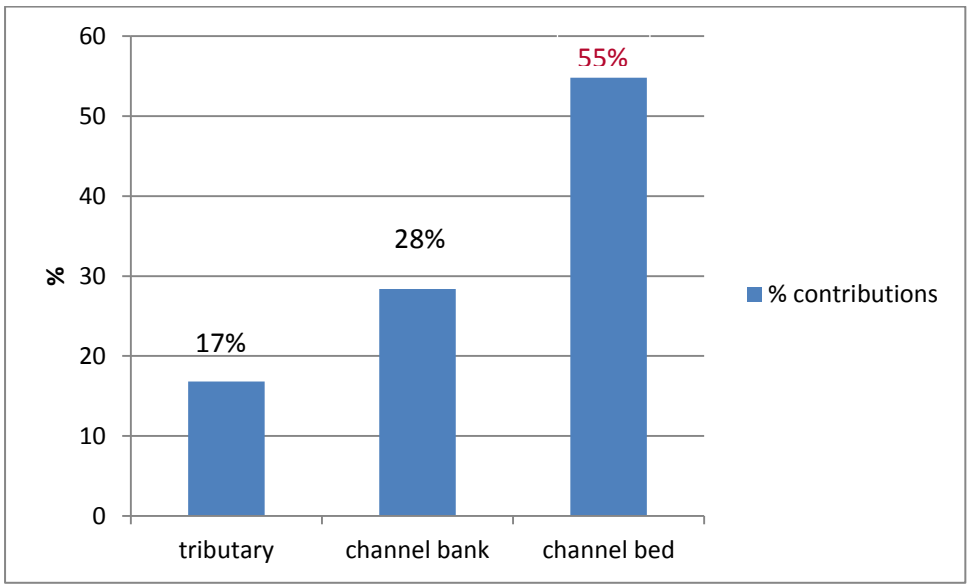


Fig. 5.38: The overall relative predicted contributions from tributaries, channel bank and channel bed within the Letaba River.

The mean absolute errors were calculated for each of the potential source areas and the results are indicted in Fig. 5.39. The model indicates high accuracy values with the median values for channel bank, channel bed and tributary of 43%, 33% and 36%, respectively (Fig. 5.39). A few of the samples also had accuracies of less than 10%, however a higher number of samples indicate high accuracies, thus indicating that the model estimated the percentage contributions with high accuracy.

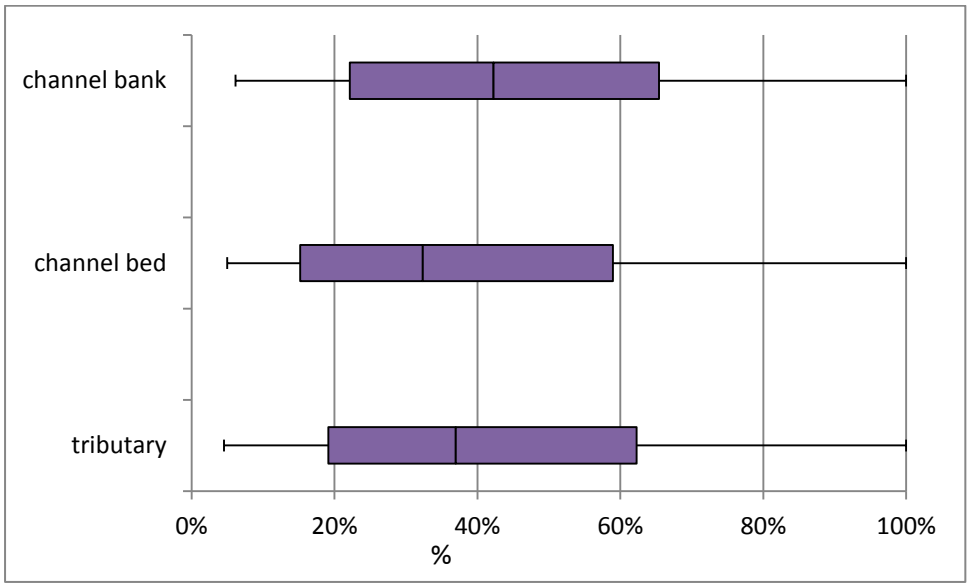


Fig. 5.39: The range of percentages obtained from calculating the mean absolute errors of the mixing model.

The percentage contribution from each source is indicated spatially in Fig. 5.40. The contributions from each source vary at each sampling site, with the relative source contributions from the channel bed being more prominent in downstream reaches. Sites 10, 12, 14 and 15 receive the highest relative contribution from channel bed sources.. Site 13 however, shows the importance of channel bank erosion, with a contribution of 62%.

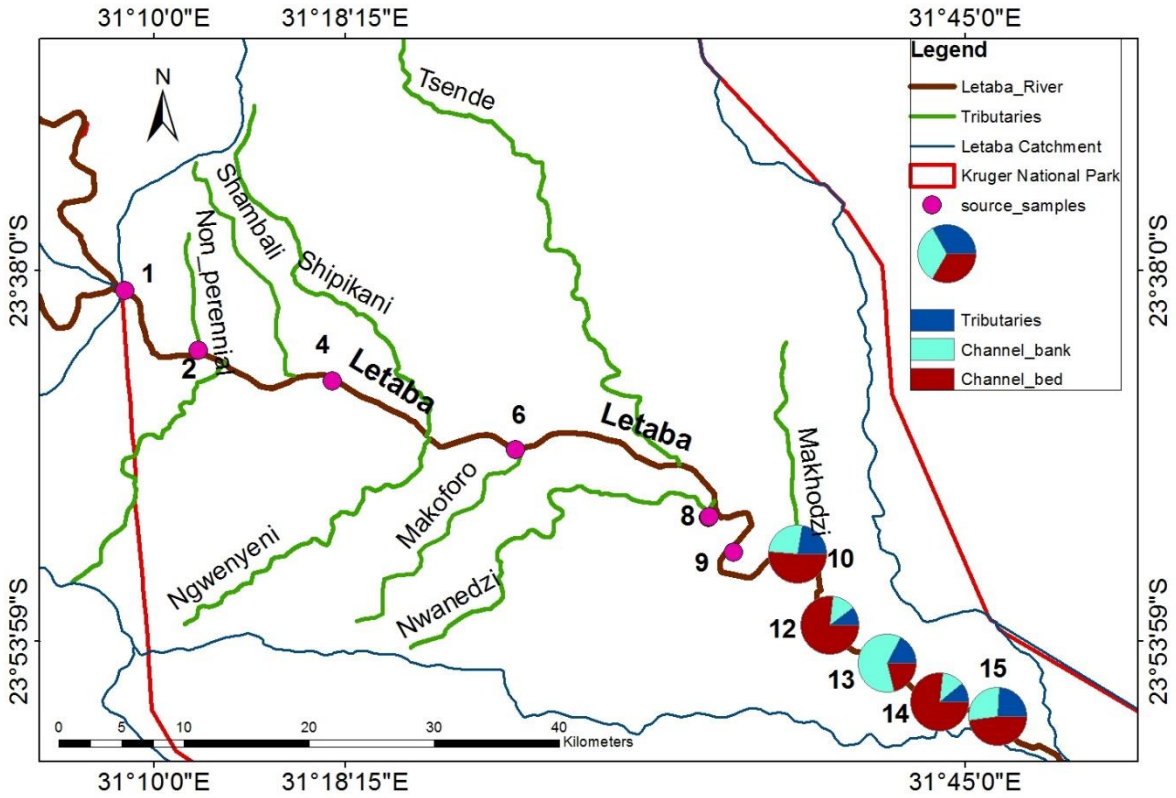


Fig. 5.40: The percentage contributions from tributaries, channel banks and channel bed in the downstream section of the Letaba River.

Chapter 6: Discussion

6.1 Landforms, sediments and grain size analysis

Objective 1: Map geomorphological features within the Letaba River, in order to produce geomorphic maps of different river reaches and identify sediment storage areas and the relationships between grain sizes and geomorphic features.

Geomorphic features along the floodplain and within the present day channel are characterised by distinctive grain size intervals (Allen, 1982; Bridge, 1993, 2003; Knight and Evans, 2017). This section describes the variable bedforms in the Letaba River, associated grain sizes, and hydraulic processes responsible for the deposition of these grain sizes and landforms. The magnitude and frequency of heavy rainfall events and associated flooding is a major determining factor on river dynamics in semi-arid regions (Wolman *et al.,* 1960, 1978; Gupta, 2000; Heritage *et al.,* 2001, 2015; Kale *et al.,* 2004; Spaliviero *et al.,* 2014). Fig. 2.5 indicates the volumes of discharge from 3 measuring stations within the Letaba River for the past 10 years. The last major flood event occurred in 2014, with the highest discharge volume of 94 m^3s^{-1} measured at the Black Heron Dam in January 2014. The Engelhardt and the Letaba Ranch measuring stations measured discharges of 50.7 m^3s^{-1} and 35.2 m^3s^{-1} respectively for January 2014, thus indicating the spatial variability of the flood. Spatial variations in the characteristics of a flood influence the geomorphic modifications that will take place (Cenderelli *et al*., 2003). These include deposition of coarse material on the floodplain (Magilligan *et al.,* 2015), bar formation (Hooke, 2016; Kochel *et al.,* 2016) and the influx of abundant sediment into the river (Heritage *et al.,* 2015).

Field mapping enabled the identification of certain geomorphic features characteristic of each river reach along the Letaba River. These features include flat-topped and ridge-like sandbars on the floodplain, 3D subaqueous dunes, overbank deposits, levee deposits, inactive channels, gravel bars, and in-channel sand bars. The characteristic grain sizes on these features will be discussed in order to examine relationships between sediment patterns and water/sediment movement. The presence of 3D subaqueous dunes (Fig. 5.2c) is indicative of migrating bedforms that developed in high energy environments and is associated with high magnitude floods (Allen, 1982; Bartholdy *et al.,* 2005; Knight and Evans, 2017). These subaqueous dunes are characterised by 25.8% and 58.8% very coarse and coarse sand, respectively, supporting the notion that dunes are developed in high energy conditions. Inactive channels that have cut through the floodplains of this river (Fig. 5.2c) also serve as evidence of the flood-dominated morphology of the Letaba River. Inactive channels contain elongate clusters of cobbles, pebbles and coarse sand (Fig. 5.7b). The presence of cobbles and pebbles indicates bedload transport under high energy conditions. Knight and Evans (2017) also attributed the presence of abandoned channels in the Sabie River to a high magnitude flood which took place in the year 2012. Levee deposits have a high percentage of fine sediment. This was seen in sample 4.2 composed of fine (56.6%) and very fine (22.2%) sand. Sample 9.1 likewise consists of 94% of fine sediment.

Levee deposits form when fine grained suspended sediment emanates from the channel during floods and is deposited adjacent to the river channel (Allen, 1982; Bridge, 2003).

Sediment from the present day channel bar (sample 7.3) is made up of very coarse (14.4%), coarse (39.1%) and medium (41.6%) sand. This river reach is underlain by sandstone and represents an area where the underlying lithology has impacted on the grain size distribution. There is a reduction in the coarse grain size interval and an increase in the medium to fine grain size interval compared to other sites that are not underlain by sandstone where bedrock erosion increases the supply of these grain sizes.

The exposed eroded cross section of a sandbar in the floodplain (Fig. 5.13b) at site 5 indicates sheet flows, which deposited sediment at variable time periods. A coarsening upwards trend can be seen, where the bottom layers are fine grained, followed by an organic rich layer and the top layer consists of coarse gravel. This arrangement of sediment was also observed in the Sabie River and corresponding to rising and waning flows of a flood event (Knight and Evans, 2017). The importance of vegetation in trapping sediment is seen at sites 6 and 10, where vegetation traps coarse sediment on the floodplain and hinders further downstream movement. Omengo *et al.* (2016) attributed variable sedimentation rates on the floodplain to differences in the amount of vegetation present at different river reaches. Samples 6-1 and 6-2 consist of high percentages of very coarse sand, of 63.2% and 52.2% respectively, which may reflect reduction in flow velocity around vegetation. The relationship between water velocity and coarse grain sizes is also seen in overbank deposits.

Overbank deposits indicate floodplain inundation and deposition during high water levels (Bridge, 2003). Overbank deposits are present at sites 1, 10, 12 and 14. A sample collected closest to the active channel (sample 10.2) contains very fine gravel (0.1%), very coarse sand (1.9%), coarse sand (49.4%), medium sand (40.3%) and fine sand (7.2%) (Appendix B). Sample 10.1, collected further away from the active channel, contains very coarse sand (1.2%), coarse sand (29.9%), medium sand (46.9%) and fine sand (17.8%). Another example is site 14, where a sample furthest from the active channel (sample 14.1) is abundant in fine sediments (70.8%), samples from the middle floodplain contain very fine gravel (0.9-4.0%) and very coarse sand (49.9-52.3%). Sediment fining away from the active channel is indicative of overbank deposits (Bridge *et al.,* 1979; Marriot, 1992; Miller *et al.,* 1999; Owens *et al.,* 1999).

A different trend was observed in site 13, where samples from the floodplain (samples 13.5 and 13.6) display abundant coarse grain sizes (42.7%-64.9%), with sediment in the mid-floodplain (sample 6) being coarser than sediment closer to the channel. At sites 10 and 12, sediment becomes finer with distance from the main channel but this is not the case at site 13. This may be that during flood events, new channels formed on the floodplain and deposited sediment during waning flows. This notion is supported by the elongate clusters of pebbles within abandoned channels on the floodplain (Fig. 5.20).

The floodplain of site 15 consists of pebbles and boulders from the upstream reaches of basalt, sandstone, diorite, granitic gneiss and rhyolite, between 2 cm and 4 m in diameter (Fig. 5.24b). Wohl (1992) suggested that only flows with a velocity of 8000 m^3s^{-1} or greater are able to transport boulders that make up boulder bars. Baker *et al*. (1987) noted that a discharge of 6000 m^3s^{-1} transported boulders of up to 3 m diameter in Katherine Gorge, Australia. The discharge volumes within the Letaba River in the past 10 years do not reach these values (Fig. 2.5) and may indicate that some of the largest boulders may have been moved by these recent floods, but maybe by higher magnitude events in the past.

Anthropogenic influences on the river are seen in the areas where dams and bridges have been constructed. This can be seen in the large amount of very coarse (48.2%) to coarse (38.3%) and very fine gravel (2.8%) sediment on a sandbar in the present day channel (site 11), downstream of the Engelhardt Dam, which can be attributed to the sudden reduction in flow velocity caused by the dam and leading to rapid sediment deposition. A flow velocity of 50.7 m^3s^{-1} was recorded at the Engelhardt Dam for the last heavy rainfall event in 2014 (Fig. 2.4), indicating high flow velocities which is able to carry coarse grained sediment. The low water bridge at site 14 traps the majority of sediment flowing in this reach and results in the formation of multiple coarse grained sandbars on the upstream side of the bridge (Fig. 5.22a).

Mean grain size indicates the averaged energy conditions of the transporting and depositing agent (Sahu, 1964). Grain size distribution displays a general fining downstream trend in modern rivers where there is no input from tributaries or valley sides (Parker, 1991; Paola *et al.,* 1995; Pizzuto, 1995; Ferguson *et al.,* 2006; Singh *et al*., 2007). The downstream fining trends were explained by hydraulic sorting and abrasion, where fine grained sediment is transported further downstream and sediment grain sizes decrease through abrasion with distance (Singh *et al.,* 2007). However this is not the case on the Letaba River. Even though the percentage of fine grained sediment increases on bedforms in a downstream direction, inconsistent changes in sediment grain size were observed throughout. This could be caused by fluctuations in water volumes and sediment availability and an increase in the intensity of floods in a downstream direction, as is seen in Fig. 2.5.

Changes in median grain sizes can be seen in Fig. 5.26, which indicates that upstream reaches (e.g. site 1) are dominated by medium to coarse sand (500 to 950 µm), with middle reaches (sites 4 to 13) showing an increase in fine grains (160 to 1100 µm), and downstream reaches (20 to 80 km downstream, sites 14 to 15) showing an increase in coarse grains (750 to 1200 µm). The range of sediment grain sizes on bedforms of different river reaches (Fig. 5.30) indicates sediment movement between storage areas and input of coarse sediment either from the bedrock or from lateral sources, and also the importance of hydraulic sorting on grain size distributions (Wohl *et al.,* 2001).

During flood events, coarse grains are deposited on the river bed and result in the development of distinctive bedforms such as subaqueous dunes, in-channel sand bars and

gravel bars. The abundant coarse grained bedforms indicate that the morphology of the Letaba River is regulated by the occurrence of floods (Heritage *et al.,* 1997, 2015; Sargood, 2015). The geomorphic features and sediment distribution discussed here are similar those of other semi-arid regions where floods play a major role in development of river landscapes (Wolman *et al.,* 1978; Spaliviero *et al.,* 2014; Heritage *et al.,* 2015; Kochel *et al.,* 2016; Omengo *et al.,* 2016; Knight and Evans*,* 2017).

Grain size parameters such as skewness, sorting and kurtosis are sensitive to hydraulic processes. The majority of sediments in the Letaba River are negatively skewed (88%) and this corroborates with the dominantly coarse sediment present (Fig. 5.28) associated with high energy conditions (Angusamy *et al.,* 2006). However, some sediment samples are positively skewed, indicating an abundance of fine sediment deposited in a low energy environment (Duane, 1964; Rajmohan *et al.,* 2012). Samples 1 and 2 from site 4 follow this order, where the samples are dominated by fine to very fine sediment, making up 63% to 78.8% of the samples respectively, and are positively skewed. However two samples from sites 5 and 15 are positively skewed but are dominated by medium to coarse sand (Table 5.3). This could be explained by the fact that during high energy flows, water is able to entrain both fine and coarse sediment and deposition occurs rapidly due to a sudden reduction in flow velocity. Martins *et al.* (2005) found a similar trend of alternating positive and negative skewness values in various rivers around the world. The change in underlying lithology is also seen to influence skewness. Site 4 in the present study marks the contact between diorite and granitic gneiss, and marks a change from negatively to positively skewed distributions. The input of grains from the coarser granitic gneiss results in a positively skewed distribution.

Sorting can be used to identify the depositional environment and also whether energy conditions were stable or not (Lewis *et al.,* 1994; Okeyode *et al.,* 2012; Masselink *et al.,* 2015). Sorting of sediment is not uniform in the geomorphic units within this river. The majority of sediments from floodplains are moderately to moderately well sorted, with only two of the samples showing poor sorting, which may indicate that sediment was deposited without further reworking (Table 5.3). Sediment stored on the channel banks and bedrock-cored bars is well sorted, indicating that the sediment has been reworked by the active channel. Poor sorting is associated with coarse grain sizes (Angusamy *et al.,* 2006; Anthony *et al.,* 2007; Pan *et al.,* 2015). This accords in part with observations of this study where most poorly sorted sediments are dominated by medium to coarse sand (Table 5.3). However, one sample from the channel bank of site 12 is dominated by fine sand but is poorly sorted (Fig. 5.33b). The sediment was likely transported as suspended load (Bridge, 2003) and the poor sorting attributed to turbulence and a short traveling distance. Folk and Ward (1957) found that medium and fine sands are better sorted. This corresponds with the findings of Angusamy *et al.* (2006) where fine grained sediment was found to be moderately to better sorted. Edwards (2001) also suggested that fine grained sediments are characterised by better sorting values.

Sediments within the Letaba River are mainly mesokurtic to leptokurtic (Fig. 5.72). High kurtosis values (leptokurtic) are typical of better sorted sediments (Zhang *et al*., 2016) and suggest deposition in a moderate to high energy environment. Mesokurtic distributions indicate a high energy environment where moderate winnowing took place (Rajmohan *et al.,* 2012). Sediments with high kurtosis values in the present study are moderately well sorted to poorly sorted (Table 5.3). Only two of the samples (sites 9 and 11) are platykurtic and indicate that there was little winnowing and sorting during transport and depostion (Rajmohan *et al.,* 2012). However, one sample (site 11-1) with a platykurtic and unimodal distribution is moderately sorted, and one sample (site 9-4) with a platykurtic and trimodal distribution is poorly sorted (Appendix C). The modes of the poorly sorted, platykurtic sample are in the coarse and fine grain size intervals, indicating that the sediment might have been deposited through a sudden reduction in flow velocity. Sample 9-4 was collected from the upstream side of an eroded sandbar, thus representing sediment which was deposited by sheet flows of previous flood events (Fig. 5.13b). The sediment consists of abundant fine sand (33.5%) and poor sorting might be a result of the mixture of sediment from different flood events.

6.2 Mineral analysis

Objective 2: Determine patterns of heavy mineral assemblages, magnetic susceptibility and trace elements by collecting sediment samples on geomorphic features in order to identify sediment patterns.

The factors that influence heavy mineral assemblages on the Letaba River include the underlying geology, hydraulic processes and the present morphology of the river. The importance of underlying geology can be seen by the abundance of minerals present at different river reaches and their variable grain sizes, which are characteristic of different sedimentary, igneous and metamorphic rocks (Deer *et al.,* 1966; Klein *et al.,* 2013). Stable heavy minerals such as rutile, zircon, garnet and tourmaline are present in low quantities, with concentrations ranging from less than 1% to 8.5% within each sample. These minerals were also identified by Derkachev *et al.* (1995), Tsikouras *et al*. (2011) and Khalil *et al*. (2016) in fluvial systems around the world, underlain by similar geologies as the Letaba River. Other common rock-forming minerals such as quartz, plagioclase and orthoclase are also present, with quartz being the most abundant, making up 36.05% to 54.89% of the samples (Table 5.4). The differences in the sizes of minerals at different reaches are possibly due to hydraulic sorting (Tsikouras *et al.,* 2011), different transport distances and sediment influx from different sources (Garzanti *et al.,* 2005). This can be seen from the different sizes of clinopyroxene grains, with site 1 having large grains (150 µm) and site 3 having smaller grains (50 µm) (Fig. 5.31e, k). The differences of grain sizes of the same mineral in different river reaches can also be attributed to the underlying geology. The size of a mineral depends on the rock type and rock forming processes of the parent rock (von Eynatten *et al*., 2012). Site 1 is underlain by metamorphic rocks and site 3 by igneous rocks, and this may help

explain the different sizes of clinopyroxene grains. The influence of tributary sources was highlighted by the abundance of certain minerals. The non-perennial tributary at site 2 is an important source of olivine (7.5%), clinopyroxene (6.4%), muscovite (8.04%) and rutile (Table 5.4). The Shambali River is underlain by gabbro and the sediment contains abundant clinopyroxene (7.06%) and zircon (3.5%). The olivine grains from this site contain inclusions of plagioclase which is distinctive of gabbro rocks (MacKenzie *et al.,* 1994). The non-perennial Shambali and Makoforo rivers contain very low percentages of magnetite, ilmenite and hematite, making up only 0.8 to 3.2%, indicating low contributions of iron hydroxide minerals (Table 5.4). The Nwanedzi River (site 8) on the other hand contains iron hydroxide-rich mineral assemblages with concentrations ranging between 3.9% and 4.4%, indicating the importance of this river in contributing these minerals to the Letaba River (Table 5.4).

The effects of hydraulic sorting are seen clearly in the areas underlain by the same lithology but consisting of different mineral assemblages. Sites 4, 5 and 6 are underlain by granodioritic biotite gneiss, but each site is characterised by variable abundances of each mineral (Table 5.4). Site 5 contains 11.3% biotite, 6% muscovite, 12% magnetite and 8.5% rutile, whereas site 6 contains similar biotite (11.5%), muscovite (5.2%), and much less magnetite (1.47%) and hematite (0.1%) (Table 5.4). The effects of hydraulic sorting can be seen in the differences in opaque mineral concentrations in the present day channel, floodplain and tributaries (Table 5.5). The present day active channel has the highest concentrations of magnetite, ilmenite and hematite with concentrations of 0.3% to 15.8% (Table 5.5). These high values may arise possibly because the minerals have high densities and require high flow velocities for transport. Kermani *et al.* (2016) observed a similar trend where low density heavy minerals were transported for longer distances and high density minerals accumulated closer to the source area. The overall highest concentrations of magnetite (34.5%), hematite (18.5%) and ilmenite (9.8%) are found in the sediment within the active channel (Table 5.5). The grain sizes associated with the different minerals also indicate the importance of hydraulic sorting. Derkachev *et al.* (2007) showed that high density minerals (zircon, garnet, opaque minerals) accumulate in areas of coarse sediment and low density minerals (micas and hornblende) are characteristic of fine sediments. Samples 4-2, 7-2 and 9-1 have the high percentages of fine sediment, making up 78%, 47.9% and 94.7% respectively (Appendix B), and also have high percentages of biotite and muscovite (between 13.9% and 29%) (Appendix E).

The morphology and hydraulic processes of a river also influence the concentration of heavy minerals. Morton *et al.* (1999) indicated that the heavy mineral concentration in an active channel differs from that on the floodplain due to the different flow conditions operating on these features. The proportion of stable minerals will be the highest in transport-limited river reaches (Morton *et al.,* 1999). Hattingh *et al.* (1992) observed an increasing trend in heavy mineral concentrations away from the active channel. However, this trend is not present in the sediments collected from the Letaba River, where heavy mineral

concentrations vary across the floodplain (Appendix E). An example of this can be seen in site 1 where sample 1-1 from the margin of the floodplain contains the highest percentage of biotite (11.4%), orthopyroxene (36.8%), magnetite (11.7%), ilmenite (3.7%) and hematite (4%). Sample 1-2 is characterised by lower concentrations of magnetite (1.5%), hematite (1.1%), ilmenite (0.3%) and orthopyroxene (35%) and no biotite (Appendix E). This sample was collected from an inactive channel in the middle of the floodplain, and the lower concentrations of these minerals are possibly due to hydraulic sorting. Denser (magnetite, ilmenite, hematite) and coarse grained (quartz and orthopyroxene) minerals were most commonly deposited and the smaller and less dense minerals such as biotite are either not present or have low concentrations, e.g. muscovite (1.9%). This indicates the role of selective deposition in determining heavy mineral assemblages throughout the river. Mineral density also plays a role in determining heavy mineral assemblages (Ridley, 2013). Ridley (2013) suggested that settling equivalence of minerals with variable density and size is an important factor, suggesting that larger and denser minerals are deposited closer to source. Sample 1-4 deposited closer to the active channel has slightly higher concentrations of biotite (2.5%), magnetite (2.5%), hematite (1.8%) and orthopyroxene (63.8%). The variable concentrations of these heavy minerals indicate the importance of hydraulic sorting and the underlying lithology in mineral assemblages.

6.3. Magnetic susceptibility

MS values vary throughout the different river reaches with values ranging between 0.13×10^{-6} m^3 kg^{-1} and 3.15×10^{-6} m^3 kg^{-1} (Fig. 5.34). These values are consistent with those found in other semi-arid catchments underlain by sedimentary and igneous rocks (van der Waal *et al.,* 2015; Pulley *et al.,* 2016; Rowntree *et al.,* 2017). Since MS is a measure of magnetic minerals in the sediment, the percentage of magnetic minerals within the sediment should correspond with MS readings in the sediments. All the samples analysed had a percentage between 1.5% and 18% of magnetite minerals in total and less than 1% to 8.2% of hematite minerals in particular (Table 5.5), indicating the importance of ferrimagnetism (Mullins, 1977; Maher, 1998). The last major flood event on the Letaba River in 2014 produced discharges of between 35.2 m^3s^{-1} and 94 m^3s^{-1} (Fig. 2.5), indicating that there was enough energy to transport and distribute coarse grained material from the igneous and metamorphic rocks. Increased concentrations of ferromagnetic magnetite were correlated with increasing rainfall trends in the soils of four regions in North African (Lyons *et al.,* 2010), indicating the importance of rainfall for the distribution of magnetic minerals, activated during river floods. The MS values in this research were only measured during one field trip, thus no correlation could be made with the rainfall trends within this river.

A positive relationship between grain size and MS has been identified in various rivers across the world, where coarse grained sediment was associated with low MS values and fine grained sediment with higher MS values (Foster *et al.,* 1998; Maher, 1998; Blake *et al.,*

2006; Hatfield *et al.,* 2009). This would require the sediment grain sizes to be measured separately for magnetic susceptibility; however the MS values within this study were measured in the field with size ranges and thus no correlation was done between grain size and MS values (Fig. 5.35). When considering the underlying geology, there is no significant difference between MS values from igneous and sedimentary rocks (Table 5.6). Sediment from igneous rocks was found to have higher MS values than sediment derived from sedimentary rocks in the Wilgerbosch River in the Great Karoo, South Africa (Pulley *et al.,* 2016). An opposite trend was observed in the Thina Catchment, South Africa, where MS values indicated that the dominant sediment source was from sedimentary rocks, with igneous rock contributing only a small percentage (van der Waal *et al.,* 2015). On the Letaba, MS values from the reach underlain by sedimentary rocks (site 7) are high, ranging from 0.43×10^{-6} m^3 kg^{-1} to 1.56×10^{-6} m^3 kg^{-1}. The relatively high values may result from deposition of magnetic minerals from upstream igneous reaches. Mzobe (2014) indicated that high MS values for sediment from igneous rocks are higher because they contain more iron-containing minerals when compared to sedimentary rocks.

Šroubek *et al.* (2007) indicated that high MS values are associated with larger grain sizes of magnetite minerals and a high concentration of magnetite minerals in the Spiralka Cave, Czech Republic. The MS readings at site 13 on the Letaba River floodplain range between 1.7 and 2.06×10^{-6} m^3 $kg^{-1}$and this site is also characterised by a high percentage of magnetite minerals (Table 5.6). The highest concentration of magnetite (17.7%) is present in sample 13-2, and this sample has a high MS value of 2.06×10^{-6} m^3 kg^{-1}. Sample 1-1 which also has a high concentration of magnetic minerals (8.5%) also has a high MS value of $3.15\times10^{-6}m^3$ kg^{-1}. The low MS value ($0.13\times10^{-6}m^3$ kg^{-1}) of sample 6-1 corresponds with a very low concentration (0.9%) of magnetic minerals (Table 5.6). Sample 6-1 was collected on a ridge-like sandbar, thus a long storage period might have resulted in dissolution of magnetic minerals (Maher, 1998). This idea can be used to explain the variable spatial distribution of MS values obtained at the different sampling sites (Fig. 5.34).

6.4 Trace element distribution

Trace element concentrations varied widely throughout the Letaba River (Fig. 5.36). Background concentrations of trace elements in sediments are determined by the physical and chemical weathering of parent rock (Kabula-Pendias, 2011). Zirconium (Zr) is the most abundant element and the most abundant concentrations are in samples 2-1, 9-4 and 12-3 (Fig. 5.36) with concentrations of 2262 ppm, 2601 ppm and 2511 ppm, respectively. Zirconium is derived from zircon which is an abundant detrital mineral and which is weathered from igneous and metamorphic rocks and present in sediment due to its high durability (Deer *et al.,* 1966; Thomas, 1987, 2011; Klein *et al.,* 2013). This is supported by the strong positive relationship between zircon and Zr (0.61) (Appendix J). Selective deposition might be the reason why zircon is abundant in fluvial sediment. According to Rubey (1933),

high density minerals settle together with coarse grained low-density minerals such as quartz. Zircon has a specific gravity between 4.0-4.7 (Ďud'a and Rejl, 1986) and would require high flow velocities and turbulent flow to be transported and deposited. Zr has a weak relationship with very coarse sand and fine sand (Appendix I). Very fine gravel has a significant relationship with Sc, V, Zn, Ga and Nb. These five minerals are present in low quantities within the analysed sediment (Fig. 5.36) possibly due to dissolution or low quantities present in parent materials.

When taking into account inputs from tributaries, high Zr concentrations were also derived from the Makoforo River (site 16-4) and another non-perennial tributary entering the Letaba River (site 2-1) (Fig. 5.40). Sediment samples from these rivers contain Zr concentrations of 2262 ppm and 1080 ppm respectively. Other abundant elements are Sr, Ba and Cr with concentrations of 465 ppm, 790 ppm and 863 ppm respectively. High concentrations of V, Cr, Co, Ni, Sr, Y, Zr, Nb, Mo, Ba, Th and U are present at the junction of the Makoforo and Letaba rivers, and their concentrations decrease as the sediments mix within Letaba river sediments on the different bedforms. This is an example showing the importance of tributaries and how sediments mix within a river reach. High concentrations of Cr (466 and 623 ppm) and Ni (237 and 198 ppm) were sampled from the Nwanedzi River (site 8) which enriches the Letaba River with Cr and Ni.

Trace elements have also been noted to concentrate in areas close to the active river channel and to decrease away from the river channel (Graf *et al.,* 1991; Ciszweski, 2003; Falkowska *et al.,* 2015). This trend is not present in the samples from the Letaba River. An example can be seen at site 4, where concentrations of Cr, Zr, Ba, Th and Zn are higher in distal parts of the floodplain (Fig. 6.1). This serves as evidence that the trace elements were deposited as overbank deposits by fluvial processes (Martin, 2004). In natural settings, trace elements are transported in suspension which might mean that the majority of trace elements would most likely be deposited in bedforms characterised by fine sediments (Martin *et al.,* 1979). However, higher concentrations of high density minerals with Ba, Sr and Zr are present in coarse sediments (Appendix I).

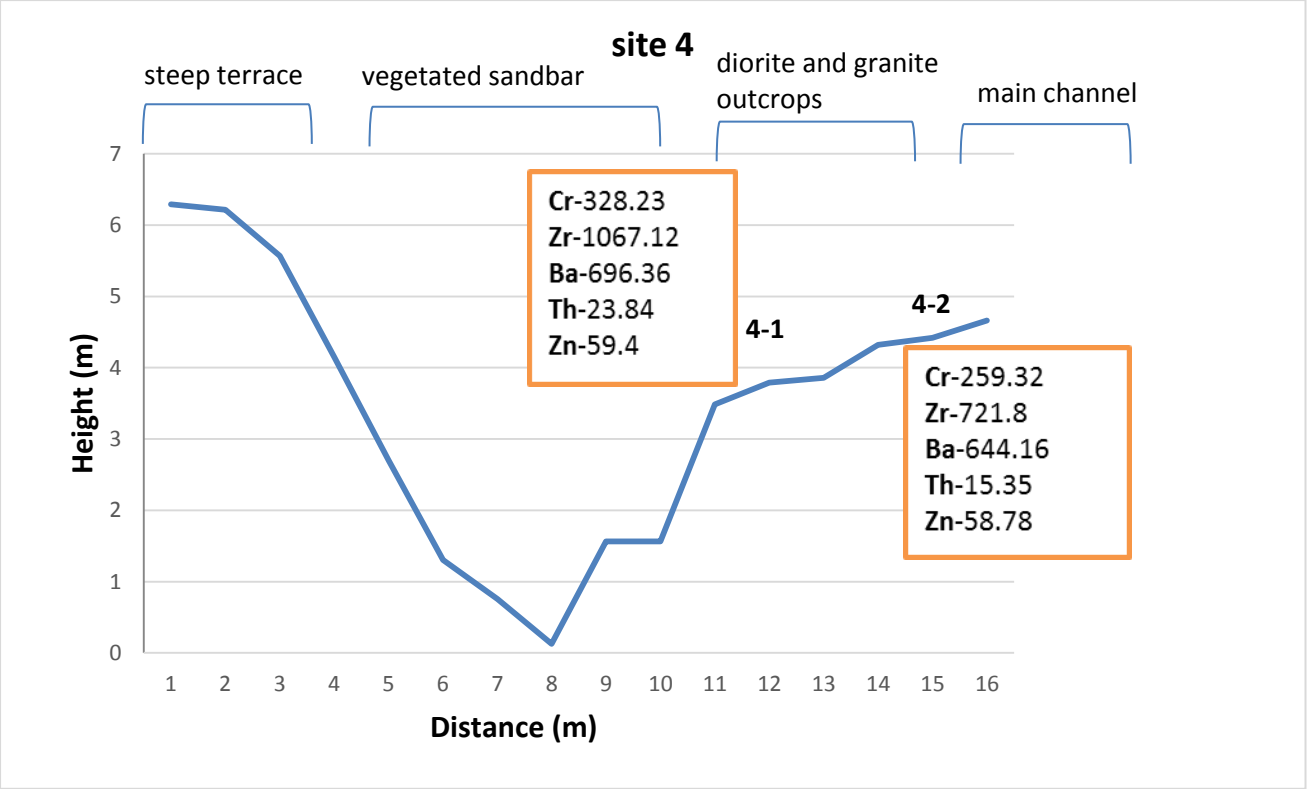


Fig. 6.1. The concentrations of five trace elements (values in ppm) at samples 4-1 and 4-2. Values decrease towards the present day active channel.

Table 5.7 indicates the results from the principal component analysis of trace element concentrations. The significant positive relationship between the first principal component and Zn, V, Sc, Nb, Cu, Ga and Co indicates that these trace elements have a similar distribution and thus may be enriched from the same source. The minerals Zn, V, Sc, Cu, Co, and Nb are all transition metals and have similar chemical properties, which may mean that they have the same behaviour when transported and thus would have a similar spatial distribution. This relationship corresponds with the results obtained from the correlation analysis between the trace elements, where strong significant relationships exist between V, Co, Cu, Zn and Nb (Appendix G). This indicates that samples with very high concentrations of these minerals might have been sourced from the same area. The overall highest concentrations of these elements were found in samples 2-1, 8-1, 8-2, 9-1, 12-2, 12-3, 13-2, 14-2, and 15-3 (Fig. 5.36). There is some indication of enrichment in downstream reaches. Guo *et al.* (2014) also found a similar trend in the Hanjiang River in China, where concentrations of trace elements were higher in downstream reaches, attributed to an increase from anthropogenic sources. The Letaba River however is still in a largely natural state, with no dense residential areas, agricultural land use or mines adjacent to the river, and so enrichment of these elements be attributed to anthropogenic sources. However, increased river discharge in a downstream direction (Fig. 2.5) might have increased the transport of trace elements and the resultant mineral deposition. The co-varying

relationship between the second principal component and Th, Cr, Zr, Y, Ni and Pb indicates a similar distribution of these elements and a possible similar source. These elements do not fall under the same mineral group on the periodic table and their chemical properties differ, however.

Trace elements were correlated with heavy minerals present within the samples, in order to find the sources of these trace elements (Appendix J). Rock-forming minerals are associated with certain trace elements which make up the mineral grains (Deer *et al.,* 1966). For example, Zr is derived from zircon (Tsikouras *et al.,* 2011) and U, V, Th and Nb can be derived from rutile (Meinhold, 2010; Meyer *et al.,* 2011). Magnetite and hematite were seen to have high significance values of 0.52 and 0.40 respectively with V (Appendix J). Vanadium concentrations were positively correlated with iron hydroxide concentrations (Larron, 2014), indicating the co-existence of iron hydroxide and V. The distribution of trace elements is also determined by the underlying lithology (Miller *et al.,* 2007; Falkowska, 2009; Otamendi *et al.,* 2016). Otamendi *et al.* (2016) noted that high concentrations of Cr, Ni, Co, Zn and V were associated with olivine-rich mineral assemblages. Olivine has high correlation values of 0.58 and 0.52 with Ba and Pb, respectively, and a low but significant relationship with Ni, Sc and Rb (Appendix J). High concentrations of Zn have been attributed to emissions from cars passing near various river systems (Callender *et al.,* 2000; Yesilonis *et al*., 2008; Coxon *et al*., 2016; Gerber *et al.,* 2016). However the Letaba River is not close to big roads and Zn concentrations were relatively low. Zn is therefore likely to have been derived from heavy minerals as Zn has positive relationships with zoisite (0.70), garnet (0.43) and zircon (0.40). These positive correlations indicate that trace elements were possibly derived from the underlying geology of the Letaba River and surrounding tributaries.

6.5 Mixing models and sediment sources

Objective 3: Identify potential sediment source contributions using the modified Collins mixing model in order to identify major sediment sources at the downstream river reaches and the processes responsible for sediment generation.

6.5.1 Sediment sources

A mixing model was used to calculate the relative contribution of sediment from different sources within and surrounding the river (Miller *et al.,* 2013). The high variability in the concentrations of trace elements from the different source areas that were sampled shows that trace elements can be used to discriminate between different sources (Table 5.11). Several authors have indicated that the contributions from different potential sources are highly influenced by land use and erosional processes characteristic of those river reaches (Carter *et al.,* 2003; Hughes *et al.,* 2009; Miller *et al.,* 2013). The different sites sampled indicate different proportions of sediment derived from upstream sources (Fig. 5.38).

River reaches with high sediment contributions from tributaries indicate the influence of high rainfall events on sediment delivery. The tributaries sampled were dry during fieldwork sampling, which is an indication that they only become active during high rainfall events, which would result in sediment being transported into the Letaba River. The importance of tributaries as the dominant source contributor diminishes in downstream reaches, possibly because their signatures are diluted as more sediment is contributed from channel sources (Fig. 5.40). Examples of this are the downstream samples of sites 12, 13 and 14, where tributary sources contribute lower percentages of 10%, 17% and 11%, respectively.

Channel bed samples contributed the highest percentage of sediment at sites 10, 12 and 14 with values of 51%, 77% and 77%, respectively (Fig. 5.37). These samples also had the lowest contributions from tributary sources. However, sediment derived from tributaries still remains relatively important in the downstream reacges of the river. The results from the Letaba can be compared to those obtained by Wilkinson *et al.* (2013) who found low tributary contributions in the Burdekin River Basin, Australia. During a flood, sediment is eroded from the channel bed and underlying bedrock due to high water velocities and this causes the channel depth to increase, resulting in the production of more sediment within the river (Hancock *et al.,* 1998; Thompson *et al.,* 2013; Magilligan *et al.,* 2015; Collins *et al.,* 2016). Thus the high contribution of channel sediment within these reaches shows the importance of bed erosion during flood events, especially in the downstream reaches. The relative contributions from potential sources vary in the Letaba, indicating the importance of variable erosional processes in sediment supply to the river system (Fig. 5.40).

6.5.2 Sediment source apportionment at different sampling sites

Site 10 has a 51% contribution from the channel bed, 27% from the channel bank and 22% from tributary sources (Fig. 5.37a). The single straight channel of this river reach (Fig. 5.15a, b) is favourable for channel bed erosion as the energy of the water is concentrated in a single channel and thus a higher stream power would result (Seidl *et al.,* 1992). Yang *et al.* (1998) noted that straight channels have higher flow velocities and this might have influenced channel erosion at this reach. High water velocities not only erode the channel bed here but also cause lateral erosion of the channel bank, which results in a wide and deep channel. Channel bed and bank erosion during floods was noted by Kochel *et al.* (2016) and Surian *et al.* (2016).

The high contribution from channel bed sources (77%) at site 12 can be attributed to the influence of bedrock outcrops (Fig. 5.18a). Bedrock-influenced channels vertical incision of the channel bed through plucking during high flows (Seidl *et al.,* 1992; Allen *et al.,* 2013; Collins *et al.,* 2016). This can result in the production of sediment and the resultant high contribution of channel bed sediment in this reach.

Only one site has a dominant contribution from the channel bank. At site 13 this contribution is 62%, and the lowest contribution of 17% from tributary sources (Fig. 5.37c). This is a bedrock-influenced channel with more than 50% bedrock outcrops and very little sediment between the outcrops. Bedrock-influenced channels experience both vertical and lateral erosion of the bed and banks. Lateral erosion is responsible for channel widening and a resultant increase in sediment supply and sediment carrying capacity within the channel (Whitbread *et al*., 2015; Surian *et al.,* 2016). Bedrock channels are known to experience channel widening during floods (Wohl *et al.,* 2001; Hancock *et al.,* 2011; Allen *et al.,* 2013; Spotila *et al.,* 2015). Sportila *et al.* (2015) suggested that bedrock-influenced channels experience lateral erosion at bedrock discontinuities. The river bank was also exposed at this reach, with no riparian vegetation present, thus encouraging erosion of the river bank.

Site 14 has a high contribution (77%) from the channel bed. The channel bank contributes 12% and tributary sources 11% of the sediment (Fig. 5.37d). This river reach has a narrow channel and a high sediment deposition on the floodplain upstream of the low-water bridge (Fig. 5.22a). This large mass of sediment suggests reworking and deposition from the channel bed. Channel bed sources also dominate at site 15, contributing 48% of the sediment. There is also an increased contribution from the channel bank and tributary sources, at 28% and 24% respectively. Increased contribution from tributaries can be explained by sediment storage on the floodplain of this river reach which consists of boulders of basalt, diorite, granite and sandstone (Fig. 5.24b), eroded from the upstream reaches. However tributary sources were sampled upstream reaches and these contributions decrease in a downstream direction at sites 12, 13 and 14, with an increase at site 15 (Fig. 5.40). It is unlikely that contributions from tributary sources would outweigh

channel sources in this downstream reach, thus posing a potential limitation in the multivariate model's ability to accurately apportion sediment sources in this reach. The potential sediment sources predicted from the mixing model from tributary, channel bed and channel bank sources vary in the downstream reach of the Letaba River, and indicate complex spatial patterns of flood-influenced sediment influx and deposition within this river.

The erosion of the channel bed and channel bank within the Letaba is controlled by the width of the river valley and the type of channel, being either bedrock-influenced or an alluvial channel. This can be seen by the erosion processes at bedrock-influenced channels, such as sites 12 and 13, where the presence of bedrock results in vertical or lateral erosion. Straight and deep channels experience higher channel bed and channel bank erosion rates such as site 10 which was apportioned 51% channel bed and 27% channel bank sources, as energy is concentrated in a single channel. River reaches with very wide valleys such as site 6 experience less erosion of the channel bed and bank, as water is distributed over a larger area during flood events.

7. Conclusions

This study set out to investigate sediment distributions and identify relative sediment contributions from different source areas within the catchment. Sediment patterns are important as they influence the functioning of river systems. The increased sediment influx and dynamics of the Letaba River associated with floods has generated an increased need to understand these sediment patterns for better management of the river system. The main findings of this research are indicated below:

- Relationships between sediments and landforms along different river reaches were identified through fieldwork and lab analysis, in order to identify the main driving processes of sediment distributions. The characteristic coarse grained bedforms in the Letaba River indicate the importance of floods in regulating the morphology and sediment patterns of this river. The bedforms identified include sandbars on the floodplain, gravel bars, 3D subaqueous dunes and in-channel bars. The relationship of these landforms to high energy flood events are supported by grain size, skewness, kurtosis and sorting values of the sediment which indicate the role of high energy flow events in the transport and distribution of sediment within the river.
- The analysed grain size intervals of the samples collected indicate that there is no fining downstream pattern in the Letaba River, with sediments showing fluctuations in grain sizes and sediment properties throughout. Grain size analysis also showed the distribution of sediment as overbank deposits with increased fining in the distal parts of the floodplain, which are characteristic of flood deposits. Other overbank deposits were present as large boulders scattered across the floodplain, which could have only been carried by water moving at a high velocity.
- The heavy minerals identified are characteristic of the underlying sedimentary, igneous and metamorphic rocks within the Letaba River catchment. Heavy mineral assemblages identified vary depending on hydraulic processes and selective deposition. Differences in the concentrations of minerals on different landforms and according to grain sizes of these minerals indicate hydraulic sorting at high flow velocities. The patterns of heavy mineral assemblages vary across the floodplains of the sampled reaches, with higher concentrations of denser minerals closer to the active channel.
- Magnetic susceptibility results showed that samples with higher concentrations of magnetic minerals have higher magnetic susceptibility values. However, magnetic susceptibility values were not able to distinguish between sedimentary, igneous or metamorphic sources. Correlations between magnetic susceptibility and grain size were not investigated in this study.
- The use of principal component analysis and correlation coefficients enabled relationships between trace elements to be identified. The abundance of the element Zr within the sediments highlights the effects of high velocity flows in transporting denser minerals. Tributaries as potential sources of sediment were seen in the high concentrations of trace elements such as Cr, Ni, Zr, Ba and Cr. Trace

element concentrations are seen to increase in a downstream direction, suggesting the effects of an amplified intensity of floods in a downstream direction.

- The use of minor trace elements as tracers in the Collins mixing model enabled the relative sediment contributions from different sources to be identified. The mixing model results indicated that the greatest potential source of sediment within the Letaba River overall is from the channel bed, contributing on average 55% of the sediment within the samples analysed, however this is highly variable spatially. High erosion rates and sediment production from the channel bed supports the main sediment distribution process proposed in this study, which is by flood events. Tributaries were apportioned the lowest contribution, however, contributions from tributaries indicate the role of high rainfall in episodically contributing sediment to the Letaba River. The results indicated that sediment source apportionment can be used to identify the areas with different spatial patterns of erosion within the river system.

7.1 Implications of this study for river management

Water is a scarce resource in semi-arid regions and thus the correct management of this resource is essential. This research can be used to facilitate the implementation of better water management practices on rivers in semi-arid regions. The geomorphology of a river provides services for riparian vegetation (van Coller *et al.,* 1997) and for riverine species (Meissener *et al.,* 2016), thus it is essential to understand the geomorphology and dynamics of a river in order to ensure that catchment management plans incorporate and uphold the geomorphic behaviour of the river system. Studies of sediment source identification can be used to identify the areas within the catchment where most erosion takes place and thus measures targeted at reducing erosion can be implemented (Walling *et al.,* 2013). The sediment tracing method has not been widely used in South Africa for river management practices, thus river managers can incorporate this method with their current practices in order to understand sediment movements and the distribution of trace elements or pollutants within a river system. The distribution of trace elements and heavy minerals can then be used to identify potential areas of pollutant storage. With the use of sediment sources and distributions, environmental managers can work with researchers in order to understand sediment movements and inform relevant management plans (Mzobe, 2014). Geo-engineers can use information about the distribution of grain sizes and heavy minerals to inform decisions when constructing dams and reservoirs. Research of this type has not been previously conducted on the Letaba River, thus this research opens the door for further research of sediment dynamics within semi-arid rivers in South Africa. This study indicated that sediment contributions from potential sources vary throughout the river system and thus the results of this study can be used to implement appropriate measures to reduce the influx of sediment and decrease erosion from the potential sources contributing the majority of the sediment.

7.2 Limitations of this study

Not all the samples were used for the XRF analysis because there was not enough sediment below 63 µm. During the field sampling period, more sediment could have been collected in order to ensure enough for each analysis. Magnetic susceptibility was measured in the field, on mixed grain sizes and this limited the ability for grain sizes to be correlated with magnetic susceptibility. Magnetic susceptibility could be measured once the sediment had been sieved into different grain size intervals to ensure that a comparison can be made for a more accurate interpretation of the results. Only one magnetic susceptibility reading was collected at every sampling location and this had implications for the analysis of the results. At least three to four readings could be recorded at each sampling location to ensure that enough data is collected. A point counting method was used to count the individual heavy mineral grains, but the use of an automatic point counter could be beneficial as it would reduce the possibilities of counting errors and would minimize the time used for this method. Only three sediment source categories were used within in this study which leaves out contributions from other potential sources within the river system. The addition of more potential source categories would also add value to the results obtained as more possible potential sources would be accounted for. Sediment samples were only collected during one field trip and this limited the amount of sediment collected in order to successfully understand the movement of sediment using mixing models. Sediment samples should be collected over a longer time period and repeated, possibly before and after a heavy rainfall season, in order to fully assess how sediment moves between different storage areas within the Letaba River. The model was not applied to the upstream reaches independently as there would not be suitable number of source samples to calculate the parameters that are needed in the model. Thus, because all the source samples lie in the upstream reaches of the river, these samples were used to model the source contributions in the downstream reaches of the river, from site 10 to 15. The collection of more sediment source samples in the upstream reaches would enable the application of the model in the upstream reaches.

Reference list

Allen, R. L. 1982. *Sedimentary structures, their character and physical basis* (Vol. 1). Elsevier, Amsterdam.

Allen, G.H., Barnes, J.B., Pavelsky, T.M. and Kirby, E. 2013. Lithologic and tectonic controls on bedrock channel form at the northwest Himalayan front. *Journal of Geophysical Research: Earth Surface.* Vol. 118. No.3. Pp.1806-1825.

Amos, C.B. and Burbank, D.W. 2007. Channel width response to differential uplift. *Journal of Geophysical Research: Earth Surface*. Vol. 112. doi:10.1029/2006JF000672.

Ando, S., Garzanti, E., Padoan, M. and Limonta, M. 2012. Corrosion of heavy minerals during weathering and diagenesis: A catalogue for optical analysis. *Sedimentary Geology*. Vol. 280. Pp. 165-178.

Anthony, E.J. and Héquette, A. 2007. The grain-size characterisation of coastal sand from the Somme estuary to Belgium: Sediment sorting processes and mixing in a tide-and storm-dominated setting. *Sedimentary Geology*. Vol. 202. No.3.Pp.369-382.

Angusamy, N. and Rajamanickam, G.V. 2006. Depositional environment of sediments along the southern coast of Tamil Nadu, India. *Oceanologia*. Vol. 48. No.1. Pp. 87-102.

Arnold, J.G., Williams, J.R. and Maidment, D.R. 1995. Continuous-time water and sediment-routing model for large basins. *Journal of Hydraulic Engineering*. Vol. 121. No.2. Pp.171-183.

Attal, M. and Lave, J. 2009. Pebble abrasion during fluvial transport: Experimental results and implications for the evolution of the sediment load along rivers. *Journal of Geophysical research.* Vol. 114. doi: 10.1029/2009JF001328.

Baartman, J. E. M, Keesstra, S. D., Masselink, R. and Temme, J. A. M. 2013. Linking landscape morphological complexity and sediment connectivity. *Earth Surface Processes and Landforms*. Vol. 38. Pp. 1457-1471.

Bahlburg, H. 1998. The geochemistry and provenance of Ordovician turbidites in the Argentine Puna. *in:* Pankhurst, R. J. and Rapela, C. W. (eds). *The Proto-Andean Margin of Gondwana.* Geological Society. London. Special Publications. No.142. Pp. 127-142.

Baker, V. R. 1994. Geomorphological understanding of floods. *Geomorphology*. Vol. 10. Pp. 139-156.

Baker, V. R. and Pickup, G. 1987. Flood geomorphology of the Katherine Gorge, Northern Territory, Australia. *Geological Society of America Bulletin*. Vol. 98. Pp. 635-646.

Baker, R. and Kale, V. S. 1998. The role of extreme floods in shaping bedrock channels. In: Tinkler, K. J. and Wohl, E. E. (eds). *Rivers over rock: Fluvial processes in bedrock channels*. American Geophysical Union. Washington, DC. Pp. 153-165.

Bartholdy, J., Flemming, B.W., Bartholomä, A. and Ernstsen, V.B. 2005. Flow and grain size control of depth-independent simple subaqueous dunes. *Journal of Geophysical Research: Earth Surface*. Vol. 110(F4). doi: 10.1029/2004JF000183.

Batalla, R.J., Gomez, C.M. and Kondolf, G.M. 2004. Reservoir-induced hydrological changes in the Ebro River basin (NE Spain). *Journal of Hydrology*. Vol. 290. No.1.Pp.117-136.

Bernet, M., Brandon, M.T., Garver, J.I. and Molitor, B.R. 2004. Fundamentals of detrital zircon fission-track analysis for provenance and exhumation studies with examples from the European Alps. in Bernet, M. and Spiegel. C. (eds). *Detrital thermochronology-Provenance analysis, exhumation and landscape evolution of mountain belts*. Boulder, Colorado. *Geological Society of America Special Papers*. Vol. 378. Pp.25-36.

Blake, W.H., Wallbrink, P.J., Doerr, S.H., Shakesby, R.A. and Humphreys, G.S. 2006. Magnetic enhancement in wildfire-affected soil and its potential for sediment-source ascription. *Earth Surface Processes and Landforms*. Vol. 31. No.2. Pp.249-264.

Blott, S. J. and Pye, K. 2001. Gradistat: A grain size distribution and statistics package for the analysis of unconsolidated sediments. *Earth Surface Processes and Landforms*. Vol. 26. Pp.1237-1248.

Bridge, J. S. and Leeder, M. R. 1979. A simulation model of alluvial stratigraphy. *Sedimentology.* Vol. 26. No. 5. Pp. 617-644.

Bridge, J.S. 1993. The interaction between channel geometry, water flow, sediment transport and deposition in braided rivers. in Best, J.L. and Bristow, C. S. (eds). *Braided Rivers.* Geological Society, London, Special Publications. Vol.75. No.1 .Pp.13-71.

Bridge, J.S. 2003. *Rivers and floodplains: forms, processes, and sedimentary record*. John Wiley & Sons, UK.

Bristow, J. W., Sweeney, R. and Venter, F. J. 1986. Geological guide to selected areas of the Krugr National Park. *Koedoe*. Vol. 29. Pp. 183-202.

Bui, E. N., Mazzullo, J. M. and Wilding, L. P. 1989. Using quartz grain size and shape analysis to distinguish between Aeolian and fluvial deposits in the Dallol Bosso of Niger. *Earth Surface Processes and Landforms.* Vol.14. Pp. 157-166

Bull, L. J. and Kirkby, M. J. 2002. *Dryland Rivers: Hydrology and geomorphology of semi-arid channels.* John Wiley & Sons. Ltd. England.

Bunn, S.E. and Arthington, A.H. 2002. Basic principles and ecological consequences of altered flow regimes for aquatic biodiversity. *Environmental Management*. Vol. 30. No.4. Pp.492-507.

Burkham, D. E. 1972. Channel changes of the Gila River in Safford valley, Arizona, 1846-1970. *Geological Survey Professional Paper*. No. 655-G. Pp. 1-24.

Callender, E. and Rice, K.C. 2000. The urban environmental gradient: anthropogenic influences on the spatial and temporal distributions of lead and zinc in sediments. *Environmental Science & Technology*. Vol. 34. No. 2. Pp.232-238.

Caracciolo, L., Orlando, A., Marchev, P., Critelli, S., Manetti, P., Raycheva, R. and Riley, D. 2016. Provenance of Tertiary volcanoclastic sediment in the NW Thrace (Bulgaria). *Sedimentary Geology*. Vol. 336. Pp. 120-137.

Carter, J., Owens, P.N., Walling, D.E. and Leeks, G.J. 2003. Fingerprinting suspended sediment sources in a large urban river system. *Science of the Total Environment*. Vol. 314. Pp. 513-534.

Cenderelli, D. A. and Wohl, E. E. 2003. Flow hydraulics and geomorphic effects of glacial lake outbursts in the Mount Everest region, Nepal. *Earth Surface Processes and Landforms.* Vol. 28. Pp. 385–407.

Chanson, H. 1999. *The Hydraulics of Open Channel Flow: an Introduction*. Sediment Transport Mechanisms 1. Bed-load Transport. Butterworth-Heinemann London. UK. Pp. 195-209.

Chatanantavet, P., Lajeunesse, E., Parker, G., Malverti, L. and Meunier, P. 2010. Physically based model of downstream fining in bedrock streams with lateral input: downstream fining in bedrock streams. *Water Resources Research*. Vol. 46. doi: 10.1029/2008WR007208.

Collins, A.L., Walling, D.E. and Leeks, G.J.L. 1997. Source type ascription for fluvial suspended sediment based on a quantitative composite fingerprinting technique. *Catena*. Vol.29. No.1. Pp.1-27.

Collins, A. L., Walling, D. E., Sichingabula, H.M. and Leeks, G. J. L. 2001. Suspended sediment source fingerprinting in a small tropical catchment and some management implications. *Applied Geography*. Vol. 21. Pp. 387-412.

Collins, A. L. and Walling, D. E. 2002. Selecting fingerprint properties for discriminating potential suspended sediment sources in river basins. *Journal of Hydrology*. Vol. 261. Pp. 218-244

Collins, A. L., Walling, D. E. Webb, L. and King, P. 2010a. Apportioning catchment scale sediment sources using a modified composite fingerprinting technique incorporating property weightings and prior information. *Geoderma*. Vol. 155. Pp. 249-261.

Collins, A.L., Zhang, Y., Walling, D.E., Grenfell, S.E. and Smith, P. 2010b. Tracing sediment loss from eroding farm tracks using a geochemical fingerprinting procedure combining local and genetic algorithm optimisation. *Science of the Total Environment*. Vol. 408. No.22. Pp. 5461-5471.

Collins, B.D., Montgomery, D.R., Schanz, S.A., Larsen, I.J. 2016. Rates and mechanisms of bedrock incision and strath terrace formation in a forested catchment, Cascade Range, Washington. *Geological Society of America Bulletin*. Vol. 128. Pp. 926-943.

Collins, A.L., Pulley, S., Foster, I.D., Gellis, A., Porto, P. and Horowitz, A.J. 2017. Sediment source fingerprinting as an aid to catchment management: a review of the current state of knowledge and a methodological decision-tree for end-users. *Journal of Environmental Management.* Vol.194. Pp.86-108.

Cooper, R.J., Krueger, T., Hiscock, K.M. and Rawlins, B.G. 2015. High-temporal resolution fluvial sediment source fingerprinting with uncertainty: a Bayesian approach. *Earth Surface Processes and Landforms*. Vol. 40. No.1. Pp.78-92.

Cox, S. and Nibourel, L. 2015. Bedload composition, transport and modification in rivers of Westland, New Zealand, with implications for the distribution of alluvial pounamu (jade). *New Zealand Journal of Geology and Geophysics*. Vol. 58. Pp. 154-175.

Coxon, T.M., Odhiambo, B.K. and Giancarlo, L.C. 2016. The impact of urban expansion and agricultural legacies on trace metal accumulation in fluvial and lacustrine sediments of the lower Chesapeake Bay basin, USA. *Science of the Total Environment*. Vol. 568. Pp.402-414.

Dean, D. J. and Schmidt, J. C. 2013. The geomorphic effectiveness of a large flood on the Rio Grande in the Big Bend region: Insight on the geomorphic controls and post-flood geomorphic response. *Geomorphology*. doi:10.1016/j.geomorph.2016.02.002.

Deer, W. A. 1966. *An introduction to the rock-forming minerals*. Longman. London.

Derkachev, A. N. and Nikolaevia, N. A. 1995. Heavy mineral associations found in sediments of the East China Sea and adjacent Ryukyu and Taiwan areas. *Terrestrial, Atmospheric and Oceanic Sciences*. Vol. 6. No. 1. Pp.75-90.

Derkachev, A. N. and Nikolaeva, N. A. 2007. Multivariate analysis of heavy mineral assemblages of sediments from the marginal seas of the Western Pacific. *Developments in Sedimentology*. Vol. 58. Pp.439-464.

Department of Water Affaires and Forestry. 2012. *Classification of water resource and determination of the resource quality objectives in the Letaba River*. Report Number: RDM/WMA02/00/CON/CLA/0112.

Department of Water Affairs and Forestry. 2006. *Letaba catchment reserve determination study*. Water Quality Report. Report Number: RDM/B800/01/CON/COMP/0804.

Department of water Affairs and Forestry. 2010. *Groot Letaba River Water Development Project: Water Resource Analysis Report.* Volume 5. Report Number: P 02/B810/00/0608/5.

Devereux, O.H., Prestegaard, K.L., Needelman, B.A. and Gellis, A.C. 2010. Suspended-sediment sources in an urban watershed, Northeast Branch Anacostia River, Maryland. *Hydrological Processes*. Vol. 24. No.11. Pp.1391-1403.

Duane, D. B. 1964. Significance of skewness in recent sediments, western Pamlico Sound, North Carolina. *Journal of Sedimentary Research*. Vol. 34. No. 4. Pp.864-874.

Ďud'a, R. and Rejl, L. 1986. *Minerals of the World*. Spring Books. England.

Edwards, A. C. 2001. Grain size and sorting in modern beach sands. *Journal of Coastal Research*. Vol. 17. No. 1.Pp.38-52.

Erlank, A. J. 1984. *Petrogenesis of the volcanic rocks of the Karoo Province*. The Geological Society of South Africa. Special Publication No. 13. 395p.

Evrard, O., Navratil, O., Ayrault, S., Ahmid, M., Nemery, J., Legout, C., Lefevre,I., Poirel, A., Bonte, P and Esteves, M. 2011. Combining suspended sediment monitoring and fingerprinting to determine spatial origin of fine sediment in a mountainous river catchment. *Earth Surface Processes and Landforms*. No. 36. Pp. 1072-1089.

Evrard, O., Poulenard, J., Némery, J., Ayrault, S., Gratiot, N., Duvert, C., Prat, C., Lefèvre, I., Bonté, P. and Esteves, M. 2013. Tracing sediment sources in a tropical highland catchment of central Mexico by using conventional and alternative fingerprinting methods. *Hydrological Processes*. Vol. 27. No. 6. Pp. 911-922.

Eze, P.N., Knight, J. and Evans, M. 2016. Tracing recent environmental changes and pedogenesis using geochemistry and micromorphology of alluvial soils, Sabie-Sand River Basin, South Africa. *Geomorphology*. Vol. 268. Pp. 312-321.

Falkowska E. 2009. Glacial morphogenesis of upland of Warta Glaciation in Poland as a control on heavy metal distribution in deposits. *Geological Quarterly.* Vol. 53. Pp 293–304.

Falkowska, E. and Falkowski, T. 2015. Trace metals distribution pattern in floodplain sediments of a lowland river in relation to contemporary valley bottom morphodynamics. *Earth Surface Processes and Landforms*. Vol. 40. No. 7. Pp. 876-887.

Favaro, C. A. and Lamourex, S. F. 2015. Downstream patterns of suspended sediment transport in a high Arctic river influenced by permafrost disturbance and recent climate change. *Geomorphology*. Vol. 246. Pp. 359-369.

Ferguson, R. I., Cudden, J.R., Hoey, T.B. and Rice, S.P. 2006. River system discontinuities due to lateral inputs: generic styles and controls. *Earth Surface Processes and Landforms*. Vol. 31. No. 9. Pp.1149-1166.

Folk, L. R. and Ward, C. W. 1957. Brazos River bar: A study in the significance of grain size parameters. *Journal of Sedimentary Petrology*. Vol. 27. No. 1. Pp. 3-26.

Foster, I. D., Lees, J.A., Owens, P.N. and Walling, D.E. 1998. Mineral magnetic characterization of sediment sources from an analysis of lake and floodplain sediments in the catchments of the Old Mill reservoir and Slapton Ley, South Devon, UK. *Earth Surface Processes and Landforms*. Vol. 23. No. 8. Pp. 685-703.

Foucher, A., Laceby, P.J., Salvador-Blanes, S., Evrard, O., Le Gall, M., Lefèvre, I., Cerdan, O., Rajkumar, V. and Desmet, M. 2015. Quantifying the dominant sources of sediment in a drained lowland agricultural catchment: The application of a thorium-based particle size correction in sediment fingerprinting. *Geomorphology.* Vol.250. Pp.271-281.

Fox, J. F. and Papanicolaou, A.N. 2008. Application of the spatial distribution of nitrogen stable isotopes for sediment tracing at the watershed scale. *Journal of Hydrology*. Vol. 358. No. 1. Pp.46-55.

Friedman, G. M. 1979. Differences in grain size distribution of populations of particles among sands of various origins*. Sedimentology.* Vol. 26. Pp. 3-32.

Friedman, G.M., 1967. Dynamic processes and statistical parameters compared for size frequency distribution of beach and river sands. *Journal of Sedimentary Research*, Vol.37. No.2. Pp.327-354.

Fryirs, K. 2013. (Dis) Connectivity in catchment sediment cascades: a fresh look at the sediment delivery problem. *Earth Surface Processes and Landforms*. Vol. 38. No.1.Pp.30-46.

Fryirs, K. A., Brierly, G. J., Preston, N. J. and Kasai, M. 2007. Buffers, barriers and blankets: The (dis)connectivity of catchment scale sediment cascades. *Catena* 70. Pp 40-67.

Garçon, M., Chauvel, C. 2014. Where is basalt in river sediments, and why does it matter? *Earth and Planetary Science Letters*. Vol. 407. Pp. 61-69.

Garzanti, E., Vezzoli, G., Andò, S., Paparella, P., Clift, P.D. 2005. Petrology of Indus River sands: a key to interpret erosion history of the Western Himalayan Syntaxis. *Earth and Planetary Science Letters.* Vol.229. Pp. 287-302.

Garzanti, E., Andò, S., Vezzoli, G., Ali Abdel Megid, A., El Kammar, A. 2006. Petrology of Nile River sands (Ethiopia and Sudan): Sediment budgets and erosion patterns. *Earth and Planetary Science Letters*. Vol. 252. Pp. 327-341.

Gazanti, E., Vezzoli, G., Ando, S., Lave, J., Attal, M., France-Lanord, C. and DeCelles, P. 2007a. Quantifying sand provenance and erosion (Marsyandi River, Nepal Himalaya). *Earth and Planetary Science Letters.* Vol. 258. Pp. 500-515.

Garzanti, E., Andò, S. 2007b. Heavy Mineral Concentration in Modern Sands: Implications for Provenance Interpretation. In: Mange, M. and Wright, D. (eds). *Heavy minerals in use. Developments in Sedimentology Series 58*. Elsevier. Amsterdam. Pp. 517-545.

Garzanti, E., Limonta, M., Resentini, A., Bandopadhyay, P. C., Najman, Y., Ando, S. and Vezzoli, G. 2013. Sediment recycling at convergent plate margins (Indo-Burman Ranges and Andaman-Nicobar Ridge). *Earth-Science Reviews*. Vol. 123. Pp. 113-132.

Garzanti, E. 2016. From static to dynamic provenance analysis—Sedimentary petrology upgraded. *Sedimentary Geology*. Vol. 336. Pp. 3-13.

Gerber, R., Smit, N.J., van Vuren, J.H. and Wepener, V. 2016. Metal concentrations in Hydrocynus vittatus (Castelnau 1861) populations from a premier conservation area: relationships with environmental concentrations. *Ecotoxicology and Environmental Safety.*Vol. 129. Pp. 91-102.

Gertenbach, W. P. D. 1983. Landscapes of the Kruger National Park. *Koedoe*. Vol. 26. Pp. 9-121.

Gellis, A.C. and Walling, D.E. 2011. Sediment source fingerprinting (tracing) and sediment budgets as tools in targeting river and watershed restoration programs. *Stream Restoration in Dynamic Fluvial Systems.* Pp.263-291.

Graf,W.L., Clark,S.L., Kammerer,M.T., Lehman,T., Randall,K., Schroeder,T.R. 1991. Geomorph ology of heavy metals in the sediments of Queen Creek, Arizona, USA. *Catena.* Vol. 18. Pp 567–582.

Gruszowski, K. E., Foster, I. D. L., Lees, J. A. and Charlesworth, S. M. 2003. Sediment sources and transport pathways in a rural catchment, Herefordshire, UK. *Hydrological Processes.* Vol. 17. Pp. 2665–2681.

Guo, Y., Huang, C., Pang, J., Zha, X., Li, X. and Zhang, Y. 2014. Concentration of heavy metals in the modern flood slackwater deposits along the upper Hanjiang River valley, China. *Catena*. Vol.116. Pp.123-131.

Gupta, A. 2000. Hurricane floods as extreme geomorphic events. in Slaymaker, O. and Hassan, M.A. (eds). *The Hydrology-geomorphology interface: Rainfall, floods, sedimentation, land use* (Proceedings of the Jerusalem Conference, May 1999). IAHS Publication. No. 261. Pp. 215-228.

Guzmán, G., Quinton, J.N., Nearing, M.A., Mabit, L. and Gómez, J.A. 2013. Sediment tracers in water erosion studies: current approaches and challenges. *Journal of Soils and Sediments.* Vol.13. No.4. Pp.816-833.

Gyamfi, C., Ndambuki, J.M. and Salim, R.W. 2016. Simulation of Sediment Yield in a Semi-Arid River Basin under Changing Land Use: An integrated approach of hydrologic modelling and principal component analysis. *Sustainability*. Vol.8. No.11. doi:10.3390/su8111133.

Haddadchi, A. Ryder, D. S. Evrard, O. and Olley, J. 2013. Sediment Fingerprinting in Fluvial Systems: Review of Tracers, Sediment Sources and Mixing Models. *International Journal of Sediment Research*. Vol. 28. Pp. 560–578.

Haddadchi, A., Olley, J. and Laceby, P. 2014a. Accuracy of mixing models in predicting sediment source contributions. *Science of the Total Environment*. Vol. 497. Pp.139-152.

Haddadchi, A., Nosrati, K. and Ahmadi, F. 2014b. Differences between the source contribution of bed material and suspended sediments in a mountainous agricultural catchment of western Iran. *Catena*. Vol.116.Pp.105-113.

Haddadchi, A., Olley, J. and Pietsch, T. 2016. Variable source contributions to river bed sediments across three size fractions. *Hydrological Processes*. Vol. 30. No.10. Pp.1609-1623.

Hancock, G. S., Anderson, R. S. and Whipple, K. 1998. Beyond power: Bedrock river incision process and from. in Tinkler, K. J., and Wohl, E. E. (eds). *Rivers over rock: Fluvial processes in bedrock channels: Washington*, D.C. American Geophysical Union. Pp.35-60.

Hancock, G. S. and Small, E. E., Wobus, C. 2011. Modeling the effects of weathering on bedrock-floored channel geometry. *Journal of Geophysical Research.* Vol. 116. doi: 10.1029/2010JF001908.

Harrison, L. R., Legleiter, C. J., Wydzga, M. A. and Dunne, T. 2011. Channel dynamics and habitat development in a meandering, gravel bed river. *Water Resource Research*. Vol. 47. doi: 10.1029/2009WR008926.

Hatfield, R.G. and Maher, B.A. 2009. Fingerprinting upland sediment sources: Particle size-specific magnetic linkages between soils, lake sediments and suspended sediments. *Earth Surface Processes and Landforms*. Vol. 34. No.10. Pp.1359-1373.

Heritage, G. L., Van Niekerk, A. W., Moon, B. P. L. J, Broadhursk, L. J., Rogers, K. H. and James, C. S. 1997. *The geomorphological response to changing flow regimes of the Sabie and Letaba River systems*. WRC. Report No. 376/1/97. University of the Witwatersrand. South Africa.

Heritage. G. L., Moon, B.P., and Large, A. R. G. 2001. The February 2000 floods on the Letaba River, South Africa: an examination of magnitude and frequency. *Koedoe*. Vol. 44. No.2. Pp. 1-6. doi: 10.4102/koedoe.v44i2.171

Heritage, G.L., Large, A.R.G., Moon, B.P. and Jewitt, G. 2004. Channel hydraulics and geomorphic effects of an extreme flood event on the Sabie River, South Africa. *Catena*. Vol. 58. No. 2. Pp. 151-181.

Heritage, G. L., Tooth, S., Entwhistle, N., Milan, D. 2015. Long-term flood controls on semi-arid river form: evidence from the Sabie and Olifants rivers, eastern South Africa. IAHS Publication 367. Pp. 141–146.

Hillier, S. 2001. Particulate composition and origin of suspended sediment in the R. Don, Aberdeenshire, UK. *Science of the Total Environment*. Vol. 265. Pp. 281–293

Hooke, J. M. 2016. Geomorphological impacts of an extreme flood in SE Spain. *Geomorphology.* Vol.263. Pp. 19-38.

Huang, G. W. 2011. Dual behaviour of suspended sediment concentration in a regulated river. *World Journal of Mechanics*. Vol. 1. Pp. 115-121.

Huckleberry, G. 1994. Contrasting channel response to floods on the middle Gila River, Arizona. *Geology*. Vol. 22. No.12. Pp.1083-1086.

Hudson, P. F, and Moosa, J. 1997. Suspended sediment transport effectiveness of three large impounded rivers, U.S. Gulf Coastal Plain. *Environmental Geology.* Vol. 32. No. 4. Pp. 293-273.

Hughes, A.O., Olley, J.M., Croke, J.C. and McKergow, L.A. 2009. Sediment source changes over the last 250 years in a dry-tropical catchment, central Queensland, Australia. *Geomorphology*. Vol. 104. No.3.Pp.262-275.

Jadot, H. and Boulvain, F. 2015. Sedimentology and magnetic susceptibility of recent sediments from New Caledonia. in Da Silva, A. C., Whalen, M. T., Hladil, J., Chadimova, L., Chen, D., Spassov, S., Boulvain, F. and Devleeschouwer, X. (eds). *Magnetic Susceptibility application: A Window onto Ancient Environments and Climatic Variations*. Geological Society, London, Special Publications. Vol. 414. No.1 .Pp. 111-132.

Jung, D., Paik, K. and Kim, J.H. 2013. Relationship between downstream hydraulic geometry and suspended sediment concentration characteristics. *Journal of Hydro-Environment Research*. Vol.7.No.4. Pp.243-252.

Kabata-Pendias, A. 2011. *Trace elements in soils and plants*. Fourth edition. Boca Raton. CRC Press.

Kale, V. S and Hire, P. S. 2004. Effectiveness of monsoon floods on the Tapi River, India: role of channel geometry and hydrologic regime. *Geomorphology.* Vol. 57. Pp. 275-291.

Kale, V. S. 2003. Geomorphic effects of monsoon floods on Indian rivers. *Natural Hazards*. Vol.2 8. Pp. 65-84.

Kara, F., Loewenstein, E. and Kalin, L. 2015. Changes in sediment and water yield downstream on a small Watershed. *Ekoloji*. Vol. 21. No. 84. Pp. 30-37.

Karlsen, E. 1991. Variations in grain-size distribution of suspended sediment in a glacial meltwater stream, Austre Okstindbreen, Norway. *Journal of Glaciology*. Vol. 37. No.125. Pp. 113-119.

Kasilingam, K., Gandhi, M.S., Krishnakumar, S. and Magesh, N.S. 2016. Trace element concentration in surface sediments of Palk Strait, southeast coast of Tamil Nadu, India. *Marine Pollution Bulletin*. Vol. 111. No.1. Pp.500-508.

Katambara, Z and Ndiritu, J. G. 2010. A hybrid conceptual–fuzzy inference streamflow modelling for the Letaba River system in South Africa. *Physics and Chemistry of the Earth*. Vol. 35. Issue: 13-14. Pp. 582-595.

Kermani, S., Boutiba, M., Boutaleb, A. and Fagel, N. 2016. Distribution of heavy and clay minerals in coastal sediment of Jijel, East of Algeria: indicators of sediment sources and transport and deposition environments. *Arabian Journal of Geosciences*.Vol.9. No.1. doi: 10.1007/s12517-0152155-2.

Khalil, M.I., Khan, M.N.I., Kabir, M.Z., Majumder, R.K., Ali, M.I., Paul, D. and Islam, S.M.A. 2016. Heavy Minerals in Sands along Brahmaputra (Jamuna) River of Bangladesh. *International Journal of Geosciences*. Vol.7. No.1. Pp.47-52.

Kingsford, R.T. 2000. Ecological impacts of dams, water diversions and river management on floodplain wetlands in Australia. *Austral Ecology*. Vol. 25. No.2.Pp.109-127.

Klein, C. and Philoptts, A. 2013. Earth Materials: Introduction to mineralogy and petrology. Cambridge University Press. New York.

Knight, J. and Evans, M. 2017. The sediment stratigraphy of a flood event: An example from the Sabie River, South Africa. *Catena*. Vol.151. Pp.87-97.

Knighton, D. 1998. Channel changes through time: the effects of floods*. Fluvial forms and processes: a new perspective*. Chapter 6. London. Arnold. Pp. 295-302.

Kochel, R. C., Hayes, B. R., Muhlbauer, J., Hancock, Z. and Rockwell, D. 2016. Geomorphic response to catastrophic flooding in north-central Pennsylvania from Tropical Storm Lee (September 2011): Intersection of fluvial disequilibrium and the legacy of logging. *Geosphere.* Vol. 12. No. 1. Pp. 305-345.

Koiter, A.J., Owens, P.N., Petticrew, E.L. and Lobb, D.A. 2013. The behavioural characteristics of sediment properties and their implications for sediment fingerprinting as an approach for identifying sediment sources in river basins. *Earth-Science Reviews*. Vol.125. Pp.24-42.

Kotschy, K. and Rogers, K. 2008. Reed coral characteristics and responses to disturbance in a semi-arid river. *Aquatic Botany*. Vol. 88. Pp. 47-56.

Kouhpeima, A., Feiznia, S., Ahmadi, H., Hashemi, S.A. and Zareiee, A.R. 2011. Application of quantitative composite fingerprinting technique to identify the main sediment sources in two small catchments of Iran. *Hydrology and Earth System Sciences Discussions*. Vol.7. No.5. Pp.6677-6698.

Kouhpeima, A. and Hamid, G.S. 2013. Estimation of sediment sources using a fingerprinting procedure. *Elixir International Journal*. Vol. 56. Pp.13252-13259.

Lamba, J., Karthikeyan, K.G. and Thompson, A.M. 2015. Apportionment of suspended sediment sources in an agricultural watershed using sediment fingerprinting. *Geoderma*. Vol.239. Pp.25-33.

Larsson, M.A. 2014. *Vanadium in soils: Chemistry and Ecotoxicity* .Doctral Thesis. Swedish University of Agricultural Sciences, Uppsala. Pp.1-60.

Laceby, J.P. and Olley, J. 2015. An examination of geochemical modelling approaches to tracing sediment sources incorporating distribution mixing and elemental correlations. *Hydrological Processes*. Vol. 29. No.6. Pp.1669-1685.

La Tour, T. E. 1989. Analysis of rocks using X-ray fluorescence spectrometry. Department of Geology, Georgia State University. The Rigaku Journal. Vol. 6. No. 1. Pp. 3-9.

Lewin, J. 1989. Floods in fluvial geomorphology. in. Beven, K. J. and Carling, P. A. (eds). *Floods: hydrological, sedimentological and geomorphological implications*. Chichester. Wiley. Pp. 265-280.

Lewis, D. W. and McConchie, D. 1994. *Texture of detrital sediments*. Practical Sedimentology. Springer, US. Pp.128-150.

Lin, J., Huang,Y., Wang, M., Jiang, F., Zhang, X. and Ge, H. 2015. Assessing the sources of sediment transported in gully systems using a fingerprinting approach: An example from South-east China. *Catena.* No. 129. Pp. 9-17.

Lindholm, R. 2012. A practical approach to sedimentology. Allen and Unwin. London.

Liu, Q., Roberts, A.P., Larrasoana, J.C., Banerjee, S.K., Guyodo, Y., Tauxe, L. and Oldfield, F. 2012. Environmental magnetism: principles and applications. *Reviews of Geophysics*. Vol. 50. No. 4 .Pp. 1-50.

Lu, X. X. 2004. Vulnerability of water discharge of large Chinese rivers to environmental changes: an over view. Regional Environmental Changes. No. 4. Pp. 182-191.

Lynn, W., Thomas, J. E. and Moody, L. E. 2008. *Petrographic microscope techniques for identifying soil minerals in grain mounts*. In Methods of soil analysis: Mineralogical methods part 5. Ulery, A and Drees, R. Science society of America. Madison. Pp. 161-190.

Lyons, R., Oldfield, F. and Williams, E. 2010. Mineral magnetic properties of surface soils and sands across four North African transects and links to climatic gradients. *Geochemistry, Geophysics, Geosystems*. Vol.11.No.8. doi: 10.1029/2010GC003183.

MacKenzie, W.S. and Adams, A.E. 1994. *A colour atlas of rocks and minerals in thin section*. CRC Press. Boca Raton.

Magilligan, F.J. 1992. Thresholds and the spatial variability of flood power during extreme floods. *Geomorphology*. Vol. 5. Pp. 373-390.

Magilligan, F. J., Buraas, E. M. and Renshaw, C. E. 2015. The efficacy of stream power and flow duration on geomorphic responses to catastrophic flooding. *Geomorphology*. Vol. 228. Pp. 175-188.

Maher, B.A. 1998. Magnetic properties of modern soils and Quaternary loessic paleosols: paleoclimatic implications. *Palaeogeography, Palaeoclimatology, Palaeoecology*. Vol.137. No.1-2. Pp.25-54.

Manjoro, M., Rowntree, K., Kakembo, V., Foster, I. and Collins, A.L. 2016. Use of sediment source fingerprinting to assess the role of subsurface erosion in the supply of fine sediment in a degraded catchment in the Eastern Cape, South Africa. *Journal of Environmental Management*.Vol.194. Pp. 27-41.

Maponya, P. and Mpanedi, S. 2012. Impact of drought on food scarcity in Limpopo province, South Africa. *African Journal of Agricultural Research* Vol. 7. No.37.Pp. 5270-5277.

Martinez-Carreras, N., Gallart, F., Iffly, J.F., Pfister, L., Walling, D.E. and Krein, A. 2008. Uncertainty assessment in suspended sediment fingerprinting based on tracer mixing models: a case study from Luxembourg. *IAHS Publication*. Vol. 325. Pp.94-105.

Martin, C. W. 2004. Heavy metal storage in near channel sediments of the Lahn River, Germany. *Geomorphology*.Vol.61.No.3.Pp.275-285.

Martins, L. R., and E. G. Barboza. 2005. Sand-gravel marine deposits and grain-size properties. *Gravel.* Vol.3. Pp. 59-70.

Masselink, G., Hughes, M. and Knight, J. 2014. *Sediments, boundary layers and transport*. Introduction to coastal processes and geomorphology. Chapter5. Routledge. Pp. 105-147.

McCarthy, T. and Rubidge, B. 2005. *The story of Earth and Life*. A southern Africa perspective of a 4.6 billion year journey. Struik Publishers, Johannesburg.

McLaren, P. 1979. An interpretation of trends in grain size measures. *Journal of Sedimentary Petrology*. Vol. 51. No. 2. Pp. 611-624.

McLaren, P. and Bowles, D. 1985. The effects of sediment transport on grain-size distributions. *Journal of Sedimentary Research*. Vol. 55. No.4. Pp. 457-470.

Meade, R. H. 1982. Sources, sinks and storage of river sediment in the Atlantic drainage of the United States. *Journal of Geology*. Vol. 90. No. 3. Pp. 235-252.

Meinhold, G. 2010. Rutile and its applications in earth sciences. *Earth-Science Reviews*. Vol.102.No.1.Pp.1-28.

Meissner, A.G., Carr, M.K., Phillips, I.D. and Lindenschmidt, K.E. 2016. Using a Geospatial Model to Relate Fluvial Geomorphology to Macroinvertebrate Habitat in a Prairie River—Part 1: Genus-Level Relationships with Geomorphic Typologies. *Water*. Vol.8. No.2. doi:10:3390/w8030107.

Mentling, F., Langston, A. L. and Temme, A .J. A. M. 2015. Downstream fining, selective transport, and hillslope influence on channel bed sediment in mountain streams, Colorado Front Range, USA. *Geomorphology*.Vol.239. Pp. 91-105.

Meissner, A. G. N., Carr, M.K., Phillips, I.D. and Lindenschmidt, K.E. 2016. Using a Geospatial Model to Relate Fluvial Geomorphology to Macroinvertebrate Habitat in a Prairie River—Part 2: Matching Family-Level Indices to Geomorphological Response Units (GRUs). *Water*.Vol. 8.No. 3. Pp.1-18.

Meyer, M., John, T., Brandt, S. and Klemd, R. 2011. Trace element composition of rutile and the application of Zr-in-rutile thermometry to UHT metamorphism (Epupa Complex, NW Namibia). *Lithos*. Vol. 126. No.3. Pp.388-401.

Miller, J., Bar, R., Grow, D., Lechler, P., Richardson, D., Waltman, K., and Warwick, J. 1999. Effects of the 1997 flood on the transport and storage of sediments and Mercury within the Carson River valley, West- Central Nevada. *Journal of Geology*. Vol. 107. Pp. 313-327.

Miller, J. R., Lechler, P. J., Macklin, G., Germanoski, D., Villarroel, L.F. 2007. Evaluation of particle dispersal from mining and milling operations using lead isotopic fingerprinting techniques, Rio Pilcomayo Basin, Bolivia. *Science of the Total Environment*.Vol. 384. Pp. 355-373.

Miller, J. R., Mackin, G., Lechler, P., Lord, M. and Lorentz, S. 2013. Influence of basin connectivity on sediment source, transport, and storage within the Mkabela Basin, South Africa. *Hydrology and Earth System Sciences*. Vol.17.No.2. Pp.761-781.

Miller, K. L., Szabó, T., Jerolmack, D. J. and Domokos, G. 2014. Quantifying the significance of abrasion and selective transport for downstream fluvial grain size evolution. *Journal of Geophysical Research: Earth Surface*. Vol. 119. Pp. 2412-2429.

Montgomery, D.R., Abbe, T.B., Buffington, J.M., Peterson, N.P., Schmidt, K.M., and Stock, J.D. 1996. Distribution of bedrock and alluvial channels in forested mountain drainage basins. *Nature*. Vol. 381. Pp. 587–589.

Moon. B. P. and G.L. Heritage. 2001. The contemporary geomorphology of the Letaba River in the Kruger National Park. *Koedoe*. Vol. 44. No.1. Pp. 45-55.

Morton, A. C. and Hallsworth, C. 1999. Processes controlling the composition of heavy mineral assemblages in sandstones. *Sedimentary Geology.* Vol. 124. Pp. 3-29.

Motha, J. A., Wallbrink, P.J., Hairsine, P.B. and Grayson, R.B. 2003. Determining the sources of suspended sediment in a forested catchment in southeastern Australia. *Water Resources Research*. Vol. 39. No.3.doi:10.1029/2001WR000794.

Mueller, E. R., Smith, E. M. and Pitlick, J. 2016. Lithology-controlled evolution of stream bed sediment and basin-scale sediment yields in adjacent mountain watersheds, Idaho, USA: Lithology-controlled evolution of stream bed sediment and yields. *Earth Surface Processes and Landforms.*Vol. 14. Pp.1868-1883. doi:10.1002/esp.3955.

Mukundan, R., Walling, D.E., Gellis, A.C., Slattery, M.C. and Radcliffe, D.E. 2012. Sediment source fingerprinting: transforming from a research tool to a management tool. *JAWRA Journal of the American Water Resources Association*.Vol. 48.No.6.Pp.1241-1257.

Mullins, C.E. 1977. Magnetic susceptibility of the soil and its significance in soil science–a review. *European Journal of Soil Science*. Vol.28. No.2.Pp.223-246.

Murdock, K. J., Wilkie, K. and Brown, L.L. 2013. Rock magnetic properties, magnetic susceptibility, and organic geochemistry comparison in core LZ1029-7 Lake El'gygytgyn, Russia Far East. *Climate of the Past*. Vol. 9. No.1. Pp.467-479.

Mzobe, P. J. 2014. *Sediment linkages in a small catchment in the Mount Fletcher southern Drakensburg region, Eastern Cape, South Africa*. Unpublished MSc thesis, Rhodes University, South Africa.

Nosrati, K., Govers, G., Semmens, B.X. and Ward, E.J. 2014. A mixing model to incorporate uncertainty in sediment fingerprinting. *Geoderma*. Vol. 217. Pp.173-180.

O'Connor, J. E., Mangano, J. F., Anderson, S. W., Wallick, J. R., Jones, K. L. and Keith, M.K . 2014. Geologic and physiographic controls on bed-material yield, transport, and channel morphology for alluvial and bedrock rivers, western Oregon. *Geological Society of America Bulletin.* Vol. 126. Pp. 377-397

Okeyode, I. C. and Jibiri, N. N. 2012. Grain size analysis of the sediments from Ogun River, south western Nigeria. *Earth Science Research*.Vol. 2.No.1. doi: 10.55391/esr.v2n/p43.

Oldfield, F., Hao, Q., Bloemendal, J., Gibbs-Eggar, Z., Patil, S. and Guo, Z. 2009. Links between bulk sediment particle size and magnetic grain-size: general observations and implications for Chinese loess studies. *Sedimentology*. Vol. 56. No.7. Pp.2091-2106.

Omengo, F.O., Alleman, T., Geeraert, N., Bouillon, S. and Govers, G. 2016. Sediment deposition patterns in a tropical floodplain, Tana River, Kenya. *Catena*. Vol. 143. Pp.57-69.

Otamendi, J.E., Tiepolo, M., Walker, B.A., Cristofolini, E.A. and Tibaldi, A.M. 2016. Trace elements in minerals from mafic and ultramafic cumulates of the central Sierra de Valle Fértil, Famatinian arc, Argentina. *Lithos*. Vol. 240. Pp.355-370.

Owens, P.N., Walling, D.E. and Leeks, G.J. 1999. Deposition and storage of fine-grained sediment within the main channel system of the River Tweed, Scotland. *Earth Surface Processes and Landforms*. Vol 24. No.12. Pp. 1061-1076.

Palazón, L., Latorre, B., Gaspar, L., Blake, W.H., Smith, H.G. and Navas, A. 2015. Comparing catchment sediment fingerprinting procedures using an auto-evaluation approach with virtual sample mixtures. *Science of the Total Environment*. Vol. 532. Pp.456-466.

Paola, C. and Seal, R. 1995. Grain size patchiness as a cause of selective deposition and downstream fining. *Water Resources Research*. Vol. 31. No. 5. Pp. 1395-1407.

Pan, B., Pang, H., Zhang, D., Guan, Q., Wang, L., Li, F., Guan, W., Cai, A. and Sun, X. 2015. Sediment grain-size characteristics and its source implication in the Ningxia–Inner Mongolia sections on the upper reaches of the Yellow River. *Geomorphology*. Vol. 246. Pp. 255-262.

Parker, G. 1991. Selective sorting and abrasion of river gravel. I: Theory. *Journal of Hydraulic Engineering*. Vol.117. No.2.Pp.131-147.

Pazzaglia, F. J., Gardner, T. W. and Merritts, D. J. 1998. Bedrock fluvial incision and longitudinal profile development over geologic time scales determined by fluvial terraces. in Tinkler, K. J., and Wohl, E. E. (eds). *Rivers over rock: Fluvial processes in bedrock channels*: Washington, D.C. *American Geophysical Union*. Pp.207-232.

Phillips, J.D., Slattery, M.C. and Musselman, Z.A. 2004. Dam-to-delta sediment inputs and storage in the lower Trinity River. Texas. *Geomorphology*. Vol. 62.No.1.Pp.17-34.

Pike, A. S., Scatena, F. N. and Wohl, E. E. 2010. Lithological and fluvial controls on the geomorphology of tropical montane stream channels in Puerto Rico. *Earth Surface Processes and Landforms.* Vol.35. No.12. Pp. 1402-1417.

Potts, P. J. 2008. Introduction, Analytical Instrumentation and Application Overview. in Potts, P. J. and West, M. (eds). Portable X-ray Fluorescence Spectrometry: Capabilities for in situ analysis. Faculty of Science. *The Open University*. UK. Pp. 1-12.

Pulley, S., Foster, I. and Antunes, P. 2015a. The uncertainties associated with sediment fingerprinting suspended and recently deposited fluvial sediment in the Nene river basin. *Geomorphology.* Vol.228. Pp.303-319.

Pulley, S., Foster, I. and Antunes, P. 2015b. The application of sediment fingerprinting to floodplain and lake sediment cores: assumptions and uncertainties evaluated through case studies in the Nene Basin, UK. *Journal of soils and sediments*, Vol. 15.No.10. Pp.2132-2154.

Pulley, S. and Rowntree, K. 2016. Stages in the life of a magnetic grain: Sediment source discrimination, particle size effects and spatial variability in the South African Karoo. *Geoderma*. Vol. 271. Pp.134-143.

Pulley, S., Foster, I. and Collins, A.L. 2017. The impact of catchment source group classification on the accuracy of sediment fingerprinting outputs. *Journal of Environmental Management*. Vol.194. Pp.16-26.

Rajaguru, S .N., Gupta, A., Kale, V. S., Mishra, S., Ganjoo, R. K., Ely, L.L., Enzel, Y., Baker, V. R. 1995. Channel form and processes of the flood-dominated Narmada River, India. *Earth Surface Processes and Landforms.* Vol. 20. Pp. 407-421.

Rajmohan, S., Singarasubramanian, S.R., Suganraj, K., Sundararajan, M. and Rajganapathi, V.C. 2012. Textural characterization of Vellar River along the east coast of India. *Current Research*. Vol. 4.No. 7. Pp.169-173.

Richardson, K. and Carling, P. 2005. *A typology of sculptured forms in open bedrock channels*. Geological Society of America Special Paper 392. Colorado.

Román, J.P. and Achab, M. 1999. Grain-size trends associated with sediment transport patterns in Cadiz Bay (southwest Iberian Peninsula).*Boletin-Instituto Espanol De Oceanografia*. Vol. *15. No.*1/4. Pp.269-282.

Rountree, M. W., Rogers, K.H. and Heritage, G. L. 2000. Landscape state change in the semi-arid Sabie River Kruger National Park, in response to flood and drought. *South African Geographical Journal*. Vol. 82. No. 3. Pp. 173-181.

Rowntree, K.M., van der Waal, B.W. and Pulley, S. 2017. Magnetic susceptibility as a simple tracer for fluvial sediment source ascription during storm events. *Journal of Environmental Management*. Vol. 194. Pp.54-62.

Rubey, W.W. 1933. The size-distribution of heavy minerals within a water-laid sandstone. *Journal of Sedimentary Petrology*. Vol. 3. No. 1. Pp. 3-29.

Russell, A. J., Walling, D. E., Hodgkinson, R. A. 2001. Suspended sediment sources in two lowland agricultural catchments in the UK. *Journal of Hydrology*. No. 252. Pp, 1-24.

Sargood, M.B., Cohen, T.J., Thompson, C.J. and Croke, J. 2015. Hitting rock bottom: morphological responses of bedrock-confined streams to a catastrophic flood. *Earth Surface Dynamics*. Vol.3.No.2. Pp.265-279.

Sahu, B.K. 1964. Depositional mechanisms from the size analysis of clastic sediments. *Journal of Sedimentary Research*. Vol.34. No.1. Pp. 73-83.

Schanz, S.A. and Montgomery, D.R. 2016. Lithologic controls on valley width and strath terrace formation. *Geomorphology*. Vol. *258*. Pp. 58-68.

Schumm, S. A. and Lichty, R. W. 1963. Channel widening and flood-plain construction along Cimarron River in southwestern Kansas. *Geological Survey Professional Paper*. No. 352-D. Pp. 71-88.

Seidl, M. A. and Dietrich. W. E. 1992. The problem of channel erosion into bedrock. *Catena* 23. Pp. 101-124.

Shaltout, A. A., Welz, B. and Ibrahim, M. 2011. Influence of the grain size on the quality of standardless WDXRF analysis of river Nile sediments. *Microchemical Journal*. Vol. 99. Pp. 356-363.

Singh, M., Singh, I.B. and Müller, G. 2007. Sediment characteristics and transportation dynamics of the Ganga River. *Geomorphology*. Vol. 86. No.1.Pp.144-175.

Sinha, P. 2015. A conceptual study of Impact of climate change on reservoirs of the Letaba River Catchment. *International Conference on Civil and Structural Engineering (ICCSE 15). July 14-15. Harare. Zimbabwe*. Pp. 44-48.

Sklar, L. S. and Dietrich, W. E. 2001. Sediment and rock strength controls on river incision into bedrock. *Geological Society of America Bulletin*. Vol. 29. No. 12. Pp. 1087-1090.

Sklar, L. S., Dietrich, W. E., Foufoula-Georgiou, E., Lashermes, B. and Bellugi, D. 2006. Do gravel bed river size distributions record channel network structure?. *Water Resources Research*. Vol. 42. No. 6. doi: 10.1029/2006WR005035.

Smith, H.G. and Blake, W.H. 2014. Sediment fingerprinting in agricultural catchments: a critical re-examination of source discrimination and data corrections. *Geomorphology*.Vol 204.Pp.177-191.

Spaliviero, M., De Dapper, M. and S. Maló, S. 2014. Flood analysis of the Limpopo River basin through past evolution reconstruction and a geomorphological approach. *Natural Hazards and Earth System Science.* Vol. 14. Pp. 2027–2039.

Spotila, J. A., Moskey, K .A. and Prince, P. S. 2015. Geologic controls on bedrock channel width in large, slowly-eroding catchments: Case study of the New River in eastern North America. *Geomorphology*. Vol. 230. Pp. 51-63.

Šroubek, P., Diehl, J.F. and Kadlec, J. 2007. Historical climatic record from flood sediments deposited in the interior of Spirálka Cave, Czech Republic. *Palaeogeography, Palaeoclimatology, Palaeoecology*. Vol. 251. No.3.Pp.547-562.

State of Rivers Report. 2001. *Letaba and Luvuvhu river systems*. WRC report no: TT 165/01. Water Research Commission. Pretoria.

Surian, N., Righini, M., Lucía, A., Nardi, L., Amponsah, W., Benvenuti, M., Borga, M., Cavalli, M., Comiti, F., Marchi, L., Rinaldi, M. and Viero, A. 2016. Channel response to extreme floods: Insights on controlling factors from six mountain rivers in northern Apennines, Italy. *Geomorphology*. doi: 10.1016/j.geomorph.2016.02.002.

Terrio, P.J. 2006. Concentrations, fluxes, and yields of nitrogen, phosphorus, and suspended sediment in the Illinois River basin, 1996-2000 .No. 2006-5078.

Thomas, D.S.G. 1987. Discrimination of depositional environments using sedimentary characteristics in the Mega Kalahari, central southern Africa. *Geological Society, London, Special Publications*.Vol. 35.No.1.Pp.293-306.

Thomas, W. A. 2011. Detrital-zircon geochronology and sediment provenance. *Lithosphere*. Vol 3. No. 4. Pp. 304-308.

Thompson, C. and Croke, J. 2013. Geomorphic effects, flood power, and channel competence of a catastrophic flood in confined and unconfined reaches of the upper Lockyer valley, southeast Queensland, Australia. *Geomorphology*. Vol. 197. Pp. 156-169.

Tiecher, T., Caner, L., Minella, J. P. G. and dos Santos, R. D. 2015. Combining visible-colour-based parameters and geochemical tracers to improve sediment source discrimination and apportionment. *Science of the Total Environment*. Vol.527-528. Pp.135-149.

Tinkler, K. J., and Wohl, E. E. 1998. *Rivers over rock: Fluvial processes in bedrock channels*: Washington, D.C. American Geophysical Union.

Tsikouras, B., Pe-Piper, G., Piper, D. J. W. and Schaffer, M. 2011. Varietal heavy mineral analysis of sediment provenance, Lower Cretaceous Scotian Basin, eastern Canada. *Sedimentary Geology*. Vol. 237. Pp. 150-165.

Turowski, J. M., Hovius, N., Wilson, A. and Horng, M. 2008. Hydraulic geometry, river sediment and the definition of bedrock channels. *Geomorphology*. Vol. 99. Pp. 26–38

Turowski, J.M., Lague, D. and Hovius, N. 2007. Cover effect in bedrock abrasion: A new derivation and its implications for the modeling of bedrock channel morphology. *Journal of Geophysical Research: Earth Surface*. Vol. 112. No. 4. doi: 10.1029/2006JF000697.

van Coller, A, Rogers, K. and Heritage, G. 1997. Linking riparian vegetation types and fluvial geomorphology along the Sabie River within the Kruger National Park, South Africa. *African Journal of Ecology*. Vol. 35. No.3. Pp.194-212.

van der Waal, B., Rowntree, K. and Pulley, S. 2015. Flood bench chronology and sediment source tracing in the upper Thina catchment, South Africa: the role of transformed landscape connectivity. *Journal of Soils and Sediments*. Vol.15.No.12. Pp.2398-2411.

Venter, F. J. (1986). Soil patterns associated with the major geological units of the Kruger National Park. *Koedoe*. Vol.26. Pp. 125-138

Viljoen, M. 2015. The Kruger National Park: Geology and Geomorphology of the Wilderness. in Grab, S. and Knight, J. (eds). *Landscapes and Landforms of South Africa*. Springer International Publishing. Switzerland. Pp. 111-120

von Eynatten, H., Dunkl, I. 2012. Assessing the sediment factory: The role of single grain analysis. *Earth-Science Reviews*. Vol. 115. Pp. 97-120.

Wachecka-Kotkowska, L. and Kotkowski, P. 2011. Grain-size distribution analysis of Quaternary sediments from the southern part of the Lodz region in Poland: a computational-methods approach. *Geologos*. Vol. *17*. No.4. Pp.205-219.

Walling, D.E. and Webb, B.W. 1987. Suspended load in gravel-bed rivers: UK experience. In Thorn, C. R., Bathurst, J. C. and Hey, R. D. (eds). *Sediment Transfer in Gravel-Bed Rivers. John Wiley & Sons.* New York. Pp. 691-723.

Walling, D.E., Woodward, J.C. and Nicholas, A.P. 1993. A multi-parameter approach to fingerprinting suspended-sediment sources. *IAHS publication*. Vol.215. Pp.329-338.

Walling, D.E. and Woodward, J.C., 1995. Tracing sources of suspended sediment in river basins: a case study of the River Culm, Devon, UK. *Marine and Freshwater Research.* Vol. 46. No.1. Pp.327-336.

Walling, D.E. and He, Q. 1997. Investigating spatial patterns of overbank sedimentation on river floodplains. Evans, D. R., Wisniewski, J. and Wineiwski, J. R. (eds). *The Interactions Between Sediments and Water.* Springer, Netherlands. Pp. 9-20.

Walling, D.E., Owens, P.N. and Leeks, G.J.L. 1997. The characteristics of overbank deposits associated with a major flood event in the catchment of the River Ouse, Yorkshire, UK. *Catena*. Vol.31. No.1.Pp.53-75.

Walling, D. E. and Collins, A. L. 2000: Integrated assessment of catchment sediment budgets: A technical manual. *Department for International Development*. (Research project R6868) University of Exeter. Pp.168.

Walling DE, Owens PN, Carter J, Leeks GJL, Lewis S, Meharg AA, Wright J. 2003. Storage of sediment-associated nutrients and contaminants in river channel floodplain systems. *Applied Geochemistry* 18.Pp. 195-220.

Walling, D.E., Collins, A.L. and Stroud, R.W. 2008. Tracing suspended sediment and particulate phosphorus sources in catchments. *Journal of Hydrology*. Vol.350. No.3. Pp.274-289.

Walling, D. E. 2013. The evolution of sediment source fingerprinting investigations in fluvial systems. *Journal of Soil and Sediments*. No. 13. Pp. 1658-1675.

Wang, H., Yang, Z., Saito, Y., Liu, P. J. and Sun, X. 2006. Interannual and seasonal variation of the Huanghe (Yellow River) water discharge over the past 50 years. Connections to impacts from ENSO events and dams. *Global and Planetary Change*. No. 50. Pp. 212-225.

Weltje, G. J and von Eynatten, H. 2004. Quantitative provenance analysis of sediments: a review and outlook. *Sedimentary Geology*. Vol. 171. Pp. 1-11.

Whipple, X. K. 2004. Bedrock Rivers and the geomorphology of active orogens. *Annual Review of Earth and Planetary Sciences*. No. 32. Pp.151-185.

Whipple, X. K., Hancock, G. S. and Anderson, R. S. 2000. River incision into bedrock: Mechanics and relative efficiency of plucking, abrasion and cavitation. *Geological Society of America*. Vol. 112. No. 3. Pp. 2-19.

Whitbread, K., Jansen, J., Bishop, P. and Attal, M. 2015. Substrate, sediment, and slope controls on bedrock channel geometry in postglacial streams. *Journal of Geophysical Research: Earth Surface*. Vol. 120. No.5. Pp.779-798.

Wilkinson, S.N., Hancock, G.J., Bartley, R., Hawdon, A.A. and Keen, R.J. 2013. Using sediment tracing to assess processes and spatial patterns of erosion in grazed rangelands, Burdekin River basin, Australia. *Agriculture, Ecosystems & Environment*. Vol. 180. Pp.90-102.

Wohl, E. 2015. Particle dynamics: The continuum of bedrock to alluvial river segments. *Geomorphology*. Vol. 241. Pp.192-208.

Wohl, E. E. 1992. Gradient irregularity in the Herbert Gorge of North-eastern Australia. *Earth Surface Processes and Landforms*. Vol. 17. Pp. 69-84.

Wohl, E. E. 2014. *Rivers in the Landscape: Science and management*. Wiley-Blackwell, Chichester, UK.

Wohl, E. E. and Ikeda, H. 1998. Patterns of bedrock channel erosion on the Boso Peninsula, Japan. *Journal of Geology*. Vol. 106. No. 3. Pp. 331-346

Wohl, E. E. and Merrit, D. M. 2001. Bedrock channel morphology. *Geological Society of America Bulletin*. Vol. 113. No. 9. Pp. 1205–1212

Wolman, G. M. and Miller, J. P. 1960. Magnitude and frequency of forces in geomorphic processes. *Journal of Geology*. No. 68. Pp. 54-74.

Wolman, G. M. and Gerson, R. 1978. Relative scales of time and effectiveness of climate in watershed geomorphology. *Earth Surface Processes*. Vol. 3. Pp. 189-208.

Yamada, M., Fujino, S., Goff, J. and Chagué-Goff, C. 2016. Large-scale erosion and overbank deposition caused by the July 2013 flood of the Abu River, Yamaguchi City, Japan. *Island Arc*.Vol.25. No.5.Pp.386-399.

Yanites, B .J. and Tucker, G E. 2010. Controls and limits on bedrock channel geometry. *Journal of Geophysical Research: Earth Surface*. Vol, 115. No. F04019. Pp. 1-17. doi: 10.11.30/B30035.1.

Yanites, B.J., Tucker, G. E., Mueller, K. J., Chen, Y. G., Wilcox, T., Huang, S. Y. and Shi, K. W. 2010b. Incision and channel morphology across active structures along the Peikang River, central Taiwan: Implications for the importance of channel width. *Geological Society of America Bulletin.* Vol. 122. Pp. 1192-1208.

Yesilonis, I.D., Pouyat, R.V. and Neerchal, N.K. 2008. Spatial distribution of metals in soils in Baltimore, Maryland: role of native parent material, proximity to major roads, housing age and screening guidelines. *Environmental Pollution*. Vol.156. No.3. Pp.723-731.

Zhang, M.M., Liu, Z.J. and Fang, S. 2016. Sandstone grain size characteristics of the Upper Jurassic Emuerhe Formation in the western region, Mohe Basin (NE China). *Geological Journal*. Vol.51. Pp. 625-669.

Appendices

Appendix A: Example of results obtained from Gradistat on Excel 2010.

SAMPLE STATISTICS

SAMPLE IDENTITY: **site1-sample1** ANALYST & DATE: Tondani,

SAMPLE TYPE: Trimodal, Moderately Sorted TEXTURAL GROUP: Slightly Gravelly Sand

SEDIMENT NAME: Slightly Very Fine Gravelly Coarse Sand

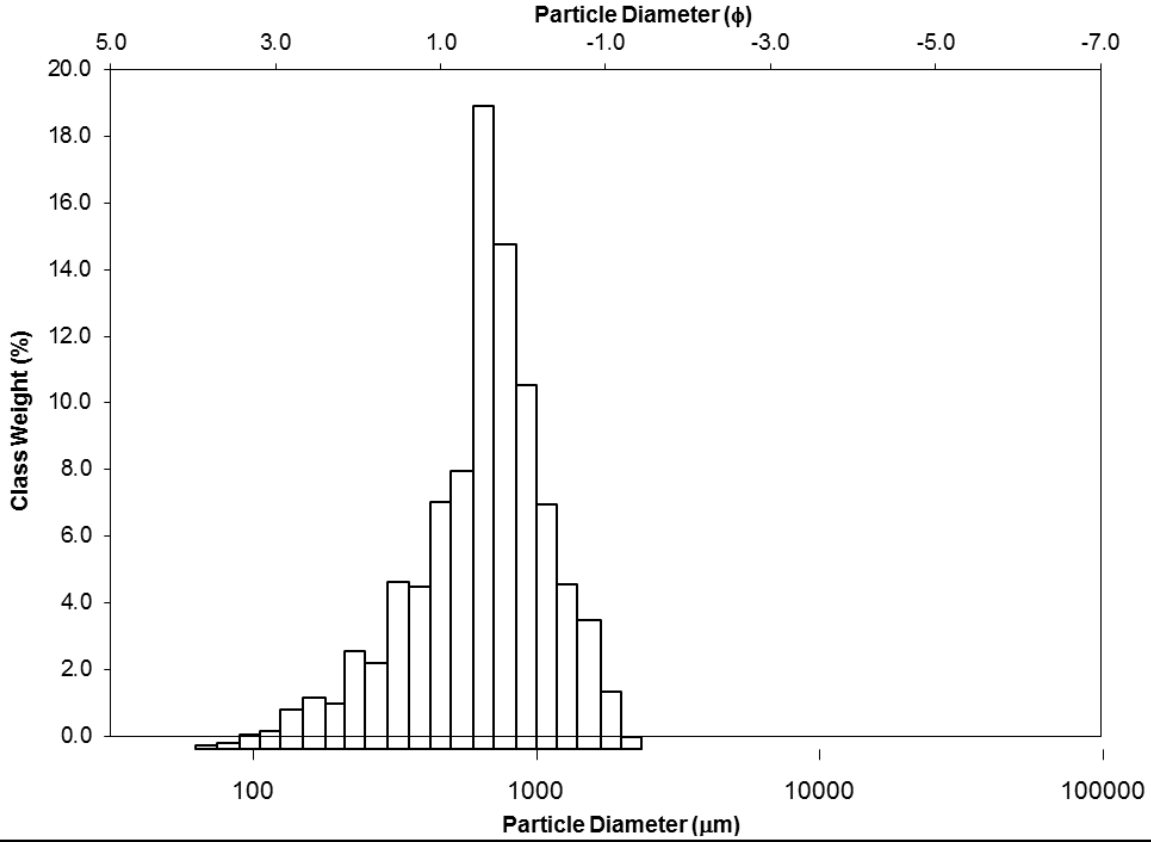
	μm	ϕ
MODE 1:	655.0	0.616
MODE 2:	327.5	1.616
MODE 3:	231.0	2.119
D_{10}:	282.1	-0.301
MEDIAN or D_{50}:	675.6	0.566
D_{90}:	1232.1	1.826
(D_{90} / D_{10}):	4.368	-6.063
(D_{90} - D_{10}):	950.0	2.127
(D_{75} / D_{25}):	1.923	7.186
(D_{75} - D_{25}):	431.9	0.944

GRAIN SIZE DISTRIBUTION

GRAVEL:	0.3%	COARSE SAND:	53.8%
SAND:	99.7%	MEDIUM SAND:	19.7%
MUD:	0.0%	FINE SAND:	7.0%
		V FINE SAND:	1.2%
V COARSE GRAVEL:	0.0%	V COARSE SILT:	0.0%
COARSE GRAVEL:	0.0%	COARSE SILT:	0.0%
MEDIUM GRAVEL:	0.0%	MEDIUM SILT:	0.0%
FINE GRAVEL:	0.0%	FINE SILT:	0.0%
V FINE GRAVEL:	0.3%	V FINE SILT:	0.0%
V COARSE SAND:	18.0%	CLAY:	0.0%

	METHOD OF MOMENTS			FOLK & WARD METHOD		
	Arithmetic	Geometric	Logarithmic	Geometric	Logarithmic	Description
	μm	μm	ϕ	μm	ϕ	
MEAN ($\bar{x}$):	726.6	625.5	0.677	634.0	0.657	Coarse Sand
SORTING (σ):	372.9	1.782	0.834	1.773	0.826	Moderately Sorted
SKEWNESS (Sk):	0.916	-0.769	0.769	-0.193	0.193	Fine Skewed
KURTOSIS (K):	4.053	3.797	3.797	1.250	1.250	Leptokurtic

GRAIN SIZE DISTRIBUTION



Appendix B: Table indicating grain size parameters for each site following Gradstat analysis.

Sample no.	very fine gravel	very coarse sand	coarse sand	medium sand	fine sand	very fine sand
site 1-1	0	2.4	48.8	35.3	11.9	1.6
site 1-2	0.8	46.3	41	7.3	3.1	1.4
site 1-3	0.2	25.3	57.8	14.1	2.5	0.1
site 1-4	0.1	29	62.6	7.9	0.4	0
site 1-5	0.1	25.8	58.8	12.2	3	0.2
site 1-6	0.1	20.3	59.7	16.8	2.7	0.3
site 1-7	0.2	23.9	53.4	18.4	3.2	0
site 2-1	0.1	10.9	41	37.1	9.5	1.5
site 3-1	0.6	28.7	47.2	21.1	2.3	0.2
site 4-1	0.4	6.6	5.8	24.2	47.3	15.7
site 4-2	0	2.2	6.8	12.2	56.6	22.2
site 5-1	0.4	31.9	45.8	17.5	3.9	0.5
site 5-2	0.1	3.4	28	52.8	13.4	2.2
site 5-3	0	1.7	28.7	59.2	9.6	0.8
site 6-1	1.8	63.2	27.6	4.2	1.5	1.7
site 6-2	0.4	17.6	30.1	25.6	20	6.2
site 6-3	1	52.2	37.8	5	2.5	1.4
site 6-4	0	1.3	5.3	59.3	28.7	5.4
site 7-1	0.1	11.3	48.2	21.8	14.8	3.8
site 7-2	0	3.2	14.5	34.4	39.5	8.4
site 7-3	0.4	14.4	39.1	41.6	4.4	0.1
site 7-4	0.5	15.7	29.8	47.8	5.8	0.4
site 8-1	0.1	4.6	11	51.2	23.6	9.4
site 8-2	0.6	39.7	31.6	11.6	12.5	3.9
site 9-1	0	1.2	1	3.2	83.9	10.8
site 9-2	0.7	40.6	42.1	10.2	5.5	0.9
site 9-3	0.2	47.7	46.1	3.1	2.2	0.7
site 9-4	0.2	7.6	39.2	14.2	33.5	5.4
site 9-5	0.2	17.7	50.8	25.2	3.8	2.3
site 10-1	0	1.2	29.9	46.9	17.8	4.2
site 10-2	0.1	1.9	49.4	40.3	7.2	1.2
site 11-1	2.8	48.2	38.3	8.6	1.7	0.4
site 12-1	0	0.9	6.3	64.3	26	2.6
site 12-2	0	1	53	38.4	6.6	1
site 12-3	0	0.3	25.6	66	7.6	0.5
site 12-	0.2	2.4	36.2	39.4	16.6	5.2

4						
site 12-5	0	0	0.1	74.9	23.7	1.3
site 13-1	0.3	18	53.8	19.7	7	1.2
site 13-2	5.4	38.1	33	12	7.1	4.2
site 13-3	2.6	59.4	28.3	6.3	2.4	0.9
site 13-4	0	0.5	1	10.2	69.8	18.5
site 13-5	1.4	42.7	39.5	11.2	2.2	3.1
site 13-6	1	54.9	38.3	2.5	1.7	1.6
site 14-1	0	0.3	0.5	12.7	70.8	15.7
site 14-2	4	52.3	23	6.7	11.6	2.4
site 14-3	0.9	49.9	37.9	7.6	2.7	1.1
site 15-1	1.2	41.9	50.5	5.4	0.7	0.4
site 15-2	0.9	25.5	50	11.5	3.9	8.2
site 15-3	3.5	63.2	26.7	2.6	1.2	2.6

Appendix C: Table indicating the mode, sediment name, kurtosis and sorting obtained from Gradstat analysis.

sample no.	Mode	sediment name	kurtosis	sorting
site 8-1	Bimodal	Slightly Very Fine Gravelly Coarse Sand	Mesokurtic	Moderately Sorted
site 8-2	Unimodal	Slightly Very Fine Gravelly Very Coarse Sand	Leptokurtic	Moderately Sorted
site 8-3	Unimodal	Slightly Very Fine Gravelly Coarse Sand	Leptokurtic	Moderately Well Sorted
site 8-4	Unimodal	Slightly Very Fine Gravelly Coarse Sand	Mesokurtic	Well Sorted
site 8-5	Unimodal	Slightly Very Fine Gravelly Coarse Sand	Leptokurtic	Moderately Well Sorted
site 8-6	Unimodal	Slightly Very Fine Gravelly Coarse Sand	Leptokurtic	Moderately Well Sorted
site 8-7	Unimodal	Slightly Very Fine Gravelly Coarse Sand	Mesokurtic	Moderately Sorted
site 9-1	Trimodal	Slightly Very Fine Gravelly Coarse Sand	Mesokurtic	Moderately Sorted
site 10-1	Unimodal	Slightly Very Fine Gravelly Coarse Sand	Mesokurtic	Moderately Sorted
site 12-1	Polymodal	Slightly Very Fine Gravelly Fine Sand	Leptokurtic	Poorly Sorted
site 12-2	Trimodal	Moderately Sorted Fine Sand	Very Leptokurtic	Moderately Sorted
site 13-1	Unimodal	Slightly Very Fine Gravelly Coarse Sand	Mesokurtic	Moderately Sorted
site 13- 2	Bimodal	Slightly Very Fine Gravelly Medium Sand	Leptokurtic	Moderately Sorted
site 13-3	Unimodal	Slightly Very Fine Gravelly Medium Sand	Leptokurtic	Moderately Well Sorted
site 16-1	Unimoda	Slightly Very Fine Gravelly Very Coarse Sand	Mesokurtic	Moderately Well Sorted
site 16-2	Polymodal	Slightly Very Fine Gravelly Coarse Sand	Mesokurtic	Poorly Sorted
site 16-3	Bimodal	Slightly Very Fine Gravelly Very Coarse Sand	Leptokurtic	Moderately Well Sorted
site 16-4	Bimodal	Slightly Very Fine Gravelly Medium Sand	Mesokurtic	Moderately Well Sorted
site 17-1	Bimodal	Slightly Very Fine Gravelly Coarse Sand	Mesokurtic	Moderately Sorted
site 17-2	Trimodal	Slightly Very Fine Gravelly Fine Sand	Leptokurtic	Moderately Sorted
site 17-3	Unimodal	Slightly Very Fine Gravelly Medium Sand	Mesokurtic	Moderately Sorted
site 17-4	Bimoda	Slightly Very Fine Gravelly Medium Sand	Mesokurtic	Moderately Sorted
site 15-1	Trimodal	Slightly Very Fine Gravelly Medium	Very	Moderately Sorted

		Sand	Leptokurtic	
site 15-2	Bimodal	Slightly Very Fine Gravelly Very Coarse Sand	Mesokurtic	Poorly Sorted
site 14-1	Bimodal	Slightly Very Fine Gravelly Fine Sand	Mesokurtic	Well Sorted
site 14-2	Trimodal	Slightly Very Fine Gravelly Coarse Sand	Leptokurtic	Moderately Sorted
site 14-3	Unimodal	Slightly Very Fine Gravelly Very Coarse Sand	Leptokurtic	Moderately Well Sorted
site 14-4	Trimodal	Slightly Very Fine Gravelly Coarse Sand	Very Platykurtic	Poorly Sorted
site 14-5	Unimodal	Slightly Very Fine Gravelly Coarse Sand	Leptokurtic	Moderately Sorted
site 5-1	Polymodal	Moderately Sorted Medium Sand	Mesokurtic	Moderately Sorted
site 5-2	Bimodal	Slightly Very Fine Gravelly Coarse Sand	Leptokurtic	Moderately Well Sorted
site 4-1	Unimodal	Slightly Very Fine Gravelly Very Coarse Sand	Platykurtic	Moderately Sorted
site 3-1	Unimodal	Slightly Very Fine Gravelly Medium Sand	Mesokurtic	Moderately Well Sorted
site 3-2	Bimodal	Slightly Very Fine Gravelly Coarse Sand	Mesokurtic	Moderately Well Sorted
site 3-3	Unimodal	Well Sorted Medium Sand	Leptokurtic	Well Sorted
site 3-4	Trimodal	Slightly Very Fine Gravelly Medium Sand	Mesokurtic	Moderately Sorted
site 3-5	Bimodal	Well Sorted Medium Sand	Mesokurtic	Well Sorted
site 1-1	Trimodal	Slightly Very Fine Gravelly Coarse Sand	Leptokurtic	Moderately Sorted
site 1-2	Polymodal	Very Fine Gravelly Very Coarse Sand	Leptokurtic	Poorly Sorted
site 1-3	Unimodal,	Slightly Very Fine Gravelly Very Coarse Sand	Leptokurtic	Moderately Sorted
site 1-4	Trimodal	Moderately Well Sorted Fine Sand	Mesokurtic	Moderately Well Sorted
site 1-5	Unimodal	Slightly Very Fine Gravelly Very Coarse Sand	Leptokurtic	Moderately Sorted
site 1-6	Unimodal	Slightly Very Fine Gravelly Very Coarse Sand	Leptokurtic	Moderately Well Sorted
site 7-1	Trimoda	Moderately Well Sorted Fine Sand	Mesokurtic	Moderately Well Sorted
site 7-2	Trimodal	Slightly Very Fine Gravelly Very Coarse Sand	Leptokurtic	Poorly Sorted
site 7-3	Unimodal	Slightly Very Fine Gravelly Very Coarse Sand	Mesokurtic	Moderately Sorted
site 6-1	Unimodal	Slightly Very Fine Gravelly Coarse Sand	Mesokurtic	Moderately Well Sorted
site 6-2	Bimodal	Slightly Very Fine Gravelly Coarse Sand	Very Leptokurtic	Poorly Sorted
site 6-3	Unimodal	Slightly Very Fine Gravelly Very Coarse Sand	Mesokurtic	Moderately Well Sorted

Appendix D: Table indicating Organic matter measured at different sites.

LOSS ON IGNITION worksheet

Soil sample	Crucible		Crucible plus soil weight (g)	Soil weight (g)	Reweigh after ignition (g)	Loss in weight (g)	% organics
	No	weight (g)					
4-1		44.93	65.23	22.31	64.73	0.50	2.25
4-2		43.17	61.97	18.62	60.92	1.14	6.15
5-3		41.37	72.42	31.06	71.85	0.57	1.85
6-1		42.39	46.30	3.91	46.15	0.16	3.96
6-2		45.41	64.38	18.96	63.77	0.60	3.19
6-3		45.11	49.01	3.89	48.81	0.19	4.98
8-1		45.09	65.46	20.36	63.67	1.79	8.78
8-2		44.15	59.62	15.50	58.39	1.23	7.95
9-2		46.07	66.41	20.34	66.14	0.27	1.36
9-5		43.64	47.71	4.06	47.43	0.27	6.73
10-1		44.31	53.12	8.80	52.57	0.55	6.25
14-1		42.78	55.51	12.72	55.18	0.33	2.57
14-3		43.37	54.00	10.63	53.56	0.35	3.33
14-4		42.40	67.08	24.67	66.75	0.33	1.32
14-5		42.90	62.63	19.73	61.97	0.66	3.36
14-6		43.68	73.97	30.29	73.54	0.43	1.43
15-2		43.30	61.07	17.76	60.05	1.02	5.75

METHOD: Burn in crucible for 8 hours at 430˚C

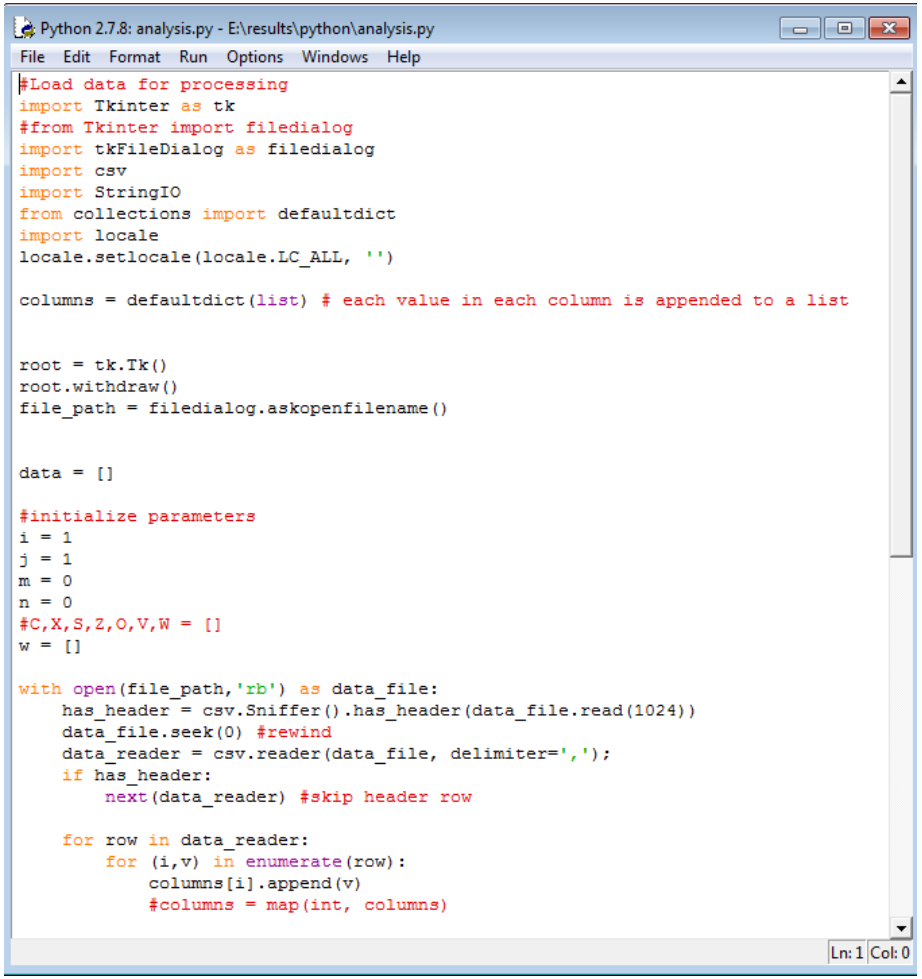
Appendix E: Table indicting the minerals counted on the thin section of each sample site.

	quartz	plagioclase	orthoclase	clinopyronene	olivine	hornblende	biotite	magnetite	hematite	ilmenite	zircon	orthopyroxene	muscovite	garnet	epidote	rutile	tourmaline	zoisite
site 1-1	155			20	4	7	74	76	28	24	9	238			7	4		
site 1-2	125			15	3			4	3	1	2	92	5		5	5		
site 1-3	259	10		7	5	8	5				3		3		5	22	3	
s1-4	62				3		7	7	5	4	2	171	11					
site 2-1-	201			24	28	7	7	12	3	3		8	30	1	3	30	3	1
site 3-1	171	15	6	20	2		20	8	4	2	10	10	15					
site 4-1	239	8				1	101	15	6	3	12		66			8		
site 4-2	417			23		5	121	78	60	24	13		83		10	8		
site 5-1	297					10	122	70	48	32	12		52		18	81	6	
site 5-2	229					16	14	69	21	18	10		29		22	22		
site 6-1	208			7	6	3	30	8	4	3		10	7		3	23		
site 6-2	422		4	25	3	7	74	11	5	4			57		10	43	3	2
site 6-3	527			37	6	10	107	10	5	3	5	13	30		12	52	1	
site 6-4	282			9	5	5	18	8	4	3	4	2	8		7	15		

site 7-1	262	2		31	2	11	89	32	15	10	1		90		15	22	2	4
site 7-2	320			37		9	105	25	13	17		8	70		21	31	8	
site 7-6	256			25		7	112	26	16	12		10	124	1	31	7	10	4
site 8-1	214	15		25	37	18	62	17	17	16		22	42		18	48	2	
site 8-2	135	3		9	6	6	18	19	15	16	13	8	17		1	7		
site 9-1	423	7				11	103	33	12	10	12		85		26	10	5	
site 9-2	175			12	6	8	13	5	5	2	1	8	19		6	21		
site 9-3	377	12		16	18	3	2	18	9	5		5	21		13	19	3	5
site 9-4	411			6	12	15	41	34	19	15	16		31			13		
site 9-5	339	12		10	23	5	17	7	6	4	2	6	17	1	5	20	9	2
site 10-1	243		5	10		4	23	28	18	12	6	16	48			10		
site 10-2	199		6	12	5	2	13	5	3	3	7	5	10		10	8		2
site 11-3	239	6		28	15	9	122	9	10	5		10	96	4	43	73	19	1
site 12-1	240			21	2	2	17	5	2		15	6	13		4	54		
site 12-3	246			25	9		63	20	9	11	12	9	21		13	24		
site 12-4	173			14		5	47	31	24	18	9					5		

site 12-5	214			19	3	21	62	4	3	3		7	40		11	33		
site 12-6	304	85		42	3		101	38	14	8			72		26	54	10	
site 13-1	167	26	10	9	21	7	1	17	4	7	1	9	20		6	19		1
site 13-2	458	5	3	31		4	30	157	68	26		20			6	21		
site 13-4	130	15	4	69	6	3	1	12	11	12	6	2		3	2	5		3
site 13-5	372		3				24	18	12	8			36		13	10		
site 13-6	200		4	6			2	8	2	2	4	45						
site 14-1	59		5	2	8		3	12	6	5	16	64						2
site 14-2	220			3	12			10	7	4	15		9			11		
site 14-3	357		1	11	9	8	33	6	2	4		12	22		10	16		
site 15-2	156		6	9		10	50	7	3	2	4		33					
site 15-3	283			62		16	305	35	16	12	4							

Appendix F: Example of the Python script used for running the mixing model.



Appendix G: Table indicating the correlation coefficient between trace elements

	Sc	*V*	*Cr*	*Co*	*Ni*	*Cu*	*Zn*	*Ga*	*Rb*	*Sr*	*Y*	*Zr*	*Nb*	*Mo*	*Ba*	*Pb*	*Th*	*U*
Sc	1																	
v	**0.909357**	1																
Cr	0.319058	0.253022	1															
Co	**0.728472**	**0.651381**	0.415473	1														
Ni	0.39067	0.224462	**0.635096**	**0.656946**	1													
Cu	**0.550541**	**0.504459**	-0.18772	0.410346	0.090059	1												
Zn	**0.852226**	**0.836412**	0.214209	**0.651861**	0.285792	**0.833037**	1											
Ga	**0.602718**	**0.601832**	-0.2318	0.405557	0.007937	**0.798474**	0.77191	1										
Rb	-0.59226	-0.67308	-0.39487	-0.34538	-0.2217	-0.03415	-0.37925	-0.0811	1									
Sr	0.216207	0.382513	-0.02325	0.112405	-0.17295	0.045279	0.169136	0.036805	-0.59844	1								
Y	**0.546156**	**0.513367**	**0.662268**	0.466034	0.24753	0.238006	**0.588929**	0.205369	-0.34951	0.149407	1							
Zr	0.304525	0.273687	**0.62696**	0.196949	0.094626	0.149481	0.419279	**0.059825**	-0.26355	0.071331	**0.895777**	1						
Nb	**0.782469**	**0.919208**	0.266121	0.460333	0.033231	0.457121	**0.790133**	**0.558799**	-0.59736	0.378243	**0.602676**	0.457721	1					
Mo	0.38057	0.417574	0.212299	0.169286	-0.07014	0.426922	**0.54697**	0.331427	-0.23028	0.226344	0.465102	**0.503127**	**0.608124**	1				
Ba	-0.26314	-0.13823	-0.19834	-0.12985	-0.31553	-0.00423	-0.1344	-0.11858	0.227439	**0.527221**	-0.02901	-0.07788	-0.05192	0.079861	1			
Pb	-0.23004	-0.27691	0.389808	-0.13534	-0.0561	-0.15379	-0.08186	-0.19389	0.361031	-0.26495	0.438107	**0.567543**	-0.06378	0.157389	0.217919	1		
Th	0.232619	0.236864	**0.679201**	0.236442	0.116135	-0.10459	0.229105	-0.09996	-0.22605	0.10819	**0.862455**	**0.859383**	0.391265	0.302951	0.132861	**0.665627**	1	
U	-0.10639	-0.11761	0.206875	-0.12535	-0.11553	-0.05585	-0.03265	-0.19282	0.141612	-0.07806	0.381	0.420825	0.041977	0.235306	0.123782	**0.561624**	0.495976	1

Appendix H: Table indicating the eigenvalues obtained following principal component analysis.

Total Variance Explained

	Initial Eigenvalues			Extraction Sums of Squared Loadings		
Component	Total	% of Variance	Cumulative %	Total	% of Variance	Cumulative %
1	6.775	37.639	37.639	6.775	37.639	37.639
2	3.696	20.531	58.170	3.696	20.531	58.170
3	2.193	12.186	70.355	2.193	12.186	70.355
4	1.865	10.363	80.718	1.865	10.363	80.718
5	1.045	5.808	86.527	1.045	5.808	86.527
6	.594	3.302	89.829			
7	.569	3.161	92.990			
8	.387	2.148	95.139			
9	.243	1.350	96.488			
10	.176	.977	97.465			
11	.140	.775	98.240			
12	.103	.572	98.812			
13	.073	.403	99.215			
14	.067	.371	99.586			
15	.033	.184	99.770			
16	.020	.111	99.881			
17	.014	.078	99.959			
18	.007	.041	100.000			

Extraction Method: Principal Component Analysis.

Appendix I: Table indicating the relationship between grain sizes and trace elements. Significant statistical relationships at P>0.5.

	Sc	**V**	**Cr**	**Co**	**Ni**	**Cu**	**Zn**	**Ga**	**Rb**	**Sr**	**Y**	**Zr**	**Nb**	**Mo**	**Ba**	**Pb**	**Th**	**U**
very fine gravel (>2 mm)	**0.56**	**0.71**	-0.23	0.24	-0.26	0.43	**0.54**	**0.52**	-0.40	0.27	0.12	-0.10	**0.71**	0.30	-0.02	-0.30	-0.11	-0.15
very coarse sand (2 mm)	0.11	0.17	-0.23	0.05	-0.17	0.19	0.13	0.26	-0.01	-0.04	-0.21	**-0.32**	0.14	-0.09	-0.10	-0.20	-0.34	-0.17
coarse sand (1 mm)	0.01	-0.01	-0.03	-0.10	0.05	0.11	0.03	0.14	-0.18	0.03	-0.17	-0.18	-0.07	-0.11	-0.06	-0.02	-0.17	-0.07
medium sand (0.5 mm)	-0.03	-0.07	0.05	0.17	0.21	-0.07	-0.04	-0.12	-0.08	0.15	0.02	0.13	-0.13	0.01	0.02	0.04	0.08	-0.07
fine sand (0.25 mm)	-0.10	-0.12	0.20	-0.11	-0.03	-0.18	-0.11	-0.26	0.20	-0.10	0.28	0.33	-0.01	0.14	0.12	0.20	0.37	0.27
very fine sand (0.125 mm)	-0.11	-0.06	0.06	-0.03	-0.01	-0.21	-0.13	-0.16	0.17	-0.07	0.14	0.11	0.01	0.05	0.05	-0.01	0.14	0.03

Appendix J: Table indicating relationships between trace elements and minerals within the sediment. Qz=quartz, plg=plagioclase, cpy=clinopyroxene, olv=olivine, hbld=hornblende, bio=biotite, mg=magnetite, hm=hematite, il=ilmenite, zcn=zircon, opy=orthopyroxene, grt=garnet, rt=rutile, tml=tourmaline. Significant statistical relationships at P>0.5 marked in bold.

	Sc	**V**	**Cr**	**Co**	**Ni**	**Cu**	**Zn**	**Ga**	**Rb**	**Sr**	**Y**	**Zr**	**Nb**	**Mo**	**Ba**	**Pb**	**Th**	**U**
qz	0.01	0.03	0.01	0.15	-0.07	-0.05	0.01	0.01	0.14	0.03	0.17	0.16	0.12	0.26	0.07	0.16	0.26	0.16
plg	-0.24	-0.15	-0.35	-0.35	0.06	-0.24	-0.28	-0.18	-0.07	0.16	-0.54	-0.67	-0.33	**-0.74**	0.05	**-0.56**	**-0.53**	-0.17
orth	0.02	-0.14	-0.01	-0.02	0.42	-0.17	-0.14	-0.09	0.00	-0.07	-0.03	-0.23	-0.29	-0.47	0.06	-0.35	-0.22	0.02
cpy	-0.02	0.04	-0.35	-0.07	-0.23	-0.02	-0.08	0.03	0.06	0.09	-0.15	-0.13	0.03	-0.03	-0.01	-0.18	-0.10	-0.13
olv	0.38	0.29	0.07	0.20	0.49	0.21	0.27	0.13	-0.35	-0.12	0.08	0.05	0.12	-0.13	**-0.58**	**-0.52**	-0.27	-0.13
hbld	-0.02	-0.03	0.27	-0.02	0.23	0.06	0.07	-0.04	0.00	-0.05	0.27	0.20	0.01	0.11	-0.11	0.04	0.12	0.29
bio	-0.09	-0.03	-0.21	-0.02	-0.23	0.01	-0.04	0.07	0.20	0.07	0.09	0.00	0.03	0.14	0.14	0.04	0.04	0.23
mg	0.30	**0.52**	-0.08	0.11	-0.22	0.29	0.38	0.37	-0.32	0.27	0.20	0.13	**0.60**	0.35	0.05	-0.05	0.28	0.30
hm	0.19	0.40	-0.02	0.13	-0.12	0.14	0.26	0.23	-0.21	0.19	0.14	0.08	0.47	0.32	0.01	-0.02	0.21	0.32
il	0.08	0.23	0.14	0.14	0.01	0.08	0.15	0.05	-0.18	0.30	0.15	0.15	0.29	0.33	0.11	0.08	0.29	**0.53**
zcn	0.22	0.28	0.37	0.18	-0.06	0.29	0.40	0.11	0.04	0.11	**0.63**	**0.61**	**0.50**	**0.67**	0.13	0.34	0.49	0.44
opy	-0.21	-0.17	-0.09	-0.24	-0.03	0.27	0.00	0.04	0.22	-0.03	-0.16	-0.14	-0.17	-0.11	0.35	0.37	-0.04	**0.51**
msc	-0.28	-0.33	-0.13	-0.20	-0.26	-0.25	-0.32	-0.24	0.27	-0.02	0.02	0.15	-0.10	0.03	0.18	0.23	0.21	0.22
grt	-0.48	-0.28	-0.30	**-0.51**	-0.27	-0.39	-0.43	**-0.63**	0.44	**0.74**	**-0.50**	-0.43	-0.37	-0.48	**0.52**	-0.17	-0.45	0.13
epi	-0.21	-0.22	-0.05	-0.14	-0.10	-0.24	-0.28	-0.25	0.36	-0.15	-0.02	0.07	-0.13	-0.01	0.23	0.40	0.24	0.40
rt	-0.12	-0.06	-0.09	0.01	-0.06	0.00	-0.01	0.07	0.13	-0.11	0.11	0.16	-0.04	-0.05	-0.19	0.14	0.12	0.38
tml	-0.13	-0.14	-0.04	-0.12	-0.05	-0.20	-0.25	-0.39	-0.02	0.18	-0.09	-0.06	-0.03	0.18	0.19	0.09	0.06	0.28
zoi	-0.29	**-0.57**	0.27	0.10	-0.09	**-0.65**	**-0.70**	**-0.58**	0.29	0.16	-0.40	-0.26	-0.49	-0.39	0.38	0.40	0.26	-0.16